NNT : 0000AIXM0000

THÈSE DE DOCTORAT

Soutenue à Aix-Marseille Université
le 13 septembre 2024 par

Pedro Miguel BELIO-MAIRAL

Functional diversity of MT5-MMP domains: mechanistic and therapeutical implications in Alzheimer's disease

Diversité fonctionnelle des domaines de MT5-MMP : implications mécanistiques et thérapeutiques dans la maladie d'Alzheimer

Discipline
Biologie Santé

Spécialité
Neurosciences

École doctorale
ED62 – Sciences de la Vie et de la Santé

Laboratoire/Partenaires de recherche
Institut de NeuropPhysiopathologie (INP)
UMR 7051 AMU/CNRS

Composition du jury

Raphaëlle PARDOSSI-PIQUARD Université Côte d'Azur	Rapporteuse
Sylvie CLAEYSEN Université de Montpellier	Rapporteuse
Nicolas SERGEANT Université de Lille	Examinateur
François DEVRED Aix-Marseille Université	Président du jury
Santiago RIVERA Aix-Marseille Université	Directeur de thèse
Emmanuel NIVET Aix-Marseille Université	Co-directeur de thèse

Affidavit

I, undersigned, Pedro Miguel BELIO-MAIRAL, hereby declare that the work presented in this manuscript is my own work, carried out under the scientific supervision of Santiago RIVERA and Emmanuel NIVET, in accordance with the principles of honesty, integrity and responsibility inherent to the research mission. The research work and the writing of this manuscript have been carried out in compliance with both the French national charter for Research Integrity and the Aix-Marseille University charter on the fight against plagiarism.

This work has not been submitted previously either in this country or in another country in the same or in a similar version to any other examination body.

Place Marseille, date 10 juillet 2024



Cette œuvre est mise à disposition selon les termes de la Licence Creative Commons Attribution - Pas d'Utilisation Commerciale - Pas de Modification 4.0 International.

Liste de publications et/ou brevets et participation aux conférences

1) Liste des publications et/ou brevet [1] réalisées dans le cadre du projet de thèse :

    1. Arnst N, Belio-Mairal P, García-González L, Arnaud L, Greetham L, Nivet E, Rivera S, Dityatev A. Deficiency in MT5-MMP Supports Branching of Human iPSCs-Derived Neurons and Reduces Expression of GLAST/S100 in iPSCs-Derived Astrocytes. *Cells*. 2021; 10(7):1705. https://doi.org/10.3390/cells10071705

    2. Belio-Mairal P, Kamitsou A, Stephan D, Jullien N, Thiane D, Ramos M, Louis L, Benoist F, Serrano B, David M, Khrestchatisky M, Lécorché P, Nivet E, Rivera S. Mutations in specific domains of MT5-MMP prevent the accumulation of toxic APP metabolites and serve as templates for peptide-based therapeutics in human in vitro models of Alzheimer's disease. *HAL*. 2024. hal-04642476

2) Participation aux conférences[2] et écoles d'été au cours de la période de thèse :
    1. **XV European Meeting on Glial Cells in Health and Disease**, virtual, 1st - 9th July 2021.
    2. **Neurodays 2021**, Marseille, France, 8th - 9th November 2021.
    3. **FENS Forum 2022**, Paris, France, 9th - 13th July 2022.
       Belio-Mairal P, Louis L, Jimenez A, Stephan D, Sonawane S, Greetham L, Di Pasquale E, Nivet E, Rivera S. S07-259: The C-terminal of MT5-MMP regulates C99 processing and amyloid-beta levels in a cell model of Alzheimer's

[1] Cette liste comprend les articles publiés, les articles soumis à publication et les articles en préparation ainsi que les livres, chapitres de livre et/ou toutes formes de valorisation des résultats des travaux propres à la discipline du projet de thèse. La référence aux publications doit suivre les règles standards de bibliographie et doit être conforme à la charte des publications d'AMU.

[2] Le terme « conférence » est générique. Il désigne à la fois « conférence », « congrès », « workshop », « colloques », « rencontres nationales et/ou internationales » … etc.

Indiquer si vous avez fait une présentation orale ou sous forme de poster.

ABSTRACT

Alzheimer's disease (AD) is a neurodegenerative disorder with two major hallmarks: 1) amyloid β (Aβ) plaques in the brain parenchyma, and 2) neurofibrillary tangles. The recent FDA approval of 3 anti-Aβ monoclonal antibodies has downplayed some of the existent doubts on the Amyloid hypothesis, but the efficacy of these treatments is limited. In this context, the precursor of Aβ, C99, is gaining momentum as a neurotoxic factor on its own, and new secretases of the amyloid precursor protein (APP) have been identified. Together, these elements provide new avenues for the study of novel pathological mechanisms and anti-amyloid strategies in AD.

Membrane-type 5 matrix metalloproteinase (MT5-MMP) is a recently described APP secretase, cleaving at the η-site. Knockout of MT5-MMP prevented amyloidogenesis and neuroinflammation in an AD mouse model, and deletion of MT5-MMP transmembrane (TM) and/or intracellular (IC) domains decreased C99 and Aβ levels in human cells. In this thesis, I explored the consequences of MT5-MMP depletion in human neurons and astrocytes and the potential of MT5-MMP TM and IC to modulate C99 and Aβ levels in an in vitro AD model. In my thesis, I describe an important role of MT5-MMP in dendritic arborization and glial physiology in human neurons and astrocytes. Moreover, I revealed the different roles of MT5-MMP TM and IC in C99 and Aβ accumulation. Modifications of the MT5-MMP IC changed C99 trafficking, with divergent consequences on C99 and Aβ levels. Finally, synthetic peptides mimicking certain MT5-MMP IC variants demonstrate the utility of MT5-MMP-based strategies to tackle C99 accumulation.

My PhD thesis expands our knowledge of the roles of specific MT5-MMP domains. Moreover, it provides a framework to exploit the potential of MT5-MMP unique properties for modulating C99 and confirms MT5-MMP as a valuable therapeutic target for preventing amyloidogenesis in AD.

Keywords: Alzheimer's disease, MT5-MMP, Aβ, C99, trafficking, human *in vitro* models.

RESUME

La maladie d'Alzheimer (MA) est un trouble neurodégénératif avec deux marqueurs majeurs dans le cerveau : 1) les plaques d'amyloïde β (Aβ) et 2) les enchevêtrements neurofibrillaires. L'approbation récente par la FDA de trois anticorps monoclonaux anti-Aβ a réduit certains doutes sur l'hypothèse amyloïde, mais leur efficacité reste limitée. Le précurseur de l'Aβ, C99, est désormais considéré comme un facteur neurotoxique à part entière, et de nouvelles secrétasses de la protéine précurseur de l'amyloïde (APP) ont été identifiées, ouvrant de nouvelles perspectives pour l'étude des mécanismes pathologiques et des stratégies anti-amyloïdes dans la MA.

La metalloproteinase matricielle de type membranaire 5 (MT5-MMP) est une sécrétase de l'APP récemment découverte, qui clive l'APP au niveau du site η. La suppression de MT5-MMP prévient l'amyloïdogenèse et la neuroinflammation dans un modèle murin d'AD, et la suppression des domaines transmembranaires (TM) et/ou intracellulaires (IC) de MT5-MMP diminue les niveaux de C99 et d'Aβ dans des cellules humaines. Ma thèse explore les conséquences de la déplétion de MT5-MMP dans les neurones humains et les astrocytes, ainsi que le potentiel des domaines TM et IC de MT5-MMP pour moduler les niveaux de C99 et d'Aβ dans un modèle in vitro de la MA. J'ai aussi étudié les rôles distincts des domaines TM et IC de MT5-MMP dans l'accumulation de C99 et d'Aβ, montrant que les modifications de MT5-MMP IC affectent le trafic de C99 avec des effets divergents sur les niveaux de C99 et d'Aβ. Enfin, des peptides synthétiques mimant certains variants du domaine IC de MT5-MMP confirment l'utilité des stratégies basées sur MT5-MMP pour réduire l'accumulation de C99.

Ma thèse élargit nos connaissances sur les rôles spécifiques des domaines de MT5-MMP et souligne MT5-MMP comme une cible thérapeutique prometteuse pour prévenir l'amyloïdogenèse dans la MA.

Mots-clés : Maladie d'Alzheimer, MT5-MMP, Aβ, C99, trafic cellulaire, modèles *in vitro* humains.

ACKNOWLEDGEMENTS

First of all, sorry to anyone I may forget… it's 19:30 of the 10th of July of 2024, I have slept probably a mean of 4 hours per day for the last 6 months because of insomnia, stress, and work. So, if I forgot to add you is not because I don't love you but because I am exhausted and on the verge of my sanity. Please contact me if you feel I didn't value enough your help and I will be happy to invite you to some drinks ☺

Thank you to the NeuroSchool for funding my PhD and thank you to their team. Gabrielle, Catherine, and specially Isabelle, thank you for always being there and being ready to give a hand. Isabelle, I don't know how many thousands of times I came to bother you, but you always answered with a smile. You are invaluable to this community!!!

Thank you also the Fondation Vaincre Alzheimer for trusting in me and funding our research and my last year of PhD.

Santi, Manu, thank you. I don't think I can say anything else but thank you. You guys gave me an opportunity when it was very easy to search for someone younger, healthier, and cleverer than me. I will always feel I owe you a big one for taking me into your teams and make me the scientist I am today. Thank you. I don't think you're aware of the impact you had in my life, but I do, and I will always be grateful for having the opportunity to grow under your supervision. Manu, special thanks to you because you believed in me and you helped me when we were only collaborators and I was trying to take a very big decision, which has completely changed my life (for good). Santi and Manu, I hope the years to come are full of collaborations, and that we can continue to be in contact for long time.

Big thanks to all the INP, from its "ex"-director, Michel, to the flamant new director François. It has been a pleasure to be part of this institute for nearly 5 years. I will definitely miss it. In fact, I think it will be tough for me to find a place as welcoming as the INP! Thank you also to all the PIs and researchers of the INP who have been always helpful with any difficulties (both technical and personal) I came across.

Special mention to the Neurocyto team, to the PhDs with whom I have shared this path, Dominic, Florian, Ciarán, Sofia, and of course Karo. You guys have been the sweetest people to hang out with (also you Louisa, even if you're a postdoc). Always there to share our problems and our glory days. I wish you all the best because you truly deserve it. Soon it will be you writing this section Sofia! En plus, un grand merci à Christophe, Nico, Fanny et Florence, toujours présents quand j'ai eu besoin d'aide, matos, ou n'importe quoi.

Sans oublier à Hervé et Fabrice. Finalement on a réussi à faire les co-IP ! Même si maintenaient c'est l'anticorps anti-Flag qui ne fonctionne pas… Merci pour le temps que vous avez dédié à m'aider. Merci Fabrice pour le temps, questions, explications techniques, et surtout pour toujours me saluer avec un sourire !

Au freak team des statistiques et l'informatique, merci beaucoup pour être tarpin gentils ! Merci Denis pour être toujours dispo pour discuter avec moi les choses les plus techniques de n'importe quoi sur les statistiques. A ti Montse, qué te voy a decir… pues nada, que gracias. No sé cuántas horas de quejas, indignación, e insultos varios a los ordenadores te has comido, pero gracias. Eres maravillosa. Un pequeño tesoro en el INP. Espero que te valoren algún día como deben.

Before going to my team colleagues… Maud, thank you. You're such a great person. I honestly hope that you can finally get your place and start developing your project. I will keep a close eye on your work, I think you have in your hands a very exciting future. I am honestly jealous of your team for having the opportunity to work with you. And I wish one day we can work this out.

Time for my teams. Thank you, Laurence, Kevin, and Dominika for welcoming me, teaching me, and always be there to give me a hand. Big thanks to Shweta also, for being my postdoc in anything that had to do with biochemistry. As soon as you arrived, I started to feel less lonely. Thank you, Eric for teaching me SO MUCH on electrophysiology. Thank you for taking your time to help me with the hiPSC and thank you for the long conversations. Gracias Laura por derrochar optimismo, energía y pasión por todas partes, empezamos en esto en países diferentes en 2016 y al final acabé heredando tu currazo, espero haber sido digno sucesor. Merci Christine, merci pour être toujours bienveillante, pour faire attention à moi, et pour être disponible pour parler n'importe quand. Merci à Diarra aussi, pour me supporter, pour fournir des efforts pour nous comprendre et pour m'aider à réussir dans cette thèse.

Iván, pibe, boludo, gracias por ser tan radiante como eres. Gracias por ser el optimista, por querer ayudar siempre, por estar siempre disponible para hablar, y por ser tan payaso. Me has ayudado mucho durante esta tesis, aunque me haya costado hacerte de psicólogo 24/7. Laurie, n'importe où tu travailles, ils auront de la chance de t'avoir. Tu as une luminosité incroyable, une passion géante pour la science, je juste espère que tu trouves un endroit où ils t'apprécient comment tu mérites. Merci encore, Angélique, parce qu'au moment critique, tu m'as aidé vraiment beaucoup à réussir et avancer avec les p*** de

neurones, avec les 3000 millions des clones, et toujours avec un sourire. Et toi Louise, quoi on ferait dans le labo sans LA personne qui pense à que ce monde soit un peu meilleur pour tous. Merci pour nôtres discussions, nôtres conversations, pour tes eyeliners, et pour t'occuper des choses plus chiantes du labo. Et alors, la reine de l'équipe, Delphine, vraiment, je ne sais pas quoi dire, je pense que je vais me mettre à pleurer. Tu vas me manquer, tellement ! Je ne sais pas comment commencer à te remercier, pour t'occuper aussi des choses plus chiantes du labo, mais surtout pour être toujours disponible pour parler, rigoler, crier, râler, discuter, ou simplement être présent. Je ne suis pas sûr que tu aies besoin d'apprendre de la communication bienveillante, mais je suis sûr que beaucoup du monde peux apprendre de toi simplement comment être une bonne personne, tu es vraiment une ange.

Half-way of my 3rd page, and I am still starting. Time for the newbies. Raph, Thaïs, Nico, Chiara, Matthew, Léana you've been such shot of fresh air. We've only been together a bit more than 6 months, but I promise you changed my life in the lab. Your energy, your smiles, the enormous support you guys have given me, I can't say thank you enough times. In very few months you already mean a lot to me, and believe me, I am VERY sad to leave without sharing part of your journeys. I have the feeling we could have done great things together. I wish you all the best. You guys are brilliant, you all have great future, I just hope everything works out and you get where you deserve. Wherever I am whenever it might be, I will be there if you need me (sounds like a song, but I didn't do it on purpose).

Thaïs, just few words for my successor. I don't know if you realize it, but apart from being a sunshine, you have an enormous talent. Squeeze it. Put it into play. Don't let anyone make you feel like you don't own that. Your thesis has to be your playground to grow and develop yourself into the great scientist you're meant to be. Be stubborn. Be all the stubborn you want. Push everything, everyone, and yourself to get the best out of you. You have a lot to give.

To the students, Elias, Charline, Camille, Albane, Mélissa, Célia, it was a pleasure to be part of your journey into science, thank you for letting me mentor you. It was a pleasure to see you guys learn so much! Marine, merci pour me faire la tête toujours, ça me mette un sourire dans la tête chaque fois que je te vois. Kalimera Thei! Thank you for being such a sweet person. And take that talent of yours and exploit it where they deserve it! And, finally, Athina, I don't know how many times I'll say this, but you saved my thesis. You're such a hard worker. Thank you, thank you, thank you, thank you, and thank you. I only

have good words for you. You're incredibly talented and such a nice person at the same time. Any lab that has you will be extremely lucky. I hope we can work together again.

Maura and Gabri, I am the last one, but we did it. The three of us. We can finally say a big f*** you all together. Thank you for your friendship, your support, and your guidance. You're incredibly valuable for me.

Que pasa Blanca, gracias por tu amistad, por tu optimismo, y por tu alegría. Has puesto muchos más esfuerzos que yo para que esta amistad se mantenga, y te lo agradezco mucho, porque vale mucho la pena tenerte cerca. Gracias por estar siempre dispuesta a ir a tomar algo, a escalar, a comer, a lo que fuera. Gracias. Pronto te toca a ti!

Sara, Raphi, what am I supposed to say now? It will break my heart to leave Marseille, but it will break my heart even more to leave you guys. You have been the cure to my darkness. You have been SO present when I needed you, and I just hope I could have had more time to be present for you, too. I will always remember our times. Some of my most precious memories (if not all) in Marseille are with you in them. Robert, I have the feeling we always come across when you come to use our bathrooms. Although I nearly killed you, after you had saved me, you have always been there. You're such a special person. You're a German that is completely the opposite of what we could expect (in the good sense). And talking about weird Germans (no judgement), Caro, Leo, and Karo, what about you, hein? What can I say? You girls arrived in my live in one of the worst moments I have gone through. And you made it all worth it again. I miss you so much since you left. I miss our little walks of 8 hours and 1000 meters slope in Les Calanques... I just wish we can share a lot more in the years to come, because it is so worth it to spend time with you.

Sonia, te he dejado para casi el final porque ya sabes lo que has significado para mí. Después del COVID, no exagero cuando digo que no tuve amigos hasta que te conocí y me sacaste de mi madriguera. Hemos compartido mucho y siempre te llevaré en el corazón. Gracias por hacerme un sitio en tu vida ♥

Jaehyeon, I know things didn't work out as we planned, but I wouldn't be here without you. The day I was diagnosed with depression was one of the hardest I have gone through. And you were there for me. We talked for hours. You supported me so much. I am sorry if I didn't do so. This thesis is also yours. Although you don't need it because you'll have yours very soon! I am sure you're gonna have a great future.

Marco, no m'oblido de tu. Gràcies per fer-me de guia. Gràcies per obrir-me els ulls moltes vegades i per ensenyar-me de què va tot això de la ciència. Que jo hagi arribat fins aquí en aquest món és gran part culpa teva. Espero que poguem continuar treballant molts anys junts. T'admiro molt i estic molt content que continuem ajudant-nos.

Als meus amics uesos. Què dir-vos? No gaire perquè segur que no us llegireu aquestes pàgines, molt menys la tesis. Moltes gràcies per fer que sempre senti que tinc un lloc on tornar. No s'em fa gens fàcil tenir-vos lluny, i menys ara que comenceu a reproduir-vos com conills, però sé que hi sou presents, i això m'ajuda a saber que si algún dia ho engego tot a la merda i torno a Girona, tornaré a casa. Us estimo.

Papa, què dir-te que no sàpigues. S'ha acabat la tortura. S'ha acabat la tesis. Ja no hauràs de passar temporades a pensar que m'estic enfonsant. Gràcies. Ara comença una nova etapa. Només que hauràs d'agafar un avió per venir a veure'm!!

Mama, bueno. Ay, mama... fa uns dies escoltàvem al Bruce cantar "Waiting on a sunny day", i sembla que ja arriben ☺ gràcies per cuidar-me. No seria qui soc si no haguèssis posat la teva vida a fer-me tirar endavant. Hem passat per molt. Però sembla que les coses marxen bé. I crec que ja ens ho mereixem que ens vagin bé. Espero aprofitar molt més de tu ara que et jubilaràs i que tu aprofitis que seré a San Francisco! Per fi anirem a veure jugar als Lakers!!!!

Et finalement, toi. Tu avais pensé que je t'avais oublié, n'est-ce pas ? Sarah, tu es mon soleil. Je vais t'écrire en catalan parce que je veux m'exprimer vraiment bien. No sé què passarà, no sé què ha de venir. No sé què será de nosaltres. Però t'estimo. Ha sigut tot una bogeria. Ha sigut dificilíssim. Ens han tocat les proves més difícils només començar la relació. I aquí estem, millor que mai diria jo. Encarant un futur junts. De moment als EEUU, després ja veurem a on. T'estimo Sarah, gràcies per portar la bogeria a la meva vida. Tinc moltes ganes de viure els pròxims anys amb tu, quan tot es calmi i de veritat poguem treure partit a la nostre relació. Quan puguem dedicar-nos simplement ha ser feliços i estimar-nos. Gràcies per ser un suport inquebrantable. Ets molt especial. I tinc sort de tenir-te al meu costat.

Thank you everyone who has shared this journey with me. I can finally say it's over, and it is all thanks to the people who surrounded me. Thank you.

TABLE OF CONTENTS

ABSTRACT 3
RESUME 4
ACKNOWLEDGEMENTS 5
TABLE OF CONTENTS 10
ABBREVIATIONS 12
INTRODUCTION 15
1. Alzheimer's disease 16
Historical context 16
Epidemiology 17
Symptoms 17
Etiology perspectives 18
Gene mutations 18
Epigenetic alterations 19
Transcriptomic changes 19
Protein aggregation 19
Synaptic dysfunction 20
Neuroinflammation 20
Lifestyle and environment 20
Neuropathology 21
Amyloid plaques 22
Amyloid hypothesis 23
Neurofibrillary tangles 24
Tau hypothesis 25
Interrelation between tau and Aβ 27
Synaptic degeneration 29
Neuroinflammation 30
2. APP 33
Gene family 33
Trafficking 35
Posttranslational modifications 36
Proteolytic processing 38
Nonamyloidogenic pathway 39
Amyloidogenic pathway 42
γ-secretase 45
APP toxic metabolites 49
APP β-CTF 49
Amyloid β 52
Alternative APP proteolytic pathways 55
MT1-MMP 58

3. MT5-MMP 61
Structure 61
Physiology 63
Pathological role in Alzheimer's disease 64
4. Peptide therapeutics 67
5. Induced pluripotent stem cells 68
Overview 68
Human *in vitro* brain models 68
Direct reprogramming 70
Drug testing 72
6. Generation and analysis of high dimensional data 74
High-content screening 74
Data analysis and machine learning 75
Bayesian statistics 77
OBJECTIVES *80*
RESULTS *82*
Artcile 1: Deficiency in MT5-MMP Supports Branching of Human iPSCs-Derived Neurons and Reduces Expression of GLAST/S100 in iPSCs-Derived Astrocytes. 83
Article 2: Mutations in specific domains of MT5-MMP prevent the accumulation of toxic APP metabolites and serve as templates for peptide-based therapeutics in human in vitro models of Alzheimer's disease 104
OTHER RESULTS *156*
DISCUSSION & PERSPECTIVES *162*
MT5-MMP regulates dendritic arborization 164
MT5-MMP deficiency alters astrocytic morphology and impairs the expression of astrocytic markers 166
Whole-domain modifications modulate MT5-MMP proamyloidogenic effects through changes in C99 trafficking 168
Changes in the MT5-MMP IC amino acid sequence preserve its capacity to modulate C99 trafficking and regulate Aβ production 171
Peptides mimicking the structure of variants of the MT5-MMP IC decrease C99 accumulation 174
REFERENCES *181*

ABBREVIATIONS

ACM	astrocyte-conditioned media
AD	Alzheimer's disease
ADAM	A Disintegrin And Metalloproteinase
AICD	amyloid precursor protein intracellular C-terminal domain
AMPAR	α-amino-3-hydroxy-5-metyl-4-isoxazolepropionic acid receptors
APH1	anterior pharynx defective-1
APOE	alipoprotein E
APP	amyloid precursor protein
APP^{d}	double copy of APP
APP_{fl}	APP full-length
BACE-1	β-site APP cleaving enzyme 1
BBB	blood-brain barrier
C1q	complement component 1q
C83	amyloid precursor protein α-C-terminal fragment
C99	amyloid precursor protein β-C-terminal fragment
CNS	central nervous system
CSF	cerebrospinal fluid
CTF	C-terminal fragment
DIV	days *in vitro*
ECM	extracellular matrix
EGF	epidermal growth factor
ER	endoplasmic reticulum
EXT	extracellular (domains)
fAD	familial Alzheimer disease
FDA	Food and Drug Administration

FTD	frontotemporal dementia
GPC4	glypican-4
GPI	glycosylphosphatidyl inositol
GSK3	glycogen synthase kinase 3
HCS	high-content screening
hESC	human embryonic stem cells
hiPSC	human induced pluripotent stem cells
hTREM2	human triggering receptor expressed on myeloid cells 2
HTS	high-throughput screening
IC	intracellular (domain)
IL	interleukin
iN	induced neurons
iPSC	induced pluripotent stem cells
LDLR	low-density lipoprotein receptor
LRP8	low-density lipoprotein receptor-related protein 8
LRP1	low-density lipoprotein receptor-related protein 1
LRP10	low-density lipoprotein receptor-related protein 10
LTD	long-term depression
LTP	long-term potentiation
MAM	mitochondria-associated endoplasmic reticulum membranes
MAPK	mitogen-activated protein kinase
MCI	mild cognitive impairment
MEA	multielectrode array
Mint	muncl8-interacting proteins
MMP	matrix metalloproteinase
MT	membrane-type
MT-MMP	membrane-type matrix metalloproteinase

MVB	multivesicular bodies
NCAM	neural cell adhesion molecules
NCSTN	nicastrin
NFT	neurofibrillary tangles
NGN2	neurogenin-2
NMDAR	N-methyl-D-aspartate receptor
NPC	neural progenitor cells
PEN2	presenilin enhancer 2
PKC	protein kinase C
PLA	proximity ligation assay
PS	presenilin (protein)
PSEN	presenilin (gene)
pTau	phosphorylated tau
PTB	phosphotyrosine binding
ROS	reactive oxygen species
sAD	spontaneous Alzheimer's disease
sAPP95	soluble amyloid precursor protein 95
Sez6	seizure protein 6
SORL1	sortilin-related receptor 1
TGN	trans-golgi network
TM	transmembrane (domain)
TNF	tumor necrosis factor
TREM2	triggering receptor expressed on myeloid cells 2
WT	wild type

INTRODUCTION

1. Alzheimer's disease

Historical context

In 1907, Alois Alzheimer described the presence of foreign bodies in the *postmortem* brain of a patient who died with severe cognitive impairment[1]. What he saw was what we later described as amyloid plaques and neurofibrillary tangles (NFT). These are the result of several years of accumulation and misfolding of amyloid beta (Aβ) and tau proteins and lead to neurotoxic events. The main hypotheses point toward these two pathological hallmarks as the strongest candidates to explain the development of Alzheimer's disease (AD)[2,3]. In recent years, other phenotypic abnormalities (neuroinflammation, vascular degeneration, synaptic dysfunction, etc.) have become increasingly important to explain the progression of AD, revealing the multifactorial character of the disease[4]. However, the accumulation of Aβ and its downstream consequences remain the most accepted candidate to explain the causality of AD.

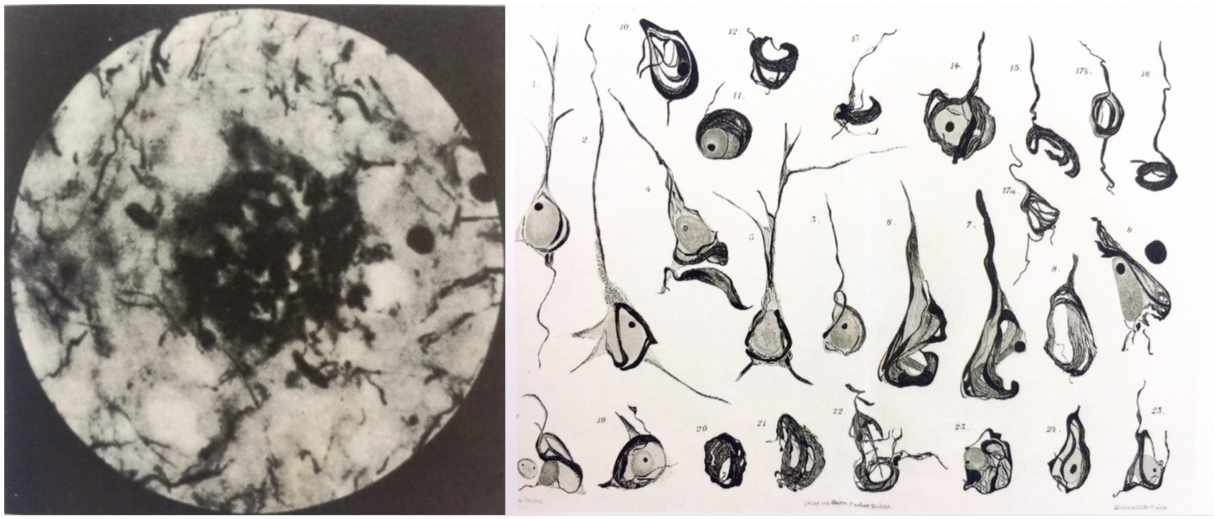

Figure 1. Original images of the plaques and the NFTs observed by Alois Alzheimer. On the left, there is a granular plaque of the brain of Auguste D., the patient from whom Alois Alzheimer did his first observations of the disease. On the right, there are the drawings that Alzheimer did after observing the NFTs present in the postmortem brain from Auguste D. Maurer K, Maurer U. Alois Alzheimer, 1864-1915: His Life and Work with Text and Photographs. 2002.

AD is a devastating neurodegenerative disorder characterized by progressive loss of cognitive function. Historically, memory lapses were the earliest clinical evidence of the disease[5]. Nowadays, more precise techniques allow for the detection of other clinical manifestations that can lead to an earlier correct diagnosis (blood and cerebrospinal fluid biomarkers, brain PET scans, genetic tests, etc.)[6]. Until recently, there was a lack of available treatments that could delay the disease, only certain treatments that could

improve specific symptoms. In 2021, 2023, and 2024, the Food and Drug Administration of the United States of America (FDA) approved three monoclonal antibodies directed against Aβ plaques after the clinical trials showed Aβ burden reduction and partial prevention of cognitive decline in patients in the early stages of AD. Nevertheless, there is still no treatment to halt or reverse the disease[7–9].

Epidemiology

Dementia is highly prevalent in more aged societies, typically associated with higher income countries, as age is the most important risk factor associated with AD[10]. The World Health Organization reported that by 2050, 2.1 billion people will be over 60 in low- and middle-income countries, and 426 million people will be over 80 years old. Thus, dementia is expected to triple by 2050, making it close to 140 million people suffering from dementia, a number similar to Mexico's or Russia's current populations[11].

AD represents approximately 60-70% of all diagnosed cases of dementia. Therefore, as the global population ages, AD is and will continue to be a major global health challenge. The associated costs of dementia represent US$1.3 trillion and are predicted to more than double by 2030[11]. Therefore, it is imperative to find a treatment that can effectively prevent or stop the development of AD.

Symptoms

Most AD cases are diagnosed after the age of 60 years, doubling its prevalence every five years[10]. This is mainly because the first detectable symptoms appear at the late stages of the pathology, when it is already well advanced.

Historically, AD clinical stages can be summarized into: 1) an early stage or preclinical phase, which is currently difficult to define due to lack of reliable markers to efficiently diagnose the disease; 2) mild cognitive impairment (MCI) phase, when the patient starts showing early symptoms of cognitive decline (the most important being memory loss); and 3) late-stage phase, where the patient shows severe cognitive impairments (*e.g.* extensive memory loss, speech problems, spatial disorientation, and apathy) and becomes completely dependent[12].

Recently, new diagnostic methodologies have been advancing the capabilities to diagnose AD at earlier stages, thus allowing for better detection, stratification, and treatment of patients[13]. However, the etiology of the disease is unclear, which limits the possibilities of intervention.

Etiology perspectives

As stated previously, AD is a multifactorial disease with no clear known causality. Age is the biggest risk factor for developing AD, similar to many other forms of dementia[14]. However, there is an extended heterogeneity of factors related to AD pathology.

Gene mutations

From a genetic perspective, several genes have been implicated in the onset of the disease. However, single genetic mutations account for approximately 1% of all AD cases, known as early-onset or familial AD (fAD). These mutations are related to the amyloid precursor protein (*APP*) gene or proteins involved in its processing, presenilin 1 (*PSEN1*) and presenilin 2 (*PSEN2*) (reviewed more in detail in the Amyloid hypothesis and the APP processing section). Since the first report of a missense mutation in the APP gene, more than 300 variants have been identified in *APP*, *PSEN1*, and *PSEN2*, which cause the onset of AD at younger ages[15,16]. Most of these mutations favor the amyloidogenic pathway, thus facilitating the production of Aβ and increasing the plaque burden, and are known to be sufficient to trigger AD[17].

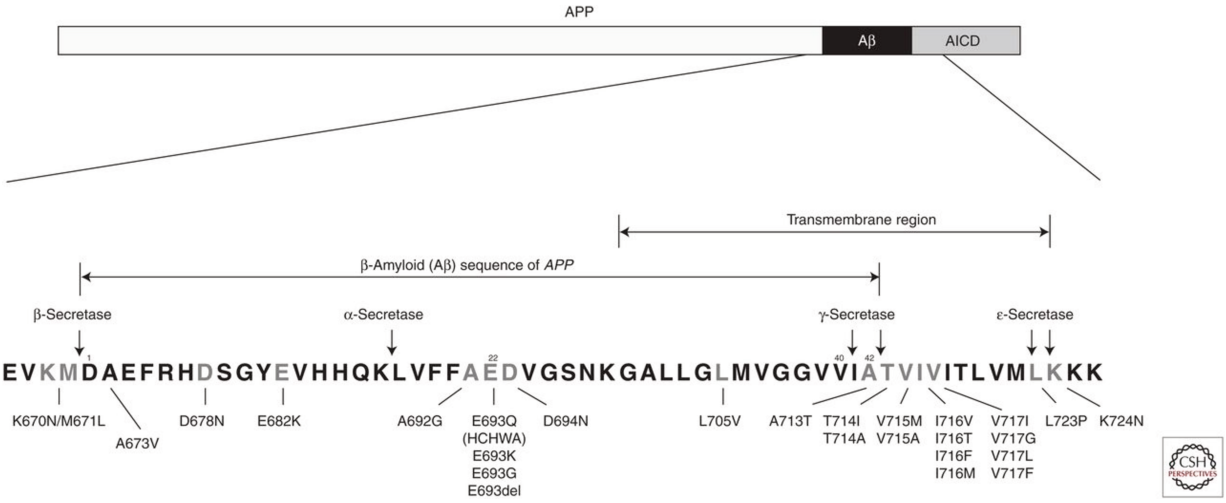

Figure 2. Genetic mutations in the APP gene associated to fAD. There exist several potential mutations in the APP gene that can increase amyloidogenesis. These mutations can affect the β-secretase cleaving site (bottom-left), the alpha-secretase site (bottom-center), or gamma-secretase (bottom-right). Mutations in α- or β-secretase cleaving sites reduce the affinity of α-secretase or increase the affinity of β-secretase. In the case of γ-secretase cleaving site, known mutations alter the ratios of Aβ42 and Aβ40, favoring the accumulation of Aβ42[17].

However, late-onset or sporadic AD (sAD), which accounts for 99% of AD cases, still lacks a clear causal factor that could explain the onset of the disease[18]. Several genetic mutations are considered major risk factors, with the most prominent being the alipoprotein E (*APOE*) allele variants; however, these mutations are insufficient to develop the pathology[19]. Thus, accumulating evidence points to different causal factors

as the driving forces of disease. In recent years, genes related to brain homeostasis, like intracellular trafficking (*SORL1*) or neuroinflammation (*TREM2*), have gained relevance in evaluating the risk of developing AD and as therapeutic targets[20,21].

Epigenetic alterations

Hypomethylation of the *APP* gene was reported in the brain of a patient with AD shortly after the discovery of the first *APP* mutation[22]. Further research has shown that several areas of the brain of AD patients have wide-spread changes in methylated and hydroxyl methylated regions, affecting several pathways involved in AD[23–25]. In general, different epigenetic modifications are observed in AD brains, although there is no clear understanding of whether these could be the cause or consequence of the preliminary stages of the disease[23].

Transcriptomic changes

With genetic and epigenetic changes, there is transcriptomic dysregulation in AD. Gene expression associated with glial homeostasis, synaptic transmission, calcium signaling, mitochondrial function, or ubiquitination, among others, is altered in *postmortem* brains from AD patients, even when compared with changes occurring during normal aging[26]. Specific transcriptional regulators drive these changes by altering the expression of specific sets of genes linked to pathological dysregulation of cellular processes[27].

Protein aggregation

One of the most prominent hallmarks of AD is protein aggregation. Whether it is Aβ, hyperphosphorylated tau, or others, it is still deemed the pivotal pathological event in AD. A lot of the ongoing AD clinical trials and the most advanced drugs approved by the FDA tackle protein aggregation, although the efficacy of these drugs is still insufficient to stop AD development[28]. However, the most consensual hypothesis of the etiology of AD is still the amyloid hypothesis (discussed in *Amyloid hypothesis*), which states that the accumulation of Aβ and the formation of senile plaques in the brain parenchyma trigger a series of downstream events that result in severe neurotoxicity, synaptic dysfunction, neuroinflammation, cognitive decline, and ultimately death[29]. Another important protein investigated in AD is tau, which also accumulates in different forms, triggering the formation of NFTs, originally observed by Alois Alzheimer, and perturbing cell trafficking[30]. Recent studies have also shown that other peptides upstream of Aβ appear

to correlate better with neurotoxicity and that different forms of Aβ may have distinct roles in fibril formation[31,32].

Synaptic dysfunction

Several transcriptional and proteomic changes are associated with the malfunction of synaptic vesicles and the overall decay of synaptic density[33]. The neurotransmitter hypothesis has been a driving force in AD for several years[34]. Although seemingly outdated, new evidence exists regarding the implications of synaptic dysregulation in the early stages of the disease[35,36]. In addition to the cholinergic and glutamatergic theories, recent studies have shown that GABAergic signaling is altered in AD[37]. Overall, synaptic deficits lead to imbalanced synaptic signaling, which causes network asynchrony and further changes in gamma oscillations[35,38]. Selective gamma stimulation modulates synaptic abnormalities and has a positive impact on several pathological processes of AD, demonstrating that synaptic changes may play a key role in AD onset and progression[39,40]. In line with findings in AD-related gene mutations associated with glial cells, reactive microglia and astrocytes also induce synapse loss in mouse models of neuronal degeneration, further disrupting normal synaptic function[41–43].

Neuroinflammation

Glial cells are indeed a main actor in AD; however, it is unclear whether their role is in the initial stages or whether it is a consequence of overall dysregulation of brain homeostasis[44]. Genes involved in neuroinflammatory pathways are rapidly dysregulated through the progression of AD–in fact, the major risk factor for developing sAD, apart from age, is APOE4[45]. Several other markers (*e.g. TREM2*) are also altered and are increasingly gaining importance to explain AD pathophysiology, most of which are implicated in the activity of glial cells, mostly astrocytes and microglia[46–48]. Neuroinflammation leads to disruption of the blood-brain barrier (BBB), allowing the entry of peripheral immune cells into the central nervous system (CNS), which increases the neuroinflammatory response and generates a feedback loop that leads to immune overactivation and worsens AD pathology[49].

Lifestyle and environment

It remains a matter of discussion whether patients with AD are genetically predisposed to exacerbated neuroinflammation or whether it depends on environmental factors, or a combination of both. For example, nanoscale particle matter induces microglial and

astrocyte activation through the upregulation of neuroinflammatory signaling pathways[50]. In fact, air pollution is correlated with an increased incidence of pathological processes related to dementia, Alzheimer's disease, and other neurodegenerative pathologies[51–53]. In addition, exposure to metals is a potential initiator of AD through interactions of different metals with Aβ in excitatory synapses[54]. In the 1990s, iron, copper, and zinc were observed in senile plaques of AD patients and were related to increased Aβ aggregation[55,56].

Exposure to harmful compounds that increase AD burden or can trigger the disease can also come from other sources (*i.e.* smoking), or other lifestyle habits (*i.e.* junk food consumption)[57,58]. Certain professions or sports involve activities that also increase the risk of developing dementia through chronic traumatic brain injury, which triggers certain pathological pathways related to AD[59,60]. But, in general, controlled physical activity has a positive impact on the prevention of dementia or cognitive decline in early dementia patients, including AD[61]. Finally, several other factors and diseases can facilitate or worsen AD symptomatology, such as sleep perturbations, obesity, education level, and hypertension[62–65].

Neuropathology

Despite the evidence presented above, the cause of AD remains unclear. During 2023, PubMed hosted around 17.000 published articles related to AD, an increasing number compared to 1993 ~2.700 articles; this is because AD has become a major public health issue. However, despite uncertainties, the pathological hallmarks of AD have been well studied.

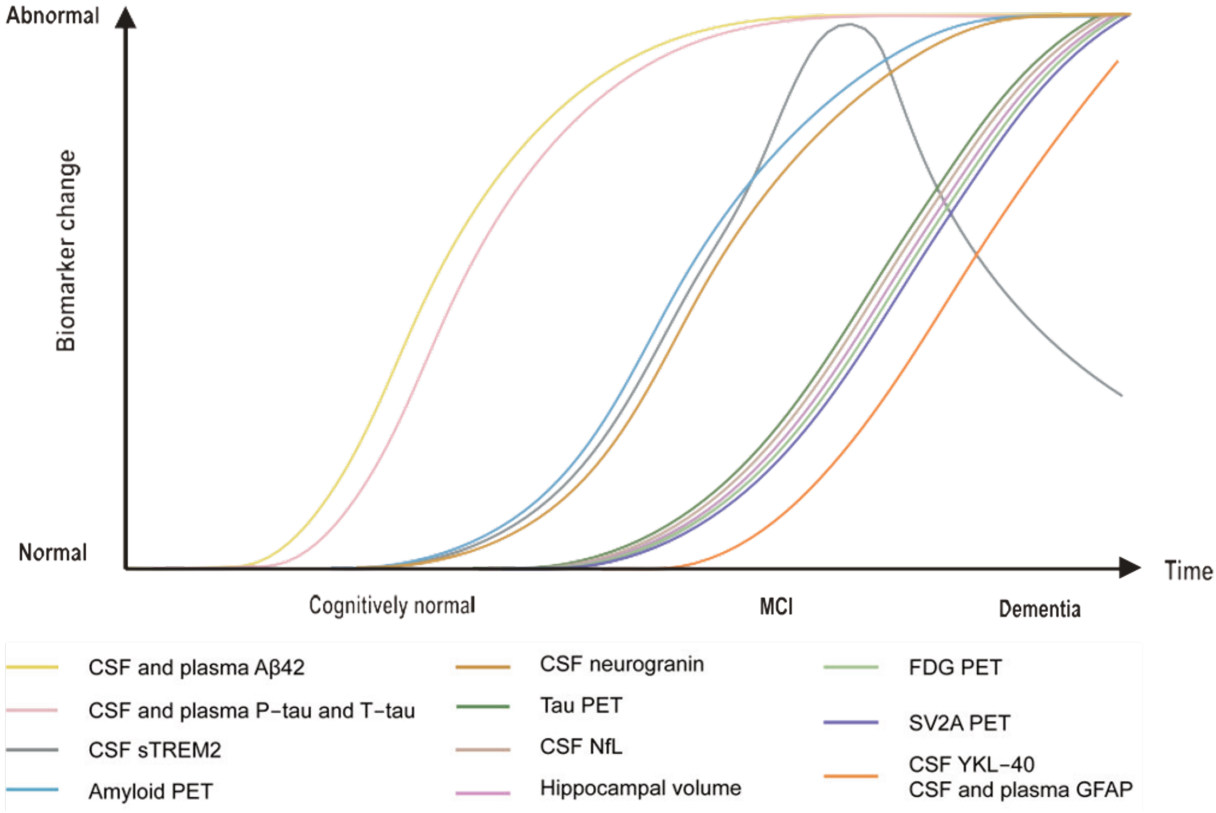

Figure 3. Model of the temporal evolution of different biomarkers along AD. The ratio of Ab42/Ab40 in CSF is the first detectable biomarker that appears early in the disease. CSF and plasma tau are detectable, probably due to the onset of neuron death. Amyloid burden can be detected with PET at the interface between cognitively normal and MCI, and microglial secreted soluble TREM2 is present in the CSF, a sign of neuroinflammation. Simultaneously, synaptic dysfunction can be detected with the appearance of neurogranin in CSF. Then, tau PET becomes positive and other markers of synaptic dysfunction and overall degeneration are detectable. Finally, astrocytic markers (CSF TKL-40 and CSF and plasma GFAP) can be detected at the late stages of the disease, already at the interface between MCI and dementia[66].

Amyloid plaques

Amyloid accumulation and deposition are particularly important in AD, although they also occur in normal aging and other neurodegenerative diseases[67]. In both forms of the disease, fAD and sAD, there is an early accumulation of Aβ in the form of extracellular plaques[29]. The Aβ peptide is heterogeneous and can have varied sizes (37-49 amino acids) depending on the γ-secretase cleaving site, although the most common forms are: a more soluble form of 40 amino acids (Aβ40) and a more hydrophobic and neurotoxic form of 42 amino acids (Aβ42)[68]. Although both forms coexist in amyloid plaques, Aβ42 is more abundant because of its higher rate of fibrillization and insolubility[69].

There are conflicting results regarding the use of Aβ40 as a biomarker, although some studies have shown specific variations in the cerebrospinal fluid (CSF) of patients with AD and correlation with other AD biomarkers[70]. In contrast, Aβ42 is a mediocre predictor

of AD because its levels are inconsistent among different patients and are insufficient to effectively separate AD from other dementias[71]. However, the Aβ42/Aβ40 ratio in CSF and plasma is a good indicator of Aβ deposition in the preliminary stages and is specific for AD[72–74].

Amyloid hypothesis

Evidence indicating a direct relationship between Aβ accumulation and AD symptoms finally crystallized into the amyloid hypothesis. It is the most accepted hypothesis for the etiology of AD and has been the focus of AD research throughout the last decades[2]. The original amyloid hypothesis states that the accumulation of Aβ in the form of plaques in the brain parenchyma causes AD, which triggers a pathological cascade that evolves into NFT generation, cytotoxicity, vascular damage, dementia, and finally death[29].

The Aβ fragment originates through the amyloid pathway: the sequential cleavage of APP by β-secretase and then γ-secretase. First, β-secretase cleaves APP at the β-cleaving site (amino acids 671-672 of the APP_{770}), producing a C-terminal fragment (CTF) of 99 amino acids known as β-CTF or C99. Then, an additional γ-secretase cleavage of C99—occurring between positions 687 and 691 of APP_{770}—generates the N-terminal fragment Aβ[75]. All the genetic mutations identified to be sufficient to provoke fAD are involved in this pathway, either in the *APP* gene or in components of the γ-secretase complex[76]. The only protective mutation against AD is also in the *APP* gene, the Icelandic mutation (A673T), which hinders β-secretase cleavage and protects against developing AD[77]. In addition, mutations in several other proteins involved in Aβ clearance and APP metabolism in different cell types are risk factors for the development of sAD[78]. Overall, these data reinforce the importance of the amyloid pathway in AD etiology.

Despite the evidence supporting the importance of the amyloid pathway in AD, several failed clinical trials targeting Aβ and studies reporting high Aβ load in cognitively normal older adults have spread doubts among the research community on the validity of the amyloid hypothesis[79]. However, the recent approval by the FDA of two drugs targeting Aβ in AD and recent studies showing a correlation between faster cognitive decline and Aβ burden in cognitively normal elders have revived the interest around the amyloid hypothesis[8,80–82] (more detailed information about Aβ pathological mechanisms in the *APP chapter*).

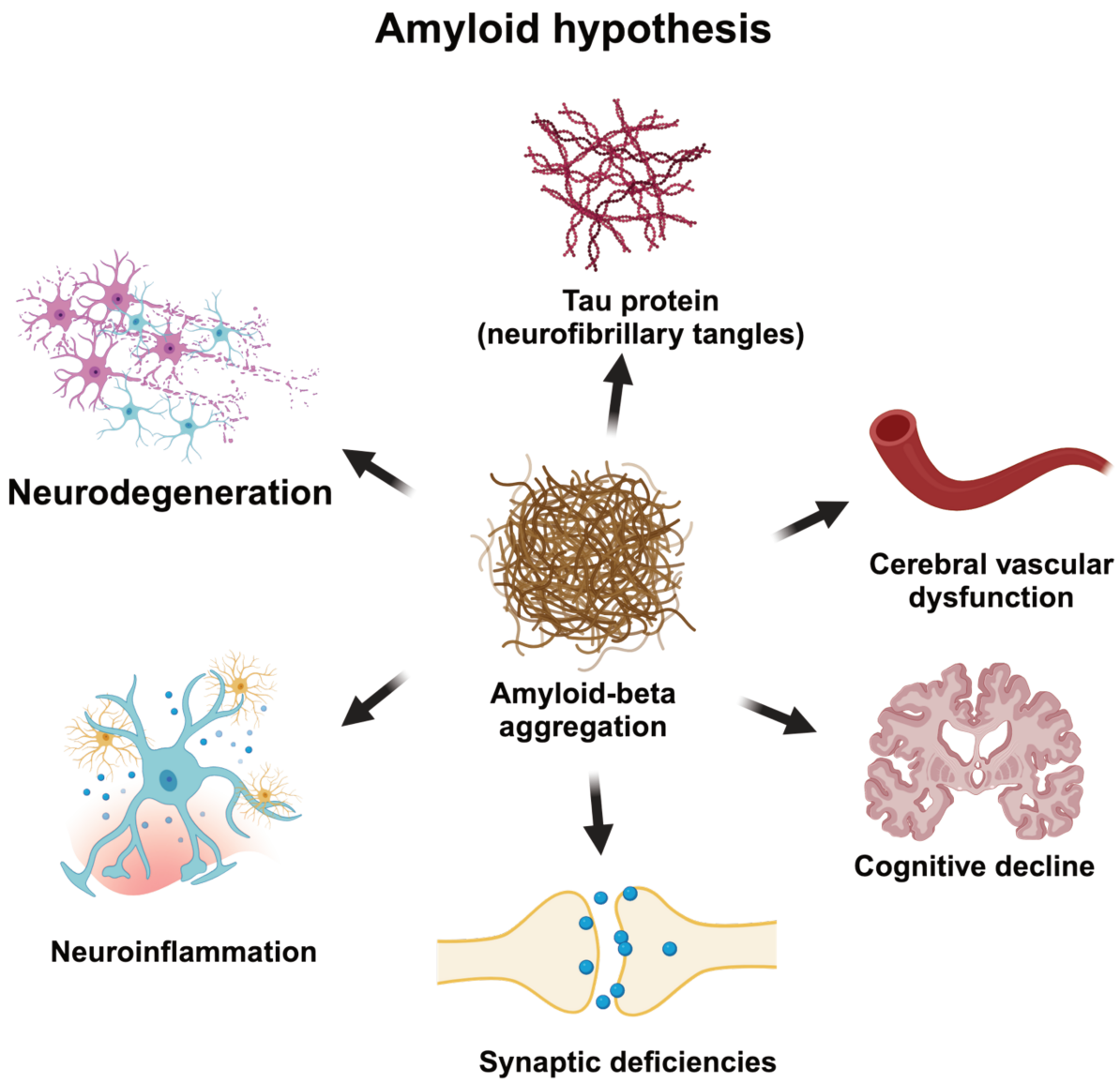

Figure 4. Graphic representation of the amyloid hypothesis. Hardy and Higgins first defined this hypothesis in 1992 with the light of the discovery of autosomal dominant mutations in APP sufficient to trigger disease onset and the definition of the amyloidogenic processing of APP that produces Aβ. Abnormal Aβ accumulation leads to its oligomerization and later aggregation in the brain parenchyma in the form of amyloid plaques. These aggregates appear in distinct areas of the brain during disease, and they trigger a series of downstream pathogenic events that decrease cognitive performance. Despite multiple advances suggesting other important factors in AD pathogenesis, the amyloid hypothesis remains one of the central theories for understanding AD onset and progression.

Neurofibrillary tangles

Together with amyloid plaques, NFTs represent a major hallmark of AD. These are abnormal aggregates primarily composed of hyperphosphorylated tau[83]. Tau is a highly dynamic soluble protein with six isoforms in the human CNS[84]. Under normal conditions, tau is a microtubule-associated protein that promotes microtubule assembly[85]. In the brain, it is a key factor in the stability of axonal microtubules—making it of pivotal importance for axonal transport[86,87]. Posttranslational modifications, particularly

phosphorylation, are essential for the regulation of tau binding to microtubules[88]. However, dysregulation of tau phosphorylation can lead to hyperphosphorylation, which drives tau aggregation into detergent-insoluble NFTs[89]. Abnormalities in tau and the generation of NFTs are important in several neurodegenerative diseases, collectively known as tauopathies[90].

The distribution of tau in neurons is heterogeneous: there is a soma-to-axonal tau gradient and a small presence in the dendrites, which suggests a potential role of tau in efficient cargo transport toward synapses[86,91]. Defects in tau posttranslational modifications trigger the destabilization of neuronal microtubules that, with the formation of NFTs, lead to disturbed cell trafficking[92]. Accordingly, the abnormal aggregation of tau in the axonal compartments and its loss of polarization severely disrupt the transport of organelles into synaptic vicinities[93,94]. Altogether, the pathological events triggered by toxic tau forms result in synaptic deficits and cognitive impairments[95,96].

Tau hypothesis

Although Aβ is detected earlier in the CSF than tau, the formation and spread of tau aggregates correlates better with the onset of AD clinical symptoms than Aβ deposition, and some studies have suggested that tau accumulation precedes Aβ pathology[97–100]. This could be because of the nature of the pathological features of both factors, as Aβ is secreted in the extracellular space—having easier access to the CSF—whereas tau is only liberated extracellularly after neuronal death[98,101]. However, CSF and plasma phosphorylated tau 181 and 217 are trustworthy biomarkers for AD diagnosis, the latter being the best biomarker to differentiate AD from other FTD-related pathologies[102,103]. And recent advances in this direction demonstrate that plasma phosphorylated tau 217 correctly predicts AD at pre-clinical stages and correlates with AD pathological hallmarks[104]. Moreover, individuals with Aβ plaques but without NFTs are cognitively normal, and transgenic mice models of amyloidosis lack NFTs and tau-related pathological events[105–108]. In fact, Aβ fails to trigger Aβ-induced tau pathology in the absence of previous tau abnormalities, suggesting a pathological feedback between Aβ and tau pathologies that potentially drive AD[109]. Elucidating the spatiotemporal sequence of this crosstalk is a priority in AD.

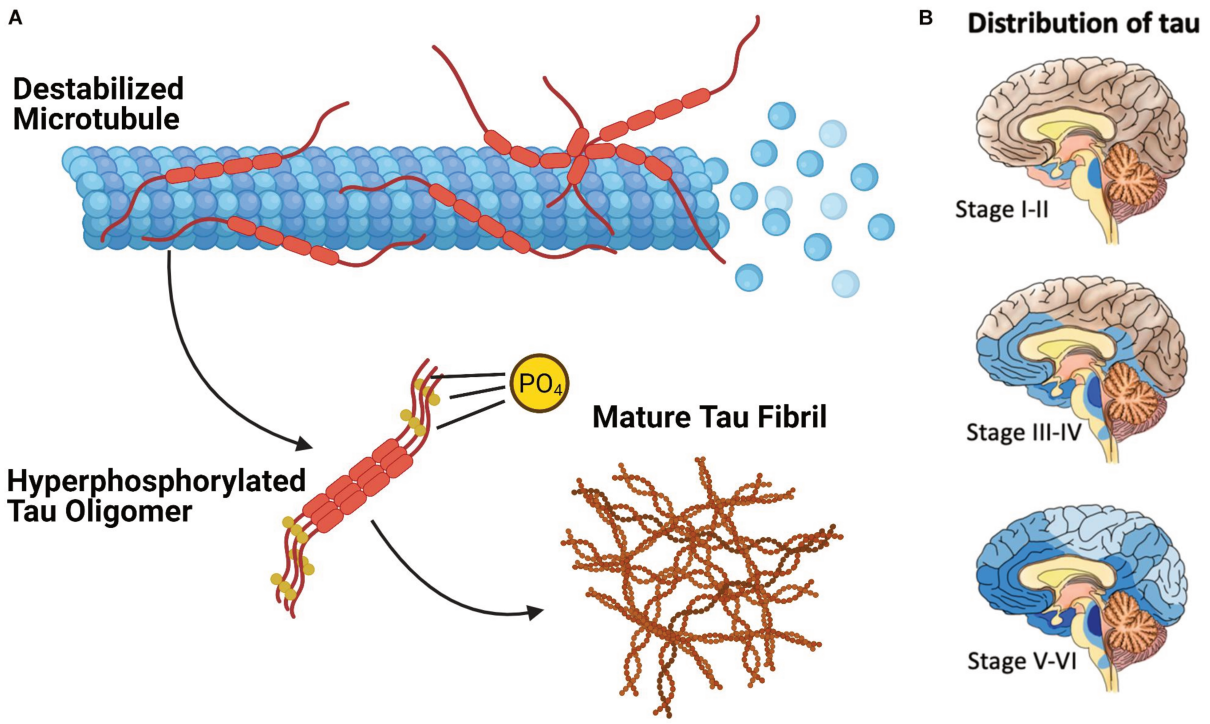

Figure 5. Tau pathology and its progression in the brains of patients with AD. (A) Early tau defects lead to microtubule destabilization and disturbed cell trafficking. Hyperphosphorylated tau aggregates in the form of oligomers that then form NFTs. (B) Braak model of tau pathology progression. Darker blue colors denote increased maturity of tau fibrils. Early tau pathology (stages I-II) starts in the subcortical nuclei and progresses through the transentorhinal region into the entorhinal region, affecting pyramidal cells. In stages III-IV, the pathology approaches the neocortex and various regions of the hippocampi. Meanwhile, areas where tau pathology is abundantly present, continue to worsen their condition. In the late stages (V-VI), tau pathology completely invades the neocortex, affecting the temporal, parietal, and frontal lobes and eventually reaching the striate area. At this stage, neuronal death can be observed in the long-term affected areas[110,111].

Tau pathology primarily affects glutamatergic neurons in the cerebral cortex[112]. Phosphorylated tau (pTau) accumulates earlier in the distal dendrites of the entorhinal cortex in both nonhuman primate models and humans, and its hyperphosphorylation increases with age[113,114]. In dendrites, tau hyperphosphorylation induces tau detachment from microtubules[115]; this leads to tau aggregation on microtubules and the calcium-storing smooth endoplasmic reticulum (ER) close to glutamate synapses, which impedes normal calcium homeostasis[113]. Accordingly, neurons with high calcium levels are the most vulnerable and earliest affected populations of tau pathology, and the expression of calcium regulators is correlated with the progression of pyramidal cell tau pathology[116,117]. These cells are more prone to develop tau pathology after receiving pTau seedings from other cells, which could explain the following: 1) the pattern seen in sAD with an early affection of cortical networks and 2) how cortical glutamate synapses can be the origin of tau pathology and its expansion[114,116,118].

Calcium dysregulation is present in the brains of patients with sAD and fAD[119,120]. Genetic mutations generally associated with the Aβ hypothesis (*i.e.,* in *PSEN1*/*PSEN2*) also impede normal calcium homeostasis from the ER[121,122]. Human *in vitro* models of fAD show aberrant calcium waves and increased neuronal activity[123,124]. And in a mouse model with APP and PSEN1 mutations, the emptying of presynaptic calcium storages normalized neuronal activity[125]. This could offer an alternative explanation for the aggressive form of AD in individuals with these mutations.

Interrelation between tau and Aβ

Intraneuronal calcium levels modulate neurotransmitter release, and changes in calcium homeostasis can lead to aberrant neuronal signaling. Neuronal hyperexcitability and impaired calcium waves correlate with elevated Aβ levels[126]. In mouse models of Aβ pathology, Aβ induces hyperexcitability by inhibiting glutamate uptake in active neurons[127]. Downstream signaling of aberrant calcium levels can alter the activity of protein kinases, which can mediate tau posttranslational modifications[128]. At the same time, hyperactive neurons increase tau secretion, which favors tau seeding in adjacent areas and in distal regions through transsynaptic seeding[129,130].

Accordingly, the spread of amyloid pathology is closely linked to tau. Although less organized, the distribution of Aβ plaque accumulation follows the axon terminals of projecting cells already affected by tau alterations[98]. Tau and Aβ may be involved in a feedback loop through the impairment of cell trafficking. The dismantling of microtubules induced by tau pathology perturbs normal cell trafficking and impedes the normal transport of organelles[93]. In the case of APP, β-secretase cleavage occurs in membrane structures inside the cell (mostly endosomes), and hyperphosphorylated tau aggregates block the normal trafficking of APP-containing endosomes on microtubules[113,131,132]. This potentially prolongs the coexistence of APP and β-secretase, thus increasing the rate of β-secretase cleavage of APP and favoring the generation of Aβ. Similarly, in AD mouse models, the expression of APOE4 in AD-free mice also alters the characteristics of early endosomes, indicating that endosomal defects may be characteristic of AD-associated pathological events[133].

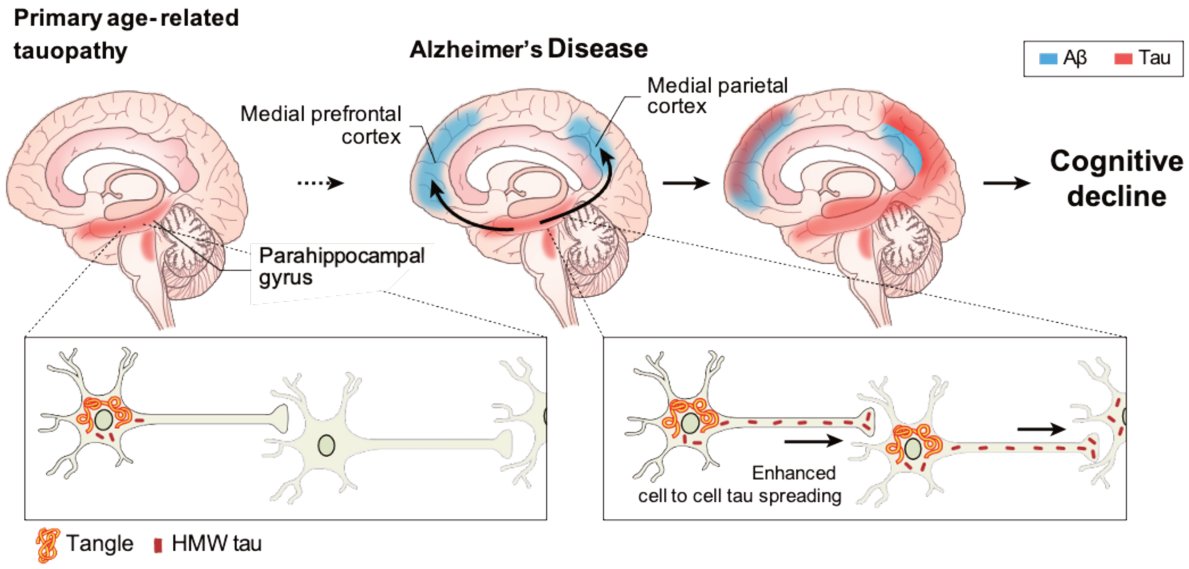

Figure 6. Graphical representation of the correlated spread of tau and Aβ pathology. From left to right, on the top, there is the evolution of tau pathology in correlation with Aβ accumulation in AD. During preliminary stages, there is an accumulation of NFTs in neurons of the subcortical areas that project towards cortical areas. In early stages of the disease, Aβ pathology starts to appear close to the axonal terminals of tau-affected neurons in the medial prefrontal and parietal cortex. Finally, Aβ and tau pathology are widespread around the cortex following a transsynaptic seeding pattern. In the bottom panels, there is a schematic representation of transsynaptic tau seeding. NFTs (tangles) and hyperphosphorylated high-molecular weight tau (HMW) start forming in vulnerable neurons. When the neurons have high levels of aberrant tau and tau aggregates, they can spread through synapses in connected neurons[134].

Different forms of Aβ can promote tau aggregation, and structure-based inhibitors of an Aβ core segment interfere in both Aβ-induced tau aggregation and tau self-seeding[135–137]. In fact, tau becomes more resistant to proteolysis in the presence of Aβ, possibly after Aβ-induced physical modifications[138]. In mouse models and *postmortem* brains of AD patients, different species of Aβ colocalize with pTau, including in synapses[139,140]. Moreover, in mouse models, both Aβ and tau target synapses, and truncating or knocking out tau protects synapses from Aβ-mediated toxicity in the postsynapse[141]. However, only a minimal percentage of human synapses (<0.02%) showed colocalization of tau and Aβ, compared to 10% Aβ positive and 0.32% tau positive human postsynaptic spines[142]. Altogether, the evidence supports the notion of an interplay between tau and Aβ beyond direct interactions.

Synaptic degeneration

Synaptic degeneration is an important hallmark of AD and is closely related to protein aggregation. Glutamatergic synapse impairment is an early trait of AD, although the exact pathogenic mechanisms are unclear. The synaptic distribution of APP toxic metabolites is particularly significant in glutamatergic synapses at early stages and is heterogeneously distributed among different compartments. C99 accumulates earlier in presynaptic buttons, and both C99 and Aβ can be located at the pre- and postsynapses along the disease[143]. Indeed, transgenic models of AD overexpressing APP_{swe} develop altered synaptic activity and deficits in long-term potentiation (LTP) before plaque formation, suggesting that β-secretase APP fragments alter normal synaptic function[36,144]. Different Aβ peptides activate N-type voltage-gated calcium channels and induce calcium overload, which correlates with neuronal hyperactivity in the early stages of AD[145]. Acute exposure to soluble Aβ oligomers also increases neuronal calcium levels *in vivo* through N-methyl-D-aspartate receptor (NMDAR)-mediated calcium influx, triggering a decrease in spine density[146]. In mouse models, dendrites near Aβ plaques show hyperactivity and calcium dysregulation, leading to the accumulation of vesicles in hippocampal presynapses[147,148].

Contrary to its rapid effect on LTP, spine density loss requires repeated exposure to Aβ for multiple days[149]. Interestingly, Aβ-induced synaptic deficits are closely related to long-term depression (LTD) caused by NMDAR overactivation via excessive glutamate release[150]. Nevertheless, NMDAR-mediated synaptic depression has been indirectly linked to hippocampal spine loss[151]. Aβ-induced LTD drives tau hyperphosphorylation, which is present in postsynaptic compartments and is necessary for LTD induction[150,152]. Aβ oligomers promote glycogen synthase kinase 3 (GSK3) activity, which is a major kinase involved in tau phosphorylation[153]. Accordingly, GSK3 activity is equivalent to that of Aβ, promoting NMDAR-mediated LTD, and GSK3 inhibitors reduce Aβ-mediated neurotoxicity[153,154]. Altogether, evidence suggests a series of sequential events involving Aβ-induced LTD through NMDAR overactivation that overstimulates GSK3 at the postsynaptic compartments, leading to tau hyperphosphorylation and hippocampal spine loss in mouse models[155].

Endocytosis deficits are characteristic of AD. Endocytosis-related proteins are upregulated and accumulate in dysmorphic endosomes in the early stages of AD[156]. Early

endosome dysfunction is Aβ-independent and correlates with APP and C99 accumulation in an AD-related Down syndrome model[157]. Overexpression of APP or C99 increases Aβ-mediated internalization of α-amino-3-hydroxy-5-metyl-4-isoxazolepropionic acid receptors (AMPAR) in hippocampal slices[158,159]. Moreover, the expression of AMPAR at the cell surface decreases in rat primary neurons treated with Aβ, accompanied by an increase in AMPAR ubiquitination and overall decreased AMPAR levels, as observed in brain lysates of AD patients[160]. Furthermore, the relationship between Aβ and AMPAR is bidirectional because recent studies have shown that AMPAR inhibition halts the β-secretase cleavage of APP and reduces C99 hippocampal levels, maintaining full-length APP (APP_{fl})[161]. Taken together, these results show that APP processing is closely related to synaptic activity and synapse homeostasis, and that toxic APP species can alter synapse composition and function, suggesting the possibility of synaptic Aβ receptors. A recent study proposed Sigma-2, a synaptic receptor, as a potential Aβ synaptic binding partner in human and mouse brains[162].

With changes in glutamatergic transmission, GABAergic interneurons adopt compensatory mechanisms to counteract hyperactivity. An increase in inhibitory sprouting in the dentate gyrus of AD mice models was partially associated with an increased presence of somatostatin-positive (SST^+) fibers[163]. In fact, subsets of SST^+ interneurons are particularly vulnerable in AD, and their loss correlates with cognitive decline[164]. Moreover, $LAMP5^+$ interneurons are associated with increased cognitive resilience in AD patients, and in mouse models of Aβ accumulation and tau pathology, they are essential for normal network synchrony and cognitive performance[164,165]. In addition, stimulation of fast-spiking interneurons to produce gamma oscillations reduces Aβ load in AD mice through stimulation of glymphatic clearance, affecting both peptide secretory interneurons and regulating glial function[40,166].

Neuroinflammation

Synaptic degeneration and protein aggregation can trigger neuroinflammation. In AD, neuroinflammation is gaining importance and is considered a key component of the disease; however, it is unclear whether it is an accelerator and/or a cause of AD. Mutations in genes involved in the neuroinflammatory response, including APOE4 and TREM2, are present in patients with sAD—APOE4 being the biggest genetic risk factor for developing the disease[167–169].

Microglia are the major resident immune cells of the CNS[170]. Under normal conditions, microglia regulate multiple processes to preserve brain homeostasis; however, with chronic inflammation, microglia can adopt a neurotoxic profile[171–174]. In AD, microglia accumulate around Aβ plaques and promote plaque clearing[175]. Overexposure of microglia to Aβ triggers a proinflammatory signature, which shifts microglia into a deleterious profile[41,176–178]. In turn, microgliosis exacerbates neurodegeneration in tau mouse models of AD and appears before the formation of neurofibrillary tangles[47,179]. Altogether, these studies indicate that both Aβ and tau pathology lead to an overactivation of microglia and promote the different types of neuroinflammatory responses, with a population of activated microglia that correlated to amyloid pathology and another population linked to tau pathology[180].

Astrocytes are the primary partners of microglia in controlling brain homeostasis. Moreover, reactive microglia trigger astrocytes into neurotoxic profiles through cytokine signaling cascades[43]. The crosstalk between microglia and astrocytes through the APOE-TREM2 axis is one of the major actors in the astrocytic and microglial responses to neurodegenerative diseases[181,182]. As stated above, APOE4 is the biggest genetic risk factor for developing AD, and its presence correlates with an increased and chronic neurotoxic inflammatory response compared with other APOE isoforms or APOE conditional knockout[46,167,169,183]. Concordantly, the specific targeting of APOE4 codeposited with Aβ in 5xFAD mice decreases cerebrovascular dysfunction and rescues the proinflammatory profiles of microglia and astrocytes[184]. In addition, the conditional knockdown of APOE3 and APOE4 in astrocytes in an AD mouse model reduces Aβ plaque load and decreases the proinflammatory profile in astrocytes and microglia distant from Aβ plaques[185]. APOE4-carrying neurotoxic astrocytes express high levels of glypican-4 (GPC4), which drives tau hyperphosphorylation and propagation. Compared with other APOE isoforms, GPC4 primarily interacts with APOE4, and the absence of GPC4 reduces APOE4-dependent tau hyperphosphorylation[186]. Generally, APOE4 expression leads to a disturbed astrocyte-mediated tau homeostasis, disturbing tau processing, which could increase the extracellular accumulation of pathogenic tau[187].

Intercellular communication between microglia and astrocytes is essential for brain homeostasis, but this crosstalk promotes neurotoxic behaviors in the context of AD. A major form of paracrine signaling between both cell types are extracellular vesicles. In a mouse model of tau propagation, inhibition of exosome secretion by microglia impeded

tau pathology[188]. In addition, microglia from AD mouse models grafted into wild-type (WT) mice were capable of spreading Aβ pathology in unaffected areas[189]. And primary rat astrocytes increased the secretion of cytokines upon receiving extracellular vesicles from ATP-activated microglia[190]. In fact, microglia signaling of interleukin 1α (IL-1α), tumor necrosis factor α (TNF-α), and complement component 1q (C1q) induces a reactive neurotoxic phenotype in astrocytes[43]. Conversely, diminishing astrocyte activation in a mouse model of AD promoted microglial accumulation around Aβ plaques, increasing the amyloid load, and suggesting that astrocytic activation within homeostatic limits is beneficial against neurotoxic insults[191]. Nevertheless, chronic exposure to Aβ hyperactivates astrocytes, which release increased levels of complement C3. In turn, chronic exposure to complement C3 impairs microglial phagocytosis, and blocking complement C3 signaling in *APP* transgenic mice diminishes amyloid pathology and microgliosis[192]. Furthermore, inflammatory effects of the interrelation between microglia and astrocytes influences also the peripheral immune system. In systemic inflammation, microglia target the astrocytic endfeet and disrupt the BBB, facilitating the infiltration of peripheral immune cells in response to neuroinflammatory cues[193,194]. In summary, AD-related pathogenic processes increase the neuroinflammatory profile of glial cells, which triggers a series of events that induce positive inflammatory feedback, leading to neurotoxicity.

2. APP

Gene family

APP is a type I single-pass transmembrane glycoprotein encoded by a gene on chromosome 21q21[195]. It is part of an evolutionarily well-preserved superfamily of genes that include APP-like proteins 1 and 2 (APLP1 and APLP2). Although having similar domains, APP is the only member of the family to have the Aβ sequence. The functions of the three homologs are redundant but poorly described. There is evidence suggesting that they can regulate synaptic function, neuronal morphology, spine density, and cognitive performance[196,197]. Accordingly, triple conditional knockout in mice leads to reduced dendritic length and spine density, synaptic dysfunctions (with impaired LTP and reduced basal activity), and cognitive impairments[198]. In addition, double knockout of APLP2 and APP is lethal in mice[199]. However, triple knockout of APLP1, APLP2 and APP has no effects in human neurons[200].

There are three major APP isoforms of different lengths: APP_{695}, APP_{751}, and APP_{770}. In normal conditions, APP_{695} is the most expressed form in the brain: 10 times more expressed than APP_{751} and 20 times more expressed than APP_{770}, although APP_{751} and APP_{770} expression is increased in some areas of AD brains[201]. Mostly, APP is composed of a large extracellular domain divided in two ectodomains (E1 and E2) that are separated by a Kunitz protease inhibitor domain (absent in APP_{695}). E1 contains a heparin-binding/growth-factor-like domain, a copper-binding domain, and a zinc-binding domain. E2 has another heparin-binding/growth-factor-like domain and a random coil[202]. Then, it follows a transmembrane domain that contains the Aβ sequence (only in APP) and a cytoplasmic tail that finishes with a phosphotyrosine binding (PTB) YENPTY motif[202,203].

APP ectodomains are essential for homo- or heterotypic dimerization, which can be modulated by heparin binding, and *cis* dimerization is reinforced by a GXXXG motif in the transmembrane region[204,205]. In addition, APP transsynaptic dimerization through their ectodomains works as a synaptic adhesion molecule, and the mutation of the secretase-cleaving sites increases synaptogenesis[206,207]. In fact, the copper-binding sites present in the ectodomains are required for the APP induction of hemisynapses[206]. The cleavage of APP releases its ectodomains, known as secreted APP or sAPP, which constitute 50% of the total APP in the brain[208]. Although similar in size, the fragments

generated by α- and β-secretase have strikingly different structures, explaining their different physiological functions[209]. Indeed, APP metabolites can act as APP ligands, and for example sAPPα induces neuroprotection through G-receptor activation by binding to cell surface APP[210].

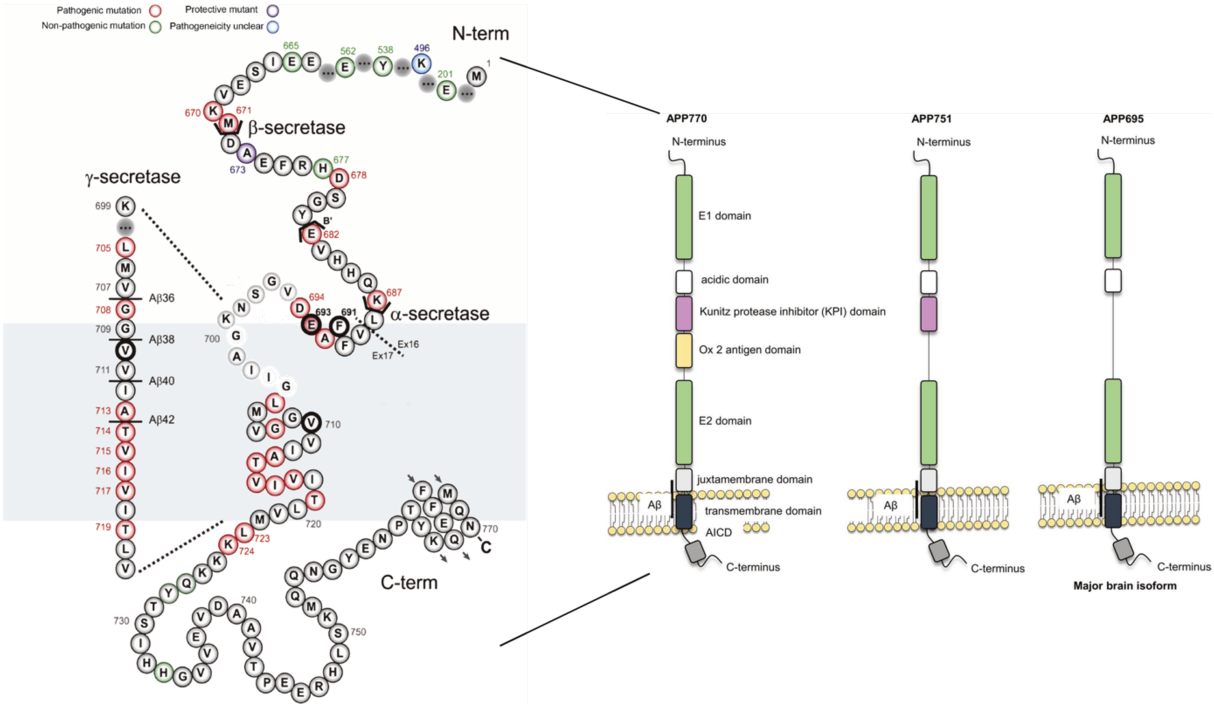

Figure 7. Potential mutation and cleaving sites of APP$_{770}$ and structures of the different isoforms. Several mutations can occur along APP. They can be divided into pathogenic, non-pathogenic, protective, or mutations with unclear pathogenicity. In the extracellular region of APP$_{770}$, there is a b-secretase cleaving site between M671 and D672. Therefore, C99 corresponds to D672 to N770 in APP$_{770}$. Alternative β-cleavage (the β'-site) occurs between Y681 and E682 in APP$_{770}$. The α-secretase cleavage site is close to the transmembrane domain, between K687 and L688 in APP$_{770}$. In the transmembrane domain, there are a series of γ-cleavage sites through which the γ-secretase complex can cleave. As a reminder, γ-secretase cleaves in a sequential manner, usually generating peptides corresponding to Aβ49 or Aβ48, which consecutively cleaves until generating shorter and more common forms of Aβ—which are represented in the image. Although domain composition differs among the other APP isoforms, the cleaving sites of canonical secretases are preserved as amino acid sequences of the APP metabolites resulting from amyloidogenic and non-amyloidogenic pathways. The longest isoform of APP contains an E1 domain at the N-terminal site, followed by an acidic domain and a KPI domain. The Ox2 antigen domain links the previous with an E2 domain. The juxtamembrane domain is present at the end of the extracellular region of APP. Finally, the TM and IC domains of APP reside in the C-terminal domain. The shorter APP isoforms maintain the same structure, but APP$_{751}$ and APP$_{695}$ lack the Ox2 antigen domain and the KPI and Ox2 antigen domains, respectively. Adapted figures[211,212] .

Trafficking

After being synthesized in the ER, APP_{fl} maturates through the Golgi/TransGolgi Network (TGN), where it undergoes multiple posttranslational modifications. APP and APLPs are abundant in intracellular membrane compartments of the secretory pathway, where APP can be processed into Aβ[213]. Once translocated into transport vesicles, APP is transported to the plasma membrane, where it can be cleaved or reinternalized through endocytosis[214]. Notably, only 10% of APP is detected at the cell surface, evidencing its rapid turnover[215]. Indeed, most APP is directly trafficked from the TGN to the early endosomes separately from β-secretase[216]. Although diverted in resting conditions, APP and β-secretase colocalize in recycling endosomes upon neuronal activity[217]. In hippocampal neurons, they converge in recycling microdomains in the dendritic spines and presynapses, and they are cotransported and interact along the axons[218]. Accordingly, Aβ secretion is observed in both dendrites and axons[213]. β-secretase processing of APP and production of Aβ mostly depend on APP intracellular trafficking, and differences in spatiotemporal subcellular distribution lead to altered levels of APP metabolites[219,220]. AD-associated mutations in APP alter its trafficking and favor Aβ production by prolonging its transit through the Golgi[219]. This could result from β-cleavage of APP in the early Golgi, which generates C99[221]. In fact, altering β-secretase post-Golgi trafficking results in higher colocalization of β-secretase and APP, and increased Aβ production[222].

Several protein families are related to APP trafficking and modulate its processing pathway. In this context, low-density lipoprotein receptor (LDLR)-related protein 1 (LRP1) interacts with APP and promotes its endocytosis, facilitating the contact of APP with amyloidogenic secretases and increasing Aβ production. In primary neurons, APP and LRP1 are transported together in fast axonal transport vesicles; however, LRP1 knockout increases APP localization at the cell surface, thus aiding its cleavage by meprin-β and α-secretase[223]. LDLR-related protein 10 (LRP10) is another member of the same family as LRP1 with analogous effects in APP sorting. LRP10 shuttles between TGN, the plasma membrane, and endosomes, and it interacts directly with the APP ectodomain. Overexpression of LRP10 sequesters APP in Golgi compartments and reduces Aβ levels in neuroblastoma cells[224]. Similarly, sortilin-related receptor 1 (SORL1)—another LDLR family protein related to AD—overexpression increases APP levels in the Golgi and reduces Aβ generation, a phenotype that is reversed by SORL1 downregulation[225]. Recent studies have shown that SORL1 depletion in human excitatory

neurons impairs APP recycling and leads to an enlargement of endosomes only alleviated after decreasing APP levels[226,227]. Interestingly, SORL1 mutations are related to different forms of AD[228]. Finally, LDLR-related protein 8 (LPR8) orchestrates APP and β-secretase endocytosis in conjunction with Muncl8-interacting (Mint) proteins[229].

Knocking out specific Mint proteins in AD transgenic mice greatly reduces APP CTF accumulation by decreasing β-secretase cleavage, without altering γ-secretase processing[230]. The C-terminal PTB motif of APP is essential for its internalization and trafficking through Mint proteins, facilitating its colocalization with PSEN1 in intracellular vesicles and increasing synaptic activity-induced Aβ production[231]. Mint1 regulates both the endocytic and secretory trafficking of APP[232]. In addition, Mint3 recruitment triggers APP transport from the Golgi into lysosomal compartments[233]. In human neuroblastoma models, Mint3 is also responsible for the APP shuttle from the TGN to the plasma membrane[234]. Accordingly, altering Mint-APP interaction proportionally modulates APP endocytosis and Aβ secretion in primary murine neurons[235]. Furthermore, Mint-dependent APP subcellular sorting affects Aβ secretion. Phosphorylation of Mint2 increases APP endocytosis through the autophagic pathway and Aβ intracellular accumulation, whereas unphosphorylated Mint2 induces APP translocation into the recycling pathway and enhances Aβ secretion[236]. Notably, APP, APLP1, and APLP2 all share the same C-terminal motif; however, APLP1 is mainly located at the cell surface, whereas APP and APLP2 are mainly located in intracellular compartments[237].

Posttranslational modifications

Posttranslational modifications determine APP intracellular trafficking. Importantly, APP_{695} cytoplasmatic tail harbors multiple phosphorylation sites, with S655 and T668 being particularly noteworthy for their roles in APP processing[238,239]. Both APP secretory trafficking and retromer-mediated transport of APP to the TGN require S655 phosphorylation, which is key to APP retrieval from endosomes[238,240]. Similarly, phosphorylation at T668 regulates APP translocation to the Golgi and its interaction with β-secretase[239]. Other phosphorylation sites also modulate APP. For instance, Y687 phosphorylation also promotes APP retention in the TGN and reduces Aβ production—this beneficial effect is halted by δ-cleavage of tropomyosin receptor kinase B[241]. Another important C-terminal phosphorylation site is Y682, which is involved in both APP intracellular sorting and APP neurotrophic effects[242,243]. Newly found APP secretases also

depend on newly found phosphorylation sites, as in the case of meprin-β-mediated APP cleavage, which greatly increases after S675 phosphorylation[244]. Although less frequent, APP ectodomain S198 and S206 can be phosphorylated under physiological conditions. Ectoprotein kinases phosphorylate S198 and S206 in post-Golgi compartments, although mature membrane-anchored APP can also undergo phosphorylation[245]. Furthermore, neuroblastoma cells carrying mutated APP at S206 or at different glycosylation sites had decreased levels of surface APP, confirming the important role of ectodomain posttranslational modifications in APP trafficking[246].

Mature APP also undergoes glycosylation. There are two main predicted sites of N-glycosylation in the ectodomains: N467 and N496. The introduction of mutated APP at both sites in COS-1 cells decreased APP secretion while augmented its cytosolic fraction[247]. The membrane-inserted APP ectodomain is essential for its axonal transport, and blocking its N-glycosylation impairs APP axonal sorting[248]. In hamsters, *in vivo* inhibition of complex N-glycan formation reduces APP translocation to synaptic membranes and its secretion[249,250]. APP trafficking is also affected by O-glycosylation. T576 is a major O-GlcNAcylation site—a novel type of O-glycosylation—and its mutation prevents APP shuttle to the plasma membrane, increasing Aβ production[251]. O-glycosylation at the cytoplasmatic tail is also involved in facilitating β-secretase cleavage. When O-glycosylation occurs in APP_{swe} at sites T663, S667, or Y681, β-secreatse APP cleavage is particularly significant and the overall amyloidogenic pathway is favored[252]. In endothelial cells, contrary to neurons, low O-glycosylated APP promotes APP externalization and reinternalization into the Golgi to be further O-glycosylated, and impeding this pathway halts Aβ production[253]. This finding is further supported by defective APP secretase processing upon removal of O-glycosilation sites[254]. Nevertheless, APP O-glycosylated at specific sites near β-secretase cleaving site also impedes proper processing of APP through the amyloidogenic pathway, highlighting the importance of APP glycosylation in its processing[255].

Moreover, APP ubiquitination triggers its degradation through the proteasome and hinders Aβ production. This depends on the E3 ubiquitin ligase complex, which ubiquitinates APP CTF and promotes its proteasomal degradation through endocytosis inhibition[256]. It also increases APP degradation through movement from endocytic compartments into multivesicular bodies (MVB), which later fuse with lysosomes[257]. In 2D and 3D human cell models, the presence of a defective variant of ubiquitin B leads to

reduced APP ubiquitination, increased APP levels, Aβ production, and formation of Aβ aggregates[258]. Accordingly, overexpression of deubiquitinase USP25 reduces APP lysosomal degradation, increasing β-secretase processing and Aβ generation[259]. On the other hand, ubiquitination of K668 sequesters APP at the Golgi and impedes its maturation and secretase processing, demonstrating the complexity of APP trafficking and the key role of posttranslational modifications in its processing[260]. This important role is also reflected in humans, where phosphorylated APP levels are increased around damaged areas of AD brains and ubiquitination-related proteins are downregulated[257,261].

Proteolytic processing

For many years, the most relevant and explored hypothesis of AD onset and progression has been the amyloid hypothesis. Thus, major efforts to decipher the molecular mechanisms of AD have focused on APP proteolytic processing. The amyloid hypothesis relies on the assumption that APP sequential cleavage by β- and γ-secretase produces the Aβ fragment, which accumulates in the brain in the form of Aβ aggregates that are neurotoxic and trigger a series of pathological events[29]. This is known as the amyloidogenic pathway. Nevertheless, APP can be also processed by α-secretase, preventing the formation of Aβ by the posterior cleavage of γ-secretase[2].

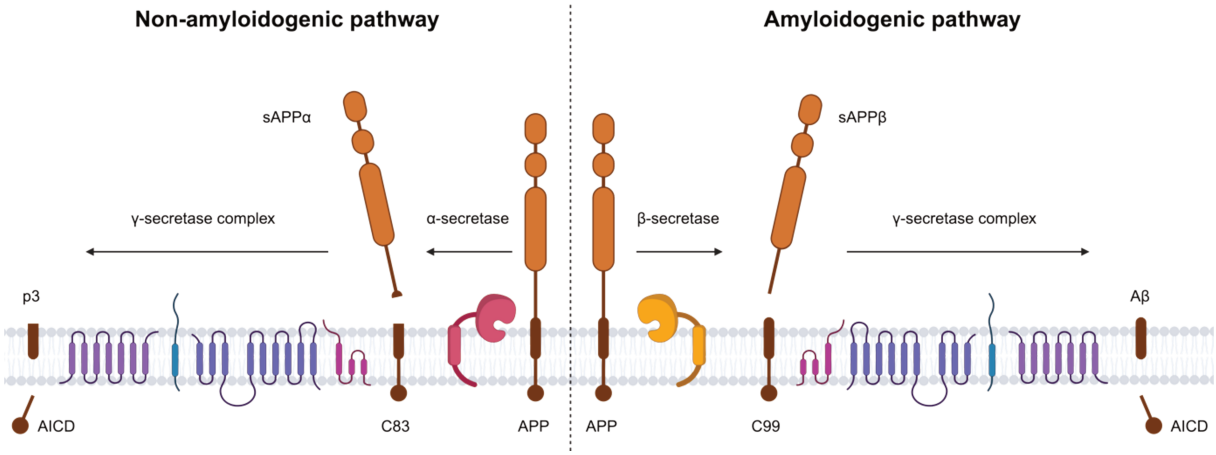

Figure 8. Canonical pathways of APP cleavage. APP is a single transmembrane protein, and the classical view of its processing involves three major secretases: α-, β-, and γ-secretases. On the one hand, in the non-amyloidogenic pathway, a-secretase cleaves APP—mostly at the plasma membrane—between K612-L613 in APP_{695}, disrupting the Aβ sequence and releasing sAPPα. Then, γ-secretase further cleaves the remaining C83, the APP-CTF remaining at the cell membrane. The final cleavage generates p3 and AICD. On the other hand, the amyloidogenic pathway starts with the β-cleavage of APP between M596 and D597 in APP_{695}. The β-secretase releases an N-terminal fragment of similar size as sAPPα, namely sAPPβ, and produces the APP-CTF C99. The γ-secretase cleavage of C99 produces the infamous Aβ peptide and AICD.

Recently, new secretases have been discovered to process APP apart from the canonical α-, β-, and γ-secretases. Therefore, various APP fragments with positive or negative effects on Aβ generation and brain homeostasis have been described[262]. However, most of their functions remain elusive and are currently being investigated.

Nonamyloidogenic pathway

As mentioned above, multiple secretases process APP. In 1990, α-secretase was described to cleave APP within the Aβ sequence, this is between K612-L613 in APP_{695}, impeding Aβ generation[263]. APP proteolytic processing by α-secretase occurs mostly at the plasma membrane[214]. After α-secretase cleavage, APP is separated into a 100kDa soluble fragment (sAPPα) and a CTF fragment of 10kDa (α-CTF or C83). This membrane-bound peptide is further cleaved by γ-secretase, releasing a 3kDa peptide named p3. Because α-secretase processes APP without generating Aβ, this sequential proteolytic process is known as the nonamyloidogenic pathway.

Various proteins have α-secretase activity cleaving APP. The most prominent α-secretases are from the A Disintegrin And Metalloproteinase (ADAM) family, specifically: ADAM9, ADAM10, and ADAM17[264]. The ADAM protein family has highly conserved domains, and their functions as α-secretases may be redundant and compensatory[265]. From these, ADAM10 has the most prominent constitutive α-secretase activity compared with the other members of the family in primary murine neurons, and it directly competes with other secretases to cleave APP at the cell surface[266]. Indeed, ADAMs are membrane-anchored proteins, where they mostly cleave APP[214]. However, ADAM10 and ADAM17 also compete with β-secretase to cleave APP in the TGN upon activation from protein kinase C (PKC)[267].

After treatment with phorbol esters, potent PKC activators, sAPPα increases in cultured AD fibroblasts, indicating a higher activity of α-secretase[268]. Receptor-mediated PKC activation through neuropeptide signaling also triggers α-secretase cleavage of APP[269]. However, both PKC-dependent and -independent mechanisms are involved in α-secretase neurotransmitter-dependent modulation through changes in intracellular calcium levels[270,271]. In fact, phorbol esters can also elevate calcium levels and activate calpain, leading to increased α-secretase activity[272]. Continuing with this theory, NMDAR activation and extracellular calcium influx increased 2.5 times α-secretase cleavage of APP[273]. Moreover, other types of receptors also regulate α-secretase.

Activation of tyrosine kinase receptors stimulate sAPPα production without affecting APP mRNA levels[274]. Accordingly, upon inhibition with genistein (a tyrosine kinase inhibitor), neuroblastoma cells decrease sAPPα release[275]. Different α-secretase activation mechanisms activate mitogen-activated protein kinase (MAPK), and MAPK inhibition reduces sAPPα secretion[276]. In human astrocytes, both the PKC and tyrosine kinase pathways converge at MAPK activation and its downstream signaling[277]. Overall, α-secretase activation is highly regulated through extra- and intracellular factors and occurs through different compensatory signaling pathways.

Activation of ADAM10 contributes to diverse cellular mechanisms other than APP processing. In both frontotemporal dementia (FTD) and AD, FTD missense mutations abolish ADAM-mediated cleavage of TREM2. Consequently, CSF TREM2 levels are practically inexistent and TREM2-expressing cells have disrupted phagocytic activity, indicating an impairment in TREM2 maturation[278]. However, ADAM17 can also cleave TREM2 and decrease its presence at the plasma membrane, reducing its ability to recognize Aβ[279]. Other proteins from the ADAM family impair amyloidogenesis. For instance, ADAM30 upregulation decreases Aβ42 secretion in primary cultures in coordination with lysosomal Cathepsin D activity, reducing amyloid load and rescuing long-term potentiation alterations[280]. Nevertheless, most therapeutic research using ADAM10 or other α-secretases continues toward modulating AD pathological traits through its APP cleaving activity.

Stimulating the nonamyloidogenic pathway has been widely explored as a potential treatment for AD. One approach is to facilitate ADAM10 and APP colocalization. In AD, increased ADAM 10 endocytosis diminishes its presence at the plasma membrane and reduces its α-secretase APP cleavage[281]. Indeed, synaptic ADAM10 partners are also downregulated in AD, decreasing the proteinase contact with APP at the cell surface[282]. Notably, acetylcholinesterase inhibitors, which are largely used to treat symptomatic aspects of AD, increase ADAM10 presence in membrane compartments in differentiated human neuroblastoma cells, increasing the release of sAPPα without affecting APP levels[283]. In addition to modulating ADAM10 trafficking, directly stimulating ADAM10 activity by overexpression in a mouse model with human APP increased sAPPα levels while reducing Aβ, and prevented amyloid deposition[284]. Similarly, molecular induction of ADAM10 catalytic activity increases sAPPα generation and suppresses Aβ production[285,286].

Neurons exposed to sAPPα had increased long-term survival and neurite growth[287]. In stem cell-derived neurons, depolarization-mediated neurite outgrowth through NMDAR activation requires sAPPα recruitment of MAPK[288]. Additionally, sAPPα competes with APP binding to integrin β1, promoting neurite outgrowth[289]. It also competes with APP binding to β-secretase, inducing a decrease in brain Aβ load in AD transgenic mice overexpressing sAPPα[290]. This decrease is a dual effect of impeding APP cleavage by β-secretase and inhibiting β-secretase enzymatic activity[209]. Moreover, sAPPα impedes hypoglycemic damage derived from excessive intracellular calcium concentration in primary neurons, protecting against excitotoxicity[291]. The neuroprotective functions of sAPPα extend to counteract Aβ-induced oxidative stress in primary rat hippocampal neurons[292]. Apart from increasing neuroprotection, sAPPα rescues hippocampal cell proliferation in 8-month-old AD mice and increases the density of astrocytes in the granule cell layer of the hippocampus[293]. Indeed, it promotes the proliferation of adult neural progenitor cells of the subgranular zone and their differentiation into astrocytes, while promoting their survival[294]. Nevertheless, sAPPα impact surpasses gliosis because it promotes neurogenesis through epidermal growth factor (EGF)-responsive cell proliferation in the subventricular zone of the lateral ventricle[295].

In contrast to the large body of evidence existing for α-secretases and sAPPα, the physiological functions or potential therapeutic roles of the CTF products of α-secretase cleavage are poorly understood. However, there is evidence supporting a beneficial effect of the substrate inhibitory domain of C83 in inhibiting γ-secretase *in vitro* and *in cellulo*, which could reduce Aβ production[296]. Curiously, α-secretase can also cleave C99, producing C83 and, thus, reducing Aβ levels[297]. After γ-secretase cleavage, two fragments are generated: p3 and the APP intracellular C-terminal domain (AICD). Both APP secreting pathways generate AICD, but the amyloidogenic pathway is the main contributor to AICD production[298]. Computational models indicate that AICD triggers synaptic dysfunction and reduced LTP in hippocampal neuronal models[299]. Accordingly, AICD weakens CA1 neuronal firing activity, modifies γ-oscillatory waves, and impairs spatial memory in mice[300]. In flies and rodent models, perturbed AICD nuclear localization alters core clock gene expression and leads to sleep disruptions, another common symptom of AD[301]. Although initially categorized as non-amyloidogenic, the p3 fragment localizes in diffused plaques and dystrophic neurites in AD and Down's Syndrome brains[302,303]. There are conflicting results regarding its capacity to form fibrillar

structures and aggregates, with studies showing both that p3 can form fibrils and aggregates or that it is soluble and unable to form oligomers[304,305]. Further research is needed to delve deeper into the mechanisms, physiological functions, and potential neurotoxic or therapeutic properties of APP metabolites generated in the nonamyloidogenic pathway.

Amyloidogenic pathway

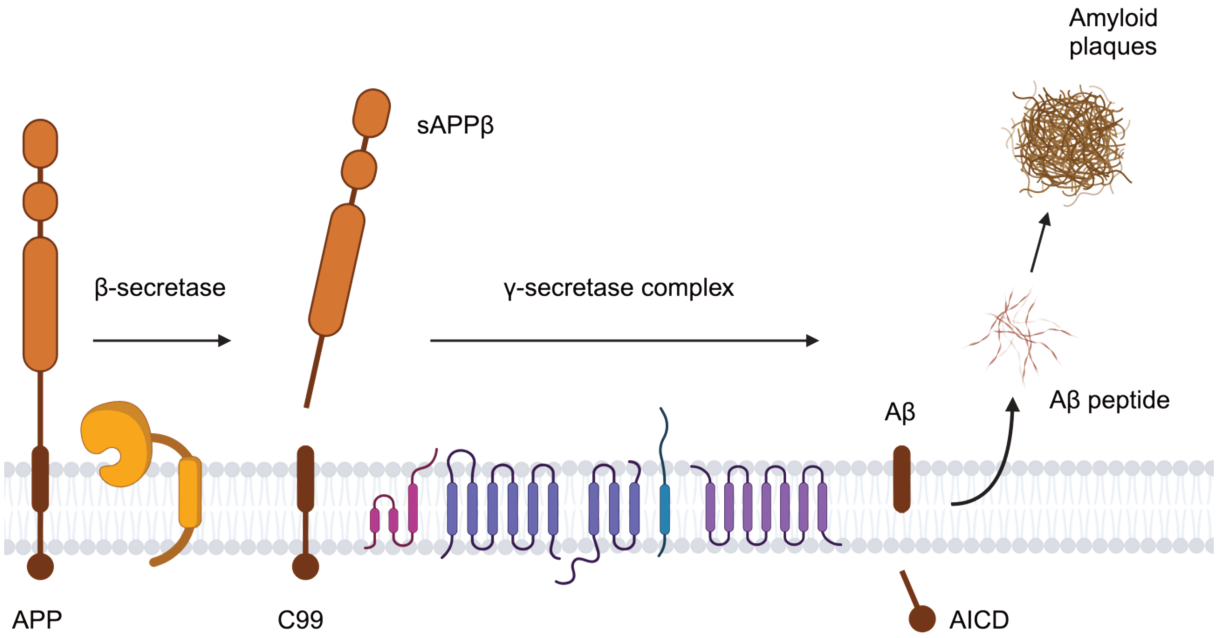

Figure 9. Amyloid pathway in detail. APP co-localizes with β-secretase in different cellular compartments with membrane structures (*e.g.* TGN, early endosomes, MVB, MAM). In these organelles, β-secretase cleaves APP, liberating sAPPβ and generating C99. Then, intracellular trafficking of C99 regulates its metabolization. The translocation of C99 into endolysosomal compartments facilitates γ-secretase cleavage, since γ-secretase is particularly active in acidic environments. The γ-secretase cleavage of C99 is sequential and generates multiple Aβ forms. Thus, the isoforms of the γ-secretase components determine the subcellular localization and efficiency of γ-secretase in the generation of certain Aβ peptides. Some of these peptides (like Aβ42) are more prone to aggregation and form Aβ fibrils, which finally generate Aβ plaques in the brain parenchyma. According to the Amyloid Hypothesis, these Aβ plaques are the cause and driving force of AD pathogenesis.

Although a robust body of information exists for the nonamyloidogenic pathway, the most studied and well-known sequential cleavage of APP is in the amyloidogenic pathway. This pathway is the major cause of Aβ accumulation and its downstream consequences. Similar to the nonamyloidogenic pathway, APP is first cleaved at the interface of the ectodomain and the transmembrane region; in this case, β-secretase cleaves at the β-site cleavage between M596 and D597 in APP_{695}. This cleavage also generates a soluble APP fragment, known as sAPPβ, and the transmembrane fragment C99. Then, the membrane-bound γ-secretase complex further cleaves C99 to produce the

Aβ fragment and AICD[29]. However, an alternative β-site cleavage exists between Y606 and E607 in APP_{695}, known as the β'-cleaving site, which produces a shorter CTF version of 89 amino acids (C89). When γ-secretase cleaves C89, it generates a truncated Aβ peptide (Aβ11-40/42)[306].

The β-site APP cleaving enzyme 1 (BACE-1) is the major β-secretase in the brain[307]. It is a type I transmembrane aspartyl protease of the pepsin family. Structurally, it has an ectodomain with a signal peptide and propeptide at the N-terminal and a large catalytic domain that extends until the loop at the interface of the transmembrane region, which extends into a cytosolic domain[308]. BACE-1 shares high amino acid sequence homology with BACE-2, another β-site transmembrane secretase, which has an alternative cleaving site at Aβ F19-F20[309]. BACE-1 is abundantly expressed in multiple neuronal subtypes and at lower levels, under stress conditions, in glial cells[310,311]. In the ER, BACE-1 is synthesized as a proprotein, and the prodomain determines its efficient exit from the ER. However, the presence of the prodomain fails to inhibit BACE-1 enzymatic activity, and pro-BACE-1 retains normal secretase functions[312,313]. During its transit through the TGN, a furin-like proprotein convertase cleaves the BACE-1 prodomain and gives rise to the mature form, which increases its activity by twofold[313,314]. Moreover, mutations in the N-glycosylation sites of the catalytic domain significantly reduce its activity, and S498 phosphorylation is essential for BACE-1 recycling to the plasma membrane[315,316]. Thus, posttranslational modifications regulate BACE-1 activity and subcellular localization.

BACE-1 trafficking through the Golgi apparatus modulates its efficiency in APP cleaving. During homeostasis, BACE-1 matures through the TGN network, separated from APP, and then translocates into the plasma membrane in its mature form[222,317]. Afterwards, BACE-1 is endocytosed and localized in early and recycling endosomes, where it can colocalize with APP[218,222,318]. In mouse primary neurons, β-secretase cleaves APP in early endosomes in the soma, suggesting that it mainly localizes in somatic transport vesicles[319]. In addition, coupling BACE-1 with the TGN38 cytoplasmic tail alters its recycling and increases Aβ production, highlighting the importance of BACE-1 recycling in APP β-secretase cleavage[320]. As mentioned above, APP relocates from the plasma membrane into the TGN through retromer-mediated transport, which mediates Aβ production. Blocking APP recycling toward the TGN increases endocytic APP and reduces Aβ levels, demonstrating that most β-secretase processing of APP occurs in the TGN[321]. This supports the notion that Golgi fragmentation in AD favors APP β-

processing[322]. Inside the cell, BACE-1 mostly localizes in intracellular membranous structures, where it cleaves APP. With increased cholesterol, APP localized in lipid rafts becomes more available to BACE-1, increasing Aβ production[323]. In the early stages of AD, alterations in lipid membrane biophysical properties induce β-secretase accumulation within lipid rafts[324]. Consequently, BACE-1 cleavage of APP proportionally correlates with lipid raft microviscosity in the cortex of AD brains, as increased viscosity makes APP more available for β-cleavage[325]. Mitochondria-associated endoplasmic reticulum membranes (MAM) are gaining attention as major sites of BACE-1 localization and β-secretase cleavage of APP, and disruption of axonal MAM structures decreases palmytolated APP cleavage by β-secretase[322].

Axonal and dendritic localization of BACE-1 are essential for its role in synapse homeostasis. Apart from processing APP, BACE-1 has multiple alternative synaptic substrates. In fact, BACE-1 knockout mice have synaptic deficits. Both knockout and inhibition of BACE-1 result in fewer releasable and poorly docked synaptic vesicles at the synaptic active zone, which can be rescued with a metabotropic glutamate receptor I positive allosteric modulator[326]. Moreover, both BACE-1 and BACE-2 are the only known sheddases of Seizure protein 6 (Sez6). Therefore, BACE-1 inhibitors decrease Sez6 processing and alter spine density *in vivo*[327]. In addition, spine density alterations lead to LTP impairment in mice chronically treated with BACE-1 inhibitors, which depends on the effects of BACE-1 on Sez6[328]. The correct processing of certain subunits of voltage-gated potassium channels also depends on BACE-1 activity in mouse primary neurons[329]. Other important synaptic molecules are neural cell adhesion molecules (NCAM), which are also BACE-1 substrates in the brain[330]. Interestingly, in some cases, BACE-1, ADAM10, and ADAM17 share the same substrates involved in synaptic structure maintenance[331]. Inhibition of BACE-1 alters the processing of several transsynaptic proteins, including: neurexin-1α, neurexin 4, and neuroligin-1[332]. The three proteins of the APP family also play multiple roles in synaptic structure[333]. Synapse proximal membranes contain both BACE-1 and APP, but Mint sequesters APP and halts its β-secretase processing[334]. N-terminal and C-terminal labeling of APP colocalizes with synaptic vesicles and augments after treatment with BACE-1 inhibitors, suggesting that APP is also processed at synaptic terminals[335]. Furthermore, upon neuronal activity, Mint phosphorylation decreases its colocalization with APP and facilitates BACE-1 cleavage[336]. Confirming the key role of

BACE-1 activity in synapse homeostasis, recent findings demonstrate that BACE-1-mediated Aβ generation induces synaptogenesis independently from sAPPβ[337].

The N-terminal fragment of β-secretase cleavage, sAPPβ, only differs in 16 residues to sAPPα. Strikingly, sAPPβ is unable to preserve the neuroprotective and neurotrophic functions of sAPPα. As previously exposed, sAPPα protects neurons from excitotoxicity, metabolic stress, and Aβ toxicity. In the case of sAPPβ, these neuroprotective functions are 100 times more inefficient in cell lines or inexistent in mouse hippocampi[338,339]. Compared to sAPPα, the differences in sAPPβ also impair its ability to modulate LTP[340]. However, sAPP fragments contain a preserved sequence capable of inhibiting neuronal activity of CA1 pyramidal cells *in vivo* through binding to the sushi 1 domain of the $GABA_BR1a$ receptor[341]. In APP and APLP2 double knockout mice, overexpression of sAPPβ is insufficient to rescue lethality, demonstrating that it is unable to compensate for lack of APP[340]. Nevertheless, sAPPβ reduces cell adhesion and increases axonal outgrowth similarly to sAPPα in primary neurons[342]. Furthermore, human embryonic stem cells (hESC) exposed to N-terminal fragments of APP rapidly acquire a neuronal fate, with sAPPβ being more efficient than sAPPα[343]. Both N-terminal fragments also target nonneuronal cells and activate microglia to induce a neurotoxic reactive profile[344].

γ-secretase

The final step in both amyloidogenic and nonamyloidogenic pathways is γ-secretase cleavage of APP CTFs. γ-secretase is a membrane-bound aspartyl protease that cleaves type I single-span transmembrane proteins at the lipid bilayer. It is a tetrameric complex formed by nicastrin (NCSTN), presenilin enhancer 2 (PEN2), presenilin (PS) 1 or 2, and anterior pharynx defective-1 (APH1). From these, NCSTN and PEN2 are constant subunits; and APH1 (a, b, or c) and PSEN (1 or 2) present different variants that determine γ-secretase subcellular localization and substrate affinity[345,346]. PS1 or 2 is the catalytic subunit of the γ-secretase complex and undergoes autoendoproteolysis after the assembly of the four subunits to generate an N-terminal fragment and a CTF, producing the active γ-secretase form[347,348].

The diversity and abundance of γ-secretase substrates hint at a role similar to that of the proteasome but specialized for transmembrane protein degradation[349]. Recently added evidence on C99 cytotoxicity and aggregation shifts the view of γ-secretase being deleterious to potentially having a beneficial role in degrading APP CTF, despite the

undesirable secondary effects of excessive Aβ production[350]. In general, γ-secretase requires substrates with short ectodomains, either naturally short or with previous membrane-proximal cleavage[351]. NCSTN sterically blocks recruitment by the tetrameric complex in the presence of large ectodomains[352]. Only 34 amino acids are necessary for the recognition and recruitment of C99 by γ-secretase: 24 amino acids of the transmembrane helix, 7 amino acids N-terminal to it, and the 3 immediately C-terminal residues[353]. Specific residues are unnecessary for γ-secretase processing; instead, it involves region-specific cleavage at the cytosolic-adjacent transmembrane region[354]. Consequently, the γ-secretase cleavage of C99 TM generates various Aβ species of different length[355].

There is a multistep process involving the four γ-secretase components from substrate recognition to final cleavage. For instance, C99 initially interacts with NCSTN, PEN2, and PSEN exosites. PEN2, PSEN TM and its hydrophilic loop undergo multiple conformational changes during substrate translocation into the active cleaving site. The conformation of all involved components determines the resulting cleavage. Certain PSEN1 fAD mutations change C99 position in the active site region and increase Aβ42/43 production[356]. Once C99 interacts with the PSEN N-terminal fragment, its cleavage site region contacts the active site in its CTF[356,357]. C99 docking in the active site causes relaxation of the transmembrane helix around the initial cleavage site[358]. Subsequently, the unwound C99 transmembrane domain fills the subsites of the γ-secretase active site and undergoes hydrolysis. γ-secretase contains three binding subsites, leading to sequential cleavage of C99 in three amino acid residues[359]. Substrate TMs are highly dynamic, and their perturbation determines their membrane anchoring[360]. This is particularly important for C99 because it is prone to dimerization, and the affinity of C99-γ-secretase compared with C99-C99 affinity regulates its availability for cleavage. The lipid environment in the lipid bilayer modulates the competition between C99 and γ-secretase and C99 dimerization[361]. Thus, subcellular localization is essential for regulating C99 γ-secretase cleavage.

The γ-secretase tetramer complex is highly dynamic, and different isoforms of its components regulate its conformation, subcellular localization, and function. PSEN1-containing γ-secretase localizes at the cell surface and endosomal compartments in neurons and brain tissue. However, PSEN2 γ-secretase contains an ERTSML motif that binds to the Adaptor Protein 1 complex and redirects γ-secretase toward late endosomes

or lysosomes. Translocation of γ-secretase into late endosomes/lysosomes generates longer Aβ fragments, elevating Aβ42 levels[346] . PSEN2 preferentially associates with APH1a or APH1b, which further the distribution of γ-secretase in TGN, and recycling or late endosomal compartments[345]. Indeed, the endosomal-to-TGN recycling pathway modulates Aβ42 through regulation of γ-secretase activity in the mouse brain[362]. In addition, PSEN mutations associated with fAD dramatically increase Aβ42 production. Interestingly, PSEN1 fAD mutations modify the subcellular localization of PSEN1 γ-secretase, increasing its presence in endolysosomal compartments. As PSEN1 lacks the PSEN2 sorting motif, conformational changes in the highly unstable fAD γ-secretase complex may impair its normal trafficking and, thus, Aβ formation[363].

As mentioned earlier, the lipid environment influences the structure of γ-secretase, which regulates its activity. Most frequently, γ-secretase cleaves C99 in three or four sequential steps, first generating Aβ48 and Aβ49 and then successively cleaving them to produce Aβ40 and Aβ42[364]. However, in lipid rafts, γ-secretase releases penta- and hexapeptides through a four, five, or six-step cleavage that augments the number of Aβ species produced[365]. Moreover, γ-secretase can form high-molecular-weight complexes with multiple proteins. With tetraspanins, γ-secretase also forms membrane microdomains that regulate γ-secretase activity[366]. Interestingly, γ-secretase functionally interacts with ADAM10 to sequentially cleave APP[367]. In a similar manner, a recent study showed that γ-secretase also forms high-molecular-weight complexes with BACE-1[368]. These interactions are especially important for understanding APP regulated intramembrane proteolysis. However, whether these complexes form through direct physical interactions or mediated by other proteins, such as tetraspanins, remains unclear[367]. In addition, it is necessary to translate these findings into physiological conditions in order to explore their effects on the production of toxic APP metabolites.

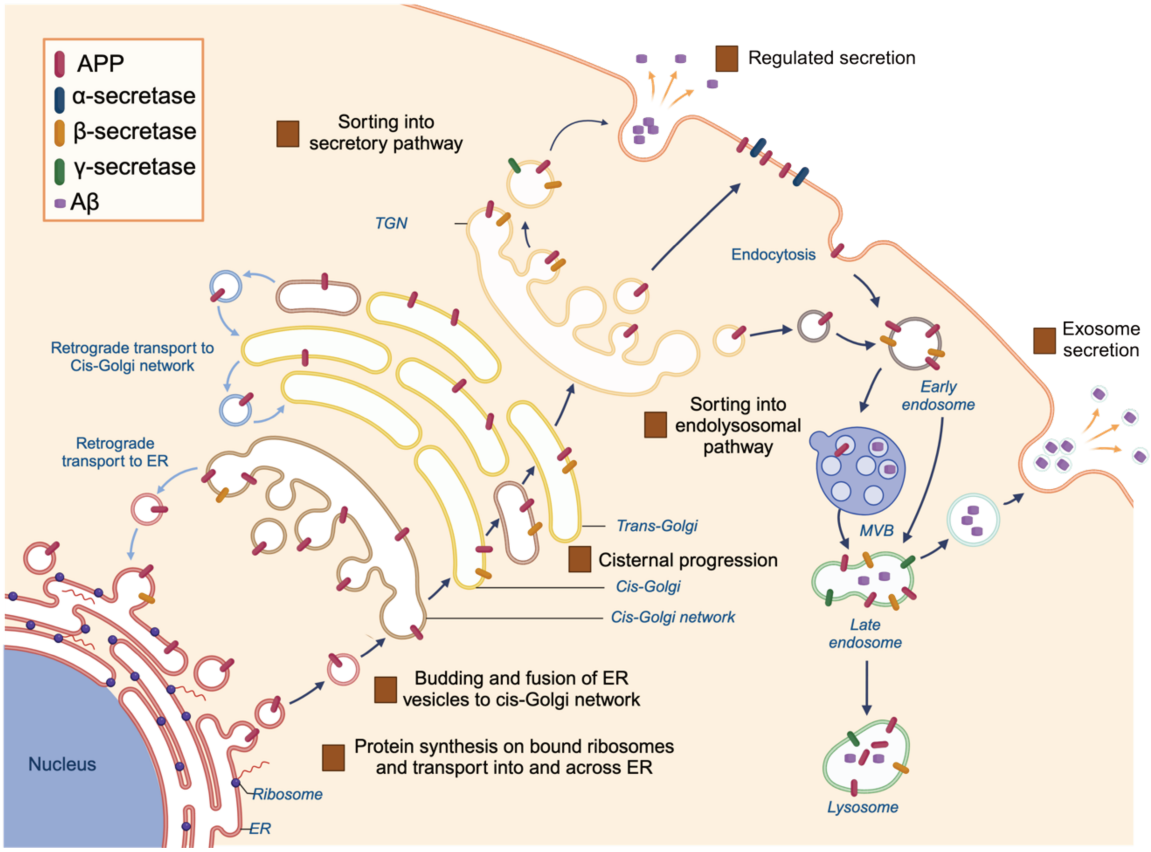

Figure 10. APP subcellular trafficking and colocalization with canonical secretases. APP is first synthesized in the ER, after which it is transported into the Golgi apparatus for further maturation. Defective APP can return to the ER. During APP transport through the Golgi apparatus, APP can already colocalize with β-secretase in the TGN and undergo β-cleavage. If intact, APP can translocate to the plasma membrane, where α-secretase is its most important metabolic partner. Otherwise, APP or C99 generated in the Golgi can follow the secretory pathway, where C99 contacts γ-secretase, facilitating the release of Aβ into the extracellular space. Another potential route of APP is the endolysosomal pathway. After translocating to the plasma membrane or immediately from the TGN, APP is endocytosed or transported into early endosomes. β-secretase is also located in early endosomes, which are important sites of C99 generation. APP-containing early endosomes mature into late endosomes or fuse with other vesicles to form MVB. Here, γ-secretase cleaves previously generated C99 to produce Aβ, which is later released through exosomes. Alternatively, APP/C99 colocalize with β-/γ-secretase in lysosomes, where Aβ is also produced. Overall, the processing of APP is highly dependent on its trafficking and it colocalizes with canonical secretases in multiple intracellular compartments. Therefore, understanding the exact locations of APP cleavage and the distribution of APP metabolites with canonical secretases is fundamental for the understanding of amyloidosis in AD. Of note, this figure is simplified, and other cellular compartments like MAMs or the presence of α-secretase in the TGN were omitted to facilitate interpretation.

APP toxic metabolites

According to the amyloid hypothesis, the amyloidogenic pathway generates a series of toxic metabolites accountable for the onset and progression of AD[29]. For many years, clinical trials evaluating drugs aimed at various pathophysiological processes previously discussed have consistently failed[369]. Thus, the amyloid hypothesis has been losing support in the scientific community (thoroughly discussed in[370–373]), until recently. In 2021, the FDA approved the first anti-amyloid immunotherapy capable of reducing amyloid pathology and cognitive decline in AD patients[8]. Since then, advances in new therapeutic strategies to decrease Aβ load and the validation of new therapeutic targets upstream of Aβ have reignite interest in the amyloid hypothesis[350,374]. Therefore, the toxic metabolites generated after β-secretase cleavage of APP are currently of high therapeutic interest.

APP β-CTF

After sAPPβ release, the β-CTF transmembrane fragment containing the Aβ sequence remains anchored to the membrane. Most of the C99 sequence passes through the membrane, with an N-helix at the N-terminal site, a hinge angle in the transmembrane part, and the AICD fragment finishing with a C-helix[375]. Traditionally, Aβ is considered to be the main toxic peptide generated in the amyloidogenic pathway. However, recent findings appoint C99 as a major contributor to pathological processes derived from APP amyloidogenic processing[376,377]. Although more prominent in fAD, C99 levels are elevated in both fAD and sAD[378]. In fact, C99 accumulates earlier than Aβ, its levels are increased in neurons and astrocytes in animal and human AD brains, and it correlates better than Aβ with neuronal vulnerability and cognitive deficits[31,376].

Even in the absence of Aβ accumulation and tau hyperphosphorylation, C99 accumulation is sufficient to alter LTP and decrease locomotor activity[377]. Indeed, the lack of effects of γ-secretase inhibitors compared to β-secretase inhibitors confirms that certain synaptic and behavioral alterations depend on C99 production rather than Aβ[379]. In early AD preplaque mice, C99 affects hippocampal network oscillations and a subset of hippocampal-related memory tasks different from those affected by Aβ[380]. Early accumulation of C99 increases the secretion of tumor necrosis factor (TNF) α, probably after microglial activation, which induces neuronal hyperexcitability[381]. Accordingly, increased BACE-1 processing of APP and increased C99 levels in rats facilitate glutamate

release in the hippocampus before the appearance of major histopathological changes[382]. Moreover, in young AD mice with hippocampal C99 but without Aβ, parvalbumin-positive (PV+) interneurons have decreased excitability and theta oscillations are less rhythmic, reflecting an overall alteration of the brain network only rescued with β-secretase inhibitors[383]. C99 also disrupts other areas of the brain, decreases the number of cholinergic neurons in the medial septal nucleus, and induces an enlargement of endosomes in the hippocampus and cortex[384].

Impaired transport and cellular distribution of C99 appears several months before Aβ in the CA1 area of the hippocampus, where C99 localizes in enlarged vesicles immunoreactive for Cathepsin-B and Aβ[376]. BACE-1 inhibition inhibits early endosomal enlargement in human fAD neurons, whereas increasing the endogenous levels of C99 is sufficient to induce early endosomal enlargement in WT human neurons[385]. Overexpression of APP or C99 alter endocytic morphology and functions in fibroblasts, and γ-secretase inhibition is sufficient to mimic it. This is also observed in fibroblasts with a double copy of APP (APP^d), where endocytic impairments are rescued after decreasing APP or BACE-1 expression[157]. Early endosomes are also enlarged in human neurons from APP^d and sAD individuals—together with increased hyperphosphorylated tau and GSK3β levels—and, contrary to γ-secretase inhibition, β-secretase inhibition reverses most of these AD-like phenotypes[386]. In a bidirectional manner, tau hyperphosphorylation induction in mice triggers C99 accumulation in axonal swellings together with transport vesicles, synaptic proteins, microtubule fragments, and transport molecules; and only β-secretase inhibition prevents C99 axonal accumulation[387,388].

Together with early endosomes, C99 accumulation alters other vesicle organelles and halts its proteolytic processing. In two different mouse models, C99 aggregation in endolysosomal compartments disrupted lysosomal proteolysis and autophagy, an Aβ-independent phenotype rescued with β-secretase inhibitors[389]. Indeed, elevated C99 levels increase lysosomal pH and impair the enzymatic activity of lysosomal hydrolases in *in vitro* and *in vivo* models of APP^d [390]. In human neurons carrying fAD mutations, reduction in C99 production rescues lysosomal defects and corrects autophagic function[391]. Consistent with these findings, the autolysosomal pathway was altered in mouse models of APP-CTF accumulation. Together with a general loss of neurons and extended gliosis, these mice display a higher number of enlarged LAMP2+ lysosomes and enhanced expression of lysosomal proteins in neurons[392]. LAMP1+ structures are also

enlarged upon C99 accumulation, and inhibiting autophagosomal activity leads to increased C99 in human cell lines. In contrast, stimulating autophagosome formation stimulates lysosomal degradation of C99[393]. This is especially important when other C99 degradation machineries are altered. For instance, ER-associated proteasomal degradation is a major C99 processing mechanism and, upon proteasome inhibition, it is redirected toward lysosomal-dependent clearing[394].

Membrane interfaces between the ER and mitochondria are increasingly recognized as important contact sites between amyloidogenic secretases and APP metabolites. In both cellular and mouse models incorporating fAD mutations, APP and its metabolites are localized in MAM together with β- and γ-secretases, and they interact with MAM proteins that modulate ER and mitochondrial functions. Furthermore, MAM contact sites are enlarged in APP_{swe}-overexpressing cells[395]. Elevated C99 levels in MAM impair lipid turnover, which alters both MAM and mitochondrial membranes. Mitochondrial stress mediated by altered lipid homeostasis leads to defects in mitochondrial respiratory supercomplexes[396]. Increasing C99 in human neuroblastoma cells increases the production of reactive oxygen species (ROS) and impairs normal mitochondrial fusion with lysosomes and overall mitophagy. This is translated into transgenic AD mice, and mitochondrial accumulation is also present in human *postmortem* AD brains[397]. Mitochondrial accumulation of APP and its metabolites disrupts mitochondria homeostasis, and pharmacological enhancement of mitochondrial function reduces toxicity in multiple AD models[398,399].

Multiple studies have demonstrated toxicity of multiple APP metabolites, but these works have focused mainly on APP and Aβ. However, C99 can also form fibrils and be neurotoxic. APP-CTFs accumulate in cultured heterologous cells in deposits similar to amyloid plaques, and induce degeneration in differentiated cell lines and in primary hippocampal neurons[400,401]. In fact, C99 contains a dimerization motif in the TM that promotes its stabilization and resistance to processing. Simulation of C99 dimerization elucidated that homodimerization stabilizes C99 extramembrane domains inducing the formation of metastable β-strands and α-helices. Indeed, the structure of extramembrane domains affects TM conformation of the C99 homodimer. These protein interactions could change C99 accessibility for further γ-secretase cleavage and regulate Aβ production[402]. Accordingly, covalent homodimerization of C99 blocks γ-secretase processing *in vitro*, and the orientation of dimeric TM GxxxG motif regulates γ-secretase

cleavage site and the Aβ form produced[403,404]. Actually, alanine mutations in the GxxxG motif are insufficient to impede C99 dimerization but define Aβ species production[405]. C99 stabilization combined with defects in the endolysosomal pathway promote its accumulation in intracellular vesicles and in exosomes[406]. A recent study demonstrated that inhibition of γ-secretase triggers C99 oligomerization. C99 oligomers were translocated into intracellular vesicles, whereas C99 monomers accumulated in the TGN. High-molecular C99 oligomers were finally detected also in extracellular vesicles in AD cells and mouse models[407]. These results suggest that secretion of C99 fibrils could be a coping mechanism for cells to reduce cytotoxicity, but it could also cause a spread of amyloid pathology.

Altogether, these elements highlight the pathological role of C99, which affects multiple cellular mechanisms altered in AD. Targeting C99 could facilitate the modulation of Aβ-associated pathologies at earlier stages and potentially prevent irreparable damage. This is particularly interesting in AD, where Aβ-targeting strategies are unable to act at early stages of the disease.

Amyloid β

The final step of APP sequential cleavage is γ-secretase cleavage of C99. This process yields two peptides: Aβ and AICD (AICD has been previously reviewed in the *Non-amyloidogenic pathway section*). In physiological conditions, these peptides have beneficial functions and regulate a number of cellular processes. Elevated Aβ levels in APP_{swe} mutant neurons induces synaptogenesis and enhances synaptic transmission. These effects could be reversed using BACE-1 inhibitors and halting Aβ production[337]. Moreover, mice with long-term treatment with BACE-1 inhibitors display reduced number of dendritic spines and impaired synaptic activity. This phenotype was recovered upon withdrawal of BACE-1 inhibitors[408]. Accordingly, BACE-1 complete or conditional knockout impaired hippocampal LTP in mice[409,410]. And BACE-1 deficient mice show signs of seizure activity and neuronal excitability mediated by increased sodium channel activity[411]. In WT mice, reduction of Aβ physiological levels impairs normal LTP and induce cognitive deficits, which are ameliorated with Aβ42 treatment[412,413]. Altogether, appoints Aβ as a major contributor to synaptogenesis and synaptic regulation.

Nevertheless, Aβ becomes harmful upon excessive production and accumulation in AD, and plays a central role in the amyloid cascade[2]. And, despite criticism, recent advances

in drug discovery in AD have solidified the concept of Aβ as an important component of AD pathogenesis[4,80]. However, mechanisms of Aβ toxicity are insufficiently understood, and ratios or mixtures of Aβ species are becoming increasingly important in elucidating Aβ toxicity.

The most abundant Aβ peptides in the CNS are Aβ40 and Aβ42. In physiological conditions, the Aβ42/Aβ40 ratio is low. However, Aβ42 is elevated in AD, and it disturbs the normal equilibrium between both peptides. Because Aβ42 is more prone to aggregation, CSF Aβ42 levels decrease in AD, making CSF Aβ42/Aβ40 ratio a reliable AD biomarker[68,414]. Additionally, *in vitro* and *in vivo* changes of Aβ42/Aβ40 ratio alter Aβ oligomerization, plaque formation, and plaque morphology. Imbalances in Aβ42/Aβ40 increase oligomer stability, governing their neurotoxicity. Altogether indicating that the Aβ42/Aβ40 ratio is more determining for neurotoxicity than the absolute value of either of its Aβ forms[415]. Indeed, total values of Aβ are insufficient to predict AD development, as some AD mutations trigger the increase of specific Aβ species production while decreasing the overall levels of Aβ. These alternative forms are N- or C-terminally truncated Aβ forms that have individual biophysical properties and, thus, instigate diverse effects[416].

Initially, differences in Aβ can come from different APP proteolytic pathways. The fragment Aβ17-40/42 is also known as p3, the resulting peptide of γ-secretase cleavage of C83 at the end of the nonamyloidogenic pathway. In a cohort of MCI patients, the Aβ17-40/Aβ11-40 ratio in CSF was the best discriminator to detect MCI subpopulations at different stages of cognitive decline[417]. Despite its nonamyloidogenic origin, p3 activated caspases-8 and -3 in two lines of human neuroblastoma, leading to cellular apoptosis[418]. Furthermore, p3 induces similar levels of mitochondrial stress to the full Aβ42, proving its capacity to disrupt cellular homeostasis[419]. Accordingly, exposure to Aβ17-40 induced glial activation through formyl peptide receptors and calcium fluxes in the human glial cell line U87[420(p1)]. In fact, Aβ17-42 can form calcium-permeable ionic channels and exerts neurotoxic effects in human cortical neurons. Other Aβ species can also form ionic channels. For instance, Aβ9-42, a structural equivalent of Aβ11-42, can form unstable ionic channels permeable to calcium. These Aβ-ionic channels-induced calcium uptake produces neurite degeneration and neurotoxicity in human neurons *in vitro*[421].

Aβ11-42 is part of the family of Aβ peptides generated within the amyloidogenic pathway. Differences in these Aβ forms originate either from initial β- or γ-secretase cleavage of APP, or from Aβ post-processing. Apart from Aβ40 and Aβ42, Aβ11-40/42 is one of the most common Aβ species and it is generated after the sequential cleavage of APP in the β'- and γ-sites. This N-terminally truncated Aβ aggregates easily and is widely found in senile plaques of AD brains, although it is less cytotoxic than other Aβ forms[422,423]. Its high affinity to copper determines its aggregation capability, and it might be the cause of high levels of copper observed in AD plaques[424,425]. As a matter of fact, Aβ N-terminal truncation exposes a copper and nickel binding motif (NH_2-Xxx-Zzz-His) with high affinity to copper[424]. And both Aβ11-x and Aβ4-x efficiently bind to copper and compete with whole Aβ peptides for copper binding, although only Aβ4-x halts copper-induced ROS production[426].

Inhibition of copper-induced ROS relies on the resistance of Aβ4-x-copper complexes to oxidation and reduction. In addition, Aβ4-x has three times more affinity to copper than its full sequence counterparts, suggesting a potential role in copper clearance during synaptic transmission[427]. However, it has a high aggregation rate, it is also neurotoxic, and it induces behavioral deficits in mice[428]. In the hippocampus and the cortex of fAD and sAD patients, Aβ4-42 is the most common species together with Aβ42[429]. Intraneuronal accumulation of Aβ4-42 starts at early stages in 5xFAD mice, and it precedes that of other well-known highly toxic Aβ forms[430]. Regarding spatial distribution, Aβ4-x localizes within the nuclei of Thioflavin S+ amyloid plaques in transgenic mice and human AD brains; differently to Aβx-34, a C-terminal truncated Aβ form, which primarily localizes outside of Thioflavin S+ aggregates[431].

Apart from N-terminal cleavage of Aβ, other Aβ peptides C-terminally truncated are detected in animal AD models and in patients. Aβ34 is a C-terminally truncated form present in AD patients CSF, and it depends on BACE-1 cleavage upon γ-secretase release of Aβ[432,433]. Other C-terminally truncated forms of Aβ usually result from γ-secretase sequential cleavage at different sites[364]. Different combinations of γ-secretase C99 sequential cleavage pathways produce different C-terminally truncated forms of Aβ[365]. And, despite most of them are related, some Aβ species are independent from the generation of other Aβ forms, and AD-related mutations or secretase inhibitors differently affect them[434,435]. From these, Aβ37, Aβ38, and Aβ39 are three of the most common intermediates generated during γ-secretase C99 processing[435]. The three

peptides are detectable in CSF of AD patients, with Aβ37 being noteworthy among them as a promising biomarker in combination with Aβ42[436,437]. Moreover, the three peptides are present in fAD mouse models and in the brain parenchyma and vasculature of AD brains. Interestingly, Aβ37 and Aβ39 were limited to the vasculature in sAD patients, while they were also located in extracellular amyloid plaques in fAD patients. In addition, the distribution of these intermediate Aβ peptides depended on specific fAD mutations[438]. In line with this, even different fAD mutations at the same codon of APP alter Aβ production and its intermediate peptides differently[439].

Some studies have identified as many as 33 different Aβ truncated peptides which are differentially present fAD and sAD[440]. And truncated species generated during Aβ degradation can increase this number. Apart from secretases involved in classical APP pathways, MMP-2 and MMP-9, two matrix metalloproteinases (MMP), cleave Aβ at C-terminal sites and produce soluble fragments without cytotoxicity[441]. Moreover, membrane-type MMP 1 (MT1-MMP) cleaves at multiple sites both Aβ40 and Aβ42 and can degrade both soluble and fibrillar Aβ[442]. These demonstrate that alternative cleavage of APP and its metabolites contribute to the generation of amyloid peptides.

Alternative APP proteolytic pathways

Since the establishment of the amyloid hypothesis, a plethora of anti-Aβ drugs have entered clinical trials. These drugs focused on modulating Aβ by directly targeting Aβ to facilitate its degradation or by halting its production upstream through β- or γ-secretase inhibition. Most of these strategies dropped out of clinical trials because of lack of efficacy or strong secondary effects[4]. However, recent, although limited, success of anti-Aβ monoclonal antibodies demonstrates that the amyloid pathway is a coherent therapeutic axis in AD[7–9].

Non-canonical APP proteinases are gaining importance in understanding the toxic effects of APP processing. Caspases, metalloproteinases, cathepsin D, or rhomboid-like protein-4 are some of the examples of enzymes that generate alternative APP fragments. In general, canonical and non-canonical secretases can combine their cleavage activity to generate different forms of sAPP and APP-CTFs with specific properties[262]. But the role of these fragments and their amyloidogenic activity are poorly understood, and recent discoveries demonstrate that some of these proteinases have a central role in AD[443].

MT1-MMP and MT5-MMP, the latter being another member of the MT-MMP family, are two recently described pro-amyloidogenic enzymes. Although, as mentioned before, MT1-MMP degrades different forms of Aβ, recent studies demonstrated that it also favors amyloidogenesis[442,444]. Similarly, MT5-MMP has a clear involvement in amyloidogenesis and neuroinflammation in the context of AD[443].

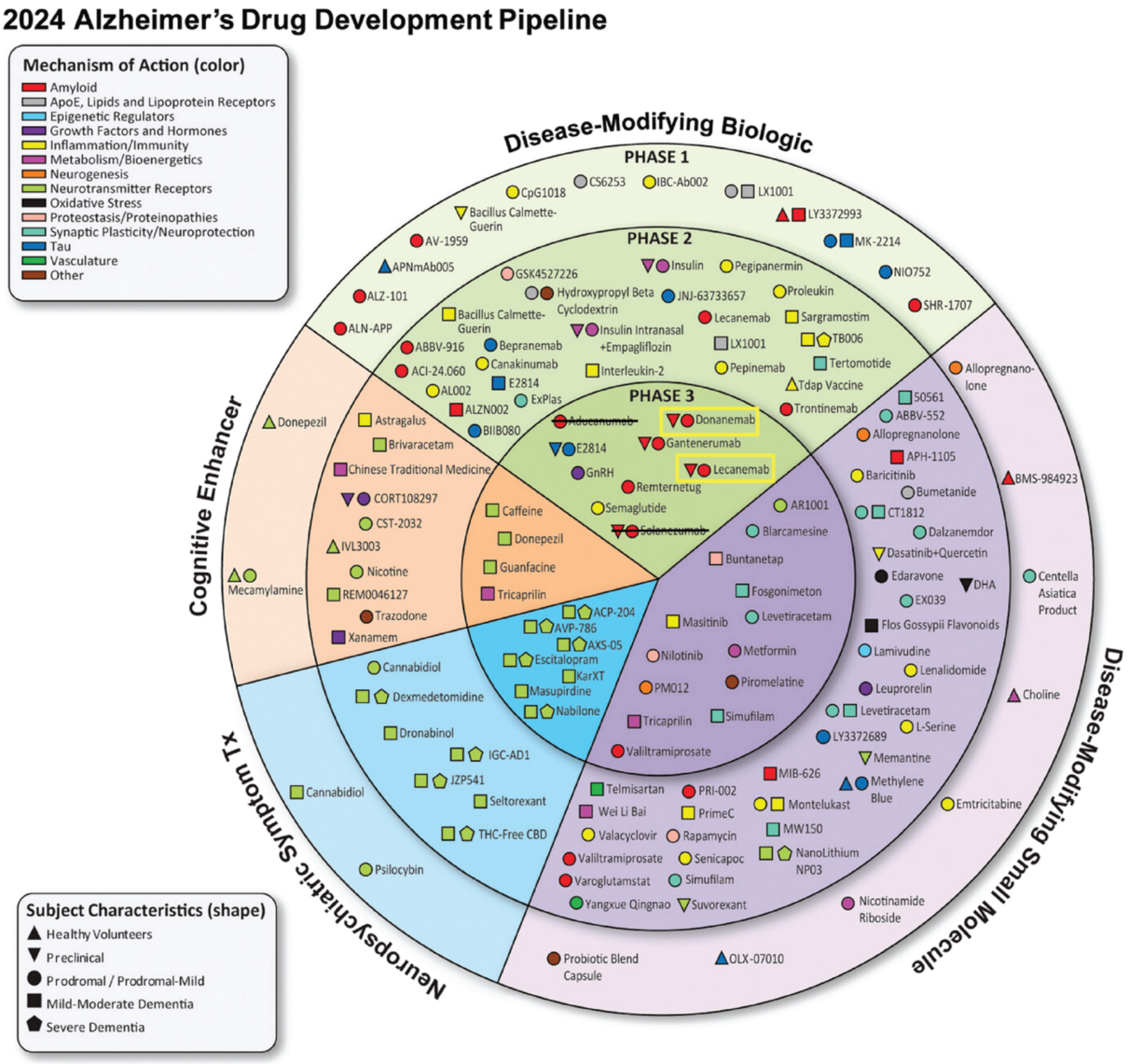

Figure 11. Pipeline of developing drugs for AD. Numerous drugs are in development to target multiple factors involved in AD pathogenesis. This is a classification of AD drugs currently in clinical phases. The outer ring represents Phase I, the middle ring represents Phase II, and the inner ring represents Phase III. They are divided into four categories disease-modifying biologic, which refers to drugs that hinder the development of certain pathogenic traits. Several mechanisms of action are involved in this category, similar to disease-modifying small molecules. However, the former involves biological agents (e.g. antibodies, vaccines), whereas the latter are small molecules (drugs less than 0,5kDa). The neuropsychiatric symptom category includes drugs that address neuropsychiatric and behavioral impairments. Cognitive enhancers are agents targeting cognitive symptoms. Importantly, in the last two categories, there are only drugs addressing symptoms of AD progression, but incapable of modifying the evolution of the disease. Aducanumab and Solanezumab are crossed because their development is discontinued, and Donanemab and Lecanemab are highlighted because they have already been approved: Donanemab in the United States of America; and Lecanemab in Japan, China, and the United States of America. Adapted figure[28].

MT1-MMP

As other MMPs, MT1-MMP has multiple physiological functions, and is homogeneously expressed in the body. In the CNS, it is principally expressed in neurons, astrocytes, and microglia[444,445]. One of its most important functions is to cleave extracellular matrix (ECM) proteins, such as: type I and III collagen, fibronectin, laminin, and proteoglycans[446]; and its first known substrate was pro-MMP2, which MT1-MMP cleaves into its active form at the cell surface[447]. MT1-MMP also cleaves pro-TNFα into active TNFα, or inactivates complement protein C3, or interleukin (IL)-8, indicating an important role in cytokine processing to modulate inflammation[448,449]. Moreover, MT1-MMP plays a role in signal transduction through cellular receptors and membrane protein processing, and MT1-MMP knockout mice are unviable after one month of age due to impaired collagen turnover[448,450]. Furthermore, it has a prominent role in cell migration in various cell types, which depends on its protein-protein interactions through the MT1-MMP cytoplasmatic tail and is independent from its catalytic activity[451,452]. Take together, these data reinforce the importance and complexity of MT1-MMP in multiple homeostatic functions and in development.

Among its physiological functions, MT1-MMP cleaves APP_{770} between positions N579 and M580 upon activation by concavalin A, releasing a sAPP fragment of 95 kDa (sAPP95) and an anchored CTF fragment of 30kDa (CTF-30)[453]. In addition, MT3-MMP, an MMP with the same APP cleavage site as MT1-MMP, cleaves APP within the Aβ sequence without modulating Aβ levels when it is overexpressed in HEK cells[454]. Demonstrating its anti-amyloid activity, MT1-MMP degraded exogenous Aβ added to COS cells overexpressing MT1-MMP and in brain slices of Tg2576 mice[442]. In addition, co-expression of C99 and a mutant MT1-MMP with an IC deletion, increased C99 and C83 levels in HEK cells, indicating a potential role of intact MT1-MMP in APP-CTF clearing dependent on the IC[455]. However, upon overexpression of MT1-MMP in HEK cells expressing APP_{swe}, there was an increase in Aβ levels[456].

Indeed, 5xFAD mice have upregulated MT1-MMP in the cortex and hippocampus at early stages of AD-like pathology, and this spatiotemporally correlated with an increase in C99 levels[444]. Moreover, MT1-MMP has APP cleavage activity, and half of this activity depends on interactions with MMP2, which is a soluble protein. MT1-MMP cleavage of pro-MMP2 at the cell surface activates the enzyme, and thus could facilitate MMP2 cleavage of APP. Furthermore, MT1-MMP simultaneously increased the levels of CTF-30 and C99,

suggesting that MT1-MMP-mediated cleavage of APP facilitates further β-secretase processing of CTF-30 to generate C99. At the same time, MT1-MMP overexpression in APP_{swe} overexpressing HEK cells rescues Aβ levels after BACE-1 inhibition, suggesting that it can compensate β-secretase activity upon BACE-1 inhibition[457]. Thus, although its physiological anti-amyloidogenic activity, MT1-MMP can exhibit amyloidogenic functions. However, the mechanisms behind MT1-MMP preference toward these different functions remain unclear. Other MT-MMPs, particularly MT5-MMP, have clear amyloidogenic functions and its pathological mechanisms are being elucidated in recent years.

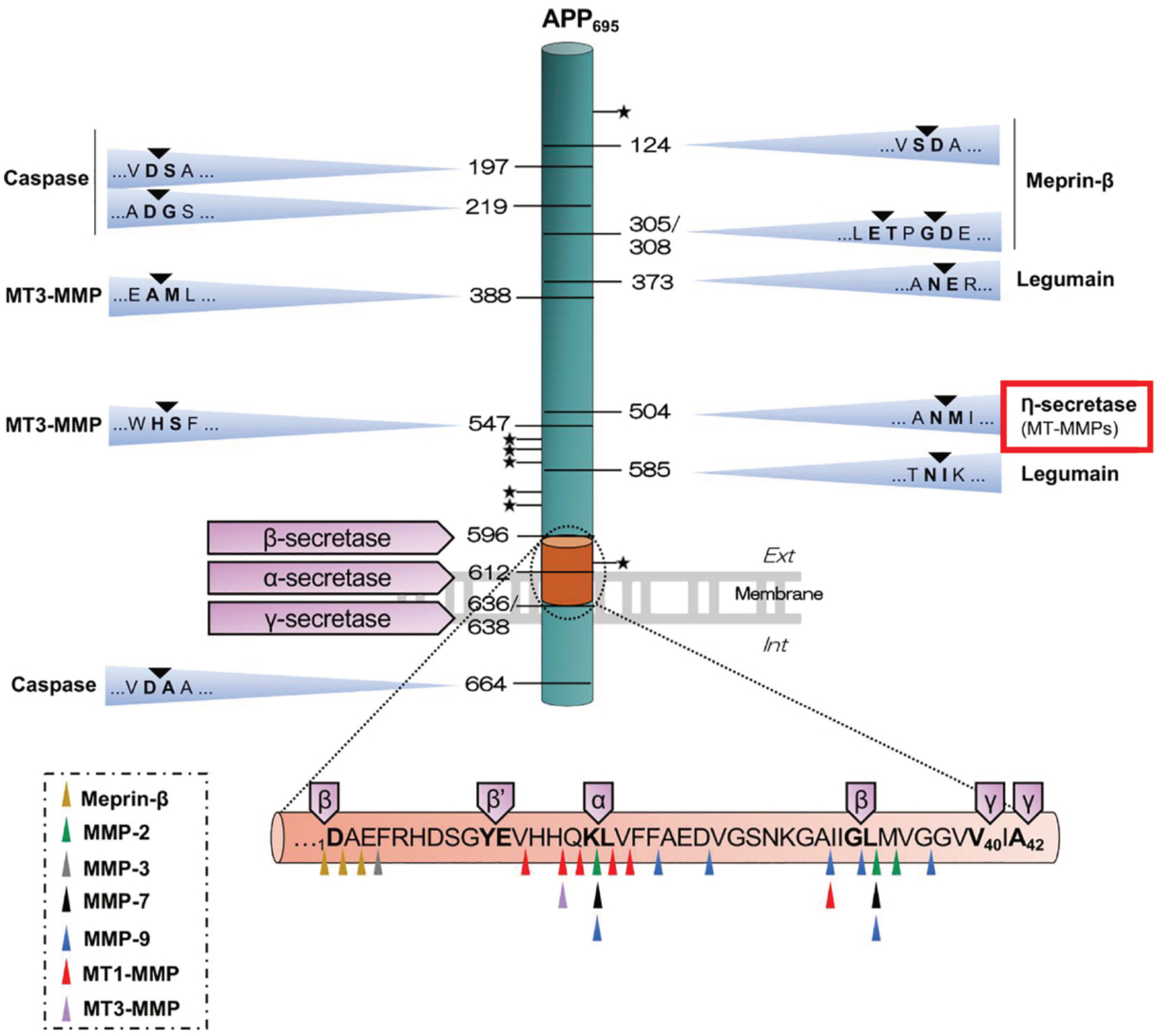

Figure 12. Scheme of different APP cleaving sites with its corresponding secretases. In addition to canonical APP secretases (α-, β-, and γ-secretase), various alternative proteinases can cleave APP at multiple sites. Caspase, meprin-β, legumain, and others (including other MMPs) produce multiple APP fragments. However, they are out of the scope of this thesis; thus, the focus will be on η-secretase (MT5-MMP or MT1-MMP). Both MT1-MMP and MT5-MMP cleave between N504 and M505 of APP_{695}, generating a soluble fragment known as sAPPη and an APP-CTF transmembrane fragment (η-CTF/CTF-30). CTF-30 can be further cleaved by canonical secretases. Indeed, $A_{η-α}$ and $A_{η-β}$ are N-terminal fragments resulting from the α- or β-secretase cleavage of CTF-30, generating either C83 or C99, respectively. Moreover, MT1-MMP also cleaves in multiple sites of the Aβ sequence, suggesting that it can degrade Aβ. Whether MT5-MMP maintains the same cleavage sites as MT1-MMP inside Aβ remains unknown. These newly described secretases represent new opportunities to modulate APP or its metabolites in the context of AD. Adapted figure[262].

3. MT5-MMP

Structure

Although MT5-MMP is becoming increasingly known for its role in AD, its physiological roles are less clear. It is a close homologue of MT1-MMP and shares the same structure of other MT-MMP. These are part of a bigger family, MMP, which are encoded by 24 genes in humans—and where MT5-MMP is encoded by the gene *MMP24*. MMP are zinc-endopeptidases with multiple physiological roles[457]. Structurally, MMP are heterogeneous, but all of them contain a catalytic domain with a pro-peptide and a signal peptide at the N-terminal. MMP usually contain also an hemopexin domain attached at the C-terminal of the catalytic domain by a linker (or hinge) region. Other MMP include more domains C-terminally from the hemopexin domain, and even some of them lack an hemopexin domain and incorporate a disintegrin domain[458]. In fact, the hemopexin domain is essential for substrate specificity and interaction with tissue inhibitors of MMP, but dispensable for normal catalytic activity[459,460(p2)]. The signal peptide at the N-terminal directs MMP toward secretion to act in the extracellular matrix in hippocampal rodent neurons[461]. During their trafficking, the pro-peptide maintains MMP inactive by a "cysteine-switch" bonded to the zinc in the active zone of the catalytic domain, which needs to be disrupted to trigger its catalytic activity[457,462]. MT-MMP are an exception to this since their activation occurs in the Golgi and they are active during their trafficking toward their target cellular compartment, allowing them to process intracellular substrates[463,464].

There are two types of MT-MMPs: the transmembrane type (where we find MT5-MMP) and the glycosylphosphatidyl inositol (GPI) type. The difference between these two subtypes is that the first contain a transmembrane and an intracellular domain, while the seconds have a GPI anchor. Transmembrane type MT-MMP share in common with other MMP the presence of a signal peptide and a pro-peptide at the N-terminal, which links with the catalytic domain. Next, there is a hinge region that connects the catalytic domain to an hemopexin domain. The last is connected to the transmembrane domain through a stem domain. And, finally, there is an intracellular domain that finishes with a PDZ binding motif at the cytoplasmatic tail[465].

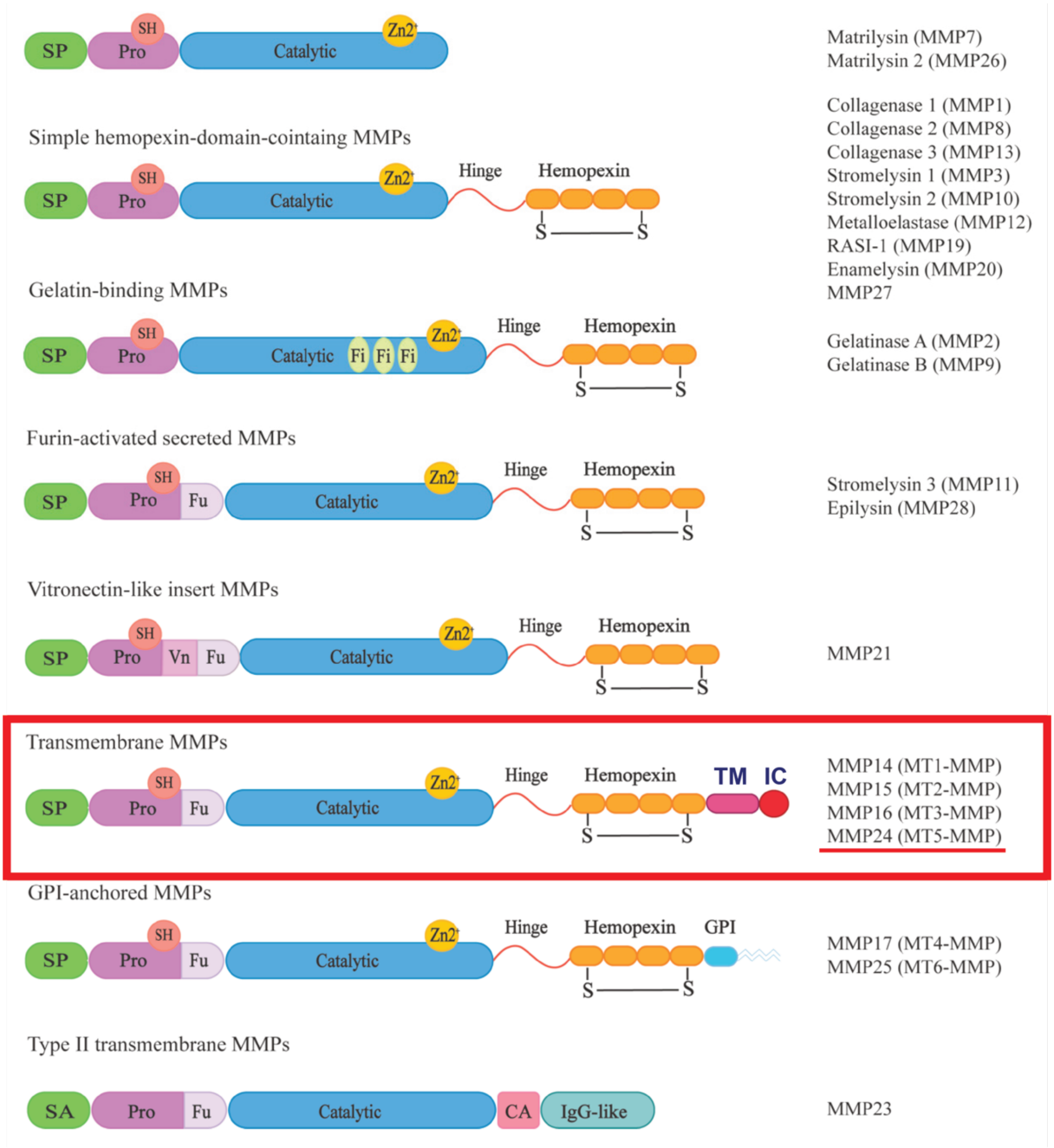

Figure 13. General structure of MMP subfamilies. All MMPs contain a catalytic domain preceded by a propeptide (Pro), signal peptide (SP) or signal anchor (SA), which are removed during maturation in the ER/Golgi traffic. In MT-MMPs (highlighted in red), the propeptide contains a thiol group (SH) and furin (Fu) cleavage side at the interface with the catalytic domain. Apart from Type II transmembrane MMPs, MMPs contain a zinc-binding site (Zn2+) in their catalytic domain. Following the catalytic domain, MMPs contain a hinge region linking to a hemopexin domain, with the exception of Type II transmembrane MMPs and matrilysins. MT-MMPs and GPI-anchored MMPs are the only MMPs containing membrane-bounding domains, whereas MT-MMPs are the only members of the family containing TM and IC (highlighted in dark blue). In the context of AD, these C-terminal domains are particularly important in MT5-MMP (underlined in red) and are the main focus of this thesis. Adapted figure[466].

The cytoplasmatic domain of MT-MMPs is crucial for their trafficking. Preservation of the LLY573 motif in MT1-, MT2-, and MT3-MMP is essential for their efficient internalization, and defective internalization of MT1-MMP impairs its physiological functions. Similarly, MT5-MMP lacks this motif, leading to less efficient

internalization[467]. MT5-MMP intracellular domain significantly differs from its close homologues, but it is also critical for MT5-MMP normal trafficking and recycling[465,467]. The C-terminal EWV PDZ-binding motif mediates MT5-MMP recycling back to the plasma membrane, which is dependent on Mint3. This interaction begins at the TGN, where MT5-MMP and Mint3 colocalize, and from where Mint3 facilitates MT5-MMP recycling to the cell surface[467]. Of note, as previously mentioned, Mint3 also colocalizes with APP and is also responsible for APP translocation from the TGN to the cell surface, what indicates that Mint3 could be a potential mediator of the recently described MT5-MMP modulation of APP and other physiological functions[233,234,468].

Physiology

From the MT-MMP subfamily, MT1-MMP is the best studied member, and, as detailed before, it has well-known physiological and pathological functions. As a close homologue of MT1-MMP, MT5-MMP shares structural characteristics, but with important functional and distribution differences. In adult rats, MT5-MMP is mostly expressed in the brain, particularly in the cerebellum. Moreover, it is also homogeneously expressed in multiple areas of the forebrain, and it was detected in membrane structures of hippocampal and cortical neurons in rats[469]. During rat embryonic development, MT5-MMP increments its expression, reaching maximum levels just before birth. MT5-MMP expression is particularly important in areas of high plasticity after birth, and it can be localized distributed around the brain parenchyma. However, after P14 its expression decreases significantly and remains restricted to areas of neuronal plasticity in the adult brain[470]. Accordingly, MT5-MMP cleavage of N-cadherin is necessary for the activation of neural stem cells and rapid progression through the cell cycle[471]. And its coordinated action with N-cadherin and ADAM-10, particularly in astrocytes, controls synaptogenesis after traumatic brain injury in the entorhinal cortex of rats[472].

Synapse modulation is an important function of MT5-MMP. However, knockout of MT5-MMP in mice results in morphologically normal individuals without obvious histopathological defects in the nervous system, suggesting potential compensatory mechanisms of other related proteins[473]. MT5-MMP knockout effects are nonetheless present in pathological contexts. Although apparently normal in phenotype, MT5-MMP knockout mice have altered dermal neuro-immune synapses as a consequence of inexistent MT5-MMP cleavage of N-cadherin. On one hand, in physiological conditions MT5-MMP knockout mice develop hyperinnervation of peptidergic sensory neurons in

the skin, which increases sensitivity to harmful thermal stimuli. On the other hand, upon cytokine-induced inflammatory conditions, MT5-MMP knockout prevented hyperalgesia in a mouse model of thermal pain[474]. Additionally, MT5-MMP knockout prevented aberrant axonal growth—thus, development of neuropathic pain—in mice with sciatic nerve injury[473].

MT5-MMP was also observed at the tips of axonal growth cones in immature primary rat hippocampal neurons, and it redistributed into synapses along maturation—where it may cleave cadherins or ECM molecules. Accordingly, MT5-MMP was enriched in rat brain-extracted synaptosomes[475]. In fact, MT5-MMP is more enriched in the post-synaptic fraction, but it has proteolytic functions at both sides of the synapse[476]. Before reaching the membrane, furin cleaves the pro-peptide domain of MT5-MMP in the TGN, allowing the protein to be activated during its trafficking[477]. Interestingly, in rat primary hippocampal neurons, MT5-MMP co-immunoprecipitated with AMPAR binding protein and glutamate receptor interaction protein, two post-synaptic density PDZ domain proteins. These two proteins mediated MT5-MMP membrane trafficking and synapse localization. The deletion of MT5-MMP C-terminal PDZ binding motif altered its membrane translocation and halted MT5-MMP colocalization with synaptic markers, demonstrating that MT5-MMP C-terminal domain is essential for its transport into synapses[475]. Noteworthy, the cytoplasmatic domain of MT5-MMP also modulates some of its recently discovered pathological roles in AD[455].

Pathological role in Alzheimer's disease

Despite the scarce information available of its physiological functions, MT5-MMP is gaining attention as an important component in AD pathogenesis[468]. MT5-MMP colocalizes with Aβ specifically in amyloid plaques around dystrophic neurites[469]. Additionally, MT5-MMP cleaves APP between N504 and M505 of APP_{695}, in a similar manner to MT1-MMP, in heterologous cell lines[453,454]. However, in AD mice, MT5-MMP cleaved APP at this site, known as the APP η-cleaving site, whereas MT1-MMP knockout was insufficient to alter APP η-cleavage. Comparatively to α- and β-secretases, η-secretase cleavage of APP generates an N-terminal fragment of 95kDa known as sAPPη (or sAPP95) and a transmembrane APP CTF named η-CTF (or CTF-30)[443,478]. In humans, η-CTF is particularly high in the CSF of AD patients with PSEN1 mutations, in sAD patients, and in demented Down syndrome individuals[479]. Upon BACE-1 inhibition in primary rat neurons, there was an increase in released Aη-α, a small peptide resulting

from the sequential cleavage of MT5-MMP and α-secretase. In a similar manner, ADAM10 inhibition resulted in Aη-β generation by MT5-MMP and β-secretase. Notably, both Aη-β and Aη-α impaired normal synaptic activity and impaired LTP *ex vivo*[480]. Indeed, knocking out MT5-MMP in a 5xFAD mouse model of AD (5xFAD$^{MMP24-/-}$) restored normal LTP levels compared to WT mice, altogether indicating an important participation of MT5-MMP in AD-related impaired synaptic plasticity[443].

Increased immunodetection of synaptic markers corroborated a preserved synaptic network in 5xFAD$^{MMP24-/-}$ mice, which probably facilitated an intact LTP despite the presence of fAD mutations in this animal model. Moreover, knocking out MT5-MMP had an impressive effect on other neuropathological hallmarks associated to 5xFAD mice. Specifically, MT5-MMP knockout reduced C99 and Aβ levels, together with a decrease of respectively 66% and 74% of the number of amyloid plaques in the hippocampus and neocortex of 5xFAD$^{MMP24-/-}$. This was concomitant with a decrease of 70% and 90% in GFAP immunostaining, and a decrease in the number of Iba1+ microglial cells around amyloid plaques of 67% and 47% in the same brain areas. The overall amelioration of AD symptomatology was translated into preserved cognitive performance in 5xFAD$^{MMP24-/-}$ mice compared to WT, reflected in improved learning in behavioral tasks. Therefore, the effect of knocking out MT5-MMP in 5xFAD mice extended to plaque formation, neuroinflammation, synaptic network preservation, and cognitive performance—that is, the main pathogenic hallmarks of AD[443,481].

Although significantly diminished, sAPP95 persisted in 5xFAD$^{MMP24-/-}$ mice, suggesting that alternative η-secretases can partially compensate MT5-MMP knockout effects in APP processing in mice. However, inactivation of the catalytic domain of MT5-MMP eliminated sAPP95 in human heterologous cells expressing APP_{swe}, while intact MT5-MMP generated the 95kDa band corresponding to APP η-cleavage. In addition, APP co-immunoprecipitated with MT5-MMP in the same cell model, which demonstrates direct or indirect physical interactions between MT5-MMP and APP[443]. Similarly to APP, MT5-MMP interacts with Mint3 through its PDZ binding motif at its cytosolic tail[467]. This could favor the conjoint internalization of MT5-MMP and APP into the same cellular organelles. In fact, APP metabolites detected with 6E10 antibody colocalize with MT5-MMP in early endosomes in HEK cells with APP_{swe}[481]. Sorting of MT5-MMP and APP metabolites into endosomal compartments might facilitate η-CTF translocation into exosomes which later neurons endocytose, which could be an additional mechanism for

amyloid spread[482]. In this context, in HEK cells overexpressing C99, the deletion of MT5-MMP intracellular domain (IC) reduces C99 localization in early endosomes, while the deletion of the extracellular domains of MT5-MMP—thus, only transmembrane domain (TM) and IC remaining—increases C99 presence in the same organelles[455].

How MT5-MMP IC and APP exactly interact is yet unclear, but the specific functions of MT5-MMP specific domains in APP metabolism are starting to be elucidated. Further than being just an η-secretase, the deletion or disruption of MT5-MMP catalytic domain was ineffective in reducing the levels of C99 or Aβ in HEK cells overexpressing C99. In fact, only the deletion of both MT5-MMP TM and IC or only IC significantly decreased both C99 and Aβ. In an opposite manner, following the same experiment, MT1-MMP IC deletion increased C99 levels. Interestingly, the high homology in the amino acid sequence of both MT1-MMP and MT5-MMP changes in the IC, where it decreases to a 20% sequence identity. Thus, specific amino acids in MT5-MMP IC might be responsible for C99 metabolization. This aligns with the differences in C99 processing pathways depending on the presence of MT5-MMP variants lacking specific domains. Upon treatment with Bafilomycin A1 (BAFA1), an inhibitor of the autophagolysosomal pathway, or DAPT, a γ-secretase inhibitor, C99 levels increased in HEK cells co-expressing C99 and a variant of MT5-MMP containing only the TM and IC. Contrary, the expression of MT5-MMP lacking TM and IC or only the IC failed to increase C99 levels upon BAFA1 or DAPT treatment. Therefore, appointing MT5-MMP TM and IC as key components of MT5-MMP in favoring C99 trafficking within endolysosomal compartments and facilitating γ-secretase cleavage, enhancing Aβ production[455]. Taken together, MT5-MMP TM and IC modulate C99 by promoting its translocation into specific cellular compartments, stimulating its amyloidogenic processing. The primary aim of this thesis was to elucidate the role of MT5-MMP TM and IC in C99 modulation using multiple MT5-MMP variants incorporating mutations in both domains. And, finally, generate synthetic peptides mimicking MT5-MMP variants with anti-amyloidogenic potential.

4. Peptide therapeutics

Deep molecular understanding of pathogenic proteins represents an opportunity to engineer therapies relying on some of their unique properties while avoiding its pathogenic mechanisms. In the early XXth century, the discovery and purification of insulin to treat diabetes paved the way to use peptides with therapeutic objectives. Globally, more than 400 peptide-based drugs are currently under clinical development and 60 are already approved for human use[483]. State-of-the-art technologies produce synthetic or recombinant peptides mirroring naturally occurring peptides that can overcome their low delivery efficacy and tissue/cellular penetrance. Thus, today it is possible to design peptides to preserve or enhance specific desired functionalities, while bypassing their limitations.

Aggregation of toxic peptides is a major pathogenic hallmark in multiple neurodegenerative diseases, and peptide interference is an efficient strategy to block Aβ fibril formation. A peptide derived from the prion protein coupled to a portion of NCAM1 impaired Aβ fibril formation, and the substitution of the prion protein part with a polycationic Aβ region maintained a similar function. Moreover, both peptides equally increased cell viability of N2a neuroblastoma cells, demonstrating the potential of producing peptides that retain specific functions of *a priori* toxic proteins in disrupting Aβ aggregation and toxicity[484]. Following a similar approach, an hexapeptide inspired in Aβ42 self-recognition component altered Aβ42 aggregation capacities, and treatment with this peptide resulted in increased cell viability in neuroblastoma cells exposed to Aβ42[485]. The efficacy of peptide-based anti-amyloid strategies expands to *in* vivo models, and systemic intraperitoneal injection of amylin short sequence peptides reduced amyloid pathology, neuroinflammation, and synaptic and behavioral deficits in 5xFAD mice[486]. Overall, peptides that reflect specific parts or domains of certain proteins, even proteins considered to be harmful, modulate pathogenic mechanisms leveraging on their physicochemical properties. Chemical modifications or addition of cell penetrant agents can further expand the use of peptides by increasing their intracellular presence in target tissues, increasing their efficacy. In the context of AD, peptides based on proteins involved in APP metabolism and conjugated with vectors that facilitate BBB crossing could represent a novel therapeutic strategy to regulate amyloidosis. Moreover, pre-screening of functional peptides in human *in vitro* neuronal models could improve their translational potential to be further developed *in vivo*.

5. Induced pluripotent stem cells

Overview

Limited access to human material has been a major burden to study human diseases in a human context. Drug discovery relying only on animal models leads to extended clinical failures during drug development in diseases occurring exclusively in humans (like AD)[487]. Human models were reduced to *in vitro,* or *ex vivo* models with tissue coming from restricted sources, like biopsies, *post-mortem* tissue, or sample donations. Therefore, apart from a material constraint, ethical implications in the use of human models confined them to very specific conditions. Differentiation of embryonic stem cells facilitated obtaining certain cell types difficult to access, like brain cells, without invasive methods. However, technical challenges, ethical concerns, and social stigma marginalized the use of these techniques in disease modeling.

This situation changed upon the development of induced pluripotent stem cells (iPSC), a technology based on the reprogramming of differentiated somatic cells into a pluripotent-like state using overexpression of defined transcriptional factors[488]. Originally, human fibroblasts were retrovirally transduced with *Oct3/4*, *SOX2*, *KLF4*, and *c-MYC* (the so-called Yamanaka factors). Continued expression of the Yamanaka factors reprogrammed differentiated cells into cells with self-renewal capacity, expression of pluripotency markers, and which could differentiate into specialized cells from the three embryonic germ layers[489]. Nowadays, human iPSCs (hiPSCs) can be obtained from most somatic cell types, and new reprogramming techniques with non-integrating methods broaden their potential[490]. Nevertheless, disease modeling and drug screening remain the two major applications of hiPSCs in neurodegeneration research.

Human *in vitro* brain models

Brain tissue scarcity has largely limited the study of both neurodevelopment and neurodegenerative diseases in human contexts, mostly relying on animal models. The arrival of hiPSC overcomes this constraint, as it can be a potential unlimited source of any type of brain cell. This allows to model specific cell types or brain areas using mono- or co-culture models, including microfluidic-based co-culture systems, as well as self-organizing 3D models (organoids). Monoculture models refer to specific cell type culture with high purity, avoiding undesired cell types. Using isolated cell types allows to investigate cell-autonomous mechanisms in specific contexts, giving a better

understanding of the role of specific cell types in specific physio or pathological contexts[167,386,491]. However, certain cells benefit from the presence of other supportive cell populations in culture, and these supportive cells are sometimes necessary for specific cellular functions. Regarding neurons, the presence of astrocytes promotes key neuronal physiological functions (*i.e.* synaptogenesis, synaptic activity, cell attachment, etc.) necessary to model certain pathologies[492,493].

Co-cultures of neurons and astrocytes are a recurrent method in hiPSC-derived neuronal models. In early phases of hiPSC-derived neuronal models, rodents were the main source of astrocytes used in co-cultures, particularly rats[494,495]. Commercially available primary human astrocytes were also commonly used, but a more limited and costly source than rodent astrocytes[386]. Recent development of increasingly easier protocols to produce hiPSC-derived astrocytes facilitates generating human models of neuron-astrocyte co-culture[496–498]. However, primary rodent astrocytes remain the more reproducible option for hiPSC-derived neuronal maturation. In addition to astrocytes, newly described methods to generate other abundant CNS cell types are leading to more complex human brain models[499]. But, despite the increasing complexity of hiPSC-based models, monolayer cultures lack 3D organization, which is particularly important in the human brain.

One of the biggest advancements in the hiPSC field was the definition of a protocol to generate 3D self-organized brain-like structures named brain organoids[500]. Since then, brain organoids are becoming increasingly accessible and reliable, representing a more complex, yet more heterogenous, model than classical 2D monolayer cultures[501]. Cerebral organoids reproduce CNS development *in vitro*, which can be controlled using different factors during the differentiation/maturation process to obtain organoids modelling specific areas of the brain with different components[500,502,503]. Chemically modulated differentiation is an undirected approach used in both 3D and 2D models, and usually generates heterogeneous cell populations[504,505]. Certain applications benefit from cell type heterogeneity in culture, but disease modelling for certain drug testing requires homogeneous cultures with well-defined cell populations.

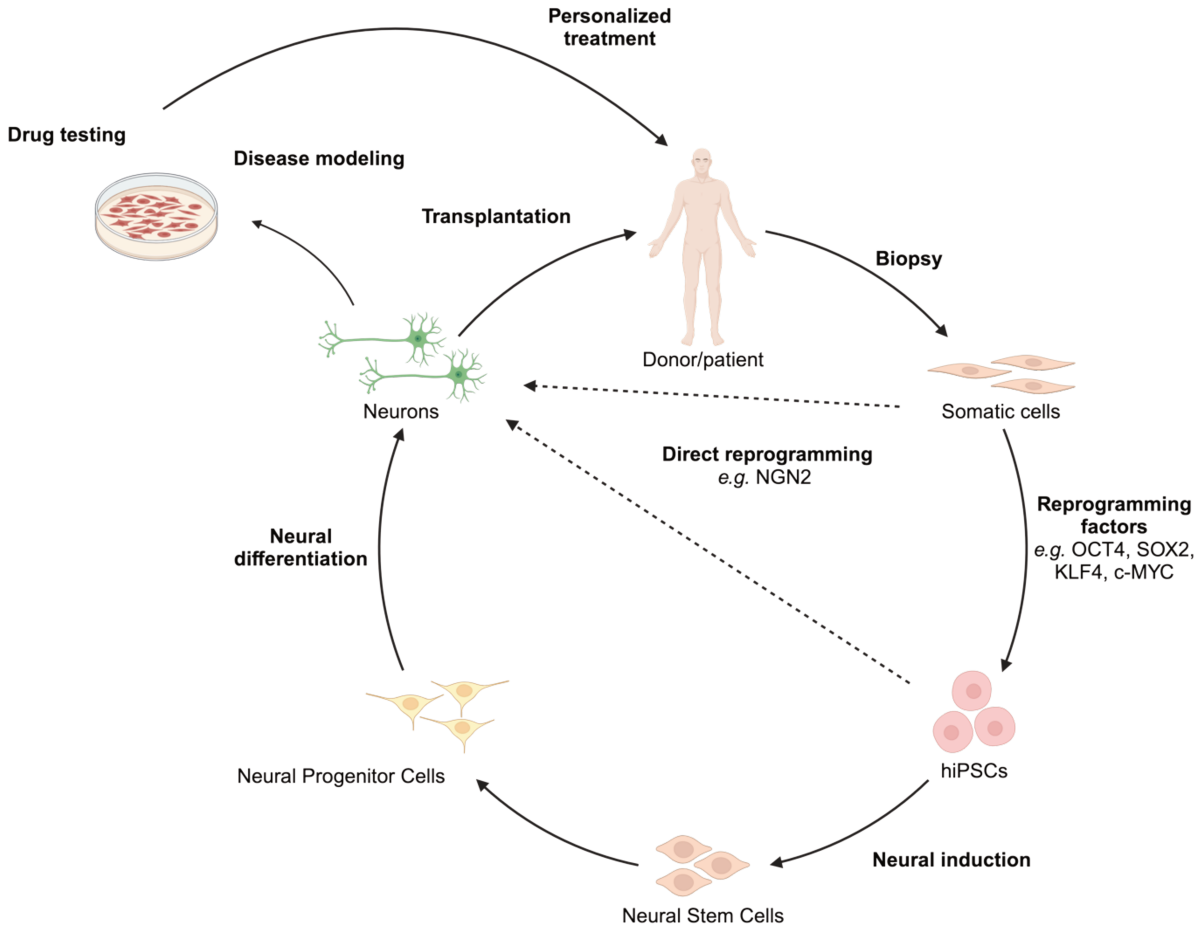

Figure 14. Current and potential applications of hiPSC. Tissue samples from patients are reprogramed into hiPSCs via the forced expression of reprograming factors. The classical Yamanaka factors are *OCT4*, *SOX2*, *KLF4*, and *c-MYC*. Importantly, direct transdifferentiation has increasingly gained prominence as a strategy for obtaining cell types that recapitulate certain diseases with genetic and epigenetic profiles similar to those of the original donor. Once reprogramed into hiPSCs, they can differentiate into any cell type. Focusing on the CNS, hiPSCs are also suitable for direct reprograming into neurons or other brain cells, or they can undergo a stepwise differentiation program based on external cues using supplemented media. Typically, these media are specific to hiPSC differentiation into specific cell types (*e.g.* NSCs), and they are combined with other media to continue the differentiation process. By either direct reprograming or stepwise differentiation, the final cell product (*e.g.* neurons) can be applied in multiple ways. In mono- or co-culture formats, hiPSC-derived cells represent an important tool for defining human-specific phenotypes through disease modeling, validating drug candidates in human contexts, performing cell therapy, or validating the efficacy of a defined drug treatment before application to the patient.

Direct reprogramming

Overcoming cell heterogeneity is a major challenge in the use of hiPSC-derived neuronal models. Differentiation using induced overexpression of certain transcription factors, also known as direct reprogramming or direct conversion, is an alternative to defined medias acting through extrinsic signaling. These techniques usually yield higher purity of specific cell types (*e.g.* highly pure neuronal populations without the presence of astrocytes) in culture without the need of purification methods[494]. Additionally, direct

reprogramming can convert differentiated cells into other target cell types without intermediate steps, opening new opportunities for treatment of neurological diseases[506,507]. Thus, direct conversion is a flexible tool that overcomes heterogeneity produced in differentiation methods based on supplemented medias.

Direct reprogramming is now extensively used to generate hiPSC-derived induced neurons (iN) rapidly, efficiently, and robustly from hiPSCs. Induced overexpression of neurogenin-2 (NGN2) in hiPSC generates mature functional neurons in less than three weeks when combined with primary rat astrocytes. After induction of NGN2 expression, hiPSC-derived neurons expressed neuronal markers MAP2 and Tuj1 in one week and had active synapses within two weeks. Moreover, it produced a 100% yield of neurons. This represented a remarkable advancement compared to supplemented medias, which needed between seven and twelve weeks to have functional synapses and produced heterogeneous cultures[494]. However, iN are also subject to certain limitations, and current methods generate different neuronal subtypes with different molecular signatures. Days of NGN2 overexpression, co-culture with astrocytes, or use of different clones all affect iN transcriptomic signature[498,508]. Therefore, the use of iN requires a thorough consideration, as any other disease models, particularly if specific neuronal subtypes need to be studied. Taken together, the advantages of rapidly obtaining pure neuronal cultures to be used in mono- or co-culture formats currently makes NGN2 direct reprogramming the most reliable 2D disease modeling approach to test neuron-targeting drugs.

Highly pure iN cultures open the door to study the effect of genetic or pharmacological modulation specifically on neurons. Combining direct conversion of hiPSC and CRISPR-Cas9 facilitates generating specific knockout neuronal models. For instance, knocking out DPYSL2-B/CRMP2-B in hiPSCs—to then perform direct reprogramming into neurons—confirmed its role in altering several neuronal pathways relevant to multiple psychiatric diseases[509]. Following the same approach, FIP200 knockout altered neuronal homeostasis and electrical activity, showing decreased autophagy and hyperactive glutamatergic synapses[510]. Moreover, iN can be useful to validate pathogenic mechanisms arising from alterations observed in patients and associated to neurological diseases. CRISPR-mediated mutation of a gene associated to autism, DDX53, demonstrated it is insufficient to induce synaptic deficits in neurons[511]. And CRISPR-mediated insertion of APP_{swe} led to decreased dendritic mitochondrial density and length, and AMPK

overactivation in iN[512]. In a model of encephalopathy through introduction of SCN3A mutations, chemical selective blocking of Nav1.3 sodium channel reverses aberrant neuronal firing[513]. Thus, iN provide a simple, but reliable, methodology to generate specific gene modifications that recapitulate certain pathological mechanisms of neurological diseases to then perform drug screening and validation.

Drug testing

Reduced difficulty and variability of direct reprogramming-based protocols spans the use of high-throughput (HTS) and high-content screening (HCS) methodologies for drug screening using human brain cells. In hiPSC, introducing an inducible NGN2 expression cassette in the safe integration site AAVS1 reduced the differentiation protocol to a two-step 21-day protocol. The scalability and low variability of this model permitted its application into a HCS platform to screen multiple compounds of the Library of Pharmacologically Active Compounds to identify tau-lowering compounds[514]. Reproducibility among different laboratories is also indispensable to establish human neuronal models. Differently to supplemented media methods, iN can be frozen at early-mid stages of the differentiation process, increasing even more its scalability. Using this technique, it was possible to perform a HTS and HCS-based phenotypic screening assay to evaluate neurotoxicity through axonal outgrowth, demonstrating iN can be used in large-scale drug-discovery platforms[515].

When combining multiple analytical tools, iN can provide insights into effects of newly developed drugs on pathological processes occurring in neurons, but also of drugs in clinical investigation. For instance, iN coming from a patient with a mutation related to FTD revealed ruboxistaurin and enzastaurin decreased tau phosphorylation in an HCS-based analysis combined with proteomic profiling[516]. Indeed, iN are applicable to several analytical tools, and they have been used for a wide range of omics and physiological techniques. Of interest, multielectrode arrays (MEA) are becoming a complementary tool to assess neuronal activity at large scale formats. In a cohort of phenotypically different patients suffering epileptic seizures from different origin, combining patient-derived iN with MEA revealed mutation-specific neuronal network alterations, and further validated anti-seizure drugs for specific phenotypes[517]. Overexpression of ASCL1/DLX2 generates GABAergic induced neurons, which can be mixed with glutamatergic iN at different rations to investigate network responses to different spatio-temporal stimuli using MEA to understand the effects of excitation/inhibition rations on network

synchronicity[518]. Also in MEAs, iN can be stimulated to perform LTP experiments, which gives access to a human platform to delve deeper into synaptic plasticity[519]. In addition, iN can be seeded in single-cell formats to study cell morphology, synapse formation, and disease-specific changes in neuronal excitability, reveling disease-associated single-cell electrophysiological properties[520]. Overall, increased reproducibility, scalability, and simplicity of hiPSC-derived neurons production paves the way to their use as standard modeling for drug screening and validation in combination with HTS, HCS, and omics techniques. However, increasing screening capacity requires adapted systems to generate and analyze high-dimensional data while maintaining biological significance.

6. Generation and analysis of high dimensional data

Technological advances in the analysis of multiple types of models facilitate the acquisition of every time more phenotypical parameters. This grants access to a better understanding of physiological and pathological mechanisms at various biological levels. Increased computational power, performance, and efficiency have facilitated the development of tools to generate the so-called "big data", which are now accessible to the scientific community and will enhance biomarker and drug discovery[521,522]. But these advantages come at the cost of more complex analytical tools to translate the findings into biological phenomena[523].

Classical techniques to identify changes in genes, expression patterns, protein levels, or synaptic activity are being complemented, and sometimes substituted, with approaches that analyze whole-genome, whole-transcriptome, whole-cell/tissue proteome, or multiple cells electrical activity at the same time in an automatized manner. Multi-factorial diseases without a clear known etiology will largely benefit from the integration of unbiased high-dimensional data, as now it is possible to analyze the same pathological mechanisms at different levels, revealing insights into the pathological processes within a spatiotemporal frame[524].

High-content screening

With the improvement of microscopy imaging and automation has come the development of HCS. Thanks to its automatization possibilities, HCS augments the throughput of experiments, which favors the screening of several experimental conditions. Thus, although different concepts, HCS and HTS are closely related. And HTS in combination with HCS are widely used for drug discovery. In addition, HCS can provide high-resolution images to the spatial resolution of the light-diffraction limit. Therefore, HCS currently goes beyond focusing on morphological properties and includes a wide array of tests in combination with immunofluorescence or functional-based assays[525].

Merging multiple phenotypic assays in different biological models allows the validation of drug candidates using HCS. In a HCS of different chemical compounds, hippeastrine hydrobromide and amodiaquine dihydrochloride dihydrate prevented ZIKA virus infection of neuronal progenitors in different human 2D and 3D neuronal progenitor cultures. Moreover, hippeastrine hydrobromide prevented ZIKA virus propagation in the adult mouse brain, remarking the feasibility of HCS in drug validation[526]. But HCS

extends to multiple screening assays, and specific experimental setups are also useful to elucidate protein function. A screen of the human kinome using siRNA revealed multiple kinases involved in tau phosphorylation in a human cell line[527]. And, similarly, a screen of 597 shRNA identified new synaptogenesis regulators in rodent primary neurons[528]. In addition, HCS is adaptable to screen for synaptotoxic metabolites, which is a particularly important application for AD research. In mouse primary hippocampal neurons, treatment with 3xTg mice brain homogenates uncovered synaptotoxic properties of high and low molecular weight fractions—even after immunodepleting Aβ—shown by colocalization of pre- and postsynaptic markers. In fact, HCS can be used in protein colocalization and subcellular distribution in more complex assays. In primary rat hippocampal neurons, a proximity ligation assay (PLA) detected interactions between tau and bridging integrator 1, a sAD risk factor involved in tau pathology. The inclusion of HCS allowed the evaluation of approximately 1100 compounds on their modulation of PLA positive spots (*i.e.* less than 40nm proximity between both proteins). Additionally, segmentation and spot-detection algorithms facilitated the analysis of the distribution of PLA spots exclusively in neurites, highlighting the importance of adequate image and data analysis workflow after image acquisition[529].

Data analysis and machine learning

Recent development on HTS and HCS has increased the complexity of their output datasets. Nowadays, HCS-generated datasets are multidimensional—*i.e.* they include multiple features in several conditions. These need advanced analytical tools to translate them into biological significance, and classical statistical methods are limited to analyze complex multidimensional data. The advent advances of machine learning overcome these limitations, providing an interface between mathematical modeling and biological interpretation[530]. Thus, machine learning is becoming a central approach in big data analysis in biomedical research.

Machine learning is a set of mathematical techniques which use algorithms to recognize and predict data patterns[531]. Supervised and unsupervised learning are two major categories in machine learning. Supervised learning relies on previously labeled data to train the algorithm to find patterns in the data that accurately predict the labels, and the trained models are then used to label unseen data. For example, in a set of data containing certain properties of population A and population B, supervised learning is going to identify patterns in the features that relate to each population. Once trained, the

algorithm can predict if a sample with specific values in those properties belongs to population A or B. This is particularly useful in disease prediction and categorization, and opens the door to use available biomarkers as diagnostic tools for neurological diseases which are difficult to diagnose at pre-symptomatic stages, like AD. Indeed, the accuracy of various machine learning models was up to 72% to predict sAD in a cohort of patients[532]. This model was based on genetic variants, but it is possible to use multiple types of clinical data and combine them to improve model performance. In a cohort with non-demented, MCI, AD, and non-AD dementia individuals, a machine learning model could classify the patients in the four categories with a 77% accuracy, validated with neurologists. The algorithm could predict the different diagnostics based on an ensemble of demographic data, medical history, functional assessment, and neuropsychiatric tests[533]. However, the process of data labeling is tedious and both human- and time-consuming, making it difficult to apply in contexts where previous knowledge is unavailable.

The best approach in machine learning to classify unknown data is unsupervised learning, because it allows to elucidate hidden patterns in unlabeled data. It holds great potential to stratify patients when the trends that correlate the clinical data to the disease state are imperceptible for the medical professionals. In the context of AD, unsupervised learning algorithms help both differentiating normal cognitive people from AD patients and classifying AD patients into different AD subtypes. Using data from magnetic resonance imaging of the brain, an unsupervised learning algorithm could differentiate between healthy and AD individuals, taking into account only the most significant regions in the brain[534]. Moreover, unsupervised classification of AD patients—based on longitudinal neuropsychological tests and demographic data—detected a subtype of patients who were at high risk of developing AD within short periods of time[535]. In the same direction, a series of clustering methods were able to stratify AD patients with available data from the clinical history of the patients, demonstrating the potential of clustering methods to stratify AD patients to define targeted therapeutical strategies[536].

Clustering algorithms are useful to reduce data complexity, decreasing dimensionality and the number of observations. This helps to prioritize features that explain data variability, which technically and computationally simplifies the posterior analysis. With diagnostic purposes, reducing dimensionality of magnetic resonance brain imaging data with unsupervised clustering generated a simpler dataset to train a classifier that could

stratify AD patients[537]. Removing outliers is another approach to reduce the size and complexity of datasets while increasing its significance for modeling, and unsupervised clustering offers better detection efficiency than classical methods[538]. For instance, outlier detection and removal improved the accuracy from 63% to 76% of a machine learning algorithm for burn diagnostic imaging, and it improved feature extraction for image reconstruction[539,540]. Thus, unsupervised learning identifies outliers undetectable with statistical methods and reduces data complexity, facilitating posterior data analysis.

Bayesian statistics

Statistics model experimental data through mathematical tools to assess data variability, providing a quantitative output to translate the results into a biological meaning. New statistical approaches accompany the rise of big data, as in HTS and HCS set-ups, where popular methodologies are falling short. These come from new mathematical development, and also from previous strategies largely overlooked. Thomas Bayes described its theorem in the late XVIIIth century, but it was his friend Richard Price who published and promoted the Bayes theorem. Concurrently, Pierre Simon Laplace independently developed the Bayesian interpretation of probability, reproducing and extending Bayes work. But most of the statistics community ostracized Bayesian statistics until mid-XXth century, when some statisticians started to work with Bayesian frameworks to solve certain complex problems.

Frequentist statistics define theoretical mathematical models to fit experimental data and define the probability of occurrence of the data among multiple repetitions. This is the most popular approach in biology to infer population parameters from experimental data. However, frequentist statistics fall short in certain new data, and other methods outperform them and give a better and more understandable framework for data interpretation. Bayesian statistics are becoming increasingly popular in biology, particularly in handling multi-dimensional data and incorporating them in machine learning workflows. In recent years, Bayesian statistics is also gaining prominence in drug development. During the COVID-19 pandemic, Pfizer and BioNTech analyzed their vaccine candidate phase III clinical trials with Bayesian statistics to demonstrate that the probability of the vaccine efficacy being higher than 30% (the minimum requirement that the FDA dictated) was 99.99%[541]. This statistical approach granted them the FDA approval to commercialize the vaccine, which was later key in controlling the pandemia.

A Bayesian analysis starts stating a prior distribution that explains the pre-assumptions of the future experimental results. The prior distribution is often defined with previous data from similar experiments or with theoretical knowledge, which predicts data behavior. Once the results are available, the prior distribution model updates with the experimental data. The posterior distribution is the new model resulting from the combination of the prior distribution and the experimental data. Thus, it is the interface between the mathematical modeling and the biological interpretation of the data. Following this logic, an advantage of the Bayes approach is that a posterior distribution can become a prior distribution if another set of experiments is added to the analysis, facilitating a continuous update of experimental evidence[542].

The Bayes theorem defines the probability of an event as:

$$p(\theta|D,M) = \frac{p(D|\theta,M) \times p(\theta)}{p(D|M)}$$

$p(\theta|D,M)$: posterior probability

$p(D|\theta,M)$: likelihood

$p(\theta)$: prior probability

$p(D|M)$: marginal likelihood

Where $p(\theta|D,M)$ corresponds to the posterior probability of a value θ given a model M and data D. This is defined as the likelihood of the model M giving rise to data D, assuming a certain value θ, multiplied by the prior belief of θ, and divided by the probability of the data D occurring under the model M. According to this formula, the two marginal likelihoods are divided to calculate the probability of two models being different. The Bayes Factor is the value of this ratio, and it directly translates into the likelihood of the alternative or null hypothesis being more probable than its counterpart. In all, the parameters in Bayes provide a comprehensive framework to interpret the probability of experimental hypotheses and extend the potential interpretations compared to classical frequentist approaches.

The recent FDA approval of anti-amyloid therapies that moderately slow cognitive decline in AD has raised certain optimism regarding limiting the burden that AD represents for the modern world. However, these new therapies remain ineffective in stopping the disease and imply a series of side effects that limit their clinical application. Thus, more effective and safer strategies could provide a better AD treatment approach. This thesis focuses on elucidating the possibilities of using MT5-MMP-based strategies to counteract certain pathological features of AD, further extending our previous work[455]. We developed MT5-MMP variants with mutations in the TM and IC to study their effects on C99 and Aβ levels in human *in vitro* models of C99 accumulation. Using an array of well-established biochemical techniques combined with innovative microscopy and statistical tools, we established the importance of certain amino acid groups in the MT5-MMP modulation of C99. Given these findings, we developed a vectorized synthetic peptide that reduces C99 levels in human cells overexpressing C99. Overall, this thesis presents a series of important advances in 1) understanding the roles of MT5-MMP TM and IC in AD, 2) uncovering the importance of intracellular trafficking in defining C99 fate, and 3) validating MT5-MMP-based strategies as viable alternatives to target amyloidosis in AD.

OBJECTIVES

The approval of new anti-Aβ drugs in multiple countries has shed light on the future of AD therapeutics. However, the limited efficacy of these drugs tempers the enthusiasm surrounding their potential impact. Extensive research on AD pathogenesis has revealed new targets that can provide complementary or alternative therapeutic strategies for AD treatment. In the last decade, MT5-MMP has become increasingly attractive because of its various roles in multiple pathogenic pathways associated with AD. MT5-MMP is a proteinase that cleaves APP and may be involved in processing neuroinflammatory mediators. However, apart from its catalytic activity, MT5-MMP TM and IC are involved in C99 and Aβ accumulation via non-catalytic mechanisms. In the context of AD, these unique properties broaden the range of opportunities to investigate the potential therapeutic strategies based on MT5-MMP. In my thesis, I studied 1) the impact of MT5-MMP deficiency on physiological parameters of human neural cells, and 2) how modifications in the structure of various MT5-MMP domains could decrease or stabilize the toxic accumulation of C99 and Aβ. Accordingly, my PhD was developed to address four specific objectives:

Objective 1. Investigate the effects of MT5-MMP deficiency in human neurons and astrocytes. To do so, I explored the phenotypical and physiological consequences of MT5-MMP depletion in hiPSC-derived neurons and astrocytes to evaluate the potential of MT5-MMP modulation as a therapeutic strategy. This resulted in a publication as second author (*Article 1*, page 86).

Objective 2. Identify specific sets of MT5-MMP amino acids involved in the control of C99 and Aβ accumulation. To that end, I assessed the effects of introducing specific mutations in MT5-MMP TM and IC in order to identify the key amino acids involved in their pathogenic properties. I studied the processing pathways involved in C99 metabolization in the presence of MT5-MMP variants and their relationships with C99 subcellular distribution.

Objective 3. Translate MT5-MMP variants with anti-amyloidogenic properties into a potential therapeutic agent. I aimed to transform our findings on anti-C99/Aβ properties of certain MT5-MMP variants into a therapeutic strategy. We generated a vectorized synthetic peptide that mimics a specific MT5-MMP variant to modulate C99 *in vitro*. The last two objectives resulted in a pre-print and future publication as a first author (*Article 2*, page 106).

Objective 4. Optimize a drug testing platform to validate potential therapeutic agents in human neurons. Finally, I also focused on implementing/optimizing a reliable hiPSC-based neuronal model that, ultimately, could become a useful translational platform to test peptide candidates in a disease-relevant human setting.

RESULTS

Artcile 1: Deficiency in MT5-MMP Supports Branching of Human iPSCs-Derived Neurons and Reduces Expression of GLAST/S100 in iPSCs-Derived Astrocytes.

Nikita Arnst, **Pedro Belio-Mairal**, Laura García-González, Laurie Arnaud, Louise Greetham, Emmanuel Nivet, Santiago Rivera, Alexander Dityatev

Cells. 2021

DOI: 10.3390/cells10071705

Our group has consistently demonstrated the implication of MT5-MMP in AD. Among other studies, we demonstrated that knocking out *MMP24* in the 5xFAD mouse model hinders the development of AD[443,481]. Apart from strikingly reducing the number of Aβ plaques in the cortex and hippocampus, the lack of MT5-MMP reduced gliosis and glial IL-1β expression, suggesting a potential independent role for MT5-MMP in amyloidogenesis and neuroinflammation. These beneficial effects promoted the preservation of synaptic networks, LTP, and cognitive performance[443]. In a follow-up study, our team further confirmed these observations in the frontal cortex, which is a brain area particularly affected in AD. In addition to providing a better understanding of the role of MT5-MMP in APP proteolysis, these results indicate the involvement of MT5-MMP in APP trafficking[481]. Thus, MT5-MMP is a new major proteinase in AD with functions that extend beyond APP proteolysis.

Limitations in the translation of rodent models into human contexts have limited drug discovery for AD, a disease specific to humans with no equivalent in mice[543]. To better understand the potential of MT5-MMP manipulation in AD, we aimed to reproduce the deletion of MT5-MMP in a human context to better understand the effects of MT5-MMP in human cells. We generated neurons and astrocytes from hiPSCs using a multistep protocol based on supplemented media. Here, I participated in the development of differentiation protocols and MT5-MMP knockout hiPSC lines, generated mature neurons to assess synaptogenesis, performed patch-clamp to determine the physiological phenotype of MT5-MMP knockout neurons, and investigated the expression of astrocytic markers in astrocytes without MT5-MMP.

Overall, we confirmed that MT5-MMP deletion changes the phenotype of hiPSC-derived neurons and astrocytes. Although *MMP24*$^{-/-}$ neurons preserved their normal differentiation capacity, they exhibited increased dendrite arborization. However,

synaptic immaturity impeded the proper assessment of the effects of MT5-MMP deficiency on synaptic network development and activity. On the other hand, we revealed the morphological consequences of *MMP24* deletion in astrocytes, which were probably linked to changes in the expression of key astrocytic markers. These data confirm the role of MT5-MMP in dendritic arborization in a human context and uncover the effects of MT5-MMP deficiency on glial development, highlighting the importance of considering the impact of MMP depletion in pathophysiological models. Therefore, more fine-tuned approaches are needed to modulate MT5-MMP in AD pathogenesis.

This work was published in Cells and was done in collaboration with the Molecular Neuroplasticity team from the German Center for Neurodegenerative Diseases (DZNE) in Magdeburg.

cells

MDPI

Article

Deficiency in MT5-MMP Supports Branching of Human iPSCs-Derived Neurons and Reduces Expression of GLAST/S100 in iPSCs-Derived Astrocytes

Nikita Arnst [1], Pedro Belio-Mairal [1,2], Laura García-González [2], Laurie Arnaud [2], Louise Greetham [2], Emmanuel Nivet [2], Santiago Rivera [2] and Alexander Dityatev [1,3,4,*]

1 Molecular Neuroplasticity, German Center for Neurodegenerative Diseases (DZNE), 39120 Magdeburg, Germany; arnst.nikita@yandex.ru (N.A.); pedro.BELIO-MAIRAL@univ-amu.fr (P.B.-M.)
2 Inst Neurophysiopathol, CNRS, INP, Aix Marseille Université, 13385 Marseille, France; laura.garcia-gonzalez@outlook.es (L.G.-G.); laurie.ARNAUD@univ-amu.fr (L.A.); louise.GREETHAM@univ-amu.fr (L.G.); Emmanuel.NIVET@univ-amu.fr (E.N.); santiago.rivera@univ-amu.fr (S.R.)
3 Center for Behavioral Brain Sciences (CBBS), 39106 Magdeburg, Germany
4 Medical Faculty, Otto-von-Guericke University, 39120 Magdeburg, Germany
* Correspondence: alexander.dityatev@dzne.de; Tel.: +49-391-67-24526

Abstract: For some time, it has been accepted that the β-site APP cleaving enzyme 1 (BACE1) and the γ-secretase are two main players in the amyloidogenic processing of the β-amyloid precursor protein (APP). Recently, the membrane-type 5 matrix metalloproteinase (MT5-MMP/MMP-24), mainly expressed in the nervous system, has been highlighted as a new key player in APP-processing, able to stimulate amyloidogenesis and also to generate a neurotoxic APP derivative. In addition, the loss of MT5-MMP has been demonstrated to abrogate pathological hallmarks in a mouse model of Alzheimer's disease (AD), thus shedding light on MT5-MMP as an attractive new therapeutic target. However, a more comprehensive analysis of the role of MT5-MMP is necessary to evaluate how its targeting affects neurons and glia in pathological and physiological situations. In this study, leveraging on CRISPR-Cas9 genome editing strategy, we established cultures of human-induced pluripotent stem cells (hiPSC)-derived neurons and astrocytes to investigate the impact of MT5-MMP deficiency on their phenotypes. We found that MT5-MMP-deficient neurons exhibited an increased number of primary and secondary neurites, as compared to isogenic hiPSC-derived neurons. Moreover, MT5-MMP-deficient astrocytes displayed higher surface area and volume compared to control astrocytes. The MT5-MMP-deficient astrocytes also exhibited decreased GLAST and S100β expression. These findings provide novel insights into the physiological role of MT5-MMP in human neurons and astrocytes, suggesting that therapeutic strategies targeting MT5-MMP should be controlled for potential side effects on astrocytic physiology and neuronal morphology.

Keywords: Alzheimer's disease; human-induced pluripotent stem cells; disease modeling; neuronal differentiation; hiPSC-derived astrocytes; metalloproteinase; morphometry; whole-cell patch-clamp

check for updates

Citation: Arnst, N.; Belio-Mairal, P.; García-González, L.; Arnaud, L.; Greetham, L.; Nivet, E.; Rivera, S.; Dityatev, A. Deficiency in MT5-MMP Supports Branching of Human iPSCs-Derived Neurons and Reduces Expression of GLAST/S100 in iPSCs-Derived Astrocytes. *Cells* **2021**, *10*, 1705. https://doi.org/10.3390/cells10071705

Academic Editor: Claudia Spits

Received: 6 June 2021
Accepted: 1 July 2021
Published: 6 July 2021

Publisher's Note: MDPI stays neutral with regard to jurisdictional claims in published maps and institutional affiliations.

Copyright: © 2021 by the authors. Licensee MDPI, Basel, Switzerland. This article is an open access article distributed under the terms and conditions of the Creative Commons Attribution (CC BY) license (https://creativecommons.org/licenses/by/4.0/).

1. Introduction

Alzheimer's disease (AD) is a neurodegenerative brain disorder with no efficient cure to date, which is typically characterized by a progressive cognitive decline [1,2]. Many *in vitro* and *in vivo* studies have highlighted the BACE1-dependent abnormal formation and intracellular accumulation of amyloid β (Aβ) peptides as the initial cause of AD [3,4]. Therefore, BACE1 has been one of the most attractive targets for the treatment of AD for many years. Accordingly, multiple BACE1 inhibitors (MK8931, AZD-3293, JNJ-54861911, E2609, and CNP520) have been tested as potential therapeutic drugs to treat neurological diseases [5–7]. However, the high failure rate of clinic-step BACE1 inhibitor candidates

and their interference with the physiological processing of other substrates has stimulated searching for novel therapeutic targets in AD [8–10].

Matrix metalloproteinases (MMPs), enzymes controlling intracellular and extracellular amyloidogenic protein turnover, are associated with neurodegenerative diseases [11,12]. Recently, we shed light on MT5-MMP as just such a novel therapeutic target [12–14]. In good health, MT5-MMP is a multifunctional MMP with N-cadherin substrate specificity that is mainly expressed in developmental stages and remains high in adulthood in the hippocampus and cerebellum [15–18]. It may play a functional role in neural plasticity via interactions with the AMPA binding protein (ABP) and the glutamate receptor-interacting protein (GRIP) [19,20]. Besides, the localization of the metalloproteinase in filopodia at the tips of growth cones and in synaptosomes also supports the idea that MT5-MMP may regulate axon pathfinding and synapse remodeling [21,22]. MT5-MMP also regulates the activation of adult neural stem cells [23]. However, MT5-MMP is also relevant to disease, since it promotes interactions between neurons and mast cells through the cleavage of N-cadherin, required for the inflammatory response in a thermal pain model [24]. In addition, MT5-MMP was found around senile plaques in the post-mortem brains of AD patients [15]. Furthermore, the physical interaction of MT5-MMP with APP and increased production of Aβ/C99 also corroborate the idea that the proteinase is a new, full-fledged player in APP metabolism, and hence a potential new target molecule in AD treatment [25,26]. Finally, *in vitro* and *in vivo* studies revealed a novel physiological APP processing pathway, the product of which is a proteolytic fragment Aη-α capable of reducing long-term potentiation in hippocampal neurons in the CA1 pyramidal cell layer [27].

Analysis of bigenic mice, resulting from crossing the 5xFAD mouse model of AD and MT5-MMP knockout mice, revealed several positive effects of MT5-MMP deficiency at early stages of the pathology, compared to age-matched 5xFAD. These include the prevention of deficits in long-term potentiation and learning and memory, decreased levels of Aβ/C99, interleukin-1β (IL-1β) and tumor necrosis factor-α (TNF-α), as well as decreased glial reactivity [25,26]. Interestingly, MT5-MMP knockout mice showed no apparent phenotypes until the organism was subjected to stressful conditions [3,23]. In this vein, MT5-MMP knockout mice do not develop neuropathic pain, together with the absence of Aβ-fiber sprouting after sciatic nerve injury [21], and they do not develop thermal hyperalgesia during inflammation [24]. Besides, confocal imaging and qRT-PCR analyses of samples after traumatic brain injury (TBI) and bilateral entorhinal cortical lesion revealed that MT5-MMP inhibition attenuated ADAM-10 and N-cadherin [19].

Overall, MT5-MMP appears to be a pivotal enzyme in multiple physiological and pathological pathways that affect both neurons and glial cells. Accordingly, we investigated the influence of the MT5-MMP knockout state on the phenotype of human neurons and astrocytes and their possible functional crosstalk in a non-pathological situation. Using differentiated human neural derivatives from hiPSCs and CRISPR/Cas9 approaches, we showed that MT5-MMP deficiency led to changes in neuron and astrocyte morphology, characterized by the formation of more branched neurons and round-shaped astrocytes with decreased expression of S100b and GLAST. These data corroborate the multifaceted spectrum of MT5-MMP actions in the nervous system.

2. Materials and Methods

2.1. Cell Line

A commercially available human cell line was purchased from the Coriell biorepository, and originate from the CIRM iPSC Repository, under the reference CW70019. The CW70019 hiPSC line was obtained from a donor being non-demented at the time of biopsy.

2.2. hiPSC Culture

hiPSCs were cultured and maintained undifferentiated in a chemically defined growth medium (StemMACS™ iPS-Brew XF media; Miltenyi Biotec, Paris, France) onto growth-factor-reduced Matrigel (BD Biosciences, Franklin Lakes, NJ, US)-coated plates (8.6 μg/cm^2).

In short, when reaching 70–80% confluency, hiPSCs were treated with an enzyme-free solution (hereafter referred to as gentle dissociation solution) containing 0.5 mM EDTA (Lonza, Basel, Switzerland), D-PBS (Gibco Life Technologies, Scotland, UK) and 1.8 mg/mL NaCl (Sigma-Aldrich, st Louis, MO, USA). hiPSCs were incubated for 2 min in gentle dissociation solution at 37 °C, and the colonies were dispersed to small clusters and lifted carefully using a 5 mL glass pipette at a ratio of 1:3 or 1:4 for further amplification. When necessary, differentiated areas were removed from hiPSC cultures prior to passaging, in order to maintain the cultures as undifferentiated before proceeding to their differentiation. hiPSC lines were maintained in an incubator (37 °C, 5% CO_2) with daily medium changes.

2.3. CRISPR-Cas9 Plasmid Production

For the generation of CRISPR-Cas9 plasmids, we first modified the pSpCas9(BB)-2A-Puro (PX459) V2.0 (Addgene plasmid # 62988, Addgene, Teddington, UK) [28] to replace the CBh promoter with the EF1 alpha promoter by a subcloning strategy. The modified plasmid was named cAB03 (i.e., pX459-pEF1 alpha), and further used to produce two distinct plasmids, each containing a single guide RNA specific to the *MMP24* sequence (i.e., sgRNA containing crRNA + TracrRNA), aiming at generating insertions and deletions within the exon 2. To that end, CRISPR sgRNAs were designed using the Zhang lab design tool (http://CRISPR.mit.edu, accessed on 28 June 2021) and cloned into cAB03 as previously described [28]. For the sgRNA, a 20 nt *MMP24* specific sequence was selected, sgRNA1: GATCCCGGTCACCGGTGTGT. Briefly, the selected *MMP24* specific sequence was cloned by BbsI-mediated digestion of cAB03, followed by ligation using cohesive end cloning. Plasmids were transformed into DH5α chemically competent cells (Thermo Fisher Scientific, Waltham, MA, USA) and individual clones were first screened by PCR to verify the insertion, then were ultimately validated by sequencing analysis.

2.4. CRISPR-Cas9-Mediated Edition for the Generation of MMP24 Knockout hiPSCs

To generate *MMP24* knockout hiPSCs from the CW70019 hiPSC line, cells were prepared and electroporated as previously described [29]. After clonal isolation, for each clone DNA, extraction was performed using a thermocycler with the following settings: 3 h at 55 °C and 30 min at 95 °C. Then, a 10 µL PCR reaction was performed using 1 µL of the extracted genomic DNA and 9 µL of a PCR mix containing 1× of the 5× PrimeSTAR GXL buffer (Takara Bio, Shiga, Japan), PrimeSTAR GXL DNA polymerase (0.25 U/10 µL), dNTPs (200 µM each) and the following primers: *MMP24*For 5′-ACGGGCATCTGCGCTGCACTC-3′ and *MMP24*Rev 5′-GCTGGGTGCCTGCATGTGCCTG-3′ (0.3 µM each). PCR reaction was performed using the following conditions: 1 min at 94 °C for one cycle, then 10 sec at 98 °C and 1 min at 55 °C for 35 cycles, and to finish, 5 min at 68 °C for one cycle. Upon completion, the PCR product was digested using the restriction enzyme AleI (New England Biolabs, Ipswich, MA, US), and run on a 2% agarose gel electrophoresis to analyze the size of the amplicon for each individual clone (expected profiles: two bands for the wild-type clone at 466 bp and 209 bp; one band for the homozygous clone at 675 bp; three bands at 675 bp, 466 bp and 209 bp for the heterozygous clone). Only knockout clones for *MMP24* were kept and further confirmed by Sanger sequencing prior to amplification for further experiments. Three knockout clones were produced for the experiment.

2.5. Derivation of NPCs from hiPSCs

hiPSCs were differentiated into neural progenitor cells (NPCs) following a monolayer culture method with a commercial dual SMAD inhibition-mediated neural induction medium (STEMdiff™ SMADi Neural Induction Kit, Stem Cell Technologies, Vancouver, Canada), based on a previously published protocol [30]. NPCs were obtained following the manufacturer's instructions, with slight modifications. Undifferentiated cultures of hiPSCs were treated with gentle dissociation solution for 4 min, then the solution was removed and cells incubated in Accumax for 4 min. hiPSCs were then dislodged as single cells and transferred into Dulbecco's modified Eagle's medium (DMEM)-F12 + 20% knockout serum

replacement. Then, cells were centrifuged at 200× *g* for 5 min, resuspended in D-PBS, counted and centrifuged once more at 200× *g* for 5 min. Lastly, cells were resuspended in STEMdiff™ SMADi neural induction kit + 10 µM Y-27632 (Tocris Bioscience, Bristol, UK), a Rho-associated protein kinase inhibitor, plated onto growth-factor-reduced Matrigel™ (BD Biosciences, Franklin Lakes, NJ, USA)-coated plates (8.6 µg/cm^2) at 320,000 cells/cm^2, and maintained in an incubator (37 °C, 5% CO_2) with medium changes every day. Between 6 and 9 days after induction, cells were harvested as single cells using Accumax, transferred into DMEM-F12 medium, centrifuged at 200× *g* for 5 min, resuspended in STEMdiff™ SMADi medium + 10 µM Y-27632, plated onto growth-factor-reduced Matrigel-coated plates (8.6 µg/cm^2) at 270,000 cells/cm^2 and maintained in an incubator (37 °C, 5% CO_2) with medium changes every day for 5 additional days. Then, cells were passaged one more time following the same procedure. Five days after the last passage (i.e., between 16 to 19 days post-induction), differentiated cells were harvested as single cells using Accumax, centrifuged at 200× *g* for 5 min, before being resuspended in STEMdiff™ neural progenitor medium (Stem Cell Technologies, Vancouver, Canada; hereafter referred as NPC media) and seeded onto growth-factor-reduced Matrigel-coated plates (8.6 µg/cm^2) at 125,000 cells/cm^2. hiPSC-NPCs were maintained in an incubator (37 °C, 5% CO_2) with medium changes every day, and passaged with Accumax when reaching 80–90% confluency.

2.6. Neuronal Differentiation

hiPSC-derived NPCs were differentiated in accordance with a previously published protocol [31]. In brief, hiPSC-NPCs were detached using Accutase, collected, centrifuged, and gently re-suspended in NPC medium and plated onto poly-L-ornithine (PLO) (Sigma-Aldrich, st Louis, MO, USA; P3655; 15 µg/mL)/Laminin (Life Technologies, Waltham, MA, USA, 23017015; 10 µg/mL)-coated glass coverslips at a density of 50,000 cells/cm^2 and incubated overnight (37 °C with 5% CO_2). Thereafter, the NPC medium was removed and replaced by the BrainPhys™ neuronal media kit (Stem Cell Technologies, Vancouver, Canada) composed of the BrainPhys neuronal maturation medium (StemCell Technologies, Vancouver, Canada; #05793) supplemented with NeuroCult SM1 neuronal supplement (StemCell Technologies, #05711) + N2 Supplement-A (StemCell Technologies, #07152) + 20 ng/mL BDNF (Peprotech, Rocky Hill, NJ, USA; #450-02) + 20 ng/mL GDNF (Peprotech; #450-10) + 1 mM dibutyryl-cAMP (Sigma-Aldrich; D0627) + 200 nM ascorbic acid (Sigma-Aldrich; A5960). Half of the medium was gently replaced two to three times a week for 8 weeks. The plates were kept in a humified incubator at 37 °C with 5% CO_2. In all experiments, the passage number (P7–P9) and the time in culture (8 weeks) were identical.

2.7. Astrocyte Differentiation

Differentiation of hiPSC-derived NPCs into astrocyte-like cells was performed using a previously published protocol with slight modifications [32]. In short, hiPSC-NPCs were dissociated with Accutase™ and seeded at 30,000 cells/cm^2 on growth-factor-reduced Matrigel™-coated 6-well plates (8.6 µg/cm^2) in astrocyte medium (ScienCell, Carlsbad, CA, USA, 1801-b), containing 2% fetal bovine serum (0010), astrocyte growth supplement (1852) and 10 U/mL penicillin/streptomycin solution (0503). Full medium changes were performed every 72 h over a 30-day differentiation period. When cells reached 90–95% confluence (approximately 5–7 days after initial seeding), they were passaged as single cells into astrocyte medium and cultured onto growth-factor-reduced Matrigel™-coated plates (8.6 µg/cm^2) at 30,000 cells/cm^2. The cells were plated onto a non-coated plastic surface after 21 days (around 3–4 passages) to remove immature astroglial cells. The cells were used for further experiments after 45 days of incubation in astrocyte medium. The maturity of astrocytes was evaluated with immunocytochemistry (ICC) for ALDH1L1, S100β, GALST, and GFAP. In all experiments, the passage number (P7–P9) and the time in culture (45 DIV) were identical.

2.8. Immunocytochemistry

The cells were fixed with a 4% paraformaldehyde solution (PFA) (Sigma-Aldrich; 158127) in PBS (Gibco, Scotland, UK) pH 7.4, for 10 min on a bed of ice. Thereafter, the cells were incubated in a quenching solution (0.1 M aqueous glycine solution) for 5 min and washed with PBS, pH 7.4, for 5 min. The fixed cells were then incubated in a blocking solution (5% normal goat serum (Jackson ImmunoResearch, West Grove, PA, USA), 0.1% Triton X-100 (Sigma-Aldrich; 2315025) diluted in PBS, pH 7.4 for 1 h at RT. The cells were then incubated with the following primary antibodies diluted in blocking solution overnight with gentle shaking at 4 °C: SOX2 (1:1000, Abcam, Cambridge, UK; ab97959), PAX6 (1:1000, BioLegend, San Diego, CA, USA; 901302), Nestin (1:500, Merck Millipore, Burlington, MA, USA; MAB5326), NeuN (1:500, Merck Millipore; MAB377), S100β (1:100, Abcam; ab212816), vGluT1 (1:1000, Merck Millipore; AB5905), PSD-95 (1:500, Abcam; ab12093), MAP2B (1:500, Abcam; ab5392), GLAST (1:120, Thermo Fisher Scientific; PA5-34198), GFAP (1:100, Merck Millipore; AB5541), and ALDH1L1 (1:100, Abcam; ab190298). The next day, the cells were thoroughly washed three times with 0.1% PBS-Triton X-100 and incubated with the following species-specific fluorochrome-conjugated secondary antibodies diluted in PBS (1:1000) for one hour at RT: Alexa Fluor 405 anti-rabbit IgG (Abcam; ab175651), Alexa Fluor 405 anti-mouse IgG (Life Technologies; A-31553), Alexa Fluor 405 anti-chicken IgG (Life Technologies; A-11040), Alexa Fluor 488 anti-mouse IgG (Life Technologies; A-11029), Alexa Fluor 546 anti-mouse IgG (Life Technologies, A-11030), Alexa Fluor 546 anti-rabbit IgG (Life Technologies; A-11035), Alexa Fluor 568 anti-rabbit IgG (Life Technologies; A-11036), and Alexa Fluor 633 anti-guinea pig IgG (Life Technologies; A-21105). After rinsing three times with 0.1% PBS-Triton X-100, pH 7.4, the samples were counterstained with the nuclear marker DAPI. Finally, coverslips were rinsed three times with PBS, one more time with phosphate buffer (pH 7.4) and mounted with a mounting medium (Sigma-Aldrich; M1289). Microscope slides with mounted coverslips were stored at 4 °C until the next morning, when the mounting medium had dried. Then, the edges of coverslips were treated with nail polish to prevent the samples from drying out. The rest of the time, all samples were stored at 4 °C (no more than 4 days) until the imaging of samples was completed.

2.9. Confocal Microscopy and Data Collection

Serial optical z-sections were carefully collected at 0.28 µm intervals using a Zeiss Axio Imager 2 (Carl Zeiss GmbH, Jena, Germany), in combination with a Carl Zeiss LSM 700 system equipped with an EC "Plan-Neofluar" 40×/0.75 M27 and EC "Plan-Neofluar" 63×/1.40 Oil DIC M27 objectives, and 405 nm, 488 nm, 555 nm and 633 nm laser lines. Throughout all experiments, the pinhole was set to 0.5 Airy unit. The images were collected using a bidirectional scan and two frames' averages settings. The z-sections were deconvolved using a fast iterative algorithm (five iterations) integrated into Zeiss software. All images in this work were maximum intensity projections, which were analyzed using Fiji (ImageJ, NIH, USA, 1.53c) or/and Imaris software (Bitplane AG, Zurich, Switzerland, v.7.7.2).

2.10. Image Analysis

Fiji Sholl analysis (v.3.6.12) was utilized to describe neuronal arbors. For analysis, the scale-corrected maximum intensity z-stack projection images of a single neuron were obtained with EC "Plan-Neofluar" 63×/1.40 Oil DIC M27 objectives. Thereafter, the images were converted into an 8-bit grayscale format. The thresholding option was utilized to obtain a mask of the neuron. The Otsu thresholding algorithm (v.1.17.2) was consistently used throughout the Sholl image analysis. The neurites of neighboring neurons were removed with the eraser tool. Using a "Line segment tool", a single line from the center of the soma of a neuron to its longest neurites was drawn. The concentric shell rings with 5 µm steps were drawn automatically. The first shell was defined 10 µm outside of the

cell body to exclude the latter from the analysis. Thereafter, a repeated two-way ANOVA was performed.

Quantification and comparison of the neurite structures were achieved with the NeuronJ plugin (v.1.4.3) for Fiji. For analysis, the maximum intensity projection two-dimensional (2D) images were converted into 8-bit gray-scale type and loaded through the NeuronJ toolbar. Thereafter, the neurite structures were manually traced and binned into two groups, referred to as "primary" and "secondary" neurites, for further automatic analysis.

To quantify the GFAP cytoskeleton volume and surface area, images were subsequently analyzed with the Imaris software (Bitplane AG, Zurich, Switzerland) using the "Surface tool", as described elsewhere [33]. After that, the ratio between the surface area and volume was calculated using Excel.

Analysis of fluorescent intensity of astroglia markers was done with ImageJ, as described elsewhere [33]. Shortly, the cells from five random fields of three random wells of three independent differentiations were chosen for analysis. After deconvolution, the average background fluorescence, calculated from three random regions of each field of view, was subtracted. For comparisons, we used the value of mean integrated density per cell, which was measured as raw integrated pixel density divided by the number of immunoreactive cells.

2.11. Patch-Clamp Recordings

Whole-cell patch-clamp recordings of neurons were performed after 8 weeks in the absence of any receptor antagonists, as described previously [31]. The coverslips with neurons were transferred into a heated perfusion chamber with a constant flow (1 mL/min) of warm artificial cerebrospinal fluid (ACSF: 121mM NaCl, 4.2 mM KCl, 1.0 mM $MgSO_4$, 0.45 mM NaH_2PO_4, 0.5 mM Na_2HPO_4, 29 mM $NaHCO_3$, 1.1 mM $CaCl_2$, 20 g glucose, all from Sigma-Aldrich), bubbled with carbon dioxide and maintained at 37 °C. Cells were incubated at 37 °C in a perfusion chamber for 5 min before recordings, to minimize the "transfer" effects. Patch pipettes were pulled from borosilicate glass capillaries and had a resistance of 5–8 MΩ (in the whole-cell configuration). Patch electrodes were filled with internal solution containing 130 mM K-gluconate, 6 mM KCl, 4 mM NaCl, 10 mM Na-HEPES, 0.2 mM K-EGTA, 0.3 mM GTP, 2 mM Mg-ATP, 0.2 mMcAMP, and 10 mM D-glucose (all from Sigma-Aldrich). The pH and osmolality of the internal solution were 7.3 and 290 mOsm, respectively. Currents were recorded with an EPC9 (HEKA Elektronik, Lambrecht, Germany) patch-clamp amplifier. Electrode capacitances were compensated online in the cell-attached mode. We maintained the cells in voltage clamp (VC) at −70 mV. Voltage-dependent Na^+ and K^+ channel properties were examined in response to stepwise membrane depolarization, and the IV curves were computed. Spontaneous synaptic events were recorded for at least 3 min at −70 mV (close to the Cl^- reversal potential, suggesting that the recorded events were EPSCs). Then we switched to current-clamp mode to evaluate the ability of cells to generate action potentials. Data acquisition and quality were controlled in real-time by PatchMaster software (HEKA Elektronik, Lambrecht, Germany) and saved for further analysis.

2.12. Statistical Analysis

All statistical analyses were performed using GraphPad Prism version 9.0 for Windows (GraphPad Software, San Diego, CA, USA). Each experiment was performed at least three times. All the data are presented as mean ± S.E.M. Results were considered significant if $p < 0.05$. The results of Sholl analysis were evaluated with a two-way repeated-measures ANOVA, followed by Bonferroni's multiple comparison test (genotype/distance from the soma). Neuronal morphology analysis was achieved with a nested *t*-test. Data were analyzed by Shapiro–Wilks's test to determine normality. Thereafter, the log transformation was used if the data were not distributed normally. Astrocyte morphology data were analyzed with both two-way ANOVA (genotype/morphotype) and nested *t*-test (the same

morphotype comparison between WT and MT5-MMP KO). Mean fluorescence intensity per cell data were analyzed with a nested *t*-test (the same morphotype comparison in both WT and MT5-MMP KO). The data collection was not genotype-blinded.

3. Results

3.1. MT5-MMP Deficient hiPSCs Preserve the Ability to Differentiate into Neuronal Cells

To accurately assess the impact of MT5-MMP deficiency on human neural cells, we first decided to knock out the *MMP24* gene from a hiPSC line that was previously generated from a non-demented donor. Upon CRISPR-Cas9 genome editing, hiPSC clones were evaluated for insertions/deletions in the targeted exon 2 (Figure 1A). PCR-based screening (Figure 1B), further validated by Sanger sequencing, allowed us to select and confirm the generation of several isogenic MT5-MMP knockout clones. Then, the loss of MT5-MMP was further validated by genic analyses in those selected isogenic MT5-MMP KO hiPSC clones. Indeed, MT5-MMP mRNA levels were barely detectable in the validated clones by qPCR, which demonstrated CRISPR-Cas9-induced frameshift mutations, leading to functional loss of MT5-MMP (Figure 1C).

In the present study, both wild-type and isogenic MT5-MMP knockout hiPSCs were successfully converted into neural progenitor cells (NPCs). Both cell lines were characterized by the expression of neuroepithelial markers PAX6 (Figure 2A,A'), SOX2 (Figure 2B,B') and nestin (Figure 2A,B). Microscopic observations revealed neither specific morphological differences nor expression marker changes between control hiPSC-NPCs and their isogenic MT5-MMP knockout counterparts. The neuronal differentiation capacity of MT5-MMP knockout hiPSC-NPCs was similar to that of wild-type cells. After three days of neuronal differentiation onset, multiple neurite-like protrusions were observed. At that early time of the differentiation stage, MT5-MMP knockout cells showed indistinguishable morphology as compared to wild-type cells (Figure 2C,D). Besides, both wild-type and MT5-MMP knockout neuronal-like cells at DIV60 showed comparable expression of neuronal markers NeuN and MAP2B (Figure 2E–H). These findings indicate that MT5-MMP deficiency does not hamper the overall differentiation potential of hiPSCs toward a neural progenitor-like phenotype and its neuronal derivatives. However, initial visual analysis of wild-type and MT5-MMP knockout neurons after 60 days in maturation conditions revealed that neurons exhibited distinguishable morphological features related to their arborizations (Figure 2G,H).

3.2. MT5-MMP Deficient Neurons Exhibited Increased Branching of Primary and Secondary Neurites

To describe morphological changes quantitatively, we conducted a morphometric analysis of hiPSC-derived neurons. Using the Sholl analysis, we revealed that MAP2B-positive MT5-MMP-deficient neuronal cells had a significantly greater number of dendritic intersections in the interval ranging between 25 to 50 µm from neuronal soma, compared to MT5-MMP wild-type neurons (two-way repeated-measures ANOVA with Bonferroni's post hoc test, $N = 3$ culture preparations, $n = 82$ neurons, $F\ (1, 80) = 10.7$, $p = 0.002$, Figure 3A). Comparative analysis with a nested showed that MT5-MMP deficiency resulted in an increased number of primary ($N = 3$, $n = 111$, $F = 10.0$, $p = 0.03$, Figure 3B) and secondary neurites ($N = 3$, $n = 111$, $F = 42.8$, $p = 0.003$, Figure 3C). Next, we investigated whether these changes in neurite numbers were also accompanied by changes in neurite lengths. The average length of primary ($N = 3$, $n = 111$, $F = 0.0126$, $p = 0.92$, Figure 3D) and secondary ($N = 3$, $n = 111$, $F = 3.30$, $p = 0.14$, Figure 3E) neurites was not different between wild-type and MT5-MMP deficient neurons. Predictably, the total length—i.e., an average sum length of all primary and secondary neurites per neuron—was significantly higher for MT5-MMP deficient cells because of the increased number of neurites ($N = 3$, $n = 111$, $F = 28.0$, ** $p = 0.006$, Figure 3F).

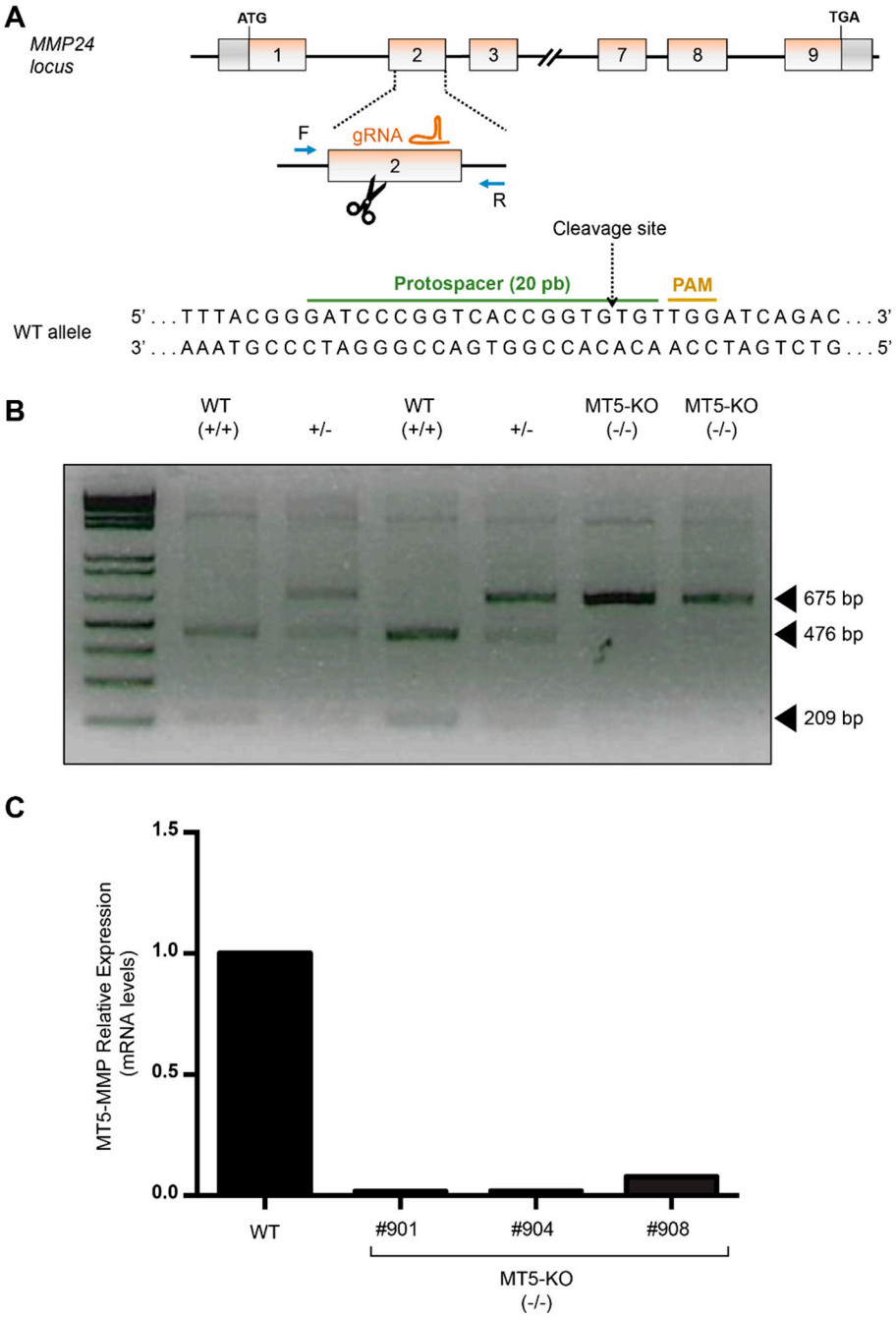

Figure 1. MT5-MMP (*MMP24*)-KO hiPSC generation by CRISPR/Cas9 genome editing. (**A**) Schematic representation of the wild-type (WT) locus and the genome editing strategy used to generate the knockout (KO) isogenic clones from a non-demented donor hiPSC line. (**B**) Representative PCR-based screening for the editing of *MMP24*: WT (+/+), heterozygous (+/−) and homozygous MT5-KO (−/−) clones. The F and R primers for *MMP24* were designed flanking the Cas9-cutting site. The PCR product was digested and run on an electrophoresis gel, to analyze the size of the amplicon for each individual clone (expected profiles: two bands at 476 bp and 209 bp (WT +/+); one band at 675 bp (restriction enzyme site obliterated, MT5-KO -/-) and three bands at 675bp, 476bp and 209bp (heterozygous clones, +/−). (**C**) After Sanger sequencing validation of MT5-KO clones (not shown), qPCR analysis revealed that *MMP24* mRNA was barely detectable in the newly generated MT5-KO clones.

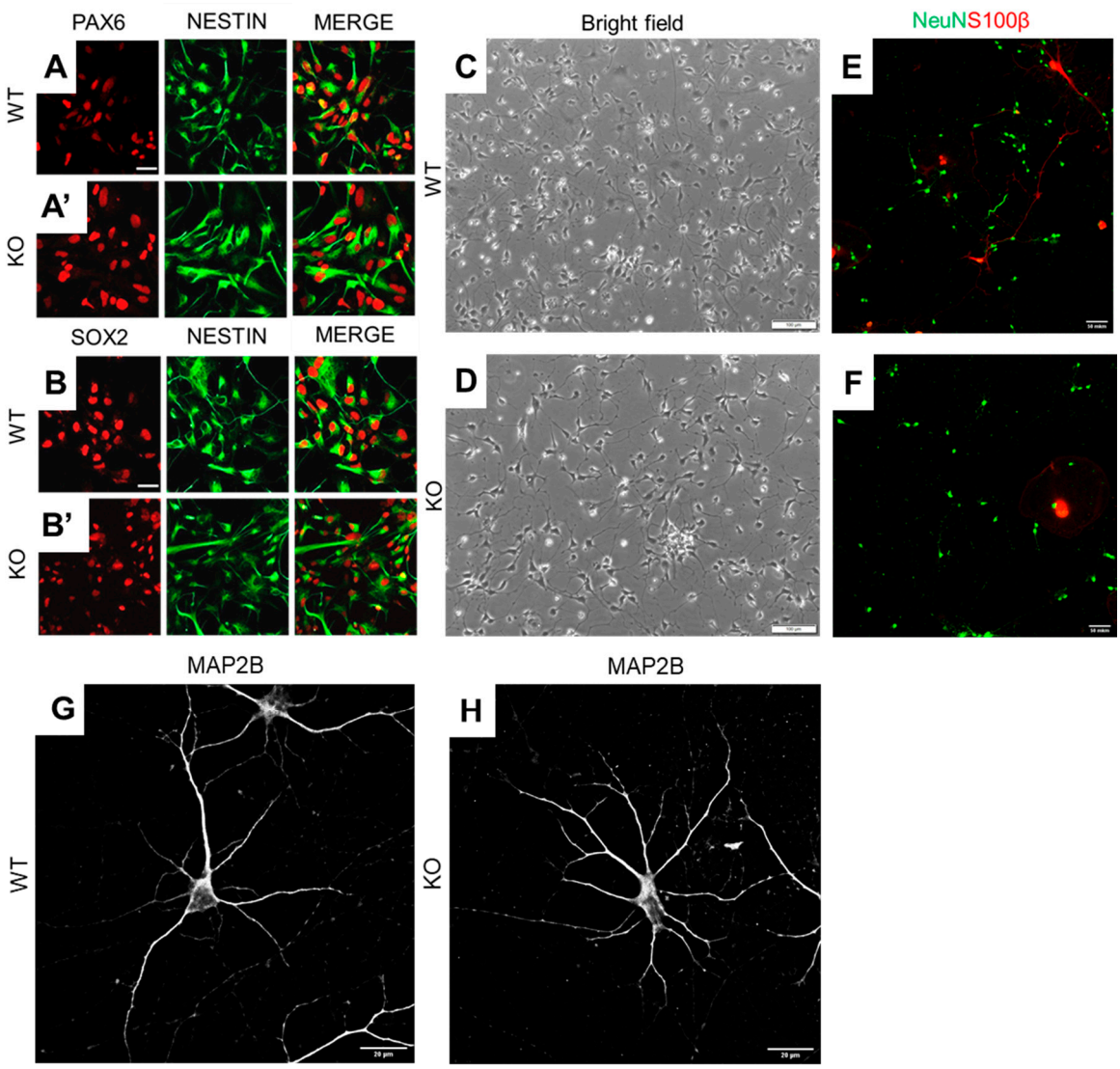

Figure 2. Efficient derivation of NPCs and neurons from wild-type and MT5-MMP-deficient hiPSCs. (**A**,**B**) Wild-type and MT5-MMP-deficient (KO) hiPSCs were efficiently differentiated into NPCs co-expressing the paired box 6 (PAX6, red) and nestin (green) (**A**,**A'**), as well as the SRY (sex-determining region Y)-box 2 (SOX2, red) and Nestin (green) markers (**B**,**B'**). Scale bar 20 µm. (**C**,**D**) Representative bright-field images of wild-type (**C**) and MT5-MMP-deficient NPCs (**D**) undergoing neuronal differentiation at DIV3, scale bar 50 µm. Note that multiple neurite-like protrusions were already observed at this early stage of differentiation, with no clearly distinct morphology between neurons of both genotypes at this stage. (**E–H**) Representative images of immunolabeled hiPSC-derived neuronal cultures immunolabelled with antibodies against the neuron-specific marker NeuN (green) and the astrocyte-specific marker S100β (red) (**E**,**F**, scale bar 50 µm) after 60 days of differentiation (DIV60). In addition, cells expressed neuron-specific cytoskeletal protein MAP2B (**G**,**H**, scale bar 20 µm).

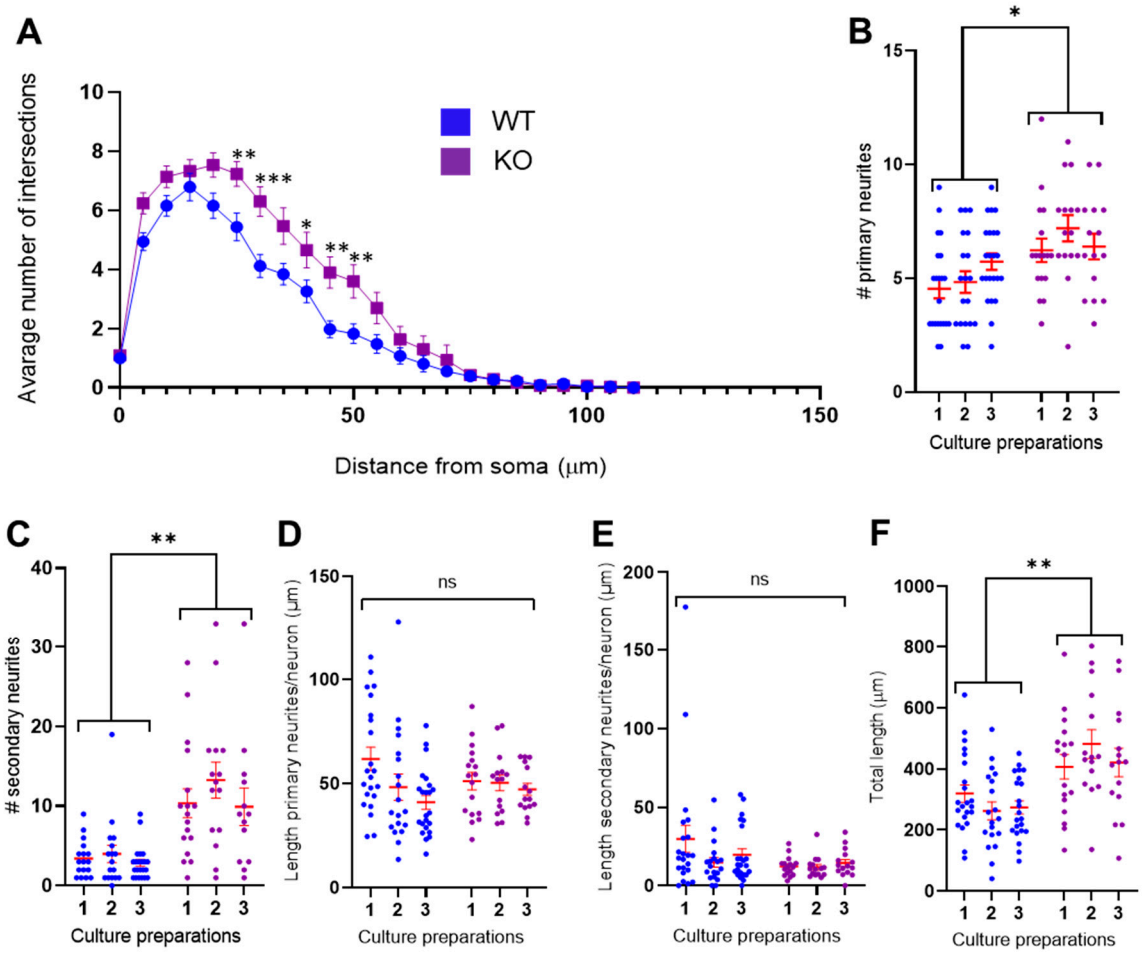

Figure 3. MT5-MMP deficiency alters neurite outgrowth in hiPSC-derived neurons. NPCs derived from wild-type and MT5-MMP KO hiPSCs were differentiated into neurons for 60 days before being subjected to the Sholl analysis. (**A**) Sholl analysis of dendrites from neurons of both genotypes (as indicated) showing the total number of intersections of MAP2B positive neurites with concentric rings, from the cell body to distal ends of dendrites (maximal distance of 110 μm, steps of 5 μm). MT5-MMP deficient neurons showed higher dendritic intersections in the 30 to 50 μm distance from soma (two-way repeated-measures ANOVA with Bonferroni's post hoc test, $N = 3$, $n = 82$, F (1, 80) = 10.7, *** $p < 0.001$; ** $p < 0.01$; * $p < 0.05$). (**B**,**C**) Bar charts depicting the counting of the number of primary (**B**) and secondary (**C**) neurites using the NeuronJ plugin. Noticeably, analyses showed that MT5-MMP deficiency significantly increases the number of primary (nested *t*-test, $N = 3$, $n = 111$, $F = 10.0$, * $p = 0.03$) and secondary neurites (nested *t*-test, $N = 3$, $n = 111$, $F = 42.8$, ** $p = 0.003$). (**D**,**E**) Bar charts depicting the average length of primary (**D**) and secondary (**E**) neurites. (**F**) Bar chart showing a significant increase of total length for MT5-MMP knockout neurons (nested *t*-test, $N = 3$, $n = 111$, $F = 28.0$, ** $p = 0.006$). Data are presented as mean ± SEM.

3.3. MT5-MMP Deficiency Does Not Alter Neuronal Activity in hiPSC-Derived Neurons

Considering the morphological differences observed in MT5-MMP-deficient neuronal cultures, we next sought whether such changes would also be accompanied by functional alterations. The presence of vGLUT1/PSD95 positive synaptic-like structures at 60DIV (Figure 4A,B) indicated that neurons could be involved in functional interactions. Therefore, whole-cell patch-clamp recordings were conducted. Neurons of both genotypes had relatively small intrinsic Na+ and K+ currents (Figure 4C,D) and generated only single-action potentials in response to the depolarization steps (Figure 4E). Nonetheless, some cells were characterized by the presence of inward spontaneous postsynaptic currents (Figure 4F). We observed that the occurrence of postsynaptic currents was limited in the generated hiPSC-derived neuronal cultures, independently of the genotype (wild-type: $n = 9$ cells out of 21; MT5-MMP knockout: $n = 7$ cells out of 23). Therefore, overall, we

did not observe genotype-associated effects on the electrophysiological properties at the studied developmental stage. However, we cannot rule out that more mature neurons would display genotype-specific differences in their functionalities.

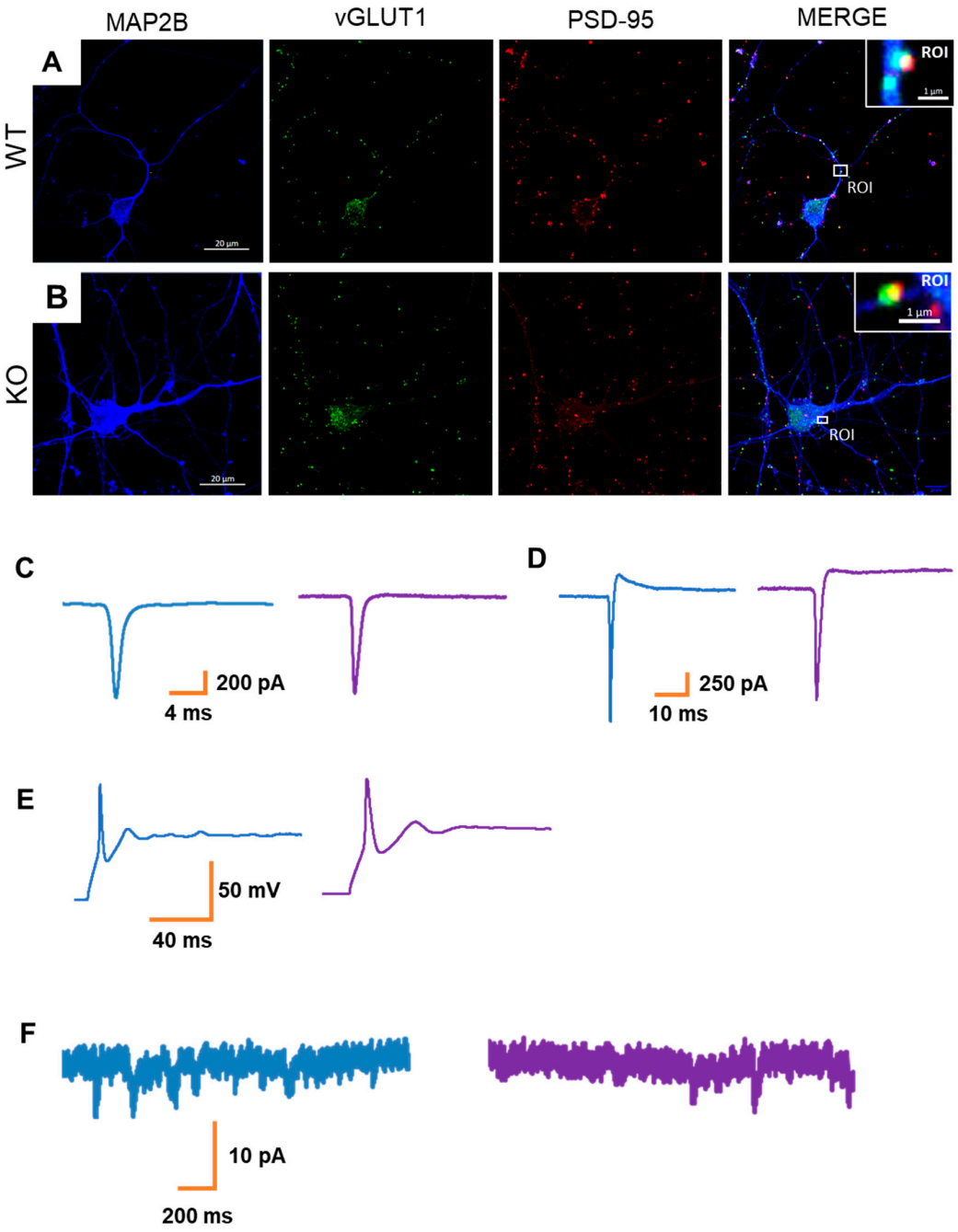

Figure 4. Synaptic connectivity and functionality of hiPSC-derived NPCs. (**A**,**B**) Representative images of wild-type (**A**) and MT5-MMP-deficient (**B**) neuronal cultures at 8 weeks of differentiation. The cells were immunostained by antibodies against MAP2B (blue), vGluT1 (green), and PSD-95 (red) as dendritic, pre- and postsynaptic markers, respectively. Scale bar 20 µm. The white rectangle depicts the ROI. Note that the juxtaposed position of pre- and postsynaptic proteins, vGluT1 and PSD95, characterized by a small area of overlapping colors, was observed for both genotypes. Scale bar 1 µm. (**C**,**D**) Representative traces from whole-cell patch-clamp recording showing that neurons were characterized by small Na^+ and K^+ currents at 60DIV. (**E**) Representative traces showing that neurons at 60DIV exhibited single action potentials in response to a depolarization step. (**F**) Representative traces from recorded neurons at 60DIV showed small inward spontaneous currents.

3.4. MT5-MMP Deficiency Induced Morphological Changes and Reduced the Expression of GLAST and S100β in Astrocyte-Like Cells

We next sought to evaluate MT5-MMP knockout effects on the most abundant neural cell type in the human brain, namely, astrocytes. To evaluate astrocyte features independently of neurons, hiPSCs were differentiated using a previously published protocol [32], with minor modifications. For both genotypes, we observed heterogeneity in cell morphology of the astrocyte-like cultures. Using the previously published method [33], we determined and binned all cells into three morphological categories for further analysis: fibroblast-like, arborized, and arrowhead (Figure 5A). Detailed analysis showed differences in the proportion of astrocytes falling into each category between genotypes, suggesting that MT5-MMP deficiency could have an impact on astrocyte morphology (two-way repeated ANOVA with Sidak's post hoc test, $N = 3$, $n = 245$, $F\ (2, 8) = 38.7$, $p < 0.001$). The comparison of morphotypes between genotypes showed that the proportion of "arborized" astrocytes was higher in wild-type astrocyte-like cultures (WT 53/131 vs. KO 14/114, $p < 0.01$), meanwhile, the number of fibroblast-like cells was higher in MT5-MMP-deficient cultures (WT 38/131 vs. KO 76/114, $p < 0.05$) (Figure 5B). A 3D IsoSurface reconstruction from serial confocal z-stacks of GFAP cells, as well as the quantification of cell surface area (SA), cell volume (Vol) and the SA:Vol ratio, revealed significant differences in cellular morphology (Figure 5C–E). Analysis of the genotype effects for each of the morphotypes (nested *t*-test, $N = 3$, $n = 73$; arborized, $n = 33$, $F = 0.013$, $p = 0.92$; arrowhead, $n = 24$, $F = 12.5$, ** $p = 0.002$; fibroblast-like, $n = 16$, $F = 13.8$, * $p = 0.02$) revealed that arrowhead and fibroblast-like MT5-MMP KO astrocytes were characterized by a bigger surface area in comparison to WT astrocytes of the same morphotype (Figure 5C). Quantification of cell volume revealed significant differences between genotypes (nested *t*-test, $N = 3$, $n = 73$; arborized: $n = 33$, $F = 3.55$, $p = 0.13$; arrowhead: $n = 24$, $F = 13.8$, *** $p < 0.001$; fibroblast-like: $n = 16$, $F = 8.98$, $p = 0.04$). MT5-MMP KO astrocytes were characterized by increased volume for arrowhead (*** $p < 0.001$) and fibroblast-like (* $p < 0.05$) astrocytes, in comparison to WT ones (Figure 4D). However, the SA:Vol ratio was higher for arborized WT compared to MT5-MMP KO astrocytes (nested *t*-test, $N = 3$, $n = 73$; arborized: $n = 33$, $F = 9.60$, ** $p = 0.004$; arrowhead: $n = 24$, $F = 4.75$, $p = 0.09$; fibroblast-like: $n = 16$, $F = 4.08$, $p = 0.06$, Figure 5E).

Astrocytes at the final stage of differentiation (45 DIV) exhibited the expression of astroglia-specific markers—GFAP, GLAST, ALDH1L1, and S100B (Figure 6A). Quantification of the fluorescence intensity of GFAP+ (nested *t*-test, $N = 3$, $n = 245$; arborized: $n = 67$, $F = 3.92$, $p = 0.12$; arrowhead: $n = 64$, $F = 0.381$, $p = 0.57$; fibroblast-like: $n = 114$, $F = 0.433$, p =0.55) and ALDH1L1+ cells (nested *t*-test, $N = 3$, $n = 121$; arborized: $n = 36$, $F = 0.04$, $p = 0.85$; arrowhead: $n = 30$, $F = 1.86$, $p = 0.24$; fibroblast-like: $n = 55$, $F = 0.746$, $p = 0.44$) revealed no difference in intensity between genotypes (Figure 6B,C). However, analysis of GLAST showed significantly decreased intensities for all three morphotypes of MT5-MMP KO astrocytes, compared to WT cells (nested *t*-test, $N = 3$, $n = 181$; arborized: $n = 57$, $F = 31.2$, ** $p = 0.005$; arrowhead: $n = 32$, $F = 5.80$, * $p = 0.02$; fibroblast-like: $n = 92$, $F = 14.0$, * $p = 0.019$, Figure 6D). Finally, analysis of S100β intensity showed significant difference between arborized MT5-MMP-deficient and wild-type astrocytes of the same morphotype (nested *t*-test, $N = 3$, $n = 139$; arborized: $n = 49$, $F = 9.67$, $p = 0.04$; arrowhead: $n = 42$, F =1.48, $p = 0.07$; fibroblast-like: $n = 48$, $F = 0.05$, $p = 0.83$, Figure 3E).

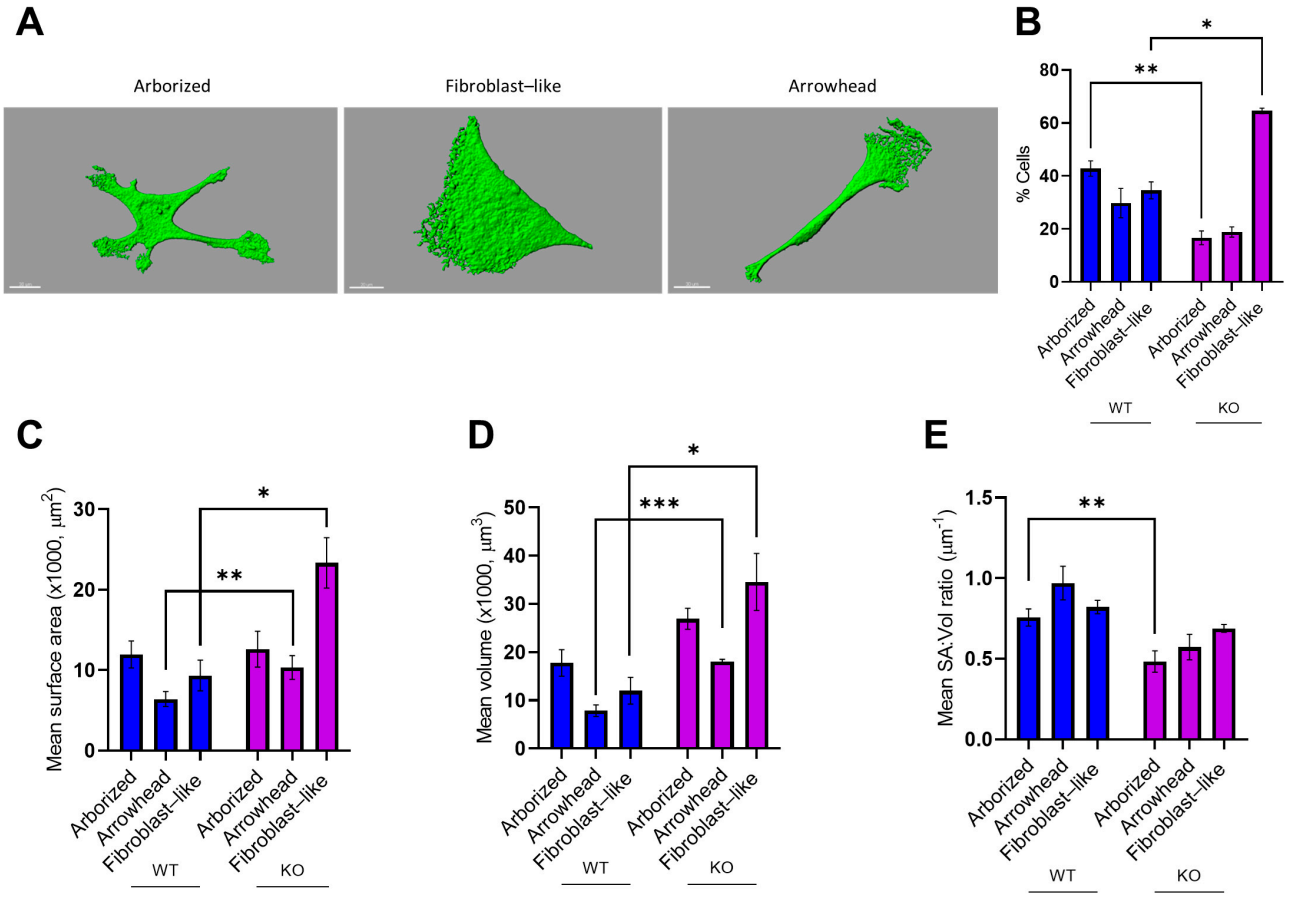

Figure 5. MT5-MMP-deficient astrocyte-like cells display morphological changes. (**A**) Representative images obtained with 3D IsoSurface reconstruction from serial confocal z-stacks of GFAP-stained astrocytes, showing clear differences in morphology, were binned into three categories: arborized, fibroblast-like, and arrowhead. (**B**) Bar chart showing the percentage of cells belonging to each of the three morphotypes from wild-type and MT5-MMP knockout (KO) astrocyte cultures. Note that MT5-MMP KO cultures showed a greater proportion of fibroblast-like astrocytes at the expense of arborized astrocytes (two-way ANOVA with Sidak´s post hoc test, $N = 3$ culture preparations, $n = 245$ GFAP+ astrocytes, $F(2, 239) = 7.72$, ** $p < 0.01$; * $p < 0.05$). (**C**–**E**) Bar charts depicting the comparative quantification of astrocyte-like cell surface area (nested *t*-test, $N = 3$, $n = 73$; arborized, $n = 33$, $F = 0.013$, $p = 0.92$; arrowhead, $n = 24$, $F = 12.5$, ** $p = 0.002$; fibroblast-like, $n = 16$, $F = 13.8$, * $p = 0.02$, in (C), volume (nested *t*-test, $N = 3$, $n = 73$; arborized: $n = 33$, $F = 3.55$, $p = 0.13$; arrowhead: $n = 24$, $F = 13.8$, *** $p < 0.001$; fibroblast-like: $n = 16$, $F = 8.98$, $p = 0.04$, in (D) and SA:Vol ratio (nested *t*-test, $N = 3$, $n = 73$; arborized: $n = 33$, $F = 9.60$, ** $p = 0.004$; arrowhead: $n = 24$, $F = 4.75$, $p = 0.09$; fibroblast-like: $n = 16$, $F = 4.08$, $p = 0.06$, in (E) between the different genotypes. Data are presented as mean ± SEM.

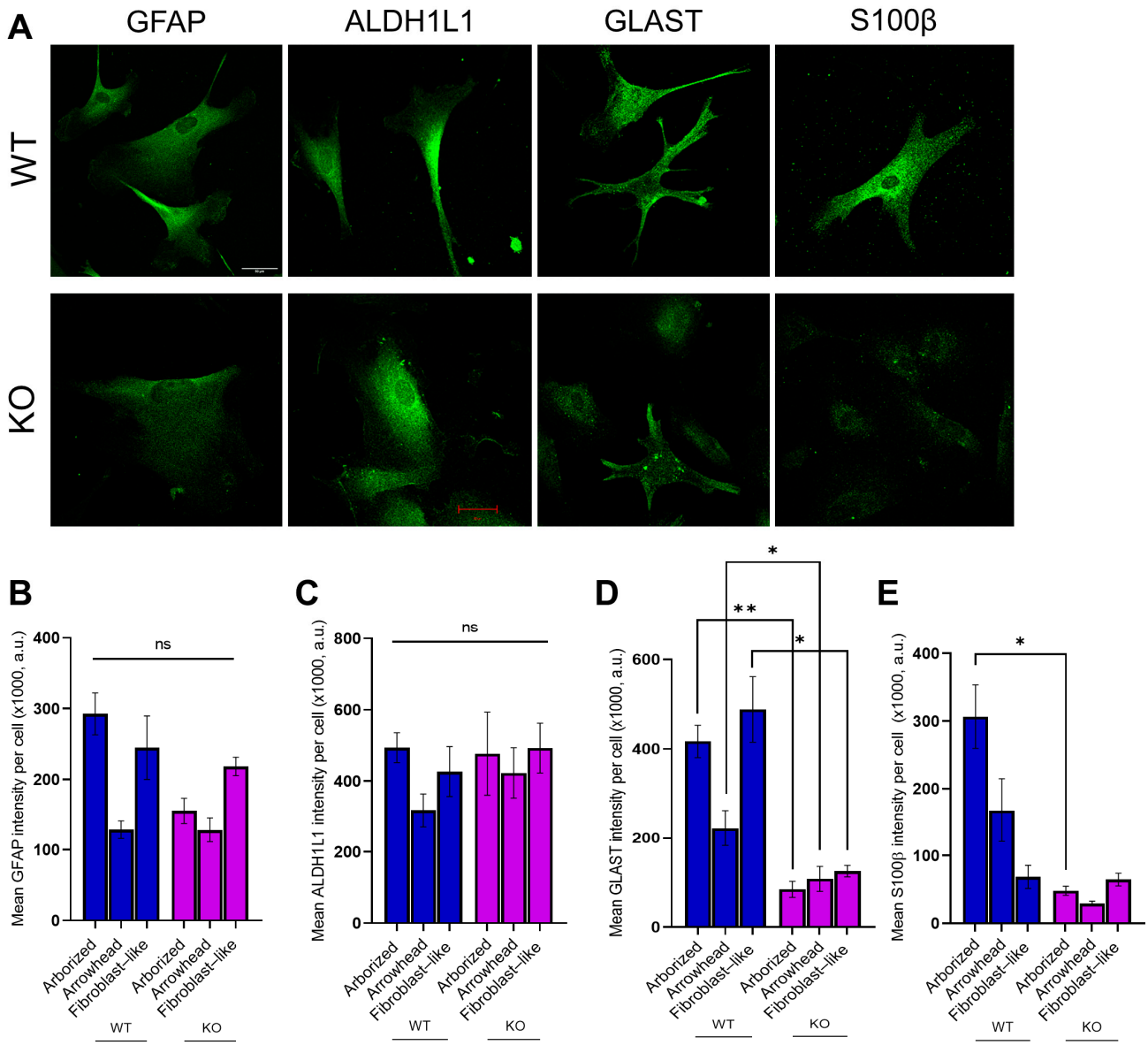

Figure 6. MT5-MMP-deficient astrocyte-like cells display altered expression of several astrocytic markers. (**A**) Representative images of hiPSC-derived astrocyte-like cells from wild-type and MT5-MMP KO hiPSCs, immunostained at DIV 45 for different astrocytic markers as indicated (scale bar: 20 µm). (**B**–**E**) Bar charts showing the quantification of the mean fluorescence intensity for different astrocytic markers within each morphological category. MT5-MMP-deficient astrocytes were characterized by no difference for GFAP (nested *t*-test, $N = 3$, $n = 245$; arborized: $n = 67$, $F = 3.92$, $p = 0.12$; arrowhead: $n = 64$, $F = 0.381$, $p = 0.57$; fibroblast-like: $n = 114$, $F = 0.433$, $p = 0.55$, in (**B**), ALDH1L1 (nested *t*-test, $N = 3$, $n = 121$; arborized: $n = 36$, $F = 0.04$, $p = 0.85$; arrowhead: $n = 30$, $F = 1.86$, $p = 0.24$; fibroblast-like: $n = 55$, $F = 0.746$, $p = 0.44$, in (**C**). Meanwhile, the significant difference was observed for GLAST (nested *t*-test, $N = 3$, $n = 181$; arborized: $n = 57$, $F = 31.2$, ** $p = 0.005$; arrowhead: $n = 32$, $F = 5.80$, * $p = 0.02$; fibroblast-like: $n = 92$, $F = 14.0$, * $p = 0.019$, in (**D**). Analysis of S100β fluorescence intensity (nested *t*-test, $N = 3$, $n = 139$; arborized: $n = 49$, $F = 9.67$, $p = 0.04$; arrowhead: $n = 42$, $F = 1.48$, $p = 0.07$; fibroblast-like: $n = 48$, $F = 0.05$, $p = 0.83$, in (**E**) reveals a significant difference between the arborized morphotype of WT and MT5-MMP KO astrocytes. Data are presented as mean ± SEM.

4. Discussion

In the present study, we demonstrated for the first time the importance of human MT5-MMP for the shape and physiology of neurons and astrocytes derived from hiPSCs. Innovative approaches based on hiPSC technologies help to bridge the genetic and phe-

notypic gap between animal models and humans for a better understanding of universal biological pathways, therapeutic target discovery and disease modeling [34–36].

We found that MT5-MMP-deficient neurons exhibited more branched morphology compared to wild-type neurons. In line with our data, Folgueras et al. showed that DRG-neurons from MT5-MMP knockout neonatal mice exhibited an increase in neurite ramification and varicosities compared to wild-type neurons, as well as in the number of branching points and in the total number of secondary neurites per neuron [24]. These data support the idea that MT5-MMP is pivotal in the developmental process of both CNS and PNS neurons. Neuritogenesis is a highly dynamic process in which N-cadherin, a substrate of MT5-MMP, participates in the stabilization of neurite branches [37]. Therefore, changes in N-cadherin processing and distribution might modulate the branched morphology of neurons. However, despite the fact that N-cadherin is an integral part of neural synapses [38,39], we did not observe any gross abnormalities in synaptic development between genotypes in a context where the electrophysiological analysis revealed the immature state of neurons. Moreover, both wild-type and MT5-MMP-deficient neurons displayed a low density of double-positive synaptic puncta even after 8 weeks *in vitro*, which further emphasizes the relative immaturity of cells. Perhaps, for this reason, the full phenotype of MT5-MMP-deficient cells in physiological conditions is not obvious at the studied developmental stage. Trial analysis (unpublished data) of vGluT1 and PSD95 showed that the number of vGluT1 positive puncta was low, even at day 60. PSD95 was detectable at early stages, i.e., at day 25–30 DIV, the expression peaked on DIV40 and remained on the same level up to DIV60, when the cultures were used for morphological analysis. In line with that, we speculate that MT5-MMP deficiency might affect axonal differentiation, as was previously demonstrated in primary neuronal cultures from E18 mouse embryos [22]. This hypothesis should be confirmed in future works with more mature human neurons derived from hiPSCs.

Astrocytes are fundamental components of the CNS. They constitute the most abundant cell type in the human brain and exhibit various morphologies, whose correlation with functional phenotypes is not yet well understood [33,40,41]. Neuron–astrocyte interactions are critical for normal neuronal functioning since astrocytes are involved in the guidance of neurons, and dynamically modulate synaptic transmission as part of the tripartite synapse [42–44]. Hence, we aimed to produce and analyze astrocytes derived from MT5-MMP knockout human iPSCs. Analysis of the fluorescence intensities of astrocytic markers, as well as of morphological features, revealed differences between wild-type and MT5-MMP KO astrocytes. High levels of GFAP mRNA and protein are recognized as a prominent feature of reactive astrocytes, although they may also reflect adaptive responses to physiological stimuli [45,46]. However, in our experiments, we did not observe a significant difference in GFAP fluorescence intensity for all morphotypes, possibly indicating a basal activation level of these cells, which is indistinguishable from the wild-type one. However, GFAP is not an absolute marker of astrocyte phenotypic and functional diversity [46]. That is why we conducted the analysis for other astrocytic markers, among which S100β is also a marker of reactivity [45,47] that turned out to be downregulated in MT5-MMP KO astrocytes. The downregulation of S100β in human astrocytes might explain an anti-inflammatory effect of MT5-MMP deficiency, which was previously shown for the 5xFAD mouse model of AD lacking MT5-MMP [25,26]. Particularly, 5xFAD/MT5-MMP KO animals showed significant reductions in key inflammatory mediators, such as interleukin-1 beta (IL-1β) and tumor necrosis factor alpha (TNFα), as well as reduced astrocyte and microglia reactivity. Since reduced neuroinflammation was concomitant with strong decreases in Aβ levels, we inferred a sequence of events where MT5-MMP deficiency caused an Aβ reduction and subsequently less inflammation. Our current data suggest that MT5-MMP can also control inflammation per se in a non-pathological state in a human setting, but it remains an open question whether basal downregulation of inflammatory markers predisposes astrocytes to decreased reactivity. In any case, our

results reinforce the idea that MT5-MMP is not only an APP-cleaving enzyme but also that its scope of activity goes far beyond that [12–14].

We found the expression of glutamate transporter GLAST is downregulated in all three morphotypes. Previously, it was shown that reductions in GLAST expression have been associated with a limited ability of astrocyte glutamate uptake from the extracellular space [48,49]. Trial co-culturing experiments showed that MT5-MMP knock-out astrocytes could not support neuronal viability, resulting in massive cell death (unpublished data). We might infer that MT5-MMP deficiency impairs the ability of astrocytes to maintain extracellular physiological levels of glutamate and, therefore, their ability to protect neurons from excitotoxicity. The verification of this hypothesis should warrant further study in neuron-astrocyte co-cultures. On the other hand, the stability of the metabolic enzyme ALDH1L1 between astrocytes of both genotypes possibly indicates the lack of MT5-MMP effects on metabolic functions in these cells.

Analysis of astrocyte morphology also revealed differences between genotypes. The round shape fibroblast-like morphotype prevailed among MT5-MMP knockout astrocytes. In addition, MT5-MMP KO astrocytes were characterized by increased surface area and volume, indicating a more "swallow" morphology. Meanwhile, the surface area/volume ratio was higher for arborized wild-type cells that again indicates a more rounded morphology of arborized MT5-MMP KO cells. We consider two possible hypotheses to explain this phenomenon. The first concerns the ability of MT5-MMP to convert by proteolysis the inactive pro-MMP-2 into the MMP-2 active form [50,51], and the fact that MMP-2 is a key enzyme for astrocyte migration and morphology [52]. Accordingly, Ogier and colleagues demonstrated, in an *in vitro* model of 2D astrocyte migration, that a selective MMP-2 inhibitor induced a round-like cell shape, coincident with impaired cell motility. In contrast, untreated cells exhibited a more elongated shape with stress fibers, filopodia and lamellipodia at the leading edge of migration [52]. Additionally, MMP-2 is considered as an enhancer of the neuroinflammatory response through the regulation of cytokine activity and release, notably in astrocytes [53]. Thus, taking into account these data, we suggest that MT5-MMP knockout astrocyte morphology may be, at least in part, the result of MMP-2 processing abnormalities that eventually downregulate inflammation.

The second hypothesis concerns the possibility that MT5-MMP is involved in astrocyte maturation, if we take into account the fact that MT5-MMP KO astrocytes are characterized by the downregulation of S100β. In particular, it was previously shown that rat primary astrocytes transiently downregulated S100β expression when exposed to the differentiating agent, db-cAMP, and re-expressed S100β at later stages of db-cAMP-induced differentiation [54,55]. Therefore, simpler morphology and a decreased expression of S100b could be the result of a developmental lag.

Overall, our study provides the first experimental evidence that MT5-MMP may affect some of the phenotypical features of cultured human neurons and astrocytes, which are reminiscent of cells at early developmental stages. This places MT5-MMP as an important enzyme in the control of neural cell development and warrants future work to identify more precisely the molecular mechanisms at stake in physiological and pathological settings.

Author Contributions: Conceptualization, E.N., S.R. and A.D.; methodology, N.A., P.B.-M., L.G.-G., L.A., L.G. and E.N.; validation, E.N., S.R. and A.D.; statistical analysis, N.A.; investigation, N.A., P.B.-M., L.G.-G., L.A. and L.G.; resources, E.N., L.G.-G. and L.G.; data curation, N.A.; writing—original draft preparation, N.A.; writing—review and editing, A.D., E.N. and S.R..; visualization, N.A., E.N. and S.R.; supervision, E.N., S.R. and A.D.; project administration, E.N., S.R. and A.D.; funding acquisition, E.N., S.R. and A.D. All authors have read and agreed to the published version of the manuscript.

Funding: This research was funded by the CNRS and Aix-Marseille Université, by CoEN grant to S.R. and E.N., by CoEN grant to A.D., by the "Fondation Plan Alzheimer" to S.R. and E.N., by Vaincre Alzheimer grants to S.R. and E.N., by public grants overseen by the French National Research Agency (ANR) MAD5 to S.R., by a grant from "La fondation NRJ-Institut de France" to E.N. and by a grant from France Alzheimer to S.R. P.B-M. was granted an International NeuroSchool doctoral

fellowship. L.G-G. was granted by the ANR and by the "Fondation pour la Recherche Médicale" FRM FDT201904008423. L.A.'s doctoral thesis was supported by the CoEN. This work also received the support of the A*Midex Foundation and the French National Research Agency funded by the French Government «Investissements d'Avenir» program (NeuroSchool, nEURo*AMU, ANR-17-EURE-0029 grant).

Institutional Review Board Statement: Not applicable.

Informed Consent Statement: Not applicable.

Data Availability Statement: The data presented in this study are openly available in Mendeley Data at DOI:10.17632/bfj8pnxfh8.1.

Acknowledgments: We thank Katrin Böhm for technical assistance.

Conflicts of Interest: The authors declare no conflict of interest.

References

1. Moussa-Pacha, N.M.; Abdin, S.M.; Omar, H.A.; Alniss, H.; Al-Tel, T.H. BACE1 inhibitors: Current status and future directions in treating Alzheimer's disease. *Med. Res. Rev.* **2020**, *40*, 339–384. [CrossRef] [PubMed]
2. Sanabria-Castro, A.; Alvarado-Echeverría, I.; Monge-Bonilla, C. Molecular Pathogenesis of Alzheimer's Disease: An Update. *Ann. Neurosci.* **2017**, *24*, 46–54. [CrossRef] [PubMed]
3. García-González, L.; Pilat, D.; Baranger, K.; Rivera, S. Emerging Alternative Proteinases in APP Metabolism and Alzheimer's Disease Pathogenesis: A Focus on MT1-MMP and MT5-MMP. *Front. Aging Neurosci.* **2019**, *11*, 244. [CrossRef]
4. Van Acker, Z.P.; Bretou, M.; Annaert, W. Endo-lysosomal dysregulations and late-onset Alzheimer's disease: Impact of genetic risk factors. *Mol. Neurodegener.* **2019**, *14*, 20. [CrossRef]
5. Mullard, A. BACE inhibitor bust in Alzheimer trial. *Nat. Rev. Drug Discov.* **2017**, *16*, 155. [CrossRef]
6. Piton, M.; Hirtz, C.; Desmetz, C.; Milhau, J.; Lajoix, A.D.; Bennys, K.; Lehmann, S.; Gabelle, A. Alzheimer's Disease: Advances in Drug Development. *J. Alzheimers Dis.* **2018**, *65*, 3–13. [CrossRef]
7. Haapasalo, A.; Hiltunen, M. A report from the 8th Kuopio Alzheimer symposium. *Neurodegener. Dis. Manag.* **2018**, *8*, 289–299. [CrossRef] [PubMed]
8. Mullard, A. BACE failures lower AD expectations, again. *Nat. Rev. Drug Discov.* **2018**, *17*, 385. [CrossRef] [PubMed]
9. Citron, M. Emerging Alzheimer's disease therapies: Inhibition of beta-secretase. *Neurobiol. Aging* **2002**, *23*, 1017–1022. [CrossRef]
10. De Strooper, B.; Vassar, R.; Golde, T. The secretases: Enzymes with therapeutic potential in Alzheimer disease. *Nat. Rev. Neurol.* **2010**, *6*, 99–107. [CrossRef] [PubMed]
11. Surguchev, A.A.; Emamzadeh, F.N.; Surguchov, A. Cell Responses to Extracellular α-Synuclein. *Molecules* **2019**, *24*, 305. [CrossRef] [PubMed]
12. Rivera, S.; García-González, L.; Khrestchatisky, M.; Baranger, K. Metalloproteinases and their tissue inhibitors in Alzheimer's disease and other neurodegenerative disorders. *Cell Mol. Life Sci.* **2019**, *76*, 3167–3191. [CrossRef]
13. Zipfel, P.; Rochais, C.; Baranger, K.; Rivera, S.; Dallemagne, P. Matrix Metalloproteinases as New Targets in Alzheimer's Disease: Opportunities and Challenges. *J. Med. Chem.* **2020**, *63*, 10705–10725. [CrossRef] [PubMed]
14. Baranger, K.; Khrestchatisky, M.; Rivera, S. MT5-MMP, just a new APP processing proteinase in Alzheimer's disease? *J. Neuroinflamm.* **2016**, *13*, 167. [CrossRef]
15. Sekine-Aizawa, Y.; Hama, E.; Watanabe, K.; Tsubuki, S.; Kanai-Azuma, M.; Kanai, Y.; Arai, H.; Aizawa, H.; Iwata, N.; Saido, T.C. Matrix metalloproteinase (MMP) system in brain: Identification and characterization of brain-specific MMP highly expressed in cerebellum. *Eur. J. Neurosci.* **2001**, *13*, 935–948. [CrossRef] [PubMed]
16. Itoh, Y. Membrane-type matrix metalloproteinases: Their functions and regulations. *Matrix Biol.* **2015**, *44–46*, 207–223. [CrossRef] [PubMed]
17. Pei, D. Identification and characterization of the fifth membrane-type matrix metalloproteinase MT5-MMP. *J. Biol. Chem.* **1999**, *274*, 8925–8932. [CrossRef]
18. Jaworski, D.M. Developmental regulation of membrane type-5 matrix metalloproteinase (MT5-MMP) expression in the rat nervous system. *Brain Res.* **2000**, *860*, 174–177. [CrossRef]
19. Warren, K.M.; Reeves, T.M.; Phillips, L.L. MT5-MMP, ADAM-10, and N-cadherin act in concert to facilitate synapse reorganization after traumatic brain injury. *J. Neurotrauma.* **2012**, *29*, 1922–1940. [CrossRef] [PubMed]
20. Monea, S.; Jordan, B.A.; Srivastava, S.; DeSouza, S.; Ziff, E.B. Membrane localization of membrane type 5 matrix metalloproteinase by AMPA receptor binding protein and cleavage of cadherins. *J. Neurosci.* **2006**, *26*, 2300–2312. [CrossRef] [PubMed]
21. Komori, K.; Nonaka, T.; Okada, A.; Kinoh, H.; Hayashita-Kinoh, H.; Yoshida, N.; Yana, I.; Seiki, M. Absence of mechanical allodynia and Abeta-fiber sprouting after sciatic nerve injury in mice lacking membrane-type 5 matrix metalloproteinase. *FEBS Lett.* **2004**, *557*, 125–128. [CrossRef]
22. Hayashita-Kinoh, H.; Kinoh, H.; Okada, A.; Komori, K.; Itoh, Y.; Chiba, T.; Kajita, M.; Yana, I.; Seiki, M. Membrane-type 5 matrix metalloproteinase is expressed in differentiated neurons and regulates axonal growth. *Cell Growth Differ.* **2001**, *12*, 573–580.

23. Porlan, E.; Martí-Prado, B.; Morante-Redolat, J.M.; Consiglio, A.; Delgado, A.C.; Kypta, R.; López-Otín, C.; Kirstein, M.; Fariñas, I. MT5-MMP regulates adult neural stem cell functional quiescence through the cleavage of N-cadherin. *Nat. Cell Biol.* **2014**, *16*, 629–638. [CrossRef]
24. Folgueras, A.R.; Valdés-Sánchez, T.; Llano, E.; Menéndez, L.; Baamonde, A.; Denlinger, B.L.; Belmonte, C.; Juárez, L.; Lastra, A.; García-Suárez, O.; et al. Metalloproteinase MT5-MMP is an essential modulator of neuro-immune interactions in thermal pain stimulation. *Proc. Natl. Acad. Sci. USA* **2009**, *106*, 16451–16456. [CrossRef]
25. Baranger, K.; Marchalant, Y.; Bonnet, A.E.; Crouzin, N.; Carrete, A.; Paumier, J.-M.; Py, N.A.; Bernard, A.; Bauer, C.; Charrat, E.; et al. MT5-MMP is a new pro-amyloidogenic proteinase that promotes amyloid pathology and cognitive decline in a transgenic mouse model of Alzheimer's disease. *Cell Mol. Life Sci.* **2016**, *73*, 217–236. [CrossRef] [PubMed]
26. Baranger, K.; Bonnet, A.E.; Girard, S.D.; Paumier, J.M.; García-González, L.; Elmanaa, W.; Bernard, A.; Charrat, E.; Stephan, D.; Bauer, C.; et al. MT5-MMP Promotes Alzheimer's Pathogenesis in the Frontal Cortex of 5xFAD Mice and APP Trafficking in vitro. *Front. Mol. Neurosci.* **2017**, *9*, 163. [CrossRef] [PubMed]
27. Willem, M.; Tahirovic, S.; Busche, M.A.; Ovsepian, S.V.; Chafai, M.; Kootar, S.; Hornburg, D.; Evans, L.D.B.; Moore, S.; Daria, A.; et al. η-Secretase processing of APP inhibits neuronal activity in the hippocampus. *Nature* **2015**, *526*, 443–447. [CrossRef] [PubMed]
28. Ran, F.A.; Hsu, P.D.; Wright, J.; Agarwala, V.; Scott, D.A.; Zhang, F. Genome engineering using the CRISPR-Cas9 system. *Nat. Protoc.* **2015**, *8*, 2281–2308. [CrossRef]
29. Rontani, P.; Perche, O.; Greetham, L.; Jullien, N.; Gepner, B.; Feron, F.; Erard-Garcia, M. Impaired expression of the COS-MOC/MOCOS gene unit in ASD patient stem cells. *Mol. Psychiatry* **2021**, *26*, 1606–1618. [CrossRef]
30. Chambers, S.M.; Fasano, C.A.; Papapetrou, E.P.; Tomishima, M.; Sadelain, M.; Studer, L. Highly efficient neural conversion of human ES and iPS cells by dual inhibition of SMAD signaling. *Nat. Biotechnol.* **2009**, *27*, 275–280. [CrossRef]
31. Bardy, C.; van den Hurk, M.; Eames, T.; Marchand, C.; Hernandez, R.V.; Kellogg, M.; Gorris, M.; Galet, B.; Palomares, V.; Brown, J.; et al. Neuronal medium that supports basic synaptic functions and activity of human neurons in vitro. *Proc. Natl. Acad. Sci. USA* **2015**, *112*, 2725–2734. [CrossRef] [PubMed]
32. Tcw, J.; Wang, M.; Pimenova, A.A.; Bowles, K.R.; Hartley, B.J.; Lacin, E.; Machlovi, S.I.; Abdelaal, R.; Karch, C.M.; Phatnani, H.; et al. An Efficient Platform for Astrocyte Differentiation from Human Induced Pluripotent Stem Cells. *Stem Cell Rep.* **2017**, *9*, 600–614. [CrossRef] [PubMed]
33. Jones, V.C.; Atkinson-Dell, R.; Verkhratsky, A.; Mohamet, L. Aberrant iPSC-derived human astrocytes in Alzheimer's disease. *Cell Death Dis.* **2017**, *8*, e2696. [CrossRef] [PubMed]
34. Penney, J.; Ralvenius, W.T.; Tsai, L.-H. Modeling Alzheimer's disease with iPSC-derived brain cells. *Mol. Psychiatry* **2020**, *25*, 148–167. [CrossRef] [PubMed]
35. Shi, Y.; Inoue, H.; Wu, J.C.; Yamanaka, S. Induced pluripotent stem cell technology: A decade of progress. *Nat. Rev. Drug Discov.* **2017**, *16*, 115–130. [CrossRef] [PubMed]
36. Liu, G.; David, B.T.; Trawczynski, M.; Fessler, R.G. Advances in Pluripotent Stem Cells: History, Mechanisms, Technologies, and Applications. *Stem Cell Rev. Rep.* **2020**, *16*, 3–32. [CrossRef]
37. Ye, B.; Jan, Y.N. The cadherin superfamily and dendrite development. *Trends Cell Biol.* **2005**, *15*, 64–67. [CrossRef]
38. Obst-Pernberg, K.; Redies, C. Cadherins and synaptic specificity. *J. Neurosci. Res.* **1999**, *58*, 130–138. [CrossRef]
39. Tanriover, G.; Kayisli, U.A.; Demir, R.; Pestereli, E.; Karaveli, S.; Demir, N. Distribution of N-cadherin in human cerebral cortex during prenatal development. *Histochem. Cell Biol.* **2004**, *122*, 191–200. [CrossRef] [PubMed]
40. Ramos-Gonzalez, P.; Mato, S.; Chara, J.C.; Verkhratsky, A.; Matute, C.; Cavaliere, F. Astrocytic atrophy as a pathological feature of Parkinson's disease with LRRK2 mutation. *NPJ Parkinsons Dis.* **2021**, *7*, 31. [CrossRef] [PubMed]
41. Zhou, B.; Zuo, Y.X.; Jiang, R.T. Astrocyte morphology: Diversity, plasticity, and role in neurological diseases. *CNS Neurosci. Ther.* **2019**, *25*, 665–673. [CrossRef]
42. Chung, W.-S.; Allen, N.J.; Eroglu, C. Astrocytes Control Synapse Formation, Function, and Elimination. *Cold Spring Harb. Perspect. Biol.* **2015**, *7*, a020370. [CrossRef]
43. Clarke, L.E.; Barres, B.A. Emerging roles of astrocytes in neural circuit development. *Nat. Rev. Neurosci.* **2013**, *14*, 311–321. [CrossRef] [PubMed]
44. Johnson, M.A.; Weick, J.P.; Pearce, R.A.; Zhang, S.-C. Functional neural development from human embryonic stem cells: Accelerated synaptic activity via astrocyte coculture. *J. Neurosci.* **2007**, *27*, 3069–3077. [CrossRef] [PubMed]
45. Escartin, C.; Galea, E.; Lakatos, A.; O'Callaghan, J.P.; Petzold, G.C.; Serrano-Pozo, A.; Verkhratsky, A. Reactive astrocyte nomenclature, definitions, and future directions. *Nat. Neurosci.* **2021**, *24*, 312–325. [CrossRef] [PubMed]
46. Escartin, C.; Guillemaud, O.; Carrillo-de Sauvage, M.A. Questions and (some) answers on reactive astrocytes. *Glia* **2019**, *67*, 2221–2247. [CrossRef]
47. Michetti, F.; D'Ambrosi, N.; Toesca, A.; Puglisi, M.A.; Serrano, A.; Marchese, E.; Geloso, M.C. The S100B story: From biomarker to active factor in neural injury. *J. Neurochem.* **2019**, *148*, 168–187. [CrossRef]
48. Pajarillo, E.; Rizor, A.; Lee, J.; Aschner, M.; Lee, E. The role of astrocytic glutamate transporters GLT-1 and GLAST in neurological disorders: Potential targets for neurotherapeutics. *Neuropharmacology* **2019**, *161*, 107559. [CrossRef]

49. Schousboe, A.; Scafidi, S.; Bak, L.K.; Waagepetersen, H.S.; McKenna, M.C. Glutamate Metabolism in the Brain Focusing on Astrocytes. In *Glutamate and ATP at the Interface of Metabolism and Signaling in the Brain*; Parpura, V., Schousboe, A., Verkhratsky, A., Eds.; Springer: Cham, Switzerland, 2014; Volume 11. [CrossRef]
50. Llano, E.; Pendás, A.M.; Freije, J.P.; Nakano, A.; Knäuper, V.; Murphy, G.; López-Otin, C. Identification and characterization of human MT5-MMP, a new membrane-bound activator of progelatinase an overexpressed in brain tumors. *Cancer Res.* **1999**, *59*, 2570–2576.
51. García-González, L.; Paumier, J.M.; Louis, L.; Pilat, D.; Bernard, A.; Stephan, D.; Rivera, S. MT5-MMP controls APP and β-CTF/C99 metabolism through proteolytic-dependent and -independent mechanisms relevant for Alzheimer's disease. *FASEB J.* **2021**, *35*, e21727. [CrossRef]
52. Ogier, C.; Bernard, A.; Chollet, A.M.; Le Diguardher, T.; Hanessian, S.; Charton, G.; Rivera, S. Matrix metalloproteinase-2 (MMP-2) regulates astrocyte motility in connection with the actin cytoskeleton and integrins. *Glia* **2006**, *54*, 272–284. [CrossRef] [PubMed]
53. Hannocks, M.J.; Zhang, X.; Gerwien, H.; Chashchina, A.; Burmeister, M.; Korpos, E.; Sorokin, L. The gelatinases, MMP-2 and MMP-9, as fine tuners of neuroinflammatory processes. *Matrix Biol.* **2017**, *75–76*, 102–113. [CrossRef] [PubMed]
54. Sorci, G.; Bianchi, R.; Riuzzi, F.; Tubaro, C.; Arcuri, C.; Giambanco, I.; Donato, R. S100B Protein, A Damage-Associated Molecular Pattern Protein in the Brain and Heart, and Beyond. *Cardiovasc. Psychiatry Neurol.* **2010**, *2010*, 656481. [CrossRef] [PubMed]
55. Raponi, E.; Agenes, F.; Delphin, C.; Assard, N.; Baudier, J.; Legraverend, C.; Deloulme, J.-C. S100B expression defines a state in which GFAP-expressing cells lose their neural stem cell potential and acquire a more mature developmental stage. *Glia* **2007**, *55*, 165–177. [CrossRef]

Article 2: Mutations in specific domains of MT5-MMP prevent the accumulation of toxic APP metabolites and serve as templates for peptide-based therapeutics in human in vitro models of Alzheimer's disease

Belio-Mairal P, Kamitsou A, Stephan D, Jullien N, Thiane D, Benoist F, Ramos M, Louis L, Khrestchatisky M, Lécorché P, Nivet E, Rivera S.

HAL. 2024
hal-04642476

Increasing evidence demonstrates the possibility of targeting MT5-MMP to halt multiple pathogenic events in AD. Depletion of MT5-MMP in the 5xFAD mouse model inhibits amyloidogenesis and neuroinflammation at early and advanced stages of the disease. In HEK cells, MT5-MMP overexpression increased C99 and Aβ levels and APP translocation into early endosomes[443,481]. Thus, the molecular mechanisms underlying the amyloidogenic properties of MT5-MMP are related to its proteolytic activity and the modulation of APP trafficking. However, further investigation of the pathogenic mechanisms of MT5-MMP demonstrated that inactivated MT5-MMP preserved its capacity to increase Aβ levels in a β- and γ-secretase-independent manner, suggesting an important pro-amylodogenic role of MT5-MMP via APP trafficking modulation. Whole-domain deletions in MT5-MMP confirmed that a lack of the TM and IC domains, or only the IC domain, was sufficient to prevent C99 and Aβ accumulation in HEK cells[455]. The major pro-amyloidogenic roles of MT5-MMP TM and IC led us to explore the possibilities of modulating their capacity to regulate the fate of C99.

MT5-MMP is involved in multiple crucial homeostatic roles in neurons, and its deficiency alters the phenotype of human neurons and astrocytes from healthy individuals[544]. Thus, reducing MT5-MMP expression in the CNS is a strategy with poor translational potential. Here, we aimed to explore the molecular mechanisms of MT5-MMP TM and IC domains. Specifically, which amino acid groups are involved in the MT5-MMP TM and IC roles in C99 and Aβ accumulation. Identifying the pro-amyloidogenic components of the C-terminal non-catalytic domains of MT5-MMP could facilitate the development of therapeutic strategies leveraging the molecular properties of these two domains. We demonstrated that MT5-MMP TM and IC play different roles in C99 metabolization, with

TM inducing C99 stabilization and IC inducing its cleavage by γ-secretase and its degradation. Contrary to deletions, the substitution of specific amino acid groups in MT5-MMP IC promotes C99 degradation with differing effects on Aβ levels. Only the substitution of KNKTG in MT5-MMP IC resulted in a consistent decrease in C99 and Aβ levels. Moreover, we observed that mutations in MT5-MMP TM and IC induced changes in the subcellular distribution of C99, likely affecting its fate. Ala substitutions of the MT5-MMP IC EWV PDZ-binding motif located at the C-terminus, altered C99 trafficking, suggesting an important role for Mint proteins in MT5-MMP-mediated trafficking of C99. Based on our findings, we designed a peptide mimicking MT5-MMP IC with KNKTG substitutions, which reduced C99 levels in HEK cells overexpressing C99. In summary, our efforts to understand the molecular mechanisms of MT5-MMP TM and IC in C99 and Aβ accumulation uncovered new possibilities for designing MT5-MMP-based therapeutic strategies without altering endogenous MT5-MMP expression in an AD *in vitro* model.



Mutations in specific domains of MT5-MMP prevent the accumulation of toxic APP metabolites and serve as templates for peptide-based therapeutics in human in vitro models of Alzheimer's disease

Pedro Belio-Mairal, Athina Kamitsou, Delphine Stephan, Nicolas Jullien, Diarra Thiane, Melissa Ramos, Laurence Louis, Florian Benoist, Bastien Serrano, Marion David, et al.

▶ **To cite this version:**

Pedro Belio-Mairal, Athina Kamitsou, Delphine Stephan, Nicolas Jullien, Diarra Thiane, et al.. Mutations in specific domains of MT5-MMP prevent the accumulation of toxic APP metabolites and serve as templates for peptide-based therapeutics in human in vitro models of Alzheimer's disease. 2024. hal-04642476

HAL Id: hal-04642476

https://amu.hal.science/hal-04642476

Preprint submitted on 10 Jul 2024

HAL is a multi-disciplinary open access archive for the deposit and dissemination of scientific research documents, whether they are published or not. The documents may come from teaching and research institutions in France or abroad, or from public or private research centers.

L'archive ouverte pluridisciplinaire **HAL**, est destinée au dépôt et à la diffusion de documents scientifiques de niveau recherche, publiés ou non, émanant des établissements d'enseignement et de recherche français ou étrangers, des laboratoires publics ou privés.

Mutations in specific domains of MT5-MMP prevent the accumulation of toxic APP metabolites and serve as templates for peptide-based therapeutics in human *in vitro* models of Alzheimer's disease

Belio-Mairal P[1], Kamitsou A[1], Stephan D[1], Jullien N[1], Thiane D[1], Ramos M[1], Louis L[1], Benoist F[2], Serrano B[2], David M[2], Khrestchatisky M[1], Lécorché P[2], Nivet E[1], Rivera S[1]*.

1. Aix-Marseille Univ, CNRS, INP, Inst Neurophysiopathol, Marseille, France

2. Vect-Horus S.A.S., Faculté de Médecine, Marseille, France

* Corresponding author, santiago.rivera@univ-amu.fr

ABSTRACT

In previous work we identified key roles of membrane-type 5-matrix metalloproteinase (MT5-MMP) in Alzheimer's disease (AD) pathogenesis. More specifically, we uncovered the involvement of the C-terminal domains of the proteinase in the processing of amyloid precursor protein (APP) and the fate of some of its major toxic metabolites (*e.g.,* C99, Aβ). We further described these effects as being dependent on MT5-MMP transmembrane (TM) and intracellular (IC) domains, leading us to hypothesize that modifications in these domains could represent a therapeutic strategy to modulate toxic APP metabolites. To test this, here we generated MT5-MMP variants carrying amino acid deletions or substitutions in entire proteinase domains or in selected amino acid clusters in the IC domain. MT5-MMP variants were co-transfected in human cell lines overexpressing C99, reminiscent of an AD setting. We have identified mutations in the IC domain that induce C99 degradation and a decrease in Aβ levels, while other mutations have divergent effects on these APP metabolites. Furthermore, high content imaging revealed the importance of MT5-MMP IC modifications in C99 subcellular trafficking through the endomembrane system and how this impacts C99 processing. Proximity ligation assays also highlight the importance of the IC domain in MT5-MMP co-localization, and possible interaction, with C99. In a translational effort, we synthetized and functionalized a peptide mimicking the MT5-MMP IC domain carrying mutations in the N-terminus. We demonstrated that this synthetic peptide efficiently decreased C99 levels in our AD *in vitro* model. Overall, our study highlights the role of a selected group of amino acids in the C-terminal domains of MT5-MMP as the basis for a better understanding of the proteinase's contribution to APP metabolism. Moreover, this study provides a new approach for designing peptide-based therapeutic strategies against AD based on the properties of specific MT5-MMP domains to prevent C99 and Aβ accumulation.

INTRODUCTION

Matrix metalloproteinases (MMPs) form a multigenic family of endopeptidases with more than 20 members that display a wide spectrum of biological activities[1]. Membrane-type 5-matrix metalloproteinase (MT5-MMP, also known as MMP-24 or η-secretase), is the only MMP family member that is primarily expressed in neural cells[2,3] and contributes to a number of physiological and pathological processes in the nervous system[4,5]. Early studies demonstrated that MT5-MMP catalytic activity is required for the proper cleavage of extracellular and non-extracellular matrix proteins[5], playing a role in synaptic plasticity[6], neural stem cell differentiation[7], post-lesion synaptic reorganization[8], and axonal growth and regeneration[9].

The presence of MT5-MMP in amyloid plaques of Alzheimer's disease (AD) patients implied its possible implication in the disease pathogenesis[2]. Accordingly, MT5-MMP was found to cleave amyloid precursor protein (APP) in HEK cells[10] and murine primary neurons[11]. APP is central to the amyloid hypothesis of AD, as its processing by β-secretase generates the APP C-terminal fragment (CTF), C99, and its subsequent cleavage by γ-secretase releases the beta-amyloid peptide (Aβ)[12], which is the main constituent of amyloid plaques and a primary pharmacological target. APP cleavage was reduced in the brain of the 5xFAD mouse model of AD deficient in MT5-MMP, indicating the *in vivo* cleavage of APP by this MMP[13]. In addition, MT5-MMP deficiency in 5xFAD mice reduced the levels of Aβ and its immediate precursor C99, as well as the levels of neuroinflammatory mediators and glial reactivity, while long-term potentiation (LTP) and cognitive performance were preserved[13,14]. Furthermore, in favor of MT5-MMP involvement in AD pathogenesis, its overexpression in HEKswe cells caused the accumulation of C99 and Aβ[13]. Moreover, MT5-MMP cleavage of APP at the η-site releases η-CTFs, which carry synaptotoxic activities[15] and contribute to Aβ production[16].

Considering their increasing pathological relevance in AD, the functional interaction of MT5-MMP and C99 is of great interest. C99 buildup precedes that of Aβ in the 3xTg and 5xFAD mouse models of AD[17,18]. In humans, C99 accumulates in brains of patients with AD[19], as well as in neurons carrying familial AD mutations, leading to endosomal dysfunction[20]. We recently reported that MT5-MMP controls the metabolism of APP and its CTFs *via* both

dependent and independent proteolytic mechanisms, indicating that certain non-catalytic domains are important for regulating its functions, particularly its interactions with APP[4].

In this study, we aimed to gain a better understanding of the mechanisms underlying the control of C99 by the non-catalytic domains of MT5-MMP. We used molecular and cell biology, and structure-function approaches, to assess the relevance of specific amino acid residues in the fate of C99 and Aβ. We provide new insights into the functional interactions between MT5-MMP and C99 and provide new perspectives for adopting MT5-MMP-based therapeutic strategies to modulate C99 in mammalian cells.

MATERIALS AND METHODS

Plasmid constructs

All plasmids were constructed using a pcDNA3.1 backbone. The new plasmids used in this study (ΔEXT, TM1/IC5, TM5/IC1, all the mutated variants of TM/IC) (Fig 1A, 2A) were generated by GeneArt (ThermoFisher Scientific). Constructs encoding other MT5-MMP variants (pcDNA, TM/IC, EXT/TM, EXT) and C99 or HA-C99 were produced as previously described[4]. Plasmids were purified and amplified as previously described[4].

Cell lines

HEK cells were maintained with DMEM Glutamax (61965026, ThermoFisher Scientific) supplemented with 10% fetal bovine serum (FBS) (A3160801, ThermoFisher Scientific) and 1% penicillin/streptomycin (15140122, ThermoFisher Scientific) (hereafter referred as HEK media). For the passaging procedure, cells were washed with 5mL of DPBS (14190094, ThermoFisher Scientific) and 2 mL of 0.05% Trypsin-EDTA (25300054, ThermoFisher Scientific) were added for 2 min. Next, 8 mL of HEK medium were added to a T75 flask (353136, Corning), and cells were dissociated into single cells by gentle mechanic pipetting. Then, 3 mL of the cell suspension was replated in a new T75 flask containing 10 mL of fresh HEK medium. Geneticin (10131027, ThermoFisher Scientific) was added at a 1:100 dilution.

hTERT-RPE1 cells were cultured using the same protocol used for HEK cells but with different reagents. The medium consisted of DMEM/F12 (31331028, ThermoFisher Scientific)

supplemented with 10% FBS and 1% penicillin/streptomycin. HBSS (14025050, ThermoFisher Scientific) was used for washing. Moreover, 0.25% Trypsin-EDTA (25200056, ThermoFisher Scientific) was used for 5 min to dissociate the cells.

Transfections

The cell lines were transfected using JetPei® Polyplus (101000053, Sartorius). For 24-well plate (353047, Corning) and 96-well plate (6055300, Revvity; 353072, Corning) formats, reverse transfection (the plasmids are added to the plate and the cells are then seeded onto it) was used to limit toxicity and increase transfection efficiency in low cell density context (< 15,000 cells/well). For larger volumes or densities, classical forward transfection was used. In both cases, the manufacturer's instructions were followed with the recommended volumes of transfection reagents and DNA quantities. The cell densities were adjusted according to the cell line. HEK cells were seeded in 6-well plates (353046, Corning) at a density of 1.5 M per well. hTERT-RPE1 cells were seeded at 10 K per well in 96-well plates and 25K in 24-well plates.

All the inhibitors were diluted in DMSO (D2650, Sigma-Aldrich). Inhibitors (Table 1) were added 15–17 h after transfection. After 20 h, cells were lysed and collected for experiments.

MTT test

HEK cells were seeded at 50,000 cells/well in 96-well plates according to the recommended volumes per the JetPei Polyplus protocol. The next day, cells were transfected or treated with the corresponding peptides. At 48 h after transfection or peptide treatment, 25 µL/well of a 5 mg/mL solution of Thiazolyl Blue Tetrazolium Bromide (M5655, Sigma-Aldrich) in HEK medium were added to each well to obtain a final solution of 0.5 mg/mL. After 3 h of incubation, the culture medium was aspired, and the formazan crystals were dissolved in 100 µL/well dimethyl sulfoxide (DMSO) (D2650, Sigma-Aldrich). The plates were shaken in the dark until the crystals were fully dissolved. Finally, the plates were read in

a multiwell plate reader with an emission filter of 544-10 nm with 3 mm diameter of orbital averaging, and 10 flashes per well.

To analyze the absorbances, the average of each row and column was used to normalize technical differences and differences in plate reading. Then, the condition with the transfection reagent but without the plasmid or peptide was used as a normalizing control for all readings to compare the different biological conditions.

Protein quantification

A bicinchoninic acid assay was used to quantify the protein concentration in the cell lysates. A BCA assay kit was used (23225, ThermoFisher Scientific) following manufacturer's instructions for the multiwell plate format. Lysates from HEK cells were diluted 1:5 with lysis buffer to enter the detection range of the kit. The samples for the standard curves were obtained from a ready-to-use BSA standard kit (23208, ThermoFisher Scientific). Each multiwell plate contained the standard curve dilutions with a blank for each lysis buffer used and the different samples. All measurements were performed in two technical replicates and, when possible, standard curve dilutions and blanks were performed in triplicate. Absorbance was measured using a multiwell plate reader with a 544-10 nm emission filter.

The standard curve was calculated using the 4-parameter fit of MARS data analysis software version 2.10R3 (BMG Labtech). Concentrations were extrapolated using the same software to calculate the volumes necessary for downstream applications.

Western Blot

After protein quantification, 20 µg of protein in 15 µL for 10-well gels or 7.5 µL for 15-well gels were prepared with ultrapure H_2O (0066571E, B.Braun). Samples were mixed with the same volume of 2x Tris-Glycine (LC2676, ThermoFisher Scientific) or Tricine (LC1676, ThermoFisher Scientific) sample buffer and heated at 95°C for 5 min or 85°C for 20 min for small-sized (<20 kDa) target proteins.

The overall protocol of western blot is based on ThermoFisher's instructions using a Mini gel tank system (A25977, ThermoFisher Scientific) and a Power Blotter Semi-dry Transfer

system (PB0013, ThermoFisher Scientific). All products cited in this section were obtained from ThermoFisher Scientific unless otherwise stated. Specifically, Novex 4-20% Tris-Glycine gels with 10 wells (XP04200BOX) or 15 wells (XP04205BOX) were run at 40 mA per gel with a maximum voltage of 130 V for 1h30 or until the 10 kDa marker of the prestained protein ladder (26616) was at the lowest end of the gel. Novex 16% Tricine gels with 10-well (EC6695BOX) or 15-well (EC66955BOX) formats were used with a Multicolor Low Range protein ladder (26628), and they were run at 80 mA per gel with a maximum voltage of 130 V for 1 h 30 min or until the 10 kDa marker reached the lowest end of the gel.

The gels were transferred into 0.45µM nitrocellulose blotting membranes (10600002, Amersham) assembled with two stacks of five units of 0.34-mm Whatman papers (3030-917, Cytiva) on top of the gels and another stack below the membranes. Prior to building the stack, all components were wetted with Towbin buffer composed of double-distilled H_2O (ddH_2O) with 25 mM Tris-Base (T1503, Sigma-Aldrich), 192 mM Glycine (G8898, Sigma-Aldrich), and 20%$_{v/v}$ methanol (34860, Sigma-Aldrich) at a final pH of 8.3 ± 0.1. The stacks were then arranged in the PowerBlotter and ran in standard semi-dry mode (25 V with 1 A maximum) for 1 h.

Blotting membranes were recovered and incubated in Ponceau solution (P7170, Sigma-Aldrich) for 30 s. Ponceau staining was captured using the Preview mode on a NineAllience 9.7 17.02 (UVITec). The membranes were then blocked for 1 h in agitation at room temperature with a blocking buffer consisting of 1x PBS (ET330-A, Euromedex) with 5%$_{m/v}$ powder milk and 0.2%$_{v/v}$ Tween20 (P1379, Sigma-Aldrich). Afterwards, antibodies were diluted to 1:1000 (anti-actin antibodies were diluted 1:5000) in blocking buffer and transferred with membranes to a clean recipient for incubation overnight at 4°C with agitation. The next day, the membranes were washed 3 times for 10 min under agitation at room temperature with 1x PBS and 0.2%$_{v/v}$ Tween20 (washing buffer). The membranes were incubated with HRP-conjugated secondary antibodies (1:1,000) in blocking buffer for 1 h under agitation at room temperature. After 3 washes of 10 minutes each with wash buffer, ECL solution (RPN2106, Amersham) or ECL Prime solution (RPN2236, Amersham) was used as per the manufacturer's instructions, depending on the signal intensity, and the membranes were visualized using the chemiluminescence mode of the UVITec station.

The western blot bands were semi-quantified using Fiji's tool "Plot lanes" from the "Gels" module[21]. The actin band values were used to normalize the remaining values.

Immunocytochemistry

Cells were cultured in 12-mm glass coverslips for confocal microscopy (65.300.21, Dutscher), 1.5H coverslips for super-resolution microscopy (0117520, Marienfeld Superior), or 96-well plates (6055300, Revvity) for high-content screening microscopy.

For sample fixation, PEM buffer was prepared to obtain a final solution of PIPES 80 mM (P1851, Sigma-Aldrich), $MgCl_2$ 2mM (M9272, Honeywell), and EGTA 5mM (E4378, Sigma-Aldrich) at pH 6.8 in ddH_2O. Then, paraformaldehyde (15714, Electron Microscopy Services) was diluted at 4%$_{v/v}$ in PEM with 4%$_{m/v}$ sucrose (S0389, Sigma-Aldrich) (fixation solution).

Glass coverslips 12 mm in diameter were washed with 0.5 mL of 1x DPBS previously to adding 300µL/well of fixation solution at room temperature. After incubating the cells for 10 min at room temperature, they were washed 4 times with 0.5 mL of DPBS. Cells were later blocked and permeabilized for 1 h under gentle agitation at room temperature with 3%$_{m/v}$ bovine serum albumin (BSA) (A7906, Sigma-Aldrich), 0.1% Triton X-100 (X-100, Sigma-Aldrich), and 10% normal goat (005-000-121, Jackson ImmunoResearch) or donkey (017-000-121, Jackson ImmunoResearch) serum in 1x DPBS (block/per buffer). For organelle staining, Triton X-100 was replaced with saponine (84510, Sigma-Aldrich) at the same concentration. After blocking and permeabilization, primary antibodies were diluted to the corresponding concentrations (Table 2) in block/per buffer. Cells were incubated with diluted antibodies overnight at 4°C.

The next day, cells were washed 3 times with 1x DPBS for 5 min under gentle agitation at room temperature. The secondary antibodies (Table 2) were diluted to 1:800 in block/per buffer, and cells were incubated with the diluted secondary antibodies for 1 h under gentle agitation at room temperature and protected from light. Then, cells were washed twice with 1x DPBS for 5 min under gentle agitation at room temperature and incubated for 10 min under the same conditions with 10 µg/mL Hoechst33342 (H3570, ThermoFisher Scientific) diluted in 1x DPBS. Finally, cells were washed twice more with 1x DPBS for 5 min under gentle agitation at room temperature, and coverslips were mounted on slides using 6µL of mounting media

(P36934, ThermoFisher Scientific). Slides were allowed to dry at room temperature overnight and curated at 4°C for 48 h before imaging.

For high-content imaging, the procedures were the same with adjusted volumes, except that the plates were parafilm-sealed and kept in DPBS after the two last DPBS washes following Hoechst 33342 incubation.

Microscopy analyses

Python procedures to clean, downsize, normalize, and visualize quantitative data from the automated microscope were run in Jupyter Notebooks (available at: github.com/RiveraLabINP/BelioMairal_2024). In brief, the overlap values of individual cells were retrieved from the Operetta© software (quantification workflow available at: github.com/RiveraLabINP/BelioMairal_2024). These values were multiplied by the area of HA fluorescence to generate a new variable representing the total area of overlap of HA with each organelle. The overlap areas were normalized using the standard values of the Power Transformer function from the sklearn package. The individual cells were then clustered using KMeans from sklearn package in 9 different clusters based on the overlap area and the number of HA spots in the cell. The dataset was downsized excluding the clusters of cells with the smallest and biggest values. The mean area of overlap was calculated for each MT5-MMP variant and normalized to the pcDNA value of each independent experiment. Finally, outliers were detected with the Tukey method by discarding values outside the fences using 1.5 as the outlier multiplier. The resulting values were used to visualize the results and Bayesian statistics.

Prior to principal component analysis, the values were standardized using the StandardScaler from the sklearn package. Once normalized and standardized, the PCA function from skleanr was used with two principal components (n components=2). For cluster analysis, the function clustermap from the seaborn package was used with the metric "canberra" (metric='canberra').

A complete list of Python and package versions is provided at: github.com/RiveraLabINP/BelioMairal_2024.

ELISA

To measure secreted Aβ40 in our samples, an ELISA kit was used (KHB3481, ThermoFisher Scientific) following manufacturer's instructions. Briefly, culture supernatants were recovered in low-binding tubes (022431081, Eppendorf) and stored at -80°C or immediately used. Samples were centrifuged at 1400 rpm for 1 min at room temperature. The supernatants were transferred to new low-binding tubes, and the samples were diluted to match the detection range. The manufacturer's protocol was followed for the remaining procedures.

Absorbance was measured using a multiwell plate reader with an emission filter 450-10 nm and 10 flashes per well. The standard curve was calculated using the 4-parameter fit of the MARS data analysis software. Concentrations were extrapolated using the same software, and values from the pcDNA condition were used to normalize all other values to account for technical variability. Thus, the results are presented as fold-changes compared with cells co-transfected with empty pcDNA and C99 overexpression constructs.

Proximity ligation assay

Colocalization between C99 and MT5-MMP constructs was performed using DuoLink© In Situ system. All volumes were adjusted to perform the procedures in 96-well plates. The goat anti-rat (112-005-003, Jackson ImmunoResearch) and goat anti-rabbit (111-005-003, Jackson ImmunoResearch) unconjugated antibodies were conjugated with DuoLink© PLA orange probes (DUO96030-1KT, Sigma-Aldrich) following the manufacturer's instructions and stored at 4°C. Cells were stained using the normal immunofluorescence protocol until secondary antibody binding. Secondary antibody binding and further procedures were performed according to DuoLink© In situ orange detection kit (DUO92007-100RXN, Sigma-Aldrich). Finally, cells were stained with Hoechst 33342, as previously explained, and plates were sealed with parafilm.

Peptide synthesis and conjugations

Fmoc–amino acids were obtained from Iris Biotech (Marktredwitz, Germany). All other amino acids and reagents were purchased from Sigma-Aldrich (Saint-Quentin-Fallavier,

France) or Analytical Lab (Castelnau-le-Lez, France). Peptide assembly was performed using a Liberty (CEM®) microwave synthesizer by solid phase peptide synthesis (SPPS) based on the Fmoc strategy. Fmoc–Gly-Wang resin (loading 0.66 mmol/g) were purchased from Iris Biotech and were used as solid support.

Purification and analysis of peptide-based products

Monitoring of reactions and quality controls of the peptide-based intermediates were carried out by liquid chromatography/mass spectrometry (LC/MS) using a Thermo Fisher Scientific UltiMate®3000 system (Waltham, MA, USA) equipped with an ion trap (LCQ Fleet) and an electrospray ionization source (positive ion mode). The LC flow rate was set to 2 mL/min using H2O 0.1%TFA (buffer A) and MeCN 0.1%TFA (buffer B) as eluents. The gradient elution was 10%–90% B in 10 min (quality control) equipped with a C18 Kinetex™ (2.6 µm, 50 mm × 4.6 mm). The heated electrospray ionization source had a capillary temperature of 350 °C. Crude peptides were purified using reverse-phase (RP)-High Pressure Liquid Chromatography (HPLC) on a Thermo Fisher Scientific UltiMate®3000 system equipped with a C18 Luna™ (5 µm, 100 mm × 21.2 mm). The detection was performed at 214 nm. The elution system comprised H2O 0.1%TFA (buffer A) and MeCN 0.1%TFA (buffer B). Flow rate was 20 mL/min.

Preparation of p17 and p20

Peptide p17: H-QFAAAAAPQPVTYYKRPVQEWV-COOH and peptide p20: H-QFKNKTGPQPVTYYKRAAAEWV-COOH were synthesized using 0.1 mmol SPPS Fmoc–Gly-Wang resin under microwave activation. Resin was swollen in DMF for 10 min. Deprotection of the fmoc-protecting group was performed using a solution of 20% piperidine in DMF for 200 s under microwave activation at 75 °C. Stepwise assembly of the Fmoc–protected-amino-acids were performed under microwave activation using standard Fmoc peptide chemistry. Double coupling times of 240 s were used with a solution of Fmoc–amino acid (1 eq), Oxyma (10 eq excess; 1 M) in DMF, and DIC (5 eq excess; 1 M) in DMF under microwave activation at 90 °C. Double coupling was used for R amino acids to improve yield. Finally, the peptidyl-resin was washed 3 times with DCM and then treated with TFA/TIS/H2O

(95:2.5:2.5) containing DTT (10 mg/1mL) at room temperature for 4 h. The cleavage solution was recovered, concentrated under N2 flow, precipitated with cold diethyl ether and washed 2 times with cold diethyl ether. The crude products were dissolved in an H2O + 0.1%TFA /MeCN + 0.1% TFA (1:1) mixture and lyophilized. The crude peptide was purified using preparative RP-HPLC as described previously to obtain p17 and p20 as white powders (p17: 60 mg, 24%; p20: 52 mg, 20%).

Production of VHH C5

Phagemid encoding VHH C5 was transformed in the E. coli BL21DE3 strain. Transformed bacteria were grown in 200 ml of 2YTA until 0.5 < OD600 < 0.8 and induced with 100 µM IPTG overnight at 30 °C with shaking (250 rpm). Bacteria were pelleted and lysed by freeze-thawing and BugBuster® Protein Extraction Reagent (Novagen, Pretoria, South Africa). After a centrifugation step (3000 g, 20 min), VHH C5 was purified from the supernatant using metal affinity chromatography, TALON® Superflow™ (GE Healthcare), according to the manufacturer's instructions. Bound molecules were eluted with 250 mM imidazole, which was eliminated using PD-10 Desalting column (GE Healthcare). An additional gel filtration step using a Superdex 75 column (Cytiva, Marlborough, USA) was performed to remove endotoxins. The purified VHH was validated for its quality and purity by LC-MS on a Orbitrap Exploris apparatus (Thermo Fisher Scientific).

Chemical conjugation of VHH C5 and p17

First, C5-PEG2-BCN was prepared. An Eppendorf vial was filled with VHH C5 (8.0 mg, 539 nmol, 2.0 mL in PBS 1X), BCN-PEG2-NH2 (5.2 mg, 16170 nmol, 0.5 mL in PBS 1X) and BTG (10.8 U, 0.08 mL). The reaction mixture was left overnight at room temperature and purified by size exclusion chromatography hiload 16/600 Superdex 75 pg using PBS 1X as an eluent to give C5-PEG2-BCN as a colorless solution (6.8mg, 79%, 2.1mL in PBS 1X). Finally, in an Eppendorf vial were introduced respectively C5-PEG2-BCN (1.8 mg, 119 nmol, 557 µL in PBS 1X) and p17 (1.0 mg, 356 nmol, 234 µL in PBS 1X). The reaction mixture was left overnight at room temperature and purified by size exclusion chromatography Superdex 10/300

increase 75 GL using PBS 1X as eluent to give C5-p17 as a colorless solution (1.5mg, 72%, 290 µL in PBS 1X).

Statistics

Frequentist statistics were performed using GraphPad Prism 10.2.3 for MacOSX (GraphPad Software). Unless otherwise stated, all tests were ANOVA with Dunnett's post hoc multiple comparison test for comparison with the control condition of each experimental set. The same software was used to generate the graphs, where the p-values are represented with * p value < 0.05, ** p value < 0.01, *** p value < 0.001, and **** p value < 0.0001.

For Bayesian statistics, JASP 0.18.3 (JASP team) was used to perform Bayesian ANOVA with post hoc tests. Prior odds were unchanged from the software default values, and the Bayes factor was LogBF10 when compared with the null model.

All statistical analyses were performed using at least three independent experiments.

RESULTS

Modulation of C99 and Aβ levels by non-catalytic MT5-MMP variants

We previously showed that the removal of the MT5-MMP intracytoplasmic (IC) domain alone or together with the transmembrane (TM) domain, referred to as EXT/TM or EXT, drastically reduced C99 levels when either of these two constructs was expressed with a plasmid encoding C99 in HEK cells. In contrast, deletion of the extracellular domains (EXT) of MT5-MMP, here named TM/IC, was sufficient to reproduce pro-amyloidogenic effects of MT5-MMP in cells overexpressing C99[4]. Thus, we aimed to identify the specific residues in TM/IC that are responsible for C99 and Aβ accumulation. However, it was unclear whether proteolytic activity in the catalytic site of EXT could account for its anti-amyloidogenic effects. Accordingly, we rendered the truncated variant inactive by substituting the Glu283 residue of the catalytic site with alanine (hereafter referred as ΔEXT) (see Fig 1A for scheme of constructs). Following coexpression of MT5-MMP variants and C99, there was no decrease in cell survival (Fig 1B). However, western blot analysis using an anti-CTF antibody revealed a significant decrease of C99 levels by 83%, 71%, and 74% in cells expressing EXT, EXT/TM, and ΔEXT, respectively, compared with our pro-amyloidogenic control MT5-MMP TM/IC (Fig 1C). This indicates that the catalytic activities of EXT and EXT/TM are not responsible for the significant drop in C99 levels in the absence of the TM and IC domains. Under these conditions, we also observed a significant decrease in the supernatant Aβ levels of cells expressing EXT, as assessed by ELISA, whereas ΔEXT cells exhibited Aβ levels close to control values (Fig 1D). This suggests that the inactivation of the catalytic domain may drive part of C99 toward Aβ production, contrary to EXT.

Next, we sought to elucidate whether the effects on C99 modulation were primarily due to the exclusion of the TM or IC domain, or both. To this end, we generated whole-domain substitutions to explore whether selective modifications of the MT5-MMP TM or IC amino acid sequences were sufficient to cause a significant reduction in C99 levels. Substitutions were based on previously reported functional divergencies between MT5-MMP and MT1-MMP, where suppression of the IC domain of MT1-MMP caused a strong increase in C99 levels, in contrast to the decrease caused by suppression of the MT5-MMP IC domain herein confirmed [4]. Accordingly, we generated two chimeras combining the TM and IC domains of both

proteinases: one construct encoding the TM of MT5-MMP and the IC of MT1-MMP (namely TM5/IC1) and another with the reverse composition (TM1/IC5) (see Fig 1A). The coexpression of TM5/IC1 or TM1/IC5 constructs with C99 had contrasting effects on both C99 and Aβ levels, but no effect on cell survival (Fig 1B, E, F). On the one hand, TM5/IC1 maintained C99 levels while drastically reducing Aβ secretion by 67% (Fig 1E, F). On the other hand, TM1/IC5 significantly decreased C99 levels by 69% but maintained Aβ levels similar to those of control TM/IC (Fig 1E, F). Overall, the contrasting outcomes for C99 and Aβ with both chimeras indicate a distinct influence on C99 processing, depending on the presence of MT5-MMP TM or IC.

MT5-MMP non-catalytic variants control C99 processing

We next investigated the fate of C99 by modulating two of the main C99 degradation systems, lactacystin (LACT) to inhibit proteasome activity and ELND006 (D6) to inhibit γ-secretase. In EXT-expressing cells, we found that only LACT treatment caused a significant recovery of C99 levels, whereas D6 had no effect (Fig 1G), indicating a prominent role of proteasome over γ-secretase in C99 degradation upon co-expression with EXT. Similarly, in the ΔEXT group, treatment with LACT also induced a significant recovery of C99, whereas D6 failed to rescue C99 levels (Fig. 1H). Considering that coexpression of ΔEXT with C99 maintains Aβ levels, the lack of recovery of C99 with D6 suggests the possibility of EXT catalytic activity in impeding Aβ generation.

Our previous studies demonstrated that treatment of HEK cells with Bafilomycin A1 (BAFA1)—an inhibitor of the V-ATPase pump[22]—increased C99 in the presence of MT5-MMP TM/IC but decreased C99 in the presence of EXT, indicating that C99 is processed in the autophagolysosome pathway in a context of high Aβ production in HEK cells expressing TM/IC [4]. BAFA1 treatment induced a significant 331% recovery of C99 levels in ΔEXT-cotransfected cells, an effect that remained well below the recovery of LACT. In contrast, BAFA1 had no significant effect in EXT-expressing cells (Fig 1G, H). Therefore, the inactivation of the MT5-MMP catalytic domain along with the deletion of the TM and IC domains partially drives C99 into lysosomal compartments, although proteasomal degradation is predominant. This confirms that the proteasome is the primary processing machinery of C99

in the presence of EXT or ΔEXT, with an alternative degradation pathway involving EXT catalytic activity in lysosomal compartments. However, other enzymes present in lysosomes could also be responsible for Aβ increase in ΔEXT-expressing HEK cells.

The lysosomal enzyme cathepsin B can cleave and degrade Aβ[23]. In addition, cathepsin B colocalized with C99 in enlarged lysosomal structures and cleaves APP-CTFs at C-terminal sites, thereby removing the C99 CTF epitope[17,24]. Thus, we postulated that cathepsin B could be a potential generator of Aβ peptides detected by ELISA. However, this hypothesis was not supported after using CA-074-Me (CA074), a well-known cathepsin B inhibitor, which had no effect on canonical APP secretases[24]. This failed to recover C99 levels in EXT- or ΔEXT-expressing cells (Fig 1G, H), suggesting that inhibition of a single lysosomal enzyme is insufficient to restore C99 levels and block Aβ production.

We next used LACT and D6 to identify the main C99 processing pathways for each chimera to better understand the mechanisms underlying their differences. The outcome of C99 expression in both chimeras was completely different. Neither LACT nor D6 changed C99 levels in the presence of TM5/IC1, which was maintained close to the control DMSO-treated condition (Fig 1I). In contrast, LACT and D6 drastically increased C99 levels by 212% and 323%, respectively, when expressing the TM1/IC5 variant (Fig 1J), suggesting that both the proteasome and the γ-secretase mediate the reduction in C99 levels observed in this chimera.

Specific amino acid deletions in the IC domain reduce C99 and Aβ levels

We next investigated whether the deletion of specific IC residues could mimic the decrease in C99 levels caused by the deletion of the entire IC domain. We deleted a series of amino acids in the MT5-MMP IC domain that differed from those in MT1-MMP IC, owing to the potential role of these amino acids in the opposite effects of suppressing the IC domain of MT5-MMP and MT1-MMP as previously reported[4]. From N-terminal to C-terminal, the deletions were: KNKTG, QPVT, YK, PVQ, and EWV (Fig 2A). None of the mutations induced cytotoxicity in HEK cells expressing these constructs with C99 (Fig 2B). On average, specific deletions in the MT5-MMP IC domain tended to reduce C99 levels by 40% ± 10%, but this

decrease was insufficient to achieve statistical significance (p-values between 0.1 and 0.5) with the exception of KNKTG deletion, which significantly reduced C99 levels by 53% (Fig 2C).

Sequence substitutions in the IC domain modulate C99 and Aβ levels

The minimal differences observed in C99 levels following targeted deletions could imply changes in IC conformation that ultimately interfere with the physiological effects of MT5-MMP. We hypothesized that alanine (ala) substitutions in different groups of amino acids could better preserve the IC conformation while revealing possible functional effects of the mutations for a given group. In addition, we generated a construct in which all selected amino acids were simultaneously substituted with ala. Similar to the deletions, the substitution of specific residues with ala exhibited no effects on cell survival (Fig 2B). Upon coexpression with C99 in HEK cells, only the constructs with the substitution of KNKTG or PVQ groups exhibited significant reductions (69% and 51% respectively) in C99 levels compared with the TM/IC control, as revealed by WB using the anti-CTF antibody (Fig 2D). Seemingly, ala substitutions of all selected residues significantly decreased C99 levels by 69% (Fig 2D). In contrast, ala substitutions in the PDZ-binding EWV motif maintained high C99 levels equivalent to those of TM/IC (Fig 2D).

Only KNKTG substitution translated the C99 reduction into a significant decrease (72%) in Aβ levels (Fig 2E). Substitutions in PVQ or all targeted groups were insufficient to modulate Aβ levels, which remained close to control levels. Thus, KNKTG remained as the key amino acids for halting C99 and Aβ accumulation in HEK cells overexpressing C99, whereas EWV ala substitution preserved the same pathologic profile in both C99 and Aβ as TM/IC control.

Decreased C99 levels after KNKTG substitution in MT5-MMP IC could result from changes in the proteolytic degradation of C99. Thus, we treated HEK cells with LACT and D6 after co-transfection with C99 and one of the following: TM/IC or TM/IC(ala)KNKTG or TM/IC(ala)EWV. On the one hand, both LACT and D6 significantly restored the expression of C99 when co-transfected with TM/IC (Fig 2F). On the other hand, C99 levels in the TM/IC(ala)KNKTG group remained unchanged upon treatment with LACT or D6 (Fig 2G), suggesting an alternative degradation pathway to proteasome or γ-secretase. In HEK cells co-transfected with TM/IC(ala)EWV, D6 but not LACT increased C99 levels, highlighting the

importance of γ-secretase processing of C99 in the presence of TM/IC(ala)EWV and no proteasomal degradation (Fig 2I). These significant changes in the fate of C99 could reflect the translocation of MT5-MMP variants into subcellular compartments that facilitate C99 processing by specific proteases.

MT5-MMP variants alter the patterns of subcellular localization of C99

To determine the possible influence of MT5-MMP variants on C99 distribution and therefore on its metabolism, we co-transfected human retinal pigment epithelial cells (RPE1) with HA N-terminally tagged C99 (HA-C99) and MT5-MMP variants known to differentially modulate C99 processing (Fig. 3A). RPE1 are highly adherent and of an optimal size to facilitate microscopic observations at the subcellular level. In addition, these cells do not express detectable levels of MT5-MMP (Fig. 3B) and, similarly as neural cells, have an embryonic neuroectodermal origin[25]. We used anti-HA antibodies to detect HA-C99 and specific antibodies targeting different cell organelles from the endomembrane system (early endosomes, Golgi apparatus, endoplasmic reticulum, and lysosomes) to investigate HA-C99 subcellular localization using immunofluorescence. We acquired and analyzed the images using quantitative unbiased high content screening microscopy (HCS). We used pcDNA as a reference construct with respect to HA distribution for data normalization and calculated the increase or decrease in the percentage of MT5-MMP variants relative to pcDNA.

The distribution of the HA signal substantially changed under the influence of different MT5-MMP variants (Fig. 3C), indicating distinct distribution patterns. Notably, all MT5-MMP variants caused an overall reduction in HA signal within the Golgi apparatus (27%±12) and the endoplasmic reticulum (14%±6) relative to pcDNA control. In contrast, we observed inconsistent changes in HA signal among MT5-MMP variants in early endosomes (10%±10), accompanied by a slight increase (11%±9) in the lysosomal HA signal (Fig 3C). However, absolute quantification is insufficient to understand the complexity of HA signal distribution in different organelles and under the influence of different MT5-MMP variants.

To visualize our data structure that summarizes the effects of the MT5-MMP variants on C99 distribution, we conducted principal component analysis (PCA) using two principal components, which collectively account for 75% of the total variability of the HA signal (Fig

3D). We observed that pcDNA and TM/IC(ala)EWV were isolated from the other MT5-MMP variants, indicating that coexpression of these two constructs leads to different HA-C99 distribution patterns in heterologous cells. In addition, three differentiated groups emerged within the main cluster: those with MT5-MMP TM (EXT/TM, TM/IC, TM/IC(ala)KNKTG), those lacking MT5-MMP TM (EXT, TM1/IC5), and the TM5/IC1 chimera positioned between these groups. These findings suggest: i) that HA-C99 distribution among different organelles varies depending on the coexpression of MT5-MMP variants, and ii) that the presence of MT5-MMP TM strongly determines HA-C99 subcellular localization.

To identify which MT5-MMP constructs significantly influenced the HA-C99 distribution in each organelle we performed a cluster analysis, using Bayesian ANOVA followed by multiple comparison tests. The natural logarithm of Bayes Factor 10 (LogBF10) quantifies the likelihood of differences in means between various groups, providing a measure of the posterior odds that the alternative hypothesis holds. In other words, it makes it easier to estimate the probability that means actually differ[26]. For instance, a LogBF10 value of -1.1 infers that the null hypothesis is three times more likely than the alternative hypothesis, 0 indicates the same probability for both, and a LogBF10 value of 1 indicates a probability approximately three times greater than the alternative hypothesis. This approach provides a quantitative criterion to evaluate differences between groups without the restrictions of conventional frequentist methods, which use p-values to interpret the data. However, this approach may overlook meaningful patterns in the data and is less informative[26]. In the context of our results, LogBF10 provides us with a quantitative framework to interpret whether the differences observed in the absolute quantification of HA signals are sufficient to reject or accept the null hypothesis. It indicates whether the means are equal or different, or if there is a lack of evidence (*i.e.* high variability, small number of repetitions, etc.) to draw a solid conclusion.

We calculated the sum of LogBF10 values for each comparison of the effect of individual MT5-MMP variants on HA-C99 expression in each organelle to create a cluster map that visually represents the strength of evidence for variability in different constructs across multiple organelles (Fig 3E, F). TM/IC(ala)EWV differed from other constructs in HA signal distribution within the Golgi (16.83), endoplasmic reticulum (2.15), and lysosomes (3.63). However, other MT5-MMP variants changed HA-C99 distribution in one or other specific

cellular compartments: TM1/IC5 in the endoplasmic reticulum (ER) (4.57), EXT/TM in the endosomes (4.30), and EXT in the Golgi (1.60) (Fig 3E, F).

MT5-MMP variants heterogeneously determine HA-C99 subcellular localization

Bayesian analysis indicated that all MT5-MMP constructs altered HA-C99 subcellular distribution compared with the pcDNA control, but certain MT5-MMP variants distinctly altered HA-C99 subcellular distribution in organelles. Thus, we delved deeper into the individual differences in HA signal in each organelle for each MT5-MMP construct by analyzing the LogBF10 values for each individual comparison in the post-hoc analysis (Fig 4A-E).

First, we wondered whether the effects of MT5-MMP variants could occur in the ER, which is the endomembrane system where most protein synthesis occurs. All MT5-MMP variants reduced the levels of HA-C99 in the ER compared with pcDNA (Fig 3F, 4B), suggesting that the presence of MT5-MMP variants induces the exit of HA-C99 toward other cellular compartments. Notably, TM1/IC5 reduced of HA-C99 levels by 17% in the endoplasmic reticulum compared with pcDNA (LogBF10 = 4.68) and induced a greater reduction than TM/IC(ala)EWV (-4%) (LogBF10 = 2.05).

Next, we examined the Golgi apparatus, which is involved in protein packaging and compartmentalization. All MT5-MMP variants induced significant reductions (between 15% and 45%) in HA-C99 compared with pcDNA (Fig 3F, 4C). Among them, TM/IC(ala)EWV was the most common variant, with a particularly significant reduction of 45% and a LogBF10 of 12.89. In addition, HA-C99 reduction in the Golgi was more prominent in TM/IC(ala)EWV (-45%) than in EXT (-16%) (LogBF10 = 2.21), EXT/TM (-17%) (LogBF10 = 0.97), and TM1/IC5 (-15%) (LogBF10 = 1.78). This possibly implies that the presence of MT5-MMP TM associated with an IC structure facilitates HA-C99 translocation outside the Golgi apparatus. A mean reduction of 16% was observed for EXT and TM1/IC5, both lacking the MT5-MMP TM domain, indicating that the presence of MT5-MMP truncated forms reduced HA-C99 in the Golgi apparatus, possibly by inducing rapid entry of HA-C99 into the secretory or endolysosomal pathways.

Co-staining of EEA1 and HA (HA-C99) revealed similar levels of HA-C99 in early endosomes, irrespective of the MT5-MMP construct. However, EXT/TM (+13%) increased HA-C99 translocation into early endosomes compared with pcDNA (LogBF10 = 2.21), TM/IC (LogBF10 = 1.05), and TM5/IC1 (LogBF10 = 1.58) (Fig 3F, 4D). This suggests that MT5-MMP EXT and/or TM, but not MT5-MMP IC, favors the presence of HA-C99 in EEA1+ vesicles. Building upon our previous findings, the levels of co-localization between early endosomes and HA-C99 indicate that EXT/TM preferentially transports HA-C99 from the ER/Golgi toward early endosomes, whereas other MT5-MMP variants may mostly translocate HA-C99 into other cellular compartments.

The dynamics of HA-C99 distribution in lysosomes were similar under different conditions. The two constructs carrying mutations in the intracellular domain, TM/IC(ala)KNKTG and TM/IC(ala)EWV, mainly differed from pcDNA (Fig 3F, 4E), with an increase in HA-C99 colocalization with lysosomes of 18% (LogBF10 = 0.97) and 21% (LogBF10 = 5.27), respectively. Although TM/IC had low LogBF10 values compared with pcDNA (LogBF10 = 0.13), it increased HA-C99 in lysosomes by 18%, which was similar to that of TM/IC(ala)KNKTG and TM/IC(ala)EWV (18% and 21%), which have consistent LogBF10 values. Thus, the presence of MT5-MMP TM and IC (intact or mutated) increases the presence of HA-C99 in lysosomes.

Overall, the expression of certain MT5-MMP constructs modifies HA-C99 distribution in key components of the endomembrane system. All constructs showed a similar trend in promoting a reduction of HA-C99 in the ER and Golgi, while increasing HA-C99 in lysosomes. MT5-MMP TM and IC appeared to play an important role in HA-C99 subcellular sorting, especially in promoting HA-C99 exiting from the Golgi and HA-C99 translocation into lysosomes.

MT5-MMP modifications alter colocalization with HA-C99

On the basis of the aforementioned data, it was unclear whether changes in C99 fate were the consequence of alterations induced by MT5-MMP variants (Fig 5A) in subcellular C99 localization in the endomembrane system or whether these changes underlie proximal interactions between both proteins. To address this issue, we performed a proximity ligation

assay (PLA) using our RPE1 cell-based model[27]. PLA detects when target proteins are within less than 40 nm of each other. Here, HA-C99 and MT5-MMP were targeted using antibodies against the HA and Flag tags present in their N-termini, respectively. For quantitative analysis, we used pcDNA as a normalization control and subtracted the number of positive spots detected in pcDNA from that observed in the MT5-MMP variants. This adjustment was made by considering the number of positive spots in pcDNA as the baseline for nonspecific binding.

Quantification of HA-C99 colocalization differed between all MT5-MMP variants compared with pcDNA. Individually, TM/IC and TM1/IC5 cells had the highest number (25 each) of PLA+ spots per cell (Fig 5B, C). Despite absolute differences, TM/IC variability projects low LogBF10 numbers in individual comparisons with other constructs (Fig 5D). TM1/IC5 (25) increased colocalization with HA-C99 compared with the TM5/IC1 chimera (10) (LogBF10 = 1.56) and EXT (13) (LogBF10 = 1.41). TM/IC(ala)EWV (21) was the third construct with a high number of PLA+ spots, exceeding the 13 spots of EXT (LogBF10 = 0.51) and the 10 of TM5/ICI (LogBF10 = 0.91). Finally, compared with EXT/TM (18), TM5/IC1 (10) showed decreased colocalization with HA-C99 (LogBF10 = 1.17) (Fig 5 A-C). Taken together, our results indicate that the MT5-MMP IC domain plays a role in mediating proteinase colocalization (and eventually interactions) with HA-C99. This role can be challenged by modifications of this domain.

MT5-MMP-based peptides promote C99 degradation

In all cases, selective modifications of the MT5-MMP IC sequence reduced C99 and Aβ accumulation, which is of potential therapeutic interest. We sought to further test this idea by using MT5-MMP IC peptidomimetics containing mutations that efficiently reduced C99 levels when expressed in DNA constructs. We synthesized two peptides, hereafter referred to as p17 and p20. The peptides were co-transfected with HA-C99 in HEK cells and left for 48 h, with no cytotoxic effect revealed by the MTT test (Fig 6A, B). p20 led to a significant 38% decrease in HA-C99 only at the highest concentration of 1000 nM (Fig 6C), while p17 had a dose-response effect at log-scale concentrations of 10, 100 and 1000 nM. The levels of HA-C99 were reduced by 29%, 35%, 53%, and 41%, respectively, which was statistically significant for the last three concentrations (Fig 6D). We selected p17 to be functionalized in a way that

allows entry into cells without the use of transfecting agents. To this end, we conjugated p17 to C5 (C5p17), a VHH (nanobody) that binds to the transmembrane transferrin receptor (TfR), enabling endocytosis and internalization, as previously shown[28]. Transfection of the C5p17 conjugate reduced HA-C99 levels by 37%, 37% and 36% in HEK cells at 1nM, 10 nM and 100 nM, respectively (Fig. 6E), validating the preservation of p17 effects after conjugation.

After western blot confirmation of TfR expression in HEK and RPE1 cells and internalization of C5 in the latter (Fig 6F, G), we conducted free uptake experiments of C5p17 (without transfecting agent) 24 h after transfection of HA-C99. Free uptake of C5p17, as its unconjugated counterpart, had no cytotoxic effects on HEK cells (Fig 6H). The C5p17 conjugate significantly reduced C99 levels by 69% at the 10 nM concentration (Fig 6I).

Overall, our results demonstrate the importance of non-catalytic C-terminal domains of MT5-MMP in the regulation of C99 and Aβ fate, in concert with different degradation pathways. We also highlight the usefulness of leveraging on the molecular plasticity of the C-terminal domains of MT5-MMP to generate molecular tools that help preventing the pathogenic accumulation of C99 and Aβ, and open to the design of peptides with therapeutic potential in the context of AD.

DISCUSSION

In recent years, we have demonstrated the pathological involvement of MT5-MMP in cellular and animal models of AD[13,14,29]. We have also shown the importance of the non-catalytic MT5-MMP domains, in particular the TM and IC, in regulating the metabolism and fate of C99 and Aβ [4]. On this basis, we designed a set of mutations in the TM and IC domains to identify the amino acids responsible for the regulation of APP metabolism and amyloidogenesis by MT5-MMP. We identified key mutations in MT5-MMP residues that affect its interactions with C99 and alter its intracellular distribution and processing. Chimeric combinations of MT5-MMP and MT1-MMP TM and IC unmasked potential differences in C99 affinity and subcellular distribution between MT5-MMP TM and IC when acting separately, ultimately leading to different outcomes for C99 and Aβ accumulation. In addition, KNKTG and PVQ ala substitutions in the IC domain most effectively reduced C99 levels. However, only KNKTG substitutions concordantly reduced Aβ accumulation. Based on these results, we generated and vectorized synthetic peptides of the IC domain carrying these mutations. Only peptides with the KNKTG substitutions decreased C99 levels, reproducing the effect of the mutated DNA plasmids. Overall, the present study identified specific sets of amino acids in the TM and IC domains of MT5-MMP that play a prominent role in controlling C99 fate, opening up new opportunities to exploit MT5-MMP properties to design anti-C99/Aβ therapeutic agents.

Modifications in MT5-MMP domains alter the fate of C99

We previously demonstrated that overexpression of MT5-MMP TM/IC in HEK cells had the same effects on C99 accumulation as full-length MT5-MMP. In contrast, overexpression of MT5-MMP without TM/IC or IC significantly reduced C99 and Aβ levels, highlighting the importance of the C-terminal domains of MT5-MMP in controlling C99/Aβ metabolism[4]. Catalytic inactivation of MT5-MMP EXT (ΔEXT) did not prevent the decrease in C99 levels (mainly through proteasome activity) but restored Aβ levels. This suggests that MT5-MMP proteolytic activity was not involved in C99 degradation, but it might influence Aβ metabolism, as reported for MT1-MMP, which is a close homolog of MT5-MMP[4,30,31]. The lack of Aβ clearance after MT5-MMP EXT inactivation may reflect the ability MT5-MMP EXT to cleave

Aβ in a context of C99 accumulation. Consistent with this idea, incubation of the MT5-MMP catalytic domain and soluble Aβ in a cell-free system truncates the first 4 amino acids of Aβ (unpublished). C99 levels were minimally recovered by inhibition of the autophagolysome system but not of γ-secretase or cathepsin B, suggesting that other processing pathways may play a role in Aβ modulation.

MT1-MMP and MT5-MMP share 60% homology overall, but only ~20% for the TM and IC domains[32], possibly accounting for the opposite effects of MT5-MMP or MT1-MMP variants lacking the IC domain, which respectively decrease and increase C99 levels in HEK cells[4]. Accordingly, chimeric combinations of the TM and IC domains of both MMPs distinctly regulate C99 and Aβ levels. The lack of C99 degradation in the presence of TM5/IC1 suggests that, unlike the TM of MT1-MMP, the TM of MT5-MMP stabilizes C99 by preventing its interaction with proteasomal enzymes or γ-secretase. The lack of effect of LACT or D6 on C99 levels in HEK cells expressing TM5/IC1 supports this hypothesis. In contrast, LACT and D6 rescue C99 levels in TM1/IC5-expressing cells, indicating that the IC of MT5-MMP facilitates C99 processing. It is therefore plausible that the TM of MT5-MMP stabilizes C99, whereas the IC favors its processing, eventually influencing C99 accumulation and Aβ production.

Mutations of specific amino acids of the MT5-MMP IC prevent C99 and Aβ accumulation

Based on the sequence divergence between MT5-MMP and MT1-MMP, we deleted or substituted several amino acid groups in the MT5-MMP IC domain. Deletions barely had any effect, except KNKTG, which significantly decreased C99 levels. This feature was replicated and amplified by ala substitutions of KNKTG or PVQ. Interestingly, only KNKTG substitutions reduce also Aβ levels, indicating the prominent role of the first amino acids consecutive to the TM in the control of both C99 accumulation and Aβ production. The failure of LACT and D6 to restore C99 levels in HEK cells expressing TM/IC(ala)KNKTG may imply the existence of C99 degradation pathways alternative to the proteasome or γ-secretase. This clearly contrasts with previous reports in which it was shown that overexpressed C99 was mainly processed by the proteasome[4,33]. Thus, small modifications in the IC sequence are sufficient to significantly alter C99 processing, thereby stressing the importance of MT5-MMP regulation of C99 fate and the remarkable level of molecular plasticity of the IC domain.

Accordingly, ala substitutions in the C-terminal PDZ-binding EWV motif maintained C99 and Aβ levels compared with TM/IC. However, only D6 clearly upregulated C99 levels, demonstrating the predominant role of γ-secretase in C99 processing. In contrast in the TM/IC control group C99 levels were rescued by both LACT and D6. Altering the C-terminal PDZ-binding motif prevents MT5-MMP recycling to the plasma membrane via interactions with mint3, resulting in MT5-MMP accumulation in the TGN[34]. It is noteworthy that mint3 also binds to APP and regulates its intracellular traffic[35,36]. In our case, EWV substitution strongly reduced C99 localization in the Golgi apparatus, possibly indicating increased export of C99 toward other acidic subcellular compartments where γ-secretase is more active[37–39] and can more efficiently convert it into Aβ.

MT5-MMP variants alter the patterns of subcellular localization of C99

Our results imply potential changes in C99 subcellular distribution that could shed light on differences in C99 processing pathways under the influence of specific MT5-MMP variants. In the same vein it has been shown that subcellular localization of C99/APP influences their processing by canonical secretases and regulates Aβ production[40–42].

PCA revealed that MT5-MMP variants influence HA-C99 distribution differently, highlighting the importance of the TM domain and the PDZ-binding motif to understand these changes. Clustering of the data when all the plasmids are taken together, indicates that TM/IC(ala)EWV is the most influential construct in the subcellular localization of HA-C99, as it alters its distribution in the Golgi, endoplasmic reticulum, and lysosomes. In the case of the other MT5-MMP variants, they limit their influence to a single organelle or none. This difference between the EWV mutations and the others reflects the importance of the MT5-MMP EWV motif in the subcellular localization of C99. Apart from mint3, other members of the Mint family also interact with APP metabolites through binding domains, and overexpression of mint1 or its PTB domain decreased Aβ40 secretion through inhibition of γ-secretase cleavage of C99 in HEK cells[43]. It is thus possible that EWV mutations alter C99 trafficking in a manner that prevents its contact with mint proteins and facilitates γ-secretase cleavage.

Individual analysis for each variant and organelle revealed a general trend toward decreased HA-C99 levels. Most variants reduced HA-C99 levels in the ER, the main site of protein synthesis, possibly indicating the stimulation of C99 sorting to other compartments. We discard the possibility that MT5-MMP variants interfere with C99 synthesis because the variants decreasing C99 levels in the ER do not correlate with decreased levels of C99, as shown in our western blots. With respect to the Golgi apparatus, TM/IC(ala)EWV resulted in the greatest reduction in C99 levels (-45%) compared with the other variants. As noted previously, substitution of the PDZ-binding motif in MT5-MMP TM/IC might facilitate its intracellular localization by impeding recycling into the plasma membrane[34]. Similarly, mint3 knockdown in neuroblastoma cells rerouted APP toward the endolysosomal pathway[44]. These data support our hypothesis that EWV mutations facilitate C99 sorting in the Golgi network to cellular compartments where optimal γ-secretase activity would ensure the maintenance of Aβ levels.

MT5-MMP variants did not change the early endosome content of C99 in most cases. The slight significant increase in cells expressing EXT/TM might be related to the absence of the EWV motif. Concordantly, there is an increase in C99 in early endosomes in the presence of TM/IC(ala)EWV, but the variability in the results makes it statistically insignificant. Conducting additional experiments could provide further evidence to support this hypothesis.

Expression of the TM/IC(ala)KNKTG and TM/IC(ala)EWV variants significantly increase C99 in lysosomes. The fact that these variants had opposite effects on C99 and Aβ content, with the former being a depressant and the latter being a stabilizer, suggests changes in C99 intracellular trafficking before it translocates into lysosomes. In this line, it was shown that inhibition of the autophagosome pathway increases the levels of C99 in LAMP1+ lysosomes in human neuroglioma cells, whereas autophagosome activation causes the opposite effect[45]. However, late endosomes-lysosomes are also major sites of C99 conversion in Aβ[39]. It is possible that KNKTG and EWV mutations in MT5-MMP IC distribute C99 into distinct cellular compartments, thereby reaching lysosomes containing different proteases through separate processing pathways. In addition, TM/IC(ala)EWV increase of C99/Aβ in lysosomes could disrupt endolysosomal function, triggering a pathogenic loop where higher levels of these toxic metabolites facilitate the conversion of more C99 into Aβ[46].

We conclude that different MT5-MMP variants critically affect C99 subcellular distribution. Moreover, whole-domain or minimal mutations in MT5-MMP TM and IC distinctly redistribute C99 in the cellular compartments of the endomembrane system, indicating a key role of the C-terminal domains of MT5-MMP in C99 trafficking. Further work in this direction—incorporating other organelle markers and specific detection methods for C99 and Aβ—could help clarifying the exact correlation of patterns in the subcellular distribution of C99 and their effects on C99 and Aβ accumulation.

Mutations in the IC domain of MT5-MMP determine the interactions with HA-C99

PLA analysis provided additional information on proximal interactions between MT5-MMP variants and HA-C99. TM/IC and TM1/IC5—both containing intact MT5-MMP IC—showed the highest level of interaction with HA-C99. Striking differences emerged between the chimeras, with TM5/IC1 exhibiting low levels of PLA+ signaling. This indicates that the IC of MT5-MMP facilitates the colocalization of MT5-MMP and C99, which is consistent with data showing that the TM/IC of MT5-MMP was sufficient to coimmunoprecipitate HA-C99 in HEK cells[4]. The strong reduction in PLA+ signal upon expression of TM5/IC1 or EXT confirms the relevance of MT5-MMP IC for the proximal interaction with C99. However, the increase in EXT/TM colocalization with C99 compared with EXT may indicate that MT5-MMP TM is also important for proximal localization with C99. Together with the decrease in TM5/IC1, these data suggest that the interface between MT5-MMP TM and IC is important but not exclusive in preserving MT5-MMP and C99 proximal interactions. This would explain why mutations in EWV have little effect on proximal interactions with C99 compared with the TM/IC control, whereas KNKTG substitutions tend to decrease the number of colocalizations. These results highlight the importance of the IC domain of MT5-MMP in mediating interactions between MT5-MMP and HA-C99, which are impaired when the domain is widely mutated. Moreover, we can observe a prominent role for MT5-MMP TM when is associated with MT5-MMP domains, which would presumably better preserve its native structure. It will be important to elaborate on the impact of MT5-MMP TM mutations along with small modifications (*e.g.* EWV or KNKTG) of MT5-MMP IC to determine the residues responsible for interactions with C99.

Intracellular delivery of a synthetic MT5-MMP IC peptide mimicking the KNKTG mutation reduces C99 accumulation

Collectively, our results demonstrate that mutated variants of MT5-MMP differentially modulate C99 in heterologous cell lines. Furthermore, we have revealed the fundamental importance of the MT5-MMP IC in determining the fate of C99 through complex molecular mechanisms involving proximity interactions and the translocation of C99 into specific cellular compartments. Thus, we hypothesized that the properties of MT5-MMP non-catalytic domains possess important therapeutic potential. Synthetic peptides imitate natural amino acid structures with specific biological properties and are significant therapeutic tools extensively used[47]. As a proof-of-concept, we generated synthetic peptides mimicking the modified amino acids sequences of MT5-MMP IC that downregulate C99 levels, and vectorized them using a VHH that recognizes the TfR. We tested peptides containing the IC domain with (ala)KNKTG or (ala)PVQ sequences in HEK cells overexpressing C99. A dose-response protocol demonstrated the ability of the peptide incorporating (ala)KNKTG to greatly reduce C99 in live cells, demonstrating that it is possible to use MT5-MMP IC-based therapeutic tools to modulate C99. In this regard, a recent study showed that editing the YENPTY motif of the C99 sequence, which is essential for its trafficking, resulted in a stable reduction of C99 and Aβ levels in an AD knock-in mouse model. This highlights the importance of targeting APP metabolites using strategies that affect their trafficking and eventual production of toxic biofactors[48]. Our study adds to this work by demonstrating the possibility of using MT5-MMP as a reference to generate synthetic peptides, which is a generally safe therapeutic strategy that avoids the use of genome-modifying tools.

Declarations

Ethics approval

All the experimental procedures were conducted in agreement with the authorization by the French Ministry of Research to the laboratory (# 7950), as defined in the directive 2009/41/CE of the European Parliament and the European Council of May 6 2009 for the use of genetically modified organisms.

Availability of data and materials

All the data generated or analyzed during this study are included in this published article and are available from the corresponding author upon reasonable request.

All the analysis files in the form of Jupyter Notebook are uploaded and freely accessible at: github.com/RiveraLabINP/BelioMairal_2024

Competing interests

MK was director of the Institute of Neuropathophysiology, UMR7051 academic neuroscience laboratory supported by the CNRS and Aix-Marseille University, but also co-founder, shareholder and scientific counsel of the VECT-HORUS biotechnology company. The other authors declare that they have no competing interests.

Funding

This work was supported by funding from the CNRS and Aix-Marseille Université and by public grants to overseen by "Fondation pour la Recherche Médicale" (FRM), by the French National Agency for Research (ANR) MT5-AD and Fondation Vaincre Alzheimer to SR. PB received a doctoral fellowship from the French government under the Programme Investissements d'Avenir, Initiative d'Excellence d'Aix-Marseille Université via A*Midex (AMX-19-IET-004) and ANR (ANR-17-EURE-0029) funding through NeuroSchool/NeuroMarseille. AK received an international mobility grant under the same program. PB also received financial support from Fondation Vaincre Alzheimer.

REFERENCES

1. Rivera S, Khrestchatisky M, Kaczmarek L, Rosenberg GA, Jaworski DM. Metzincin proteases and their inhibitors: foes or friends in nervous system physiology? *J Neurosci*. 2010;30(46):15337-15357. doi:10.1523/JNEUROSCI.3467-10.2010

2. Sekine-Aizawa Y, Hama E, Watanabe K, et al. Matrix metalloproteinase (MMP) system in brain: identification and characterization of brain-specific MMP highly expressed in cerebellum: MT5-MMP: a brain-specific MMP in rat. *European Journal of Neuroscience*. 2001;13(5):935-948. doi:10.1046/j.0953-816x.2001.01462.x

3. Jaworski DM. Developmental regulation of membrane type-5 matrix metalloproteinase (MT5-MMP) expression in the rat nervous system. *Brain research*. 2000;860(1-2):174-177.

4. García-González L, Paumier J, Louis L, et al. MT5-MMP controls APP and β-CTF/C99 metabolism through proteolytic-dependent and -independent mechanisms relevant for Alzheimer's disease. *FASEB j*. 2021;35(7). doi:10.1096/fj.202100593R

5. Rivera S, García-González L, Khrestchatisky M, Baranger K. Metalloproteinases and their tissue inhibitors in Alzheimer's disease and other neurodegenerative disorders. *Cell Mol Life Sci*. 2019;76(16):3167-3191. doi:10.1007/s00018-019-03178-2

6. Monea S, Jordan BA, Srivastava S, DeSouza S, Ziff EB. Membrane Localization of Membrane Type 5 Matrix Metalloproteinase by AMPA Receptor Binding Protein and Cleavage of Cadherins. *J Neurosci*. 2006;26(8):2300-2312. doi:10.1523/JNEUROSCI.3521-05.2006

7. Porlan E, Martí-Prado B, Morante-Redolat JM, et al. MT5-MMP regulates adult neural stem cell functional quiescence through the cleavage of N-cadherin. *Nat Cell Biol*. 2014;16(7):629-638. doi:10.1038/ncb2993

8. Warren KM, Reeves TM, Phillips LL. MT5-MMP, ADAM-10, and N-cadherin act in concert to facilitate synapse reorganization after traumatic brain injury. *J Neurotrauma*. 2012;29(10):1922-1940. doi:10.1089/neu.2012.2383

9. Komori K, Nonaka T, Okada A, et al. Absence of mechanical allodynia and Aβ-fiber sprouting after sciatic nerve injury in mice lacking membrane-type 5 matrix metalloproteinase. *FEBS Letters*. 2004;557(1-3):125-128. doi:10.1016/S0014-5793(03)01458-3

10. Ahmad M, Takino T, Miyamori H, Yoshizaki T, Furukawa M, Sato H. Cleavage of amyloid-beta precursor protein (APP) by membrane-type matrix metalloproteinases. *J Biochem*. 2006;139(3):517-526. doi:10.1093/jb/mvj054

11. Willem M, Tahirovic S, Busche MA, et al. η-Secretase processing of APP inhibits neuronal activity in the hippocampus. *Nature*. 2015;526(7573):443-447. doi:10.1038/nature14864

12. Selkoe DJ, Hardy J. The amyloid hypothesis of Alzheimer's disease at 25 years. *EMBO Mol Med*. 2016;8(6):595-608. doi:10.15252/emmm.201606210

13. Baranger K, Marchalant Y, Bonnet AE, et al. MT5-MMP is a new pro-amyloidogenic proteinase that promotes amyloid pathology and cognitive decline in a transgenic mouse model of Alzheimer's disease. *Cell Mol Life Sci*. 2016;73(1):217-236. doi:10.1007/s00018-015-1992-1

14. Baranger K, Bonnet AE, Girard SD, et al. MT5-MMP Promotes Alzheimer's Pathogenesis in the Frontal Cortex of 5xFAD Mice and APP Trafficking in vitro. *Front Mol Neurosci*. 2017;9. doi:10.3389/fnmol.2016.00163

15. Mensch M, Dunot J, Yishan SM, et al. Aη-α and Aη-β peptides impair LTP ex vivo within the low nanomolar range and impact neuronal activity in vivo. *Alzheimer's Research & Therapy*. 2021;13(1):125. doi:10.1186/s13195-021-00860-1

16. Afram E, Lauritzen I, Bourgeois A, et al. The η-secretase-derived APP fragment ηCTF is localized in Golgi, endosomes and extracellular vesicles and contributes to Aβ production. *Cell Mol Life Sci*. 2023;80(4):97. doi:10.1007/s00018-023-04737-4

17. Lauritzen I, Pardossi-Piquard R, Bauer C, et al. The -Secretase-Derived C-Terminal Fragment of APP, C99, But Not A , Is a Key Contributor to Early Intraneuronal Lesions in Triple-Transgenic Mouse Hippocampus. *Journal of Neuroscience*. 2012;32(46):16243-16255. doi:10.1523/JNEUROSCI.2775-12.2012

18. Py NA, Bonnet AE, Bernard A, et al. Differential spatio-temporal regulation of MMPs in the 5xFAD mouse model of Alzheimerâ€TMs disease: evidence for a pro-amyloidogenic role of MT1-MMP. *Front Aging Neurosci*. 2014;6. doi:10.3389/fnagi.2014.00247

19. Pulina MV, Hopkins M, Haroutunian V, Greengard P, Bustos V. C99 selectively accumulates in vulnerable neurons in Alzheimer's disease. *Alzheimer's & Dementia*. 2020;16(2):273-282. doi:10.1016/j.jalz.2019.09.002

20. Kwart D, Gregg A, Scheckel C, et al. A Large Panel of Isogenic APP and PSEN1 Mutant Human iPSC Neurons Reveals Shared Endosomal Abnormalities Mediated by APP β-CTFs, Not Aβ. *Neuron*. 2019;104(2):256-270.e5. doi:10.1016/j.neuron.2019.07.010

21. Schindelin J, Arganda-Carreras I, Frise E, et al. Fiji: an open-source platform for biological-image analysis. *Nat Methods*. 2012;9(7):676-682. doi:10.1038/nmeth.2019

22. Bowman EJ, Siebers A, Altendorf K. Bafilomycins: a class of inhibitors of membrane ATPases from microorganisms, animal cells, and plant cells. *Proceedings of the National Academy of Sciences*. 1988;85(21):7972-7976. doi:10.1073/pnas.85.21.7972

23. Mueller-Steiner S, Zhou Y, Arai H, et al. Antiamyloidogenic and neuroprotective functions of cathepsin B: implications for Alzheimer's disease. *Neuron*. 2006;51(6):703-714. doi:10.1016/j.neuron.2006.07.027

24. Asai M, Yagishita S, Iwata N, Saido TC, Ishiura S, Maruyama K. An alternative metabolic pathway of amyloid precursor protein C-terminal fragments via cathepsin B in a human neuroglioma model. *FASEB J*. 2011;25(10):3720-3730. doi:10.1096/fj.11-182154

25. Klimanskaya I. Retinal Pigment Epithelium. In: *Methods in Enzymology*. Vol 418. Embryonic Stem Cells. Academic Press; 2006:169-194. doi:10.1016/S0076-6879(06)18011-8

26. Keysers C, Gazzola V, Wagenmakers EJ. Using Bayes factor hypothesis testing in neuroscience to establish evidence of absence. *Nat Neurosci*. 2020;23(7):788-799. doi:10.1038/s41593-020-0660-4

27. Söderberg O, Gullberg M, Jarvius M, et al. Direct observation of individual endogenous protein complexes in situ by proximity ligation. *Nat Methods*. 2006;3(12):995-1000. doi:10.1038/nmeth947

28. COHEN R, David M, Khrestchatisky M. Transferrin receptor-binding molecules, conjugates thereof and their uses. Published online July 16, 2020. Accessed July 8, 2024. https://patents.google.com/patent/WO2020144233A1/en

29. Pilat D, Paumier JM, García-González L, et al. MT5-MMP promotes neuroinflammation, neuronal excitability and Aβ production in primary neuron/astrocyte cultures from the 5xFAD mouse model of Alzheimer's disease. *J Neuroinflammation*. 2022;19(1):65. doi:10.1186/s12974-022-02407-z

30. García-González L, Pilat D, Baranger K, Rivera S. Emerging Alternative Proteinases in APP Metabolism and Alzheimer's Disease Pathogenesis: A Focus on MT1-MMP and MT5-MMP. *Front Aging Neurosci*. 2019;11:244. doi:10.3389/fnagi.2019.00244

31. Paumier JM, Py NA, García-González L, et al. Proamyloidogenic effects of membrane type 1 matrix metalloproteinase involve MMP-2 and BACE-1 activities, and the modulation of APP trafficking. *FASEB j*. 2019;33(2):2910-2927. doi:10.1096/fj.201801076R

32. Pei D. Identification and Characterization of the Fifth Membrane-type Matrix Metalloproteinase MT5-MMP *. *Journal of Biological Chemistry*. 1999;274(13):8925-8932. doi:10.1074/jbc.274.13.8925

33. Evrard C, Kienlen-Campard P, Coevoet M, et al. Contribution of the Endosomal-Lysosomal and Proteasomal Systems in Amyloid-β Precursor Protein Derived Fragments Processing. *Front Cell Neurosci*. 2018;12:435. doi:10.3389/fncel.2018.00435

34. Wang P, Wang X, Pei D. Mint-3 Regulates the Retrieval of the Internalized Membrane-type Matrix Metalloproteinase, MT5-MMP, to the Plasma Membrane by Binding to Its Carboxyl End Motif EWV *. *Journal of Biological Chemistry*. 2004;279(19):20461-20470. doi:10.1074/jbc.M400264200

35. Caster AH, Kahn RA. Recruitment of the Mint3 Adaptor Is Necessary for Export of the Amyloid Precursor Protein (APP) from the Golgi Complex. *Journal of Biological Chemistry*. 2013;288(40):28567-28580. doi:10.1074/jbc.M113.481101

36. Ho A, Liu X, Südhof TC. Deletion of Mint proteins decreases amyloid production in transgenic mouse models of Alzheimer's disease. *J Neurosci*. 2008;28(53):14392-14400. doi:10.1523/JNEUROSCI.2481-08.2008

37. Cai T, Hatano A, Kanatsu K, Tomita T. Histidine 131 in presenilin 1 is the pH-sensitive residue that causes the increase in Aβ42 level in acidic pH. *J Biochem*. 2020;167(5):463-471. doi:10.1093/jb/mvz110

38. Kanatsu K, Hori Y, Ebinuma I, Chiu YW, Tomita T. Retrograde transport of γ-secretase from endosomes to the trans-Golgi network regulates Aβ42 production. *Journal of Neurochemistry*. 2018;147(1):110-123. doi:10.1111/jnc.14477

39. Maesako M, Houser MCQ, Turchyna Y, Wolfe MS, Berezovska O. Presenilin/γ-Secretase Activity Is Located in Acidic Compartments of Live Neurons. *J Neurosci*. 2022;42(1):145-154. doi:10.1523/JNEUROSCI.1698-21.2021

40. Choy RWY, Cheng Z, Schekman R. Amyloid precursor protein (APP) traffics from the cell surface via endosomes for amyloid β (Aβ) production in the trans-Golgi network. *Proceedings of the National Academy of Sciences*. 2012;109(30):E2077-E2082. doi:10.1073/pnas.1208635109

41. Roselli S, Satir TM, Camacho R, et al. APP-BACE1 Interaction and Intracellular Localization Regulate Aβ Production in iPSC-Derived Cortical Neurons. *Cell Mol Neurobiol*. 2023;43(7):3653-3668. doi:10.1007/s10571-023-01374-0

42. Wang J, Gleeson PA, Fourriere L. Spatial-Temporal Mapping Reveals the Golgi as the Major Processing Site for the Pathogenic Swedish APP Mutation: Familial APP Mutant Shifts the Major APP Processing Site. *Traffic*. 2024;25(3):e12932. doi:10.1111/tra.12932

43. King GD, Cherian K, Turner RS. X11alpha impairs gamma- but not beta-cleavage of amyloid precursor protein. *J Neurochem*. 2004;88(4):971-982. doi:10.1046/j.1471-4159.2003.02234.x

44. Shrivastava-Ranjan P, Faundez V, Fang G, et al. Mint3/X11gamma is an ADP-ribosylation factor-dependent adaptor that regulates the traffic of the Alzheimer's Precursor protein from the trans-Golgi network. *Mol Biol Cell*. 2008;19(1):51-64. doi:10.1091/mbc.e07-05-0465

45. González AE, Muñoz VC, Cavieres VA, et al. Autophagosomes cooperate in the degradation of intracellular C-terminal fragments of the amyloid precursor protein via the MVB/lysosomal pathway. *FASEB J*. 2017;31(6):2446-2459. doi:10.1096/fj.201600713R

46. Bretou M, Sannerud R, Escamilla-Ayala A, et al. Accumulation of APP C-terminal fragments causes endolysosomal dysfunction through the dysregulation of late endosome

to lysosome-ER contact sites. *Dev Cell*. 2024;59(12):1571-1592.e9. doi:10.1016/j.devcel.2024.03.030

47. Vlieghe P, Lisowski V, Martinez J, Khrestchatisky M. Synthetic therapeutic peptides: science and market. *Drug Discov Today*. 2010;15(1-2):40-56. doi:10.1016/j.drudis.2009.10.009

48. Aulston BD, Gimse K, Bazick HO, et al. Long term rescue of Alzheimer's deficits in vivo by one-time gene-editing of App C-terminus. *bioRxiv*. Published online June 9, 2024:2024.06.08.598099. doi:10.1101/2024.06.08.598099

LEGENDS

Table 1. List of inhibitors. Provides a list of the inhibitors, at which stock concentration they were resuspended, at which dilution they were used, and the references.

Table 2. List of antibodies. Provides a list of the targets of the antibodies used, the host where they were produced, the working dilution, the references, and the application they were used for. PLA refers to proximity ligation assay.

Figure 1. Whole-domain modifications modulate the accumulation of C99 and the production of Aβ in HEK cells.

(A) Schematic view of different constructs generated from the MT5-MMP sequence. (B) Graph representing the absence of cytotoxicity in HEK cells measured by the MTT test 48 h after co-transfection of HEK cells with C99 and different MT5-MMP variants. Absorbance values at 450-10 nm are represented in arbitrary units (A.U) and normalized to those of samples treated only with the transfection reagent. (C) Representative western blots of HEK cells overexpressing C99 with TM/IC, EXT, EXT/TM, or ΔEXT. C99 was detected using a rabbit anti-APP-CTF antibody. The graph on the right represents the semi-quantifications of C99 levels normalized with actin as the protein load control and with pcDNA conditions to normalize each independent experiment. (D) Graphical representation of Aβ40 concentrations in the supernatants of HEK cells overexpressing C99 with TM/IC, EXT, EXT/TM, or ΔEXT. The values of each independent experiment were normalized to the pcDNA condition to control for inter-experimental variability. (E) Representative western blots of HEK cells overexpressing C99 with TM/IC, EXT, EXT/TM, TM5/IC1, or TM1/IC5. C99 was detected using a rabbit anti-APP-CTF antibody. The graph on the right represents semi-quantifications of C99 levels normalized using actin as a protein load control and with pcDNA condition to normalize each independent experiment. (F) Graphical representation of the concentrations of Aβ40 in the supernatants of HEK cells overexpressing C99 with TM/IC, EXT, EXT/TM, TM5/IC1, or TM1/IC5. The values of each independent experiment were normalized with the pcDNA condition to control for inter-experimental variability. (G-J) Representative western

blots of HEK cells overexpressing C99 with (G) EXT, (H) ΔEXT, (I) TM5/IC1 or (J) TM1/IC5 variants, and the corresponding actin-normalized quantifications below each immunoblots. Cells were treated for 20 h with inhibitors of the C99 processing pathways: proteasome (lactacystin; LACT 10 μM); γ-secretase ELND006 (D6 1 μM); cathepsin (B CA-074 Me; CA074 10 μM); and autophagolysosomal pathway (bafilomycin A1; BAFA 50 nM). DMSO was used as control. C99 was detected using a rabbit anti-APP-CTF antibody. All statistical tests were ANOVA with Dunnett's post hoc multiple comparison test compared with the control condition, with at least three independent experiments. Values are presented as mean ± SEM. P-values are represented as * $p < 0.05$, ** $p < 0.01$, *** $p < 0.001$, and **** $p < 0.0001$.

Fig 2. Mutation of specific MT5-MMP IC residues decreases C99 and Aβ levels in HEK cells.

(A) Schematic view of different constructs generated from the MT5-MMP sequence. The amino acid groups in red were either deleted or substituted with ala. These groups were: KNKTG, QPVT, YK, PVQ, and EWV. (B) Graph representing the absence of cytotoxicity in HEK cells measured by the MTT test 48 h after cotransfection of HEK cells with C99 and different MT5-MMP variants. Absorbance values at 450-10 nm are represented in arbitrary units (A.U) and normalized to those of samples treated only with the transfection reagent. (C) Representative western blots of HEK cells overexpressing C99 with TM/IC or TM/IC with deletions in KNKTG, QPVT, YK, PVQ or EWV. C99 was detected using a rabbit anti-APP-CTF antibody. The graph below represents the semi-quantifications of C99 levels normalized with actin as the protein load control and with pcDNA conditions to normalize each independent experiment. (D) Representative western blot of HEK cells overexpressing C99 with TM/IC or TM/IC with ala substitutions in KNKTG, QPVT, YK, PVQ, EWV or all the targeted groups (All). C99 was detected using a rabbit anti-APP-CTF antibody. The graph below represents the semi-quantifications of C99 levels normalized with actin as the protein load control and with pcDNA conditions to normalize each independent experiment. (E) Graphical representation of Aβ40 concentrations in the supernatants of HEK cells overexpressing C99 with mutations in the IC that reduce C99 levels or that maintain similar pathologic C99 levels to TM/IC control; these were TM/IC, TM/IC(ala)KNKTG, TM/IC(ala)PVQ, TM/IC(ala)EWV or TM/IC(ala)All. The values of each independent experiment were normalized with the pcDNA condition to control for inter-experimental

variability. (F-H) Representative western blots of HEK cells overexpressing C99 with (F) TM/IC, (G) TM/IC(ala)KNKTG, or (H) TM/IC(ala)EWV treated for 20 h with inhibitors of the C99 processing pathways: Proteasome lactacystin (LACT 10 μM); γ-secretase (ELND006; D6 1μM). All inhibitors were resuspended in DMSO at a final 1:5000 concentration. DMSO 1:5000 was used as control. C99 was detected using a rabbit anti-APP-CTF antibody. The graphs represent semi-quantification of C99 levels in western blots normalized to actin as a protein load control. All statistical tests were ANOVA with Dunnett's post hoc multiple comparison test compared with the control condition, with at least three independent experiments. Values are presented as mean ± SEM. P-values are represented as * $p < 0.05$, ** $p < 0.01$, *** $p < 0.001$, and **** $p < 0.0001$.

Fig 3. Effect of MT5-MMP IC domain residue modification on C99 subcellular distribution in RPE1 cells.

(A) Schematic view of different constructs generated from the MT5-MMP sequence. The amino acids in red represent the targeted groups that were substituted with ala. These groups were: KNKTG and EWV. (B) Western blotting demonstrating the lack of MT5-MMP expression in lysates of both HEK and RPE1 cells. (C) Heatmap representing the quantification of the area of HA+ signal overlapping with each organelle from the endomembrane system of RPE1 cells, depending on the MT5-MMP variant co-transfected with HA-C99. The values represent the percentage change in the area of overlap relative to that of pcDNA. The values that represent a decrease in the area of overlap of HA/organelle are blue and darker, whereas higher values are represented in green and lighter colors. For instance, TM/IC(ala)EWV in Golgi is represented in dark color because its area of overlap with HA/Golgi is -45% of that in pcDNA. On the contrary, there was an increase of +21% in the overlap area of HA/lysosomes in TM/IC(ala)EWV; thus, the color was light green. (D) PCA of the quantification heatmap in (C) constructed with two components representing 75% of the total variability of the data. Each MT5-MMP variant clustered with variants that had similar profiles of change with respect to pcDNA in the overlap area of HA and different endomembrane organelles. This indicates that pcDNA and TM/IC(ala)EWV are the two most different conditions compared with the other MT5-MMP variants. In contrast, EXT and TM1/IC5 cluster together, indicating similar changes in HA distribution through the endomembrane system compared with pcDNA. (E)

Cluster map representing changes in (C) based on Bayesian ANOVA. The values in the cluster map are the summed LogBF10 values of multiple comparisons between different MT5-MMP variants in each organelle, which represent the statistical strength of variability in HA overlap with organelles for each MT5-MMP variant. High values indicate stronger statistical evidence of changes in HA overlap in a given MT5-MMP variant with respect to all other variants within the same organelle. The lower the values are, the stronger is the evidence that the MT5-MMP variant does not induce changes in HA overlap within a specific organelle compared with all other MT5-MMP variants. Higher values are represented in light-to-darker red, and lower values are represented in light-to-darker blue. In this cluster map, one can understand that TM/IC(ala)EWV particularly affects HA overlap in the Golgi, ER, and lysosomes compared with all other MT5-MMP variants; and TM1/IC5 specifically affects HA signal overlap with the ER. However, compared with the other variants, EXT did not alter the HA overlap with lysosomes compared to the other variants. (F) Representative images of HA signal overlapping with immunolabelling for either early endosomes or Golgi or ER or lysosomes in RPE1 co-transfected with HA-C99 and the MT5-MMP variants used in this experiment and represented in (A). The organelles are represented in magenta, and the HA signal is represented in cyan. The multiline plots represent the fluorescence intensity distribution along the 20 μm of yellow line in the image. The scale bar represents 10 μm.

Fig 4. LogBF10 values of individual differences in HA-C99 subcellular localization in specific subcellular compartments within RPE1 cells transfected with distinct MT5-MMP variants.

(A) Schematic view of different constructs generated from the MT5-MMP sequence. The amino acids in red represent the targeted groups that were substituted with ala. These groups were: KNKTG and EWV. (B-E) The diagonal correlation matrices represent the LogBF10 values for each comparison within a Bayesian ANOVA, with post-hoc multiple comparison of the percentage of change in HA overlap with respect to pcDNA between different MT5-MMP variants; the ER (B), the Golgi (C), early endosomes (D), and lysosomes (E). Higher values are represented in light-to-darker red, and lower values are represented in light-to-darker blue. Next to each MT5-MMP variant is a color representation of the quantitative value of the area of overlap of HA and organelle previously shown in a heatmap (Fig 3C) to facilitate

interpretation of the LogBF10 values. As before, the values that represent a decrease in the area of HA/organelle overlap are blue and darker, whereas higher values are represented in green and lighter colors. Therefore, in (C) Golgi, the LogBF10 value in the comparison between TM/IC(ala)EWV and pcDNA indicates that statistical analysis strongly supports the presence of a difference in HA overlap with that observed in Golgi. Values close to 0 indicate that there is not enough evidence to determine whether there is a difference. Negative values describe strong evidence supporting the finding of no difference in the comparison of means.

Fig 5. Altering the MT5-MMP IC domain residues disrupts interactions with C99.

(A) Schematic view of different constructs generated from the MT5-MMP sequence. The amino acids in red represent the targeted groups that were substituted with ala. These groups were: KNKTG and EWV. (B) Representative images of the Operetta© HCS imaging results of PLA in RPE1 cells co-transfected with HA-C99 and various MT5-MMP variants described in (A). The orange dots correspond to PLA+ spots that translate the proximity of HA (HA-C99) and Flag (MT5-MMP variant) to less than 40 nm. Rat anti-HA and rabbit anti-Flag antibodies were used to tag the HA-C99 and MT5-MMP variants, respectively. The goat anti-rat and goat anti-rabbit conjugated to DuoLink© orange oligos were used as secondary antibodies for later ligation, amplification, and detection. The representative images show segmented cells defining the nucleus and plasma membrane. The scale bar represents 10 μm. (C) Quantification of PLA+ spots in each MT5-MMP variant. PLA+ spots in pcDNA were subtracted from the other conditions, as we considered them to represent the baseline unspecific signal. The values representing a small number of PLA+ spots are blue and darker, whereas higher PLA+ spots are represented in green and lighter colors. Here, TM/IC represents 25 PLA+ spots per cell (light green color). In contrast, pcDNA represents 0 PLA+ spots per cell; thus, it is darkly colored. (D) The diagonal correlation matrix represents the LogBF10 values for each comparison in a Bayesian ANOVA with post-hoc multiple comparisons of the number of PLA+ spots between different MT5-MMP variants. Higher values are represented in light-to-darker red, and lower values are represented in light-to-darker blue. For instance, the difference in PLA+ spots between TM1/IC5 and TM5/IC1 has a LogBF10 value of 1.56, which suggests that one can assume there is a difference in the mean number of PLA+ spots per cell between these two variants.

Figure 6. Effects of modified peptides of the MT5-MMP IC domain on C99 levels in heterologous cell lines.

(A-B) Amino acid sequence of the (A) p20 and (B) p17, corresponding to MT5-MMP IC with PVQ and KNKTG substituted with ala groups (in red), respectively. Graph representing the absence of cytotoxicity in HEK cells measured by the MTT test 48 h after cotransfection with C99 and p20 (A) or p17 (B). Absorbance values at 450-10 nm are represented in arbitrary units (A.U) and normalized to those of samples treated only with the transfection reagent. (C-E) Representative western blots of HEK cells overexpressing HA-C99 co-transfected with the peptides p20 (C), p17 (D) or conjugated p17 (C5p17) (E) at log-scaled concentrations from 0 to 1000 nM. HA-C99 was detected using a rat anti-HA antibody. The graphs represent semi-quantifications of HA-C99 levels normalized to actin as the protein load control. (F) Representative confocal images of RPE1 cells demonstrating that our TfR antibody specifically detects human TfR in human cells. (G) Western blot of TfR in HEK and RPE1 cell lysates, showing expression of TfR in both cell types. (H) As in (A-B), the graph represents the absence of cytotoxicity in HEK cells measured by the MTT test 48 h after transfection with HA-C99 and subsequent treatment with C5p17. (I) Sequence representing the VHH C5 conjugated to p17. Below is a representative image of a western blot of HEK cell lysates transfected with HA-C99 and incubated for 48 h with C5p17 at concentrations log-scaled from 0 to 1000 nM. HA-C99 was detected using a rat anti-HA antibody. The graph represents semi-quantifications of HA-C99 levels normalized to actin as the protein load control. All statistical tests were ANOVA with Dunnett's post hoc multiple comparison test compared with the control condition, with at least three independent experiments. Values are presented as mean ± SEM. P-values are represented as * $p < 0.05$, ** $p < 0.01$, *** $p < 0.001$, and **** $p < 0.0001$.

TABLES

Table 1

Inhibitors				
Inhibitor	**[Stock](µM)**	**Dilution**	**Reference**	**Company**
LACT	**10**	**1:5000**	**BML-PI104-1000**	**Enzo Life Sciences**
D6	**1**	**1:5000**	**SML2122**	**Sigma-Aldrich**
BAFA1	**250**	**1:5000**	**B1793**	**Sigma-Aldrich**
CA074	**50000**	**1:5000**	**205531**	**Sigma-Aldrich**

Table 2

Antibodies					
Target	**Host**	**Dilution**	**Reference**	**Company**	**Application**
Primaries					
APP-CTF	**Rabbit**	**1:1000**	**A8717**	**Sigma-Aldrich**	**Western blot**
Actin	**Mouse**	**1:5000**	**A1978**	**Sigma-Aldrich**	**Western blot**
TfR1	**Rabbit**	**1:1000 1:300**	**GTX102596**	**GeneTex**	**Western blot Immunofluorescence**
Nogo-B	**Sheep**	**1:25**	**AF6034**	**Biotechne**	**Immunofluorescence**
GM130	**Mouse**	**1:200**	**610823**	**BD Biosciences**	**Immunofluorescence**
EEA1	**Mouse**	**1:100**	**sc-365652**	**Santa Cruz Biotechnology**	**Immunofluorescence**
LAMP1	**Rabbit**	**1:300**	**ab24170**	**Abcam**	**Immunofluorescence**
HA	**Rat**	**1:100 1:100**	**11867423001**	**Roche**	**Immunofluorescence PLA**
Flag	**Rabbit**	**1:200**	**14793**	**Cell Signaling Technology**	**PLA**
Secondaries					
Rabbit	**Goat**	**1:800**	**111-005-003**	**Jackson ImmunoResearch**	**PLA**
Rat	**Goat**	**1:800**	**112-005-003**	**Jackson ImmunoResearch**	**PLA**
Mouse-647	**Donkey**	**1:800**	**A32787**	**ThermoFisher Scientific**	**Immunofluorescence**
Rabbit-647	**Donkey**	**1:800**	**A32795**	**ThermoFisher Scientific**	**Immunofluorescence**
Sheep-647	**Donkey**	**1:800**	**A21448**	**ThermoFisher Scientific**	**Immunofluorescence**
Rat-488	**Donkey**	**1:800**	**A48269**	**ThermoFisher Scientific**	**Immunofluorescence**
Rabbit-488	**Donkey**	**1:800**	**A-21206**	**ThermoFisher Scientific**	**Immunofluorescence**
Mouse-594	**Donkey**	**1:800**	**A-21203**	**ThermoFisher Scientific**	**Immunofluorescence**

FIGURES

Fig 1

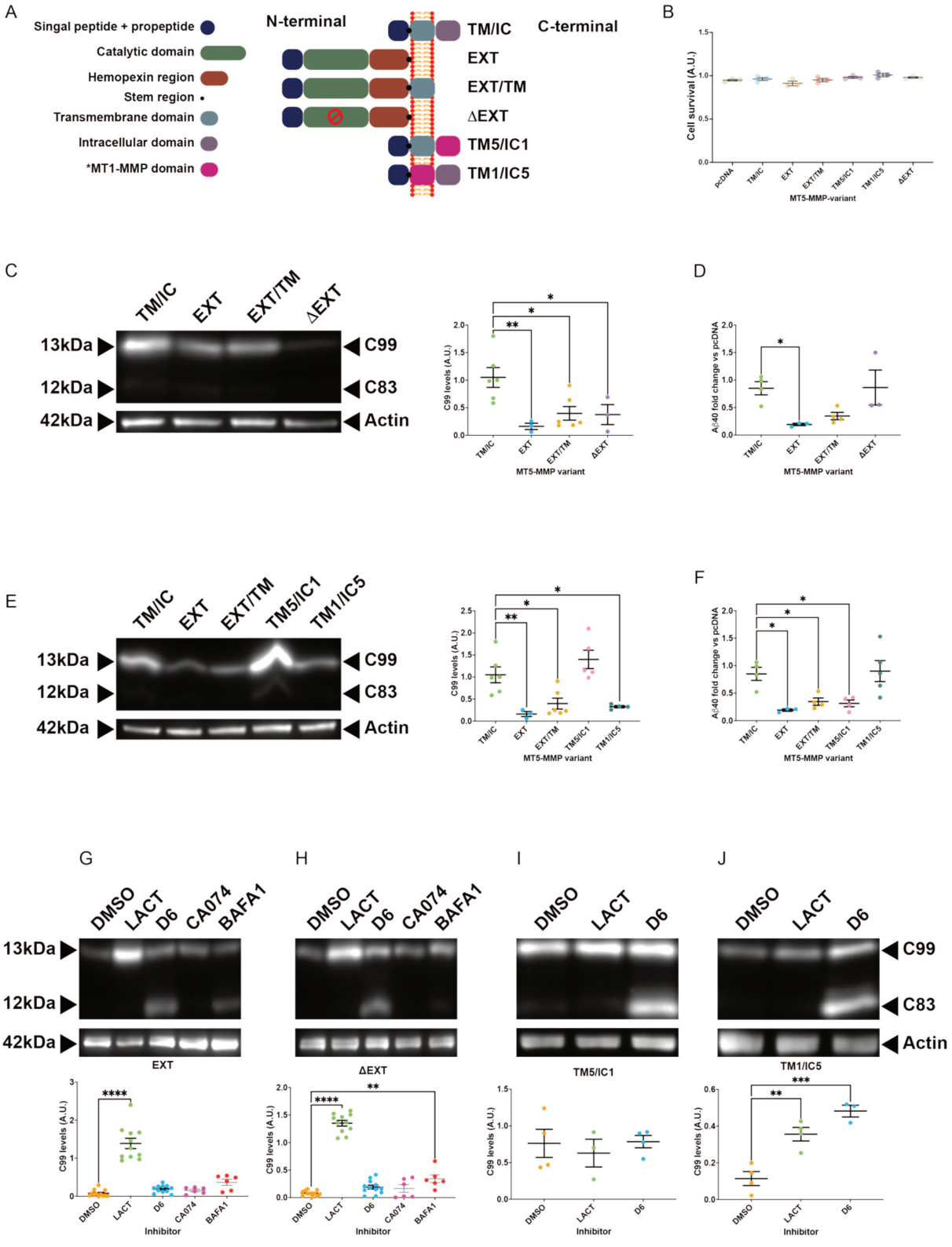

Fig 2.

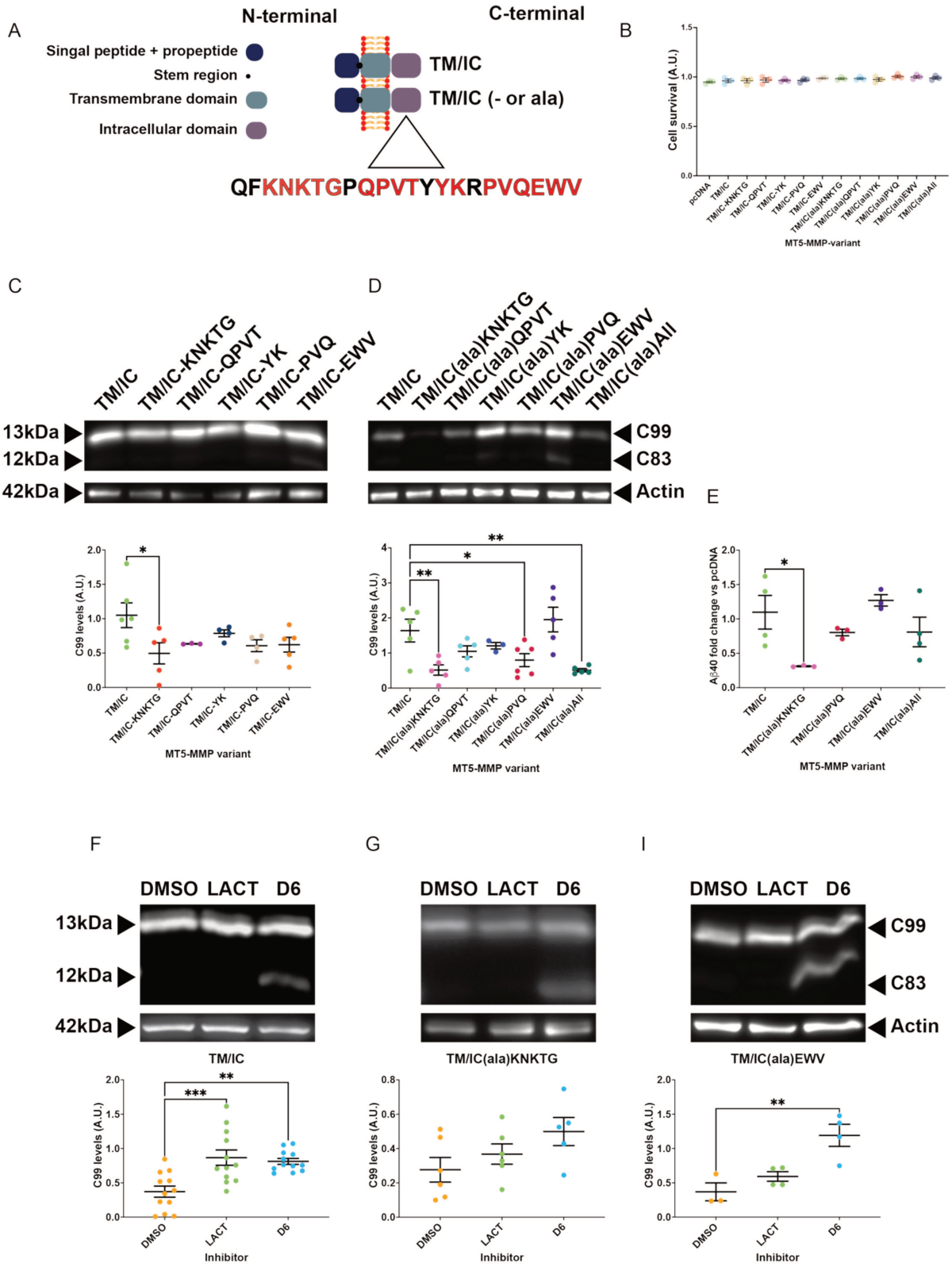
A
N-terminal
C-terminal
Singal peptide + propeptide
Stem region
Transmembrane domain
Intracellular domain
TM/IC
TM/IC (- or ala)
QFKNKTGPQPVTYYKRPVQEWV
B
Cell survival (A.U.)
pcDNA
TM/IC
TM/IC-KNKTG
TM/IC-QPVT
TM/IC-YK
TM/IC-PVQ
TM/IC-EWV
TM/IC(ala)KNKTG
TM/IC(ala)QPVT
TM/IC(ala)YK
TM/IC(ala)PVQ
TM/IC(ala)EWV
TM/IC(ala)All
MT5-MMP-variant
C
TM/IC
TM/IC-KNKTG
TM/IC-QPVT
TM/IC-YK
TM/IC-PVQ
TM/IC-EWV
13kDa
12kDa
42kDa
D
TM/IC
TM/IC(ala)KNKTG
TM/IC(ala)QPVT
TM/IC(ala)YK
TM/IC(ala)PVQ
TM/IC(ala)EWV
TM/IC(ala)All
C99
C83
Actin
C99 levels (A.U.)
MT5-MMP variant
E
Aβ40 fold change vs pcDNA
MT5-MMP variant
F
DMSO
LACT
D6
13kDa
12kDa
42kDa
TM/IC
C99 levels (A.U.)
Inhibitor
G
TM/IC(ala)KNKTG
I
TM/IC(ala)EWV

Fig 3.

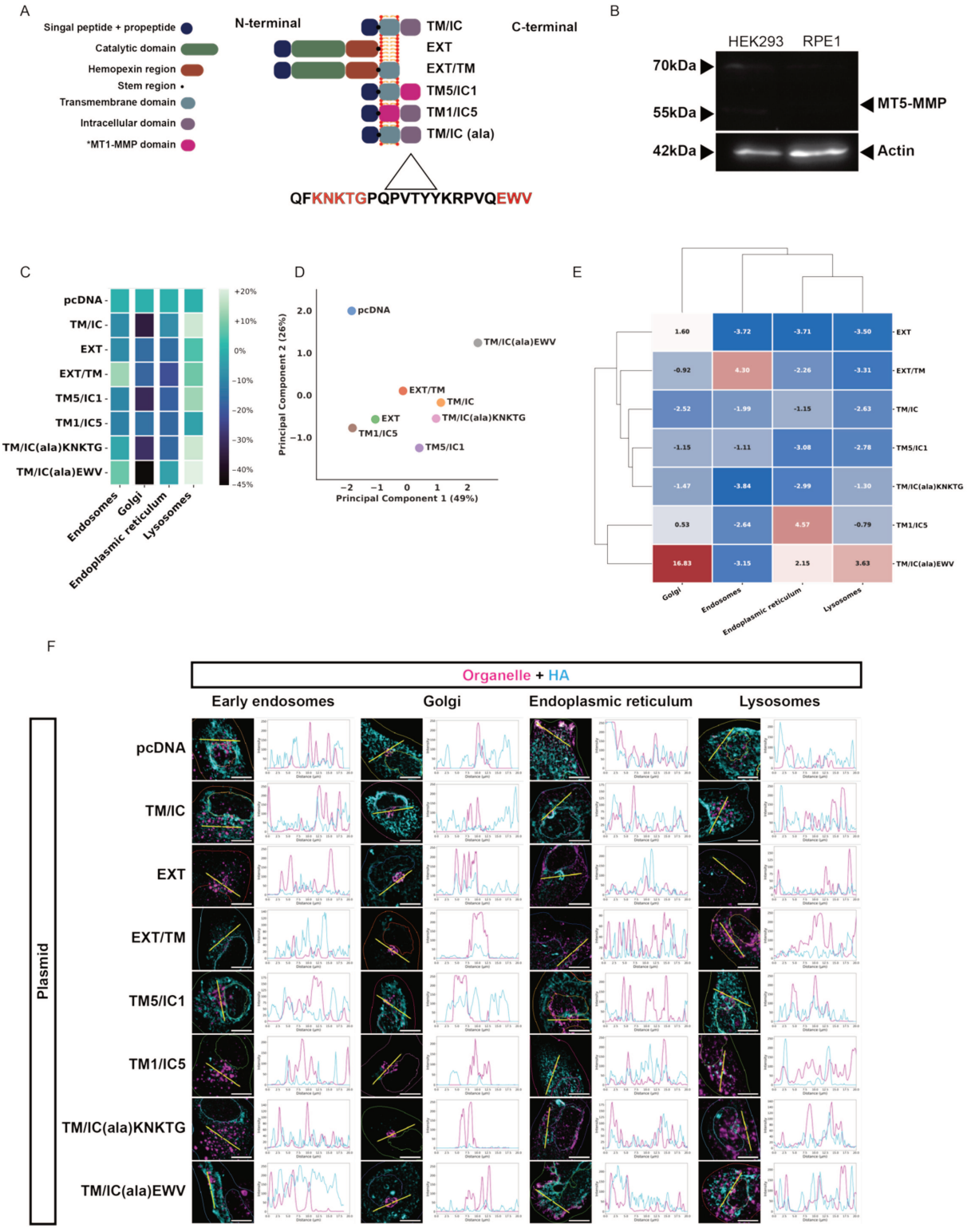
A
Singal peptide + propeptide
Catalytic domain
Hemopexin region
Stem region
Transmembrane domain
Intracellular domain
*MT1-MMP domain
N-terminal
C-terminal
TM/IC
EXT
EXT/TM
TM5/IC1
TM1/IC5
TM/IC (ala)
QFKNKTGPQPVTYYKRPVQEWV
B
HEK293
RPE1
70kDa
55kDa
42kDa
MT5-MMP
Actin
C
pcDNA
TM/IC
EXT
EXT/TM
TM5/IC1
TM1/IC5
TM/IC(ala)KNKTG
TM/IC(ala)EWV
+20%
+10%
0%
−10%
−20%
−30%
−40%
−45%
Endosomes
Golgi
Endoplasmic reticulum
Lysosomes
D
Principal Component 2 (26%)
Principal Component 1 (49%)
E
F
Organelle + HA
Early endosomes
Golgi
Endoplasmic reticulum
Lysosomes
Plasmid

Fig 4.

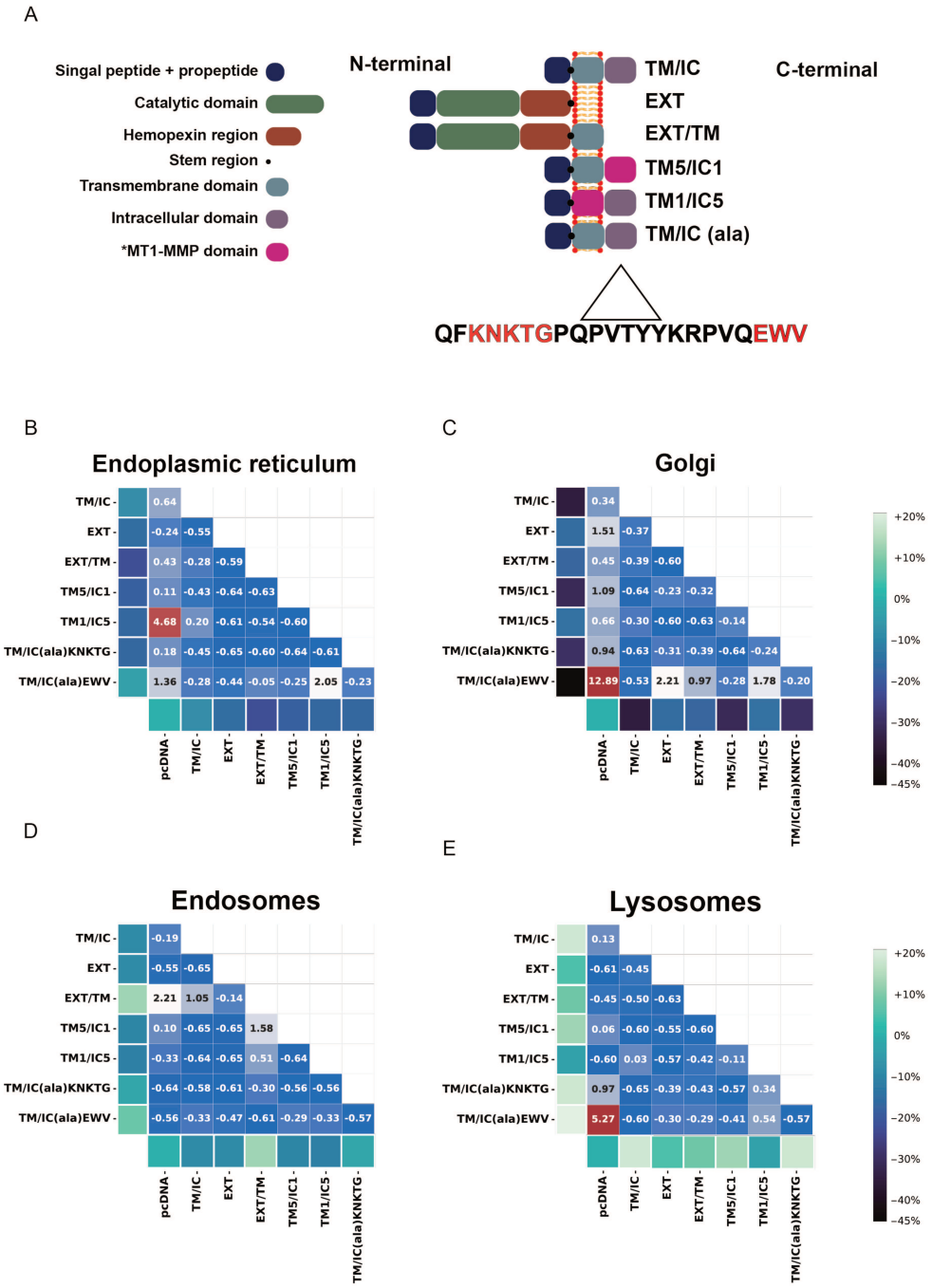
A
Singal peptide + propeptide
Catalytic domain
Hemopexin region
Stem region
Transmembrane domain
Intracellular domain
*MT1-MMP domain
N-terminal
TM/IC
EXT
EXT/TM
TM5/IC1
TM1/IC5
TM/IC (ala)
C-terminal
QFKNKTGPQPVTYYKRPVQEWV
B
Endoplasmic reticulum
C
Golgi
D
Endosomes
E
Lysosomes
TM/IC
EXT
EXT/TM
TM5/IC1
TM1/IC5
TM/IC(ala)KNKTG
TM/IC(ala)EWV
pcDNA
+20%
+10%
0%
−10%
−20%
−30%
−40%
−45%

Fig 5.

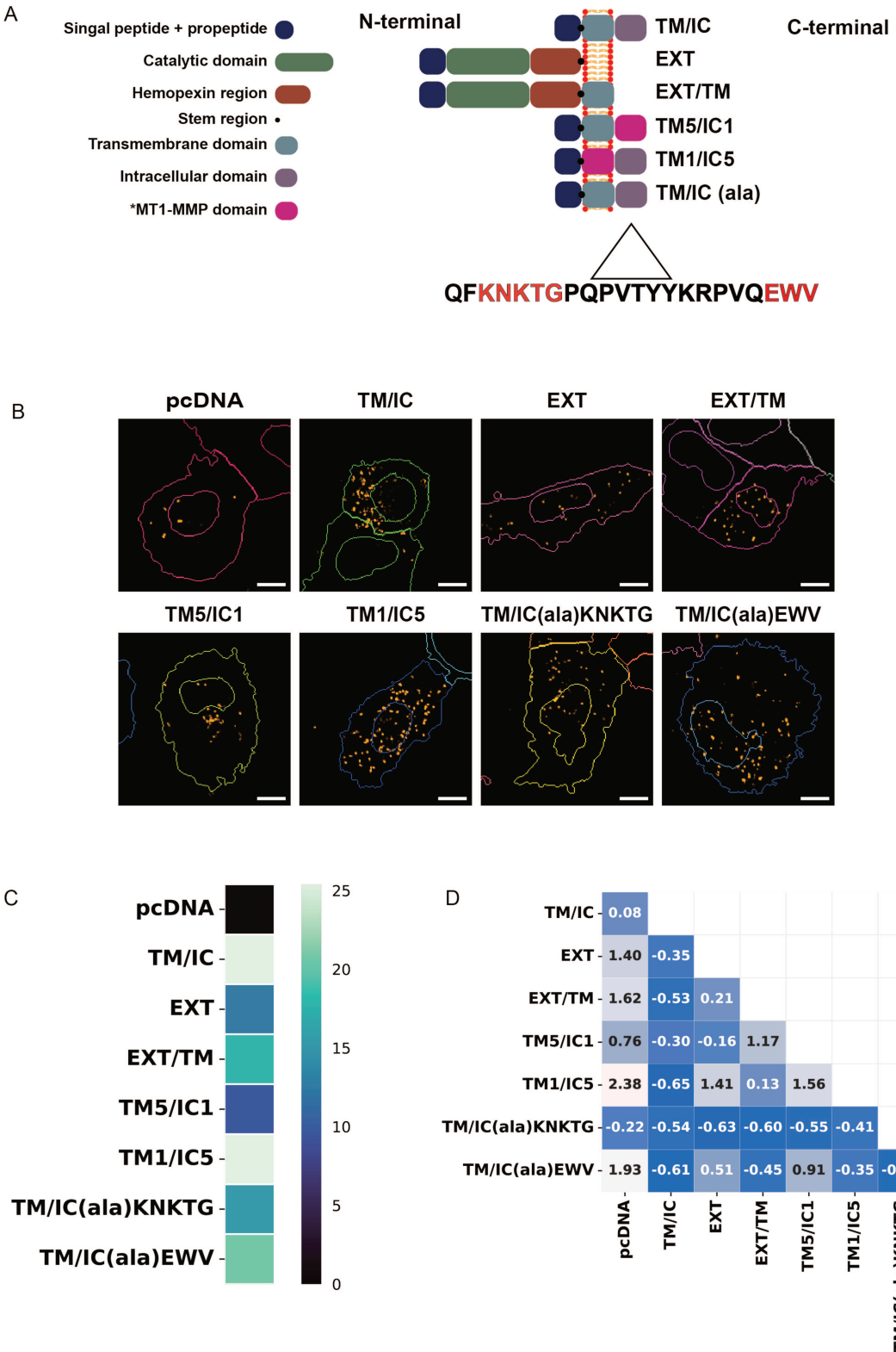
A
Singal peptide + propeptide
Catalytic domain
Hemopexin region
Stem region
Transmembrane domain
Intracellular domain
*MT1-MMP domain
N-terminal
C-terminal
TM/IC
EXT
EXT/TM
TM5/IC1
TM1/IC5
TM/IC (ala)
QFKNKTGPQPVTYYKRPVQEWV
B
pcDNA
TM/IC
EXT
EXT/TM
TM5/IC1
TM1/IC5
TM/IC(ala)KNKTG
TM/IC(ala)EWV
C
pcDNA
TM/IC
EXT
EXT/TM
TM5/IC1
TM1/IC5
TM/IC(ala)KNKTG
TM/IC(ala)EWV
25
20
15
10
5
0
D
TM/IC 0.08
EXT 1.40 -0.35
EXT/TM 1.62 -0.53 0.21
TM5/IC1 0.76 -0.30 -0.16 1.17
TM1/IC5 2.38 -0.65 1.41 0.13 1.56
TM/IC(ala)KNKTG -0.22 -0.54 -0.63 -0.60 -0.55 -0.41
TM/IC(ala)EWV 1.93 -0.61 0.51 -0.45 0.91 -0.35 -0.58
pcDNA
TM/IC
EXT
EXT/TM
TM5/IC1
TM1/IC5
TM/IC(ala)KNKTG

Figure 6.

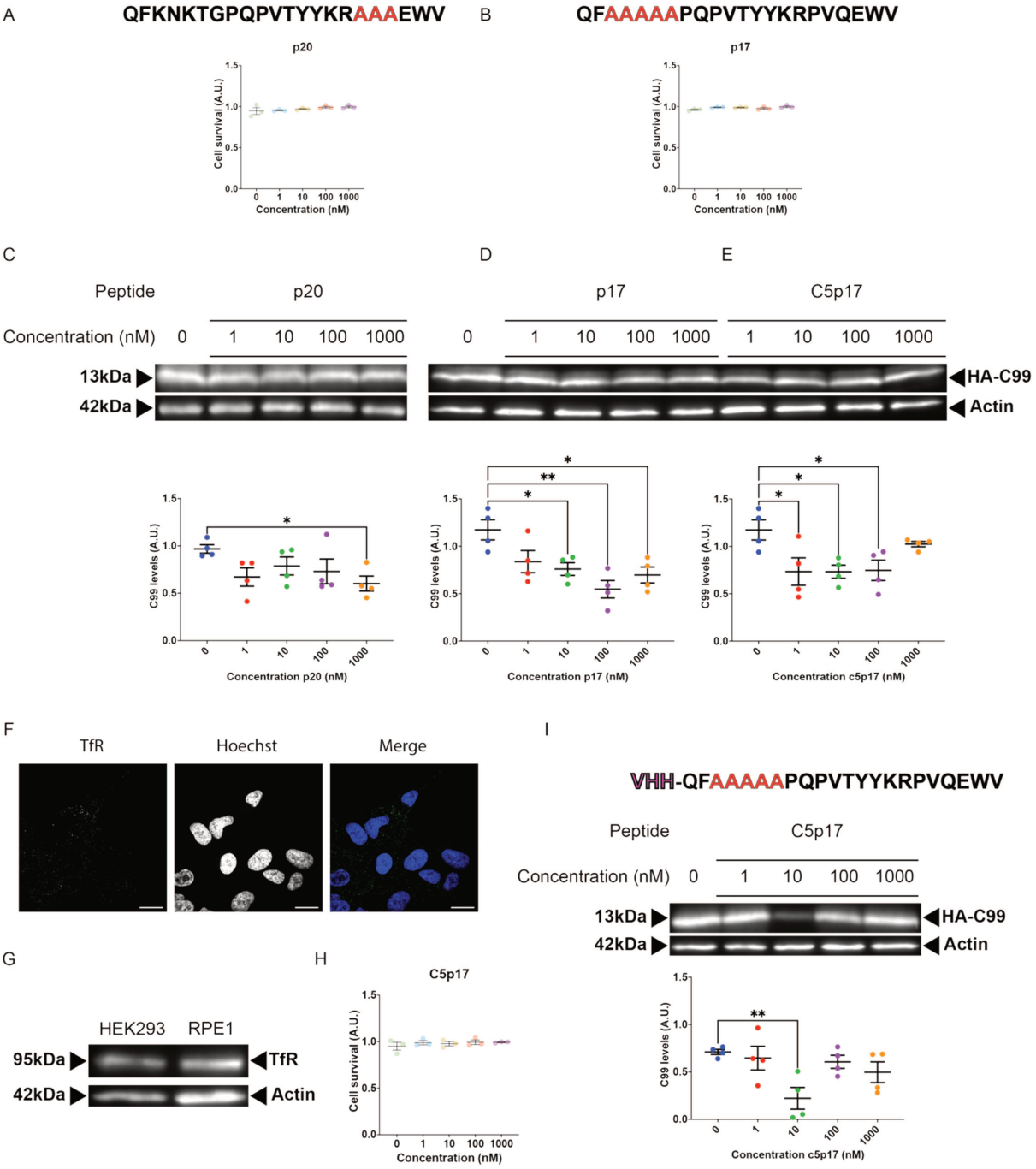
A
QFKNKTGPQPVTYYKRAAAEWV
p20
Cell survival (A.U.)
Concentration (nM)
B
QFAAAAAPQPVTYYKRPVQEWV
p17
C
Peptide
p20
Concentration (nM)
13kDa
42kDa
C99 levels (A.U.)
Concentration p20 (nM)
D
p17
Concentration p17 (nM)
E
C5p17
HA-C99
Actin
Concentration c5p17 (nM)
F
TfR
Hoechst
Merge
G
HEK293
RPE1
95kDa
TfR
42kDa
Actin
H
C5p17
I
VHH-QFAAAAAPQPVTYYKRPVQEWV

OTHER RESULTS

During the course of my PhD, in parallel of my main research project, I have been actively working at implementing a method allowing for the production of hiPSC-neurons to have access to a complementary and relevant modeling platform. Validating the ability of C5p17 to modulate C99 in a more physiological model of hiPSC-derived neurons will better help determining its therapeutic potential. There are currently multiple methods to obtain hiPSC-derived neurons (discussed in *Induced pluripotent stem cells chapter*), with their advantages and limitations. Moreover, various methods to generate disease phenotypes are available. Here, I will expose my efforts to develop a human *in vitro* model using a varied range of techniques and evaluate their validity.

Chemically defined media are widely used to induce hiPSC differentiation into different cell types. In my case, in my quest to obtain a reliable and useful model for my project, I started using a multi-step differentiation protocol to first obtain neural progenitor cells using dual-smad inhibition (NPC) and further guide their differentiation toward neurons[504,545]. Although efficient in neuronal generation, the protocol was inconsistent, resulting in heterogeneous cultures and neurons with low attachment—making it difficult to use them for further experiments. Moreover, the electrophysiological properties of neurons generated using this method were characteristic of very immature neurons, which often lacked key properties of neuronal electrical activity (*e.g.* minimal sodium currents, lack of spontaneous activity, single action potentials). In the first paper of this thesis, where I am the second author, neurons had an extremely immature profile even after 60 days of maturation from NPCs. Therefore, to overcome the shortcomings of this method we took advantage of direct reprogramming-based protocols and optimized a simple and reliable protocol that generates healthy, mature, and functional cultures within a short period of time.

Direct reprograming (discussed in the *Induced pluripotent stem cells chapter*) through NGN2 overexpression generates functional neurons within 21 days *in vitro* (DIV) when co-cultured with astrocytes. Although the original published protocol directly reprograms hiPSCs, other methods use NPCs as the starting cell type for direct reprograming. NPCs offer easier maintenance and homogeneity in the final differentiated cultures than hiPSC-based methods, and co-culture with astrocytes can be avoided. The method based on NPCs was particularly attractive because it provided us with the opportunity to investigate the modification of MT5-MMP specifically in neurons without the influence of other neural cell types. Thus, we leveraged our experience on NPC

generation to generate NGN2-expressing NPCs based on previously reported methods. We generated homogeneous cultures of NPC-derived neurons using NGN2 inducible overexpression, but we encountered similar limitations to those of our previous methods in terms of low attachment and immature physiology.

Neurons exhibit an underdeveloped synaptic network in the absence of astrocyte-secreted factors during maturation. Astrocytes are currently considered primary mediators of neuronal development and synaptic maturation. In primary rodent neurons, the addition of astrocyte-conditioned media (ACM) was sufficient to induce synaptic development and maturation in the absence of astrocyte co-culture. Thus, we combined three defined protocols to develop a maturation protocol starting from NPCs: the commercially available BrainPhys™ media previously conditioned with astrocytes to differentiate NPCs overexpressing NGN2. This method produced mature neurons in 28 DIV (Fig. 1A-I), with expression of synaptic markers (Fig. 1A) and mature synaptic network (Fig. 1C-I). Compared with non-treated ACM, ACM-treated NPC-derived NGN2 neurons showed increased staining of bassoon (pre-synapse) and Homer1 (post-synapse), and increased colocalization of both markers (synapse) (Fig. 1A). Increased synaptogenesis was correlated with more spontaneous synaptic currents and increased synaptic current amplitude (Fig. 1C-E). Moreover, ACM-treated neurons exhibited a more mature profile, with more consistent excitability at more stimulation steps (Fig. 1F), spontaneous action potential firing (Fig. 1G), and increased action potential amplitude (Fig. 1H, I). Taken together, these results demonstrate that treatment with ACM induces synaptogenesis, synaptic maturation, and correct ion channel distribution, thereby facilitating synaptic activity. Nevertheless, the inconsistency of NPC generation and scalability limitations conditioned our work toward directly optimizing NGN2 overexpression in hiPSCs.

The original protocols using direct hiPSC NGN2 reprograming were based on transducing hiPSCs with lentiviruses for every differentiation. Due to virus production limitations, batches of hiPSCs with stable expression of the inducible NGN2 transgene were a better fitted alternative. We generated three constructs to be transduced with lentiviral vectors: 1) pLV-Puro-TRE3G>hNEUROG2:P2A:TurboGFP (VB230703-1286rhg, VectorBuilder), 2) pLV-Puro-TRE3G>hNEUROG2 (VB230704-1157xpy, VectorBuilder), 3) pLV-EF1A>Tet3G:IRES:Neo (VB900088-2762aex, VectorBuilder). Following previously published protocols, mature neurons were obtained after 21 DIV of NGN2 overexpression

in hiPSCs co-cultured with rat astrocytes (Fig. 1J-L). In only 21 DIVs, direct reprograming from hiPSC in co-culture with astrocytes generated neurons with extensive expression and colocalization of synaptic markers (Fig. 1J), indicating correct synaptogenesis. Instead of assessing the electrophysiological properties of individual neurons, we evaluated the overall network synchronicity and maturation of the cultures (Fig. 1K, L). After 21 DIV and at three different seeding densities, hiPSC-derived neurons exerted neuronal activity, network synchronicity, and fired network bursts (Fig. 1K, L). From the three densities, we considered several network properties (not shown), and we chose to continue with $5x10^4$ cells/well. Our results demonstrate that mature functional neuronal cultures can be generated directly by reprograming hiPSC into neurons using NGN2-inducible overexpression. This protocol has important advantages in terms of: 1) reproducibility (*i.e.* less differentiation steps involved), 2) scalability (*i.e.* easier to increase the production of hiPSC cultures), 3) neuronal maturation (*i.e.* increased number of synapses and strong network activity), and 4) rapidity (*i.e.* cultures have mature neurons at only 21 DIV without going through NPC differentiation of 3 weeks). These benefits represent an important upgrade over our previously developed methods, facilitating the establishment of a drug testing platform. Indeed, the flexibility of this protocol helped us to optimize an AD model by inducing C99 overexpression with an AAV-PHP.S HA-C99. We are currently using this human *in vitro* model to validate the effects of C5p17 in C99 and Aβ levels and in synaptic physiology, as developed in my second article (link to second paper thesis).

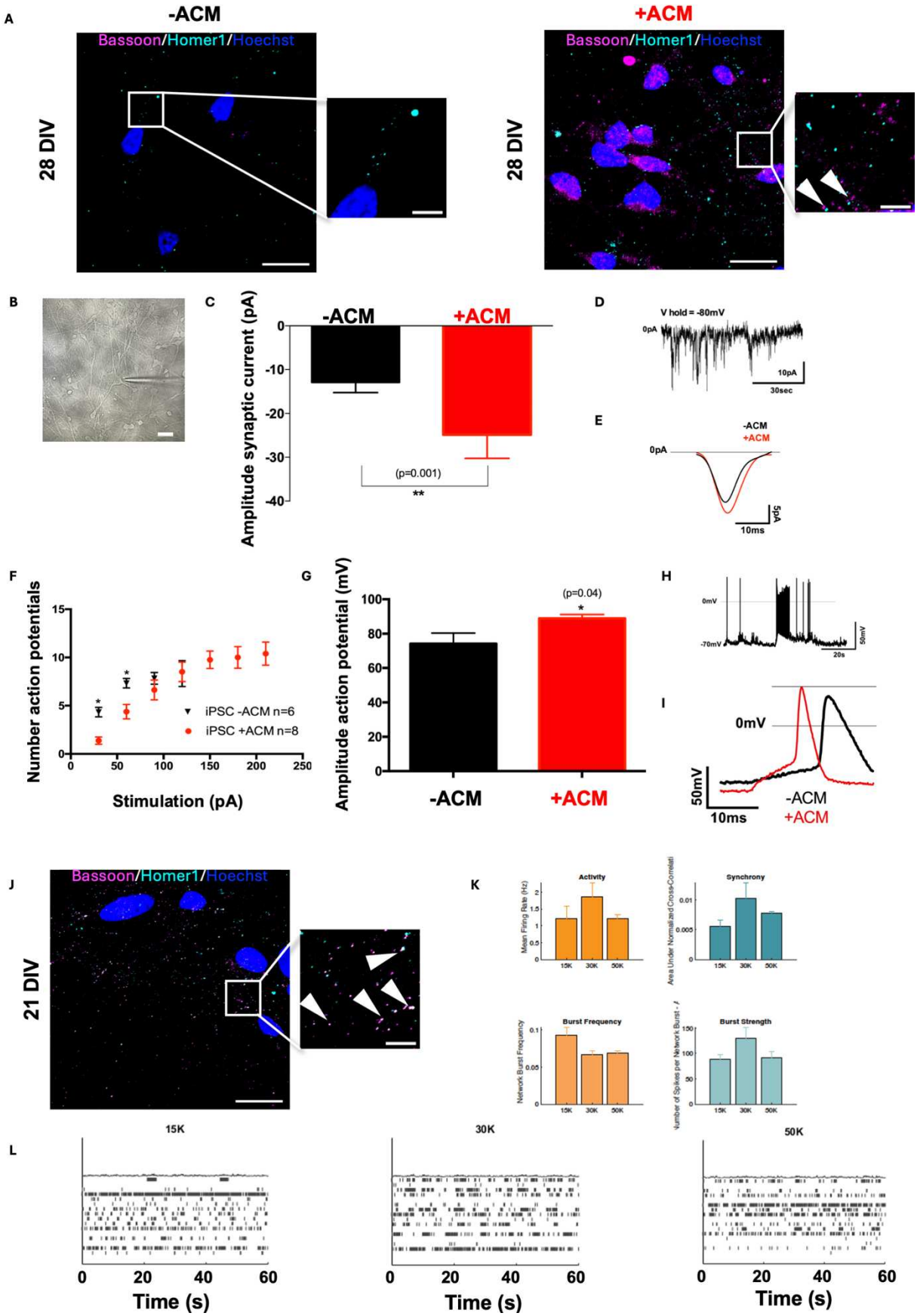
A
-ACM
+ACM
Bassoon/Homer1/Hoechst
28 DIV
B
C
Amplitude synaptic current (pA)
(p=0.001)
**
D
V hold = -80mV
0pA
10pA
30sec
E
-ACM
+ACM
0pA
5pA
10ms
F
Number action potentials
iPSC -ACM n=6
iPSC +ACM n=8
Stimulation (pA)
G
Amplitude action potential (mV)
(p=0.04)
*
H
0mV
-70mV
50mV
20s
I
0mV
50mV
10ms
J
21 DIV
K
Activity
Synchrony
Burst Frequency
Burst Strength
L
15K
30K
50K
Time (s)

Figure 1. **Inducible NGN2 overexpression rapidly generates mature neuronal cultures from different cell types.** (A) Fluorescence microphotographs of NPC-derived mature neurons differentiated for 28 DIV after NGN2 overexpression and showing extensive synaptogenesis only in the presence of ACM. Staining with the pre-synaptic and post-synaptic markers Bassoon and Homer1 demonstrated that the addition of ACM (+ACM) increased the number of synapses. White arrows point at synapses. Scale bar indicates 20µm in the big images and 5µm in the insets (B) Representative phase contrast image of patching a pyramidal neuron generated using NGN2 overexpression in NPCs. (C) Neurons differentiated in the presence of ACM exhibited significantly higher synaptic current amplitudes, indicating more mature synapses. (D) Representative trace of spontaneous synaptic currents at an imposed voltage of -80mV in NPC-derived neurons cultured with ACM. The presence of spontaneous activity denotes synaptic maturity. (E) Superposed average synaptic current traces in neurons non-treated or treated with ACM. The traces reflect the difference in synaptic current amplitude quantified in D. (F) NPC-derived neurons cultured with ACM respond to higher stimulation steps, with action potentials having a better regulated response at low stimulation steps. Immature neurons are often more excitable at low stimulation steps due to an imbalance in the distribution of ion channels. (G) ACM-treated neurons exhibit significantly increased action potential amplitudes. As mentioned in F, the presence of ACM may favor the overall maturation of neurons, providing a more balanced equilibrium of ion channels that favors deeper action potentials at more controlled rhythms. Representative traces of ACM-treated neurons with spontaneous and rhythmic depolarization, probably generated in response to network activity. (H) Representative traces of ACM-treated neurons with spontaneous and rhythmic depolarization, probably generated in response to network activity. (I) Superposed traces of single action potentials in ACM- and non-ACM–treated cells. Increased action potential amplitude and delayed depolarization evoke mature neuronal membrane profile. (J) hiPSC-derived neurons co-cultured with rat astrocytes after 21 DIV of NGN2 overexpression. Synaptic staining denotes significant synaptogenesis with generous expression of pre- and post-synaptic markers and consistent co-localization of both markers, indicative of mature synapses. White arrows point at synapses. Scale bar indicates 20µm in the big images and 5µm in the insets. (K) Quantification of channel activity, network synchrony, and burst frequency and strength in hiPSC-derived neurons seeded at $1{,}5x10^4$, $3x10^4$, $5x10^4$cells/well. Cultures with the three tested densities exhibited network activity, synchronicity, and burst firing. (L) Representative blots of 60s of neuronal firing recorded in different channels in cultures with different densities (*e.g.* 15K = $1{,}5x10^4$ cells/well). Each vertical line represents a spike detected in a single channel. Evoked spikes at high frequencies represent burst firing, and bursts aligned at similar time points in different channels represent network firing and indicate network synchronicity. All graphs are representations of means ± SEM of a minimum of 3 n. Statistical significance of t-test was considered for p-values (p) < 0.05. Each recorded cell was considered as one n.

DISCUSSION & PERSPECTIVES

More than a century after it was first described, researchers have yet to discover a cure for AD. With an overall increase in life expectancy, the burden of AD is growing exponentially. In addition, the pathogenic mechanisms underlying disease onset and progression remain elusive, hindering the development of effective treatments. Significant advances over the past 4 decades have highlighted key molecular components of AD, some of which have resulted in potential biomarkers and/or therapeutic targets. The amyloid hypothesis established Aβ as the primary instigator of the onset and progression of AD. However, the lack of success in developing efficient biomarkers and therapies targeting Aβ has raised progressively the scientific interest for other pathophysiological pathways and even questioning the amyloid hypothesis. Only recently developed treatments against Aβ, that partially prevent cognitive decline in patients, have restored confidence in delaying/halting AD by tackling the amyloid cascade. This train of thought has provided new avenues for exploring alternative targets at distinct stages of APP processing to prevent amyloidogenesis and enhance the efficiency of Aβ-targeting therapies.

Despite multiple advances in the treatment of AD, with the recently FDA-approved anti-Aβ monoclonal antibodies at the forefront, there is a lack of effective treatments that fully prevent the onset or progression of AD. Anti-amyloidogenic strategies targeting the amyloidogenic pathway at different levels have frequently ended in clinical failures. This arises from a combination of AD animal models being incapable of reflecting the full complexity of the pathology and the secondary effects associated to disrupting β- and/or γ-secretase activity. Indeed, some APP metabolites (*e.g.* Aβ, $A_{\eta\text{-}\alpha}$, $A_{\eta\text{-}\beta}$) with pathogenic roles in AD also have homeostatic functions[412,413,546]. Thus, new therapeutic strategies must target these pathogenic elements (*e.g.* APP toxic metabolites) while limiting their impact on their physiological roles. In this context, recent advances in elucidating the role of MT5-MMP in AD might facilitate the generation of therapeutic agents that can specifically target AD hallmarks with minimal effects on MT5-MMP functions.

Early research on MT5-MMP indicated that it is mainly expressed in the brain and that it colocalized with parenchymal Aβ plaques[469]. Further work demonstrated that MT5-MMP knockout in 5xFAD mice significantly reduced Aβ plaques in the hippocampus and cortex, with a concomitant reduction in neuroinflammation markers and a preservation of the synaptic network, which results in preserved LTP and cognitive function. Moreover, MT5-MMP co-immunoprecipitated with APP in HEK cells co-expressing APP and MT5-

MMP, indicating possible functional interactions between both proteins[443]. Collectively, these findings provide evidence that MT5-MMP contributes to amyloidogenesis, and to neuroinflammation and synaptic dysfunctions, in an AD context.

Advances in genetic engineering enable the modulation of specific proteins to mitigate their pathogenic functions. Multiple gene therapy strategies have had great success in AD preclinical models, but none of them have been translated into clinical applications so far[547–550]. Moreover, similar to inhibition approaches, knocking down certain proteins may lead to unwanted side effects of varying severity. In the first paper of this thesis, in which I am the second author, we aimed to corroborate the phenotypical consequences of knocking out MT5-MMP in hiPSC-derived neurons and astrocytes, two of the most important cell types affected in AD.

MT5-MMP regulates dendritic arborization

The benefits of knocking out MT5-MMP in 5xFAD mice offers a playground to investigate new approaches to decrease amyloid burden and neuroinflammation in AD, in a context where MT5-MMP deficient mice lack developmental impairments[443,473]. In line with these results, both WT and MT5-MMP knockout hiPSCs were equally capable of generating neurons and astrocytes, without clear differentiation differences with our protocols. However, knocking out MT5-MMP increased the number of primary and secondary neurites in neurons, resulting in a more arborized neuronal morphology. This correlates with previous findings in a mouse model of thermal pain, in which dorsal root ganglia exhibited increased neurite arborization under MT5-MMP knockout conditions[474]. Interestingly, one of the MT5-MMP substrates is N-cadherin, which is a cell adhesion molecule that is particularly important in synapses[471]. Indeed, in rat primary hippocampal neurons, activity-induced dendrite growth depends on N-cadherin recruitment at the plasma membrane and the consequent neuron-neuron contact through N-cadherin[551]. Accordingly, surface N-cadherin is necessary for functional synapse formation, and impeding its translocation into the membrane of rat hippocampal primary neurons reduces synapse number and impairs LTP[552]. Moreover, mice carrying a mutated N-cadherin resistant to ADAM10 cleavage had increased excitatory synaptic density in the hippocampus without altering dendritic spine morphology. In multiple behavioral tasks, mutated N-cadherin knockout improved cognitive performance compared with their WT counterparts[553]. Deleting MT5-MMP in hiPSC-derived neurons may promote N-cadherin accumulation at the cell surface, which

triggers increased complexity in dendritic arborization. However, early primary cortical neurons from MT5-MMP knockout mice exhibited normal levels of N-cadherin, suggesting that MT5-MMP deficient neurons maintain normal N-cadherin metabolism in immature primary cultures[554]. Thus, MT5-MMP knockout may affect hiPSC-derived neurons differently, or alternative mechanisms may be involved in dendrite outgrowth.

Synaptic activity triggers downstream signaling that induces transcriptional changes resulting in neurite outgrowth. After treatment with bicuculline, increased synaptic activity augmented the expression of glycolysis-related genes, facilitating lipid synthesis and hypoxia inducible factor 1α stabilization. This signaling pathway modulates neurite architecture in rodents *in vitro* and *in vivo*[555]. In a *Drosophila* model, presynaptic localization and activity also regulated dendritic outgrowth. While contact with presynaptic buttons stimulated local dendritic outgrowth, presynaptic activity inhibited global dendritic arborization[556]. However, our experimental data revealed similar electrophysiological properties and synaptic density in WT and MT5-MMP knockout hiPSC-derived neurons. In both genotypes, neuronal differentiation obtained with our protocols at that time was insufficient to generate mature neurons displaying robust synaptic density and normal electrical properties with spontaneous synaptic activity. We hypothesize that the lack of changes in MT5-MMP-deficient hiPSC-derived neurons result from cell immaturity, even at 60 DIV, which masks any potential differences in synaptic physiology. Previous data on mature mouse primary cultures support the role of MT5-MMP in neuritogenesis[557]. Furthermore, unpublished data from our group confirm deficits in cognitive performance and synaptic alterations in MT5-MMP knockout WT mice. A recent paper from our team also demonstrated unchanged synaptic activity in immature primary cortical cultures from MT5-MMP knockout WT mice. Nevertheless, inducing a stress response with IL-1β stimulation revealed increased hyperactivity of MT5-MMP-deficient neurons in the same model[554]. Therefore, the absence of MT5-MMP might induce subtle differences during neurodevelopment, which are only apparent under stressful conditions. Further work on MT5-MMP knockout in WT specimens during development and in mature conditions is needed to confirm these assumptions.

MT5-MMP deficiency alters astrocytic morphology and impairs the expression of astrocytic markers

The role of MT5-MMP extends beyond neuronal physiology, and its deficiency may affect other major cell types in the brain. In addition to a decrease in amyloidogenesis, neuroinflammatory markers (*e.g.* GFAP or IL-1β) were also decreased in 5xFAD$^{MMP24-/-}$ mice. Whether this reduction was a cause, a consequence, or an independent phenomenon of knocking out MT5-MMP was unclear[443]. Astrocyte morphology correlates with specific phenotypes, and specific morphologies were translated into differential gene expression in a mouse model of AD[558]. In accordance, morphological differences in our hiPSC-derived astrocytes may reflect alterations caused by the absence of MT5-MMP. In homeostatic conditions, astrocytes occupy extended spaces with long projections reaching hundreds of thousands of neuronal synapses. Thus, the reduction of arborized astrocytes in MT5-MMP-deficient cultures might reflect impaired differentiation or altered transcriptomic states. In fact, IL-1β stimulation of immature primary mixed cortical cultures induced a different transcriptomic response in MT5-MMP knockout mice compared with WT mice, supporting the assumption that our morphological findings may result from changes in cell homeostasis due to MT5-MMP deficiency[554].

Astrocyte diversity in the CNS has highlighted the importance of considering multiple astrocytic proteins to define their phenotype[558,559]. Both GFAP and ALDH1L1 are currently the most popular markers used to characterize astrocytes, although GFAP is increasingly considered a marker of astrocyte reactivity[560]. Accordingly, its expression is associated with neurodegenerative diseases. In AD patients, GFAP serum levels are negatively correlated with cognitive performance and brain weight and positively correlated with tau pathology, suggesting a negative outcome of increased GFAP expression[561]. Following this train of thought, knocking out MT5-MMP in hiPSC-derived astrocytes was insufficient to reduce GFAP expression in any of the three studied morphologies; however, it might be necessary to further explore differences between both genotypes upon inflammatory stimulation. ALDH1L1 levels were stable across WT and MT5-MMP knockout astrocytes, indicating normal maturation despite MT5-MMP knockout. Another marker extensively used to track astrocyte differentiation is S100β, but it is also considered to mediate astrocyte reactivity[562–564]. The involvement of MT5-MMP in neuroinflammation in 5xFAD mice may explain the decrease in S100β expression in

arborized astrocytes[443]. Overall, the results on GFAP and ALDH1L1 indicate equivalent differentiation and maturation processes between both genotypes; thus, the decrease in S100β in MT5-MMP knockout arborized astrocytes might reflect decreased basal reactivity.

Beyond their role in inflammation, synaptic regulation is one the major functions of astrocytes[565]. They are responsible for buffering perisynaptic glutamate after presynaptic release. Recent findings also demonstrate that astrocytes participate in gliotransmission—they are capable of releasing glutamate at distant synapses upon presynaptic glutamate release[566]. To do so, they express a family of glutamate transporters that are mainly located in the perisynaptic processes *in vivo*[567]. The physiology of glutamate transporters is impaired in multiple neurological diseases, where their expression, subcellular location, and trafficking are altered[568–570]. Among them, solute carrier family 1 member 3 (SLCLA3 or GLAST) is also frequently used to characterize astrocytes. In MT5-MMP knockout hiPSC-derived astrocytes, GLAST was downregulated in all three morphologies studied, indicating differences in glutamate transporter homeostasis. Defects in GLAST functionality correlate with AD, and GLAST expression was increased in astrocytes close to Aβ plaques in AD patients[571]. The decrease in GLAST levels in MT5-MMP-deficient astrocytes may reflect a beneficial effect in controlling astrocyte-induced synaptic overactivation, which could partially explain the preservation of the synaptic network and LTP in 5xFAD$^{MMP24-/-}$ mice[443].

Considering the effects of knocking out MT5-MMP in human brain cells, we explored different possibilities for using MT5-MMP-based strategies to address amyloidogenesis in AD. Although MT5-MMP is a metalloproteinase with multiple targets, its amyloidogenic effects are probably partially independent of its catalytic activity. Introducing an inactivating mutation in the MT5-MMP catalytic domain was ineffective in reducing Aβ levels in HEK cells overexpressing APP_{swe}, demonstrating that MT5-MMP catalytic activity is unrelated to Aβ production in this cellular model. Moreover, in heterologous cell lines overexpressing C99, co-expression of MT5-MMP variants with whole-domain deletions only prevented the accumulation of C99 and Aβ secretion in the case of TM and/or IC deletion. The same experiment with MT1-MMP yielded opposite results, with an increase in C99 levels upon deletion of MT1-MMP IC[455]. Therefore, the amyloidogenic effects of TM and IC are unique to MT5-MMP. In my first author paper, we explored the therapeutic potential of using certain MT5-MMP domains to take

advantage of their potential interactions with C99 and introduced specific mutations in MT5-MMP to modulate C99 fate.

Whole-domain modifications modulate MT5-MMP proamyloidogenic effects through changes in C99 trafficking

The different effects in C99 levels upon IC removal in MT1-MMP and MT5-MMP indicate distinct molecular mechanisms in their interaction with C99[455]. Interestingly, both MMPs share a high sequence homology, which is reduced to only ~20% in the TM and IC domains[465]. Thus, we hypothesized that differences in the amino acid sequence of the TM and IC could account for the MT5-MMP pathogenic effect on C99 accumulation. The persistent reduction of C99 after catalytic inactivation in the EXT construct (*i.e.* the ΔEXT) further validated the importance of MT5-MMP TM and IC in C99 accumulation, demonstrating that the reduction of C99 was unrelated to EXT catalytic activity. Moreover, under both ΔEXT and EXT conditions, proteasomal degradation was the primary processing pathway. However, ΔEXT increased Aβ levels compared with EXT. This phenomenon was related to the lysosomal processing of C99, as demonstrated with BAFA1 inhibition, but the molecular mechanisms responsible for the processing of C99 into Aβ in these conditions remain unclear. One possibility is an intensified catalytic activity of EXT derived from the lack of membrane anchoring due to the loss of TM and IC, this could imply the cleavage and inactivation of other secretases involved in Aβ modulation.

The TM is a key structural component of metalloproteinases capable of modulating their catalytic activity[572,573]. For instance, chimeric combinations of the ADAM10 catalytic domain with ADAM17 TM and IC significantly decreased ADAM10 catalytic activity[572]. Similarly, mutations in ADAM17 TM or substitutions with artificial membrane-anchoring elements evidenced distinct modulation of ADAM17 substrates depending on changes in the ADAM17 TM amino acid sequence[573]. Hence, the lack of Aβ clearance after mutation of the MT5-MMP EXT catalytic site might indicate MT5-MMP EXT capacity to cleave proteins which are key in APP processing, impeding Aβ production in the context of C99 accumulation. This could be in coordination with a potential role of ΔEXT in C99 translocation into subcellular compartments where C99 contacts canonical amyloidogenic secretases.

Endolysosomal compartments are key cellular structures for amyloid APP processing, and γ-secretase is located and active in acidic compartments, where it cleaves C99[346,389,574]. Nevertheless, D6 treatment demonstrated that normal Aβ production in HEK cells co-transfected with ΔEXT is independent of γ-secretase activity. Overexpression of a catalytically active variant of MT5-MMP (EXT) may interfere with lysosomal proteolytic activity and impede normal Aβ production. Upon inactivation of the catalytic activity by point mutation (ΔEXT), this effect is lost, and Aβ levels are recovered as in our pathological control (TM/IC). The minimal recovery of C99 after BAFA1 treatment—which blocks the autophagolysosome pathway—suggests that the recovery of Aβ levels in HEK cells co-transfected with ΔEXT depends on enzymatic activity in the lysosomes. Therefore, translocation of C99 into lysosomes could facilitate its proteolysis. Interestingly, the subcellular distribution of C99 in the presence of EXT was similar to that observed after TM1/IC5 expression, as evidenced by PCA analysis. Both constructs strongly reduced C99 levels and led to similar amounts of C99 in lysosomes, but TM1/IC5 maintained high levels of Aβ. Thus, translocation of C99 into lysosomes may facilitate its processing into Aβ, unless there is catalytic activity of MT5-MMP.

Subcellular distribution is indeed an important parameter for determining C99 fate. Compared with TM1/IC5, TM5/IC1 clusters individually in the PCA, indicating that it induces a particular distribution of C99 in the endomembrane system. Reduced proximity interactions between TM5/IC1 and C99 may explain the diametrically opposite effects of this variant on C99 and Aβ levels compared to TM1/IC5, suggesting its inability to mobilize C99 in specific compartments. Accordingly, in the presence of TM5/IC1, proteasome and γ-secretase inhibitors failed to rescue C99 levels, explaining why, contrary to TM1/IC5, C99 accumulates while Aβ levels decrease. In APP_{swe}-expressing cells, delaying the transport of APP through the Golgi apparatus correlated with increased Aβ production, and impeding APP retrograde transport from endosomes to the TGN reduced Aβ40 in HEK cells, suggesting that the Golgi is a major site for Aβ production[219,321]. Concordantly, co-expression of TM5/IC1 reduced the amount of C99 in the Golgi apparatus, which could explain the lack of C99 cleavage into Aβ. Altogether, our results indicate that whole-domain modifications critically alter the subcellular distribution of C99, which deeply affects its accumulation and transformation into Aβ. Specifically, MT5-MMP IC may increase the localization of C99 into cellular compartments where distinct enzymes can process it.

Therapeutic strategies to target MMPs in disease contexts have traditionally relayed on inhibitors. However, MMPs sequences are highly conserved—with particularly high homology in their catalytic domains—and MMPs inhibitors usually target a broad spectrum of MMPs[575]. Although new generation inhibitors show greater specificity for certain MMPs (*e.g.* MT1-MMP), specific inhibition of MT5-MMP remains challenging[576]. Thus, the role of MT5-MMP TM and IC is of great interest to leverage on their properties in regulating C99 trafficking to counteract amyloidosis. On top of that, catalytic inactivation of MT5-MMP was unrelated to Aβ production when expressed in HEK cells overexpressing C99, whereas the depletion of the IC or TM/IC domains impeded C99 and Aβ accumulation in the same model[455]. Our results further extend the role of MT5-MMP TM and IC, demonstrating that these cellular domains determine C99 fate by changing its subcellular distribution. Using modified non-catalytic domains of MT5-MMP to counteract C99 accumulation opens the door to modulate amyloidogenesis in AD without affecting endogenous MT5-MMP activity, limiting potential secondary effects.

Apart from TM and IC, other MT5-MMP domains also favor Aβ production through other molecular mechanisms. Further experiments focusing on APP could elucidate the role of MT5-MMP in facilitating β-secretase cleavage of APP. Mint proteins are required to transport APP into subcellular compartments where it contacts β-secretase, and their deletion hinders APP-CTFs accumulation in primary murine neurons[230]. One possible mechanism explaining MT5-MMP-induced increase in Aβ production could involve the cross-interaction of MT5-MMP, APP, and Mints. The CTF derived from MT5-MMP cleavage of APP (η-CTF) suffices to generate Aβ, since its overexpression in APP knockout fibroblasts leads to Aβ production. Moreover, in HeLa cells, η-CTF accumulated in the Golgi and endosomes, two locations involved in Mint-related transport of APP[577]. Therefore, a primary interaction of Mint, APP, and MT5-MMP could facilitate η-CTF transport to the plasma membrane, from where it could be internalized into endocytic vesicles containing β-secretase. Whether this would lead to a subsequent cleavage by β-secretase, and whether the catalytic activity of MT5-MMP is necessary for its pro-amyloidogenic actions is unclear. Thus, the capacity of our MT5-MMP-variants to modulate APP toxic metabolites may extend to η-secretase intermediates. However, the catalytic inactivation of MT5-MMP failed to reduce Aβ production in HEK cells with the APP_{swe} mutation[455]. Exploring the effect of MT5-MMP domains/chimeras on upstream components of C99/Aβ would clarify the therapeutic potential of these constructs to

counteract the pro-amyloidogenic roles of MT5-MMP at different stages of APP processing. In other words, MT5-MMP pro-amyloidogenic effects upstream from C99 formation may also depend on MT5-MMP modulation of APP trafficking through its C-terminal PDZ-binding domain, making MT5-MMP IC a valuable tool to modulate APP/C99 trafficking and, hence, amyloidogenesis.

Changes in the MT5-MMP IC amino acid sequence preserve its capacity to modulate C99 trafficking and regulate Aβ production

More precise modifications in the MT5-MMP IC demonstrate the importance of specific amino acids in the regulation of C99. The loss of protein structure can explain the minimal effect of IC deletions on C99 regulation. In contrast, the differences in C99 modulation upon Ala substitutions confirmed that the structure of MT5-MMP variants is important for their function. Alanine scanning is a widespread methodology for determining functional epitopes in proteins because it is a neutral amino acid that preserves the secondary protein structure[578]. As with the MT1-MMP and MT5-MMP chimeras, some MT5-MMP variants exert contrasting effects on C99 and Aβ levels, which seem to accompany differences in C99 subcellular distribution.

Both deletion and substitution of the KNKTG amino acids at the interface of MT5-MMP TM and IC drastically reduced C99 and Aβ levels, being the only modification with the capacity to reduce both peptides. Other groups of amino acid substitutions (*i.e.* PVQ and all the target amino acids) reduced C99 levels while maintaining normal Aβ generation. KNKTG substitution hinders C99 processing by γ-secretase and promotes its degradation, indicating that KNKTG is a key motif for MT5-MMP facilitation of γ-cleavage of C99. However, inhibition of γ-secretase and proteasome with either D6 or LACT failed to recover C99 levels, meaning that other processing pathways are responsible for the anti-amyloidogenic action of KNKTG mutation. However, the exact molecular mechanisms of C99 degradation in HEK cells coexpressing TM/IC(ala)KNKTG remain unresolved. The co-expression of TM/IC(ala)KNKTG increases the levels of C99 in lysosomes, whereas it decreases C99 levels in the Golgi. This distribution profile is similar to that of other constructs inducing very different outcomes, and TM/IC(ala)KNKTG clusters close to the TM/IC control in the PCA analysis, which has the exact opposite effect on C99 and Aβ levels. Moreover, TM/IC(ala)KNKTG maintains colocalization with C99 at similar levels than other constructs like TM/IC or TM1/IC5,

discarding a loss of interaction between C99 and the MT5-MMP variant that could explain the decrease in both C99 and Aβ. One possibility is the involvement of other proteins in TM/IC(ala)KNKTG-mediated trafficking of C99. The presence of the PDZ-binding motif in this variant could induce C99 modulation through interactions with Mint proteins, a family of proteins with highly preserved PDZ-binding domains, which are known to colocalize in the Golgi complex with APP, and which are necessary for Aβ production[230,233]. However, the role of Mint proteins in amyloidogenesis is contradictory. In HEK cells, overexpressing mint 1 specifically blocked γ-secretase cleavage of C99, without affecting β-cleavage of APP[579]. Therefore, Mint proteins seem to traffic APP into cellular compartments where it contacts β-secretase, while they relocate C99 into γ-secretase-free cellular sites[579,580].

Removing the PDZ-binding EWV motif in MT5-MMP IC maintains both C99 and Aβ levels. This demonstrates the importance of EWV for MT5-MMP-induced metabolization of C99. It additionally confirms that removing EWV facilitates Aβ production from C99, probably by limiting C99 trafficking with Mint proteins. In HEK cells expressing TM/IC(ala)EWV, there is an increase in C99 and Aβ levels of 20% and 15%, respectively, compared to TM/IC control. Although non-significant, this suggests a trend worth to explore in future experiments, which would confirm our observations upon treatment with γ-secretase and proteasome inhibitors. HEK cells expressing TM/IC recovered C99 levels upon treatment with LACT or D6—which means that both the proteasome and γ-secretase metabolize C99. In the case of HEK cells expressing TM/IC(ala)EWV only D6 treatment significantly increased C99 levels, confirming the hypothesis that the substitution of the PDZ-binding domain in MT5-MMP IC protects C99 from degradation while promotes its γ-cleavage. Furthermore, the number of PLA+ spots of TM/IC(ala)EWV and C99, comparable to those of TM/IC, indicate that the loss of the PDZ-binding motif is ineffective in altering TM/IC(ala)EWV-C99 colocalization, suggesting that TM/IC(ala)EWV changes C99 metabolization by altering its trafficking. In fact, TM/IC(ala)EWV stands isolated in the PCA analysis of C99 subcellular distribution, which confirms that the PDZ-binding motif is a key element of MT5-MMP-mediated subcellular localization of C99. In this vein, depletion of mint 3 in neuroblastoma cells alters APP trafficking, favoring its translocation into the endolysosomal compartments and increasing Aβ40 production[580]. In HEK cells expressing TM/IC(ala)EWV, the major decrease of C99 in the Golgi further strengthens

the hypothesis that our mutations in MT5-MMP affect its interactions with Mint proteins. Altogether, these data suggest that MT5-MMP regulates C99 trafficking under the influence of Mint proteins, and that eliminating the PDZ-binding domain exacerbates MT5-MMP pro-amyloidogenic properties.

Mint 3 regulates MT5-MMP recycling after internalization, translocating MT5-MMP from the TGN back into the plasma membrane in a PDZ-binding-dependent fashion. Inactivation of the PDZ-binding domains in mint 3 or disruption of the MT5-MMP PDZ-binding motif decreased MT5-MMP levels at the cell surface in live cells[467]. Therefore, substitution of the MT5-MMP EWV C-terminal motif with ala may change the subcellular distribution of TM/IC while preserving its structure, favoring the maintenance of C99–TM/IC interactions while altering the trafficking of both peptides. Solving intracellular trafficking defects may improve the accumulation of toxic APP metabolites. This is the case in other CNS diseases in which a decrease in the accumulation of toxic proteins in certain organelles mitigates pathological hallmarks. For instance, patients with mutations in the glucocerebrosidase gene are at increased risk of developing Parkinson's disease, and treatment with Ambroxol—a molecular chaperone that stabilizes mutant glucocerebrosidase and facilitates its translocation into lysosomes—is gaining interest as a promising drug for treating patients with Parkinson's disease[581,582]. Ambroxol induces the exit of mutant glucocerebrosidase from the ER and facilitates its transport into lysosomes, increasing their enzymatic activity[583,584]. Similarly, our MT5-MMP variants facilitate C99 localization in subcellular compartments where different enzymes can metabolize it. This represents a novel approach to addressing the amyloid burden in AD by directly targeting Aβ generation before fibrillation and accumulation in the extracellular space without affecting canonical APP secretases. In the future, combining different mutations of MT5-MMP IC, or even MT5-MMP TM, into a single therapeutic agent could enhance their effects to finely tune C99 degradation. Precise regulation of C99 could help maintain homeostatic levels of APP metabolites and prevent their pathological accumulation.

Modulation of C99 represents an opportunity to counteract amyloid pathology in AD by minimizing negative side effects. To date, C99 functions remain unclear, and evidence appoints C99 as a peptide with a relatively short half-life under homeostatic conditions[394,585]. Thus, C99 accumulation is an important abnormality, and increasing its degradation rate could represent a safer strategy than blocking its production or that of

other APP metabolites. Indeed, soluble APP fragments and Aβ are important for several homeostatic functions, and altering their production leads to unwanted side effects[327,332,342]. Certain mutations in the MT5-MMP domains revealed the potential to regulate C99 levels independently of Aβ, which could be interesting for restoring normal C99 rapid processing without affecting the homeostatic levels of Aβ. This strategy would avoid: 1) interfering with APP processing upstream of C99, 2) affecting γ-secretase activity, or 3) disturbing the homeostatic functions of Aβ. Current methods for targeting AD amyloid burden involve triggering immune reactivity to induce Aβ plaque clearing. However, neuroinflammation and immune activation are also pathological hallmarks of AD. Thus, targeting C99 could prevent Aβ accumulation without affecting normal APP metabolization, or reducing the generation of homeostatic levels of Aβ, and without inducing immune reactivity. Nevertheless, there is a lack of knowledge that hinders the design of molecular tools to counteract C99 accumulation. The MT5-MMP variants presented here represent a promising first step toward exploring their therapeutic potential to regulate C99. However, a better understanding of C99 trafficking and its metabolic partners could provide a clearer framework for developing MT5-MMP-based approaches to induce C99 metabolization. In HEK cells stably expressing the μ-opioid receptor, proximity labeling—using an engineered peroxidase that couples biotin to proteins at less than 20nm—coupled to mass spectrometry resolved the subcellular distribution and functional partners of the activated receptor at multiple time points[586]. A similar approach would offer an exciting opportunity to decipher C99 subcellular trafficking with spatio-temporal resolution and could provide information on the proximity interactions of C99 with other molecules, paving the way for the construction of more precise tools to directly modulate the fate of C99[587].

Peptides mimicking the structure of variants of the MT5-MMP IC decrease C99 accumulation

Our results demonstrate that MT5-MMP IC contains amino acid residues that are essential for MT5-MMP-mediated modulation of C99 and Aβ. Through changes in C99 trafficking, mutations in MT5-MMP domains regulate C99 accumulation and its enzymatic processing. Modifying the C-terminal PDZ-binding motif strikingly changes C99 subcellular distribution but maintains high Aβ levels, whereas mutating the KNKTG amino acids at the interface between the MT5-MMP TM and IC domains promotes C99

degradation, blocking Aβ production. Thus, introducing mutations in the structure of the MT5-MMP IC holds great potential to develop strategies to modulate C99 and Aβ.

Synthetic peptides mirrored in natural amino acid structures are a common strategy to profit from biological properties of certain protein domains. Since the discovery of insulin and the development of a synthetic alternative, peptide-based therapeutics have been a valuable therapeutic strategy[588]. One of the limitations of peptides as therapeutic molecules is tissue penetration, but recent advances in their functionalization by internalization vectors facilitate their intracellular delivery[589]. Our peptide based on TM/IC(ala)KNKTG aimed at reproducing the decrease in C99 and Aβ using only the MT5-MMP IC sequence with the KNKTG substituted with ala (named p17). The significant decrease in C99 levels in HEK cells overexpressing C99 treated with p17 demonstrates its efficacy to clear C99 already at low concentrations (from 10nM to 1000nM). This effect was specific to TM/IC(ala)KNKTG, since p20, a peptide based on TM/IC(ala)PVQ, was unable to reproduce the decrease in C99, despite the effectiveness of this sequence when overexpressed through plasmid transfection. In addition, p17 vectorization with a VHH that binds to the TfR (C5p17) increased p17 efficiency, since it strikingly reduced C99 by ~70% in HEK cells treated with 10nM of C5p17. The recovery of C99 levels at higher concentrations (100nM and 1000nM) could result from a C5p17-induced saturation of TfR, as previously reported in other contexts. For instance, treating HepG2 cells with ferric ammonium citrate, which activates TfR, saturates TfR and activates a signaling cascade that involves a decrease of TfR at the cell surface and its lysososomal degradation[590]. Therefore, higher concentrations of C5p17 may lead to a saturation of TfR activation and trigger its endocytosis and trafficking towards degradation compartments, decreasing the possibilities of internalization of the conjugated peptide and inducing the degradation of the few internalized C5p17.

Different cellular systems display distinct receptor-mediated endocytosis patterns. This is particularly significant when comparing mitotic cells with post-mitotic and terminally differentiated cells. Accordingly, expression of TfR tends to be higher in dividing cells independently from cell endocytosis dynamics[591]. In the CNS, mice display the highest peak of TfR expression between P10 and P19, reinforcing the evidence for changes in TfR expression and internalization along development[592]. We have demonstrated that our conjugated peptide regulates C99 in HEK cells, but confirming our results in differentiated cells would validate our peptide as a solid translational candidate. The

development of hiPSC technologies is shifting the workflows in drug discovery and validation. Nowadays, hiPSC-derived neurons offer a platform to validate drugs targeting CNS cell types in a human context, which is particularly important for AD. In fact, certain AD-related hallmarks, as endolysosomal defects, tau hyperphosphorylation related to APP metabolism, or synaptic defects are more prominent in hiPSC-derived models[385,386,593,594]. This could be particularly important to reveal the role of C99 in AD in humans. For instance, only BACE-1 inhibition rescued AD features in hiPSC-derived neurons with fAD and sAD mutations, and C99 directly caused endosomal abnormalities in hiPSC-derived neurons carrying APP or PSEN1 mutations[385,386]. Importantly, these models also validate the therapeutic potential of drug candidates to rescue AD phenotypes. In hiPSC-derived neurons models of fAD and sAD, the anti-inflammatory compound apigenin increased cell viability, reduced inflammatory cues, and decreased spontaneous calcium waves[595]. Similarly, inducing autophagy with bexarotene restored mitochondrial deficiencies—a well-known pathogenic trait in AD—in hiPSC-derived neurons carrying PSEN1 mutations[596]. Moreover, anti-Aβ antibodies reversed abnormal secretion of Aβ peptides and tau hyperphosphorylation in human neurons carrying the APP London mutation, showing the potential of anti-Aβ therapies in humans long before the FDA approval of anti-Aβ monoclonal antibodies[593]. In these terms, we are currently testing the C5p17 on hiPSC-derived neurons overexpressing C99 (work in progress). Delving deeper into TfR localization, endocytosis dynamics, and C5p17 internalization will uncover the suitability of targeting the TfR with C5 for intracellular delivery. Future results on Aβ, C99, and electrophysiological phenotype of these cells will further clarify the therapeutic potential of C5p17 in human neurons.

Our results confirm the potential of MT5-MMP-based strategies to modulate amyloidosis in AD *in vitro* models. But certain limitations in our experimental setup demand delving deeper on the dynamics of MT5-MMP variants and how they affect APP toxic metabolites. Here, I propose a series of perspectives that can help clarifying the future directions to continue exploring the therapeutical value of our MT5-MMP variants.

Perspective 1.

Characterization of intracellular delivery of C5p17 and its validation in human neurons.

We validated the effects of C5p17 in HEK cells overexpressing C99. However, the particular profile of C99 accumulation in HEK cells treated with varying concentrations of C5p17 suggests that there are potential areas for optimization of peptide efficiency or conjugation/delivery strategies. Furthermore, western blotting is a limited technique for obtaining quantitative readouts, and the intracellular delivery and dynamics of the peptide are unclear. To overcome these limitations, I propose flow cytometry combined with HCS microscopy to determine the cell penetrance of our peptide in HEK cells and its effects on C99 levels. We have already begun to set up an experimental design to measure intracellular C5p17 levels at different time points using flow cytometry. Moreover, we will clarify the relationship between C5p17 and C99, correlating intracellular availability of C5p17 and intracellular C99 levels. In addition, we will resolve the spatiotemporal distribution of C5p17 and C99 using HCS microscopy to provide a direct measure of the internalization dynamics of C5p17, its intracellular trafficking, and potential interactions with C99.

From a translational perspective, we must validate our findings in a more representative model of human biology that accounts for the varying receptor dynamics and APP metabolite processing in target cell types. Confirming the efficacy of intracellular delivery of the VHH-C5 vector cargo to human neurons will determine the optimization steps of C5p17. Moreover, evaluating Aβ levels, C99 accumulation, and the electrophysiological profile in a human in vitro neuronal model of AD is crucial for determining the efficacy of C5p17 as a potential therapeutic agent for AD. Thus, we incubated hiPSC-derived neurons with C5p17 previously infected with an AAV encoding C99 to induce its overexpression. Currently, Aβ40 levels in the supernatants of these neurons are being measured and correlated with intracellular C99 levels measured by PLA using a combination of N- and C-terminal antibodies of C99. Assessing the electrophysiogical

properties of hiPSC-derived neurons following C99/Aβ modulation with C5p17 will clarify the physiological implications of the peptide. We are currently assessing network synchronicity using MEA, and patch-clamp experiments will provide further insight into the efficacy and safety of C5p17 in human neurons.

Perspective 2.

***In vivo* validation of C5p17 delivery into the CNS and therapeutical efficacy.**

Our primary constraint is the absence of *in vivo* experimental results. Assessing the *in vivo* delivery system, safety, and therapeutic efficacy of C5p17 for clinical application is essential for continuing the development of C5p17. Although TfR transcytosis is an effective method for transporting therapeutic agents into the CNS the specificity of C5p17 biodistribution is unknown[589]. Having access to a 5xFAD mouse model of AD within the team enables us to assess the preclinical potential of C5p17. Measuring C5p17 concentrations in the neurons of intraventricularly injected mice will shed light on C5p17 ability to disseminate throughout the CNS. Assessing intraneuronal C5p17 levels will be essential after intraperitoneal injection. If C5p17 is detected in CNS cells under these conditions, it will confirm C5p17 capacity to reach its cellular targets *in vivo*.

Optimizing the delivery method will determine the therapeutic potential of C5p17 based on the assessment of the molecular, physiological, and cognitive markers of AD pathology. Clinical trials on Aβ monoclonal antibodies demonstrate the importance of timing in the treatment of AD. Treating 5xFAD mice with multiple C5p17 injections at early, intermediate and advanced stages of the pathology (*e.g.* 4, 6, and 12 months), would provide further evidence of its effectiveness against AD progression. First, Aβ plaque burden, C99 levels, synaptic integrity, and functionality will be essential indicators of C5p17 capabilities. The correlation of C5p17 readouts with the resolution of various AD pathogenic traits, including tau pathology, neuroinflammation, vascular dysfunction, glucose uptake, and neurodegeneration, will determine the potential scope of the treatment. Finally, assessing the cognitive abilities of treated mice will finally confirm the therapeutic value of the peptide. To evaluate whether modifications to C5p17 (*e.g.* inclusion of non-natural amino acids, introduce modifications in the delivery vector) made during *in vivo* testing have no bearing on its intracellular delivery capacity and therapeutic potential in human neurons, the final form of C5p17 should be re-evaluated in hiPSC-derived neurons.

Perspective 3.

Evaluation of the effects of MT5-MMP variants in human neurons and *in vivo*.

Distinct MT5-MMP variants exert divergent effects on C99 and Aβ levels in human cell models of AD. In this work, I focused on the MT5-MMP IC domain to rapidly translate our previous discoveries into potential therapeutic applications, leveraging on MT5-MMP IC molecular properties. However, we also demonstrated the significance of MT5-MMP TM in C99 subcellular distribution and processing, and the potential role of MT5-MMP EXT catalytic activity in preventing Aβ production. We now have a pool of MT5-MMP variants that regulate C99 and Aβ differently, translocating C99 into distinct subcellular compartments, and engaging C99 into various processing pathways.

Experimental validation of the anti-amyloidogenic potential of MT5-MMP variants in hiPSC-derived neurons will deepen our knowledge of the mechanisms of C99 degradation and will elucidate new amino acid groups, small amino acid sequences, and subdomains of therapeutic interest. The newly described groups could then develop into therapeutic agents, as we did with the substitution of KNKTG in MT5-MMP IC. Alternatively, combining these modified sequences with p17 could synergize their ability to induce C99 degradation. Generating AAVs containing these constructs opens the possibility of overexpressing them without introducing genomic changes in hiPSC-derived neurons. We are currently employing AAV vectors to evaluate the effects of EXT and TM1/IC5 on amyloidogenesis in C99-overexpressing primary cultures and in the brains of 5xFAD mice. The parallel evaluation of human *in vitro* and rodent *in vivo* AD models will provide a complete framework for the application of MT5-MMP-based strategies to halt AD pathogenesis and improve translational potential.

Perspective 4.

Understanding C99 trafficking and molecular partners.

Constructs with divergent effects on C99 and Aβ, such as TM5/IC1, offer an opportunity to specifically study the pathological consequences of C99 accumulation. Accumulating evidence suggests that C99 plays a particular role in AD pathogenesis independent of Aβ, contributing to amyloidogenesis, neurotoxicity, synaptic impairment, and endolysosomal dysfunction. To date, the manipulation of C99 has relied on knockout, chemical inhibition, or overactivation of certain proteins and pathways. Our newly described constructs accumulate C99 without altering any processing pathway outside

the C99-induced phenotype, while maintaining low or high Aβ levels. These MT5-MMP constructs are valuable for elucidating the role of C99 in AD.

Another limitation in my work is only considering endolysosomal vesicles, the ER, and the cis-Golgi as subcellular spaces where C99 localizes. In fact, other subcellular compartments, like mitochondria, TGN, or the plasma membrane, have been reported as major sites of APP/C99 processing. Recent advances in super-resolution microscopy have enabled the multiplexing of >30 proteins with a resolution of 15 nm[597]. The combination of certain MT5-MMP variants and advanced super-resolution techniques could help elucidate the specifics of C99 subcellular localization during intracellular accumulation or degradation/processing into Aβ. Proximity-labeling coupled with proteomics, as mentioned in the discussion, could spatiotemporally resolve C99 localization, further confirming C99 trafficking and defining its molecular partners. A validatory loop between proteomics and multiplexing super-resolution microscopy will help elucidate C99 dynamics in neurons. Overall, MT5-MMP variants are valuable experimental tools for clarifying the particular role of the tandem C99/Aβ in AD pathogenesis.

REFERENCES

1. Alzheimer: Die arteriosklerotische atrophie des gehirns - Google Scholar. Accessed July 9, 2024. https://scholar.google.com/scholar_lookup?hl=en&volume=51&publication_year=1895&pages=809-811&journal=Allg+Z+Psychiat&author=Alzheimer+A&title=Die+arteriosklertische+atrophie+des+gehirns

2. Selkoe DJ, Hardy J. The amyloid hypothesis of Alzheimer's disease at 25 years. *EMBO Mol Med*. 2016;8(6):595-608. doi:10.15252/emmm.201606210

3. Arnsten AFT, Datta D, Del Tredici K, Braak H. Hypothesis: Tau pathology is an initiating factor in sporadic Alzheimer's disease. *Alzheimers Dement*. 2021;17(1):115-124. doi:10.1002/alz.12192

4. Kepp KP, Robakis NK, Høilund-Carlsen PF, Sensi SL, Vissel B. The amyloid cascade hypothesis: an updated critical review. *Brain*. 2023;146(10):3969-3990. doi:10.1093/brain/awad159

5. McKhann G, Drachman D, Folstein M, Katzman R, Price D, Stadlan EM. Clinical diagnosis of Alzheimer's disease: report of the NINCDS-ADRDA Work Group under the auspices of Department of Health and Human Services Task Force on Alzheimer's Disease. *Neurology*. 1984;34(7):939-944. doi:10.1212/wnl.34.7.939

6. Porsteinsson AP, Isaacson RS, Knox S, Sabbagh MN, Rubino I. Diagnosis of Early Alzheimer's Disease: Clinical Practice in 2021. *J Prev Alzheimers Dis*. 2021;8(3):371-386. doi:10.14283/jpad.2021.23

7. van Dyck CH, Swanson CJ, Aisen P, et al. Lecanemab in Early Alzheimer's Disease. *N Engl J Med*. 2023;388(1):9-21. doi:10.1056/NEJMoa2212948

8. Budd Haeberlein S, Aisen PS, Barkhof F, et al. Two Randomized Phase 3 Studies of Aducanumab in Early Alzheimer's Disease. *J Prev Alzheimers Dis*. 2022;9(2):197-210. doi:10.14283/jpad.2022.30

9. Sims JR, Zimmer JA, Evans CD, et al. Donanemab in Early Symptomatic Alzheimer Disease: The TRAILBLAZER-ALZ 2 Randomized Clinical Trial. *JAMA*. 2023;330(6):512-527. doi:10.1001/jama.2023.13239

10. Braak H, Braak E. Frequency of stages of Alzheimer-related lesions in different age categories. *Neurobiol Aging*. 1997;18(4):351-357. doi:10.1016/s0197-4580(97)00056-0

11. International AD. World Alzheimer Report 2023: Reducing Dementia Risk: Never too early, never too late. Published online September 21, 2023. Accessed July 9, 2024. https://www.alzint.org/resource/world-alzheimer-report-2023/

12. Reisberg B, Ferris SH, de Leon MJ, Crook T. The Global Deterioration Scale for assessment of primary degenerative dementia. *Am J Psychiatry*. 1982;139(9):1136-1139. doi:10.1176/ajp.139.9.1136

13. Self WK, Holtzman DM. Emerging diagnostics and therapeutics for Alzheimer disease. *Nat Med*. 2023;29(9):2187-2199. doi:10.1038/s41591-023-02505-2

14. Wu YT, Beiser AS, Breteler MMB, et al. The changing prevalence and incidence of dementia over time - current evidence. *Nat Rev Neurol*. 2017;13(6):327-339. doi:10.1038/nrneurol.2017.63

15. Goate A, Chartier-Harlin MC, Mullan M, et al. Segregation of a missense mutation in the amyloid precursor protein gene with familial Alzheimer's disease. *Nature*. 1991;349(6311):704-706. doi:10.1038/349704a0

16. Reitz C, Pericak-Vance MA, Foroud T, Mayeux R. A global view of the genetic basis of Alzheimer disease. *Nat Rev Neurol*. 2023;19(5):261-277. doi:10.1038/s41582-023-00789-z

17. Tcw J, Goate AM. Genetics of β-Amyloid Precursor Protein in Alzheimer's Disease. *Cold Spring Harb Perspect Med*. 2017;7(6):a024539. doi:10.1101/cshperspect.a024539

18. Knopman DS, Amieva H, Petersen RC, et al. Alzheimer disease. *Nat Rev Dis Primers*. 2021;7(1):33. doi:10.1038/s41572-021-00269-y

19. Serrano-Pozo A, Das S, Hyman BT. APOE and Alzheimer's disease: advances in genetics, pathophysiology, and therapeutic approaches. *Lancet Neurol*. 2021;20(1):68-80. doi:10.1016/S1474-4422(20)30412-9

20. Mishra S, Knupp A, Kinoshita C, et al. Pharmacologic enhancement of retromer rescues endosomal pathology induced by defects in the Alzheimer's gene SORL1. *Stem Cell Reports*. 2023;18(12):2434-2450. doi:10.1016/j.stemcr.2023.10.011

21. Yoo Y, Neumayer G, Shibuya Y, Mader MMD, Wernig M. A cell therapy approach to restore microglial Trem2 function in a mouse model of Alzheimer's disease. *Cell Stem Cell*. 2023;30(8):1043-1053.e6. doi:10.1016/j.stem.2023.07.006

22. West RL, Lee JM, Maroun LE. Hypomethylation of the amyloid precursor protein gene in the brain of an Alzheimer's disease patient. *J Mol Neurosci*. 1995;6(2):141-146. doi:10.1007/BF02736773

23. De Jager P, Srivastava G, Lunnon K, et al. Alzheimery's disease pathology is associated with early alterations in brain DNA methylation at ANK1, BIN1, RHBDF2 and other loci. *Nat Neurosci*. 2014;17(9):1156-1163. doi:10.1038/nn.3786

24. Bakulski KM, Dolinoy DC, Sartor MA, et al. Genome-wide DNA methylation differences between late-onset Alzheimer's disease and cognitively normal controls in human frontal cortex. *J Alzheimers Dis*. 2012;29(3):571-588. doi:10.3233/JAD-2012-111223

25. Lunnon K, Smith R, Hannon E, et al. Cross-tissue methylomic profiling strongly implicates a role for cortex-specific deregulation of ANK1 in Alzheimer's disease neuropathology. *Nat Neurosci*. 2014;17(9):1164-1170. doi:10.1038/nn.3782

26. Morabito S, Miyoshi E, Michael N, Swarup V. Integrative genomics approach identifies conserved transcriptomic networks in Alzheimer's disease. *Human Molecular Genetics*. 2020;29(17):2899-2919. doi:10.1093/hmg/ddaa182

27. Canchi S, Raao B, Masliah D, et al. Integrating Gene and Protein Expression Reveals Perturbed Functional Networks in Alzheimer's Disease. *Cell Reports*. 2019;28(4):1103-1116.e4. doi:10.1016/j.celrep.2019.06.073

28. Cummings J, Zhou Y, Lee G, Zhong K, Fonseca J, Cheng F. Alzheimer's disease drug development pipeline: 2024. *Alzheimers Dement (N Y)*. 2024;10(2):e12465. doi:10.1002/trc2.12465

29. Hardy JA, Higgins GA. Alzheimer's disease: the amyloid cascade hypothesis. *Science*. 1992;256(5054):184-185. doi:10.1126/science.1566067

30. Mandelkow EM, Stamer K, Vogel R, Thies E, Mandelkow E. Clogging of axons by tau, inhibition of axonal traffic and starvation of synapses. *Neurobiol Aging*. 2003;24(8):1079-1085. doi:10.1016/j.neurobiolaging.2003.04.007

31. Pulina MV, Hopkins M, Haroutunian V, Greengard P, Bustos V. C99 selectively accumulates in vulnerable neurons in Alzheimer's disease. *Alzheimers Dement*. 2020;16(2):273-282. doi:10.1016/j.jalz.2019.09.002

32. Thal DR, Walter J, Saido TC, Fändrich M. Neuropathology and biochemistry of Aβ and its aggregates in Alzheimer's disease. *Acta Neuropathol*. 2015;129(2):167-182. doi:10.1007/s00401-014-1375-y

33. DeKosky ST, Scheff SW. Synapse loss in frontal cortex biopsies in Alzheimer's disease: Correlation with cognitive severity. *Annals of Neurology*. 1990;27(5):457-464. doi:10.1002/ana.410270502

34. Francis PT. The interplay of neurotransmitters in Alzheimer's disease. *CNS Spectr*. 2005;10(11 Suppl 18):6-9. doi:10.1017/s1092852900014164

35. Lauterborn JC, Scaduto P, Cox CD, et al. Increased excitatory to inhibitory synaptic ratio in parietal cortex samples from individuals with Alzheimer's disease. *Nat Commun*. 2021;12(1):2603. doi:10.1038/s41467-021-22742-8

36. van den Berg M, Adhikari MH, Verschuuren M, et al. Altered basal forebrain function during whole-brain network activity at pre- and early-plaque stages of Alzheimer's disease in TgF344-AD rats. *Alzheimers Res Ther*. 2022;14(1):148. doi:10.1186/s13195-022-01089-2

37. Salazar AM, Leisgang AM, Ortiz AA, Murtishaw AS, Kinney JW. Alterations of GABA B receptors in the APP/PS1 mouse model of Alzheimer's disease. *Neurobiol Aging*. 2021;97:129-143. doi:10.1016/j.neurobiolaging.2020.10.013

38. Verret L, Mann EO, Hang GB, et al. Inhibitory Interneuron Deficit Links Altered Network Activity and Cognitive Dysfunction in Alzheimer Model. *Cell*. 2012;149(3):708-721. doi:10.1016/j.cell.2012.02.046

39. Martorell AJ, Paulson AL, Suk HJ, et al. Multi-sensory Gamma Stimulation Ameliorates Alzheimer's-Associated Pathology and Improves Cognition. *Cell*. 2019;177(2):256-271.e22. doi:10.1016/j.cell.2019.02.014

40. Iaccarino HF, Singer AC, Martorell AJ, et al. Gamma frequency entrainment attenuates amyloid load and modifies microglia. *Nature*. 2016;540(7632):230-235. doi:10.1038/nature20587

41. Hong S, Beja-Glasser VF, Nfonoyim BM, et al. Complement and microglia mediate early synapse loss in Alzheimer mouse models. *Science*. 2016;352(6286):712-716. doi:10.1126/science.aad8373

42. De Schepper S, Ge JZ, Crowley G, et al. Perivascular cells induce microglial phagocytic states and synaptic engulfment via SPP1 in mouse models of Alzheimer's disease. *Nat Neurosci*. 2023;26(3):406-415. doi:10.1038/s41593-023-01257-z

43. Liddelow SA, Guttenplan KA, Clarke LE, et al. Neurotoxic reactive astrocytes are induced by activated microglia. *Nature*. 2017;541(7638):481-487. doi:10.1038/nature21029

44. Singh D. Astrocytic and microglial cells as the modulators of neuroinflammation in Alzheimer's disease. *J Neuroinflammation*. 2022;19(1):206. doi:10.1186/s12974-022-02565-0

45. Corder EH, Saunders AM, Strittmatter WJ, et al. Gene dose of apolipoprotein E type 4 allele and the risk of Alzheimer's disease in late onset families. *Science*. 1993;261(5123):921-923. doi:10.1126/science.8346443

46. Lin YT, Seo J, Gao F, et al. APOE4 Causes Widespread Molecular and Cellular Alterations Associated with Alzheimer's Disease Phenotypes in Human iPSC-Derived Brain Cell Types. *Neuron*. 2018;98(6):1141-1154.e7. doi:10.1016/j.neuron.2018.05.008

47. Gratuze M, Schlachetzki JCM, D'Oliveira Albanus R, et al. TREM2-independent microgliosis promotes tau-mediated neurodegeneration in the presence of ApoE4. *Neuron*. 2023;111(2):202-219.e7. doi:10.1016/j.neuron.2022.10.022

48. Wang S, Sudan R, Peng V, et al. TREM2 drives microglia response to amyloid-β via SYK-dependent and -independent pathways. *Cell*. 2022;185(22):4153-4169.e19. doi:10.1016/j.cell.2022.09.033

49. Zenaro E, Piacentino G, Constantin G. The blood-brain barrier in Alzheimer's disease. *Neurobiol Dis*. 2017;107:41-56. doi:10.1016/j.nbd.2016.07.007

50. Woodward NC, Levine MC, Haghani A, et al. Toll-like receptor 4 in glial inflammatory responses to air pollution in vitro and in vivo. *Journal of Neuroinflammation*. 2017;14(1):84. doi:10.1186/s12974-017-0858-x

51. Chen H, Kwong JC, Copes R, et al. Living near major roads and the incidence of dementia, Parkinson's disease, and multiple sclerosis: a population-based cohort study. *The Lancet*. 2017;389(10070):718-726. doi:10.1016/S0140-6736(16)32399-6

52. Mork D, Braun D, Zanobetti A. Time-lagged relationships between a decade of air pollution exposure and first hospitalization with Alzheimer's disease and related dementias. *Environ Int*. 2023;171:107694. doi:10.1016/j.envint.2022.107694

53. Calderón-Garcidueñas L, González-Maciel A, Reynoso-Robles R, et al. Alzheimer's disease and alpha-synuclein pathology in the olfactory bulbs of infants, children, teens and adults ≤ 40 years in Metropolitan Mexico City. APOE4 carriers at higher risk of suicide accelerate their olfactory bulb pathology. *Environ Res*. 2018;166:348-362. doi:10.1016/j.envres.2018.06.027

54. Bush AI, Tanzi RE. Therapeutics for Alzheimer's disease based on the metal hypothesis. *Neurotherapeutics*. 2008;5(3):421-432. doi:10.1016/j.nurt.2008.05.001

55. Lovell MA, Robertson JD, Teesdale WJ, Campbell JL, Markesbery WR. Copper, iron and zinc in Alzheimer's disease senile plaques. *J Neurol Sci*. 1998;158(1):47-52. doi:10.1016/s0022-510x(98)00092-6

56. Bush AI, Pettingell WH, Multhaup G, et al. Rapid induction of Alzheimer A beta amyloid formation by zinc. *Science*. 1994;265(5177):1464-1467. doi:10.1126/science.8073293

57. Moreno-Gonzalez I, Estrada LD, Sanchez-Mejias E, Soto C. Smoking exacerbates amyloid pathology in a mouse model of Alzheimer's disease. *Nat Commun*. 2013;4:1495. doi:10.1038/ncomms2494

58. Hill E, Clifton P, Goodwill AM, Dennerstein L, Campbell S, Szoeke C. Dietary patterns and β-amyloid deposition in aging Australian women. *Alzheimers Dement (N Y)*. 2018;4:535-541. doi:10.1016/j.trci.2018.09.007

59. Baragi VM, Gattu R, Trifan G, et al. Neuroimaging Markers for Determining Former American Football Players at Risk for Alzheimer's Disease. *Neurotrauma Rep*. 2022;3(1):398-414. doi:10.1089/neur.2022.0020

60. Small GW, Kepe V, Siddarth P, et al. PET scanning of brain tau in retired national football league players: preliminary findings. *Am J Geriatr Psychiatry*. 2013;21(2):138-144. doi:10.1016/j.jagp.2012.11.019

61. López-Ortiz S, Valenzuela PL, Seisdedos MM, et al. Exercise interventions in Alzheimer's disease: A systematic review and meta-analysis of randomized controlled trials. *Ageing Res Rev*. 2021;72:101479. doi:10.1016/j.arr.2021.101479

62. Li K, Luo X, Zeng Q, et al. Interactions between sleep disturbances and Alzheimer's disease on brain function: a preliminary study combining the static and dynamic functional MRI. *Sci Rep*. 2019;9:19064. doi:10.1038/s41598-019-55452-9

63. Charisis S, Lin H, Ray R, et al. Obesity impacts the expression of Alzheimer's disease-related genes: The Framingham Heart Study. *Alzheimers Dement*. 2023;19(8):3496-3505. doi:10.1002/alz.12954

64. Larsson SC, Traylor M, Malik R, et al. Modifiable pathways in Alzheimer's disease: Mendelian randomisation analysis. *BMJ*. 2017;359:j5375. doi:10.1136/bmj.j5375

65. Lennon MJ, Makkar SR, Crawford JD, Sachdev PS. Midlife Hypertension and Alzheimer's Disease: A Systematic Review and Meta-Analysis. *J Alzheimers Dis*. 2019;71(1):307-316. doi:10.3233/JAD-190474

66. Zetterberg H, Bendlin BB. Biomarkers for Alzheimer's disease-preparing for a new era of disease-modifying therapies. *Mol Psychiatry*. 2021;26(1):296-308. doi:10.1038/s41380-020-0721-9

67. Mann DMA, Jones D. Deposition of amyloid (A4) protein within the brains of persons with dementing disorders other than Alzheimer's disease and Down's syndrome. *Neuroscience Letters*. 1990;109(1):68-75. doi:10.1016/0304-3940(90)90539-L

68. Roher AE, Lowenson JD, Clarke S, et al. Structural alterations in the peptide backbone of beta-amyloid core protein may account for its deposition and stability in Alzheimer's disease. *J Biol Chem*. 1993;268(5):3072-3083.

69. Sánchez L, Madurga S, Pukala T, et al. Aβ40 and Aβ42 amyloid fibrils exhibit distinct molecular recycling properties. *J Am Chem Soc*. 2011;133(17):6505-6508. doi:10.1021/ja1117123

70. Lehmann S, Dumurgier J, Ayrignac X, et al. Cerebrospinal fluid A beta 1–40 peptides increase in Alzheimer's disease and are highly correlated with phospho-tau in control individuals. *Alzheimer's Research & Therapy*. 2020;12(1):123. doi:10.1186/s13195-020-00696-1

71. Baiardi S, Abu-Rumeileh S, Rossi M, et al. Antemortem CSF Aβ42/Aβ40 ratio predicts Alzheimer's disease pathology better than Aβ42 in rapidly progressive dementias. *Ann Clin Transl Neurol*. 2019;6(2):263-273. doi:10.1002/acn3.697

72. Baldeiras I, Santana I, Leitão MJ, et al. Addition of the Aβ42/40 ratio to the cerebrospinal fluid biomarker profile increases the predictive value for underlying Alzheimer's disease dementia in mild cognitive impairment. *Alzheimer's Research & Therapy*. 2018;10(1):33. doi:10.1186/s13195-018-0362-2

73. Pérez-Grijalba V, Romero J, Pesini P, et al. Plasma Aβ42/40 Ratio Detects Early Stages of Alzheimer's Disease and Correlates with CSF and Neuroimaging Biomarkers in the AB255 Study. *J Prev Alzheimers Dis*. 2019;6(1):34-41. doi:10.14283/jpad.2018.41

74. Janelidze S, Zetterberg H, Mattsson N, et al. CSF Aβ42/Aβ40 and Aβ42/Aβ38 ratios: better diagnostic markers of Alzheimer disease. *Ann Clin Transl Neurol*. 2016;3(3):154-165. doi:10.1002/acn3.274

75. Nunan J, Small DH. Regulation of APP cleavage by alpha-, beta- and gamma-secretases. *FEBS Lett*. 2000;483(1):6-10. doi:10.1016/s0014-5793(00)02076-7

76. Lanoiselée HM, Nicolas G, Wallon D, et al. APP, PSEN1, and PSEN2 mutations in early-onset Alzheimer disease: A genetic screening study of familial and sporadic cases. *PLoS Med*. 2017;14(3):e1002270. doi:10.1371/journal.pmed.1002270

77. Jonsson T, Atwal JK, Steinberg S, et al. A mutation in APP protects against Alzheimer's disease and age-related cognitive decline. *Nature*. 2012;488(7409):96-99. doi:10.1038/nature11283

78. Jonsson T, Stefansson H, Steinberg S, et al. Variant of TREM2 associated with the risk of Alzheimer's disease. *N Engl J Med*. 2013;368(2):107-116. doi:10.1056/NEJMoa1211103

79. Aizenstein HJ, Nebes RD, Saxton JA, et al. Frequent amyloid deposition without significant cognitive impairment among the elderly. *Arch Neurol*. 2008;65(11):1509-1517. doi:10.1001/archneur.65.11.1509

80. Swanson CJ, Zhang Y, Dhadda S, et al. A randomized, double-blind, phase 2b proof-of-concept clinical trial in early Alzheimer's disease with lecanemab, an anti-Aβ protofibril antibody. *Alzheimers Res Ther*. 2021;13(1):80. doi:10.1186/s13195-021-00813-8

81. Timmers T, Ossenkoppele R, Verfaillie SCJ, et al. Amyloid PET and cognitive decline in cognitively normal individuals: the SCIENCe project. *Neurobiol Aging*. 2019;79:50-58. doi:10.1016/j.neurobiolaging.2019.02.020

82. Pelkmans W, Legdeur N, Ten Kate M, et al. Amyloid-β, cortical thickness, and subsequent cognitive decline in cognitively normal oldest-old. *Ann Clin Transl Neurol*. 2021;8(2):348-358. doi:10.1002/acn3.51273

83. Grundke-Iqbal I, Iqbal K, Tung YC, Quinlan M, Wisniewski HM, Binder LI. Abnormal phosphorylation of the microtubule-associated protein tau (tau) in Alzheimer cytoskeletal pathology. *Proceedings of the National Academy of Sciences*. 1986;83(13):4913-4917. doi:10.1073/pnas.83.13.4913

84. Goedert M, Spillantini MG, Jakes R, Rutherford D, Crowther RA. Multiple isoforms of human microtubule-associated protein tau: sequences and localization in neurofibrillary tangles of Alzheimer's disease. *Neuron*. 1989;3(4):519-526. doi:10.1016/0896-6273(89)90210-9

85. Weingarten MD, Lockwood AH, Hwo SY, Kirschner MW. A protein factor essential for microtubule assembly. *Proceedings of the National Academy of Sciences*. 1975;72(5):1858-1862. doi:10.1073/pnas.72.5.1858

86. Dixit R, Ross JL, Goldman YE, Holzbaur ELF. Differential Regulation of Dynein and Kinesin Motor Proteins by Tau. *Science*. 2008;319(5866):1086-1089. doi:10.1126/science.1152993

87. Kempf M, Clement A, Faissner A, Lee G, Brandt R. Tau Binds to the Distal Axon Early in Development of Polarity in a Microtubule- and Microfilament-Dependent Manner. *J Neurosci*. 1996;16(18):5583-5592. doi:10.1523/JNEUROSCI.16-18-05583.1996

88. Cleveland DW, Hwo SY, Kirschner MW. Physical and chemical properties of purified tau factor and the role of tau in microtubule assembly. *Journal of Molecular Biology*. 1977;116(2):227-247. doi:10.1016/0022-2836(77)90214-5

89. Köpke E, Tung YC, Shaikh S, Alonso AC, Iqbal K, Grundke-Iqbal I. Microtubule-associated protein tau. Abnormal phosphorylation of a non-paired helical filament pool in Alzheimer disease. *Journal of Biological Chemistry*. 1993;268(32):24374-24384. doi:10.1016/S0021-9258(20)80536-5

90. Lee VM, Goedert M, Trojanowski JQ. Neurodegenerative tauopathies. *Annu Rev Neurosci*. 2001;24:1121-1159. doi:10.1146/annurev.neuro.24.1.1121

91. Xia D, Gutmann JM, Götz J. Mobility and subcellular localization of endogenous, gene-edited Tau differs from that of over-expressed human wild-type and P301L mutant Tau. *Sci Rep*. 2016;6(1):29074. doi:10.1038/srep29074

92. Kanaan NM, Morfini G, Pigino G, et al. Phosphorylation in the amino terminus of tau prevents inhibition of anterograde axonal transport. *Neurobiol Aging*. 2012;33(4):826.e15-826.e30. doi:10.1016/j.neurobiolaging.2011.06.006

93. Balabanian L, Lessard DV, Swaminathan K, et al. Tau differentially regulates the transport of early endosomes and lysosomes. *Mol Biol Cell*. 2022;33(13):ar128. doi:10.1091/mbc.E22-01-0018

94. Swanson E, Breckenridge L, McMahon L, Som S, McConnell I, Bloom GS. Extracellular Tau Oligomers Induce Invasion of Endogenous Tau into the Somatodendritic Compartment and Axonal Transport Dysfunction. *J Alzheimers Dis*. 2017;58(3):803-820. doi:10.3233/JAD-170168

95. Zhou L, McInnes J, Wierda K, et al. Tau association with synaptic vesicles causes presynaptic dysfunction. *Nat Commun*. 2017;8(1):15295. doi:10.1038/ncomms15295

96. Sydow A, Van der Jeugd A, Zheng F, et al. Tau-Induced Defects in Synaptic Plasticity, Learning, and Memory Are Reversible in Transgenic Mice after Switching Off the Toxic Tau Mutant. *J Neurosci*. 2011;31(7):2511-2525. doi:10.1523/JNEUROSCI.5245-10.2011

97. Brier MR, Gordon B, Friedrichsen K, et al. Tau and Aβ imaging, CSF measures, and cognition in Alzheimer's disease. *Sci Transl Med*. 2016;8(338):338ra66. doi:10.1126/scitranslmed.aaf2362

98. Braak H, Zetterberg H, Del Tredici K, Blennow K. Intraneuronal tau aggregation precedes diffuse plaque deposition, but amyloid-β changes occur before increases of tau in cerebrospinal fluid. *Acta Neuropathol*. 2013;126(5):631-641. doi:10.1007/s00401-013-1139-0

99. Giannakopoulos P, Herrmann FR, Bussière T, et al. Tangle and neuron numbers, but not amyloid load, predict cognitive status in Alzheimer's disease. *Neurology*. 2003;60(9):1495-1500. doi:10.1212/01.wnl.0000063311.58879.01

100. Braak H, Thal DR, Ghebremedhin E, Del Tredici K. Stages of the pathologic process in Alzheimer disease: age categories from 1 to 100 years. *J Neuropathol Exp Neurol*. 2011;70(11):960-969. doi:10.1097/NEN.0b013e318232a379

101. Barthélemy NR, Mallipeddi N, Moiseyev P, Sato C, Bateman RJ. Tau Phosphorylation Rates Measured by Mass Spectrometry Differ in the Intracellular Brain vs. Extracellular Cerebrospinal Fluid Compartments and Are Differentially Affected by Alzheimer's Disease. *Front Aging Neurosci*. 2019;11. doi:10.3389/fnagi.2019.00121

102. Thijssen EH, La Joie R, Strom A, et al. Plasma phosphorylated tau 217 and phosphorylated tau 181 as biomarkers in Alzheimer's disease and frontotemporal

lobar degeneration: a retrospective diagnostic performance study. *Lancet Neurol*. 2021;20(9):739-752. doi:10.1016/S1474-4422(21)00214-3

103. Mielke MM, Aakre JA, Algeciras-Schimnich A, et al. Comparison of CSF phosphorylated tau 181 and 217 for cognitive decline. *Alzheimers Dement*. 2022;18(4):602-611. doi:10.1002/alz.12415

104. Ashton NJ, Brum WS, Di Molfetta G, et al. Diagnostic Accuracy of a Plasma Phosphorylated Tau 217 Immunoassay for Alzheimer Disease Pathology. *JAMA Neurol*. 2024;81(3):255-263. doi:10.1001/jamaneurol.2023.5319

105. Weigand AJ, Bangen KJ, Thomas KR, et al. Is tau in the absence of amyloid on the Alzheimer's continuum?: A study of discordant PET positivity. *Brain Commun*. 2019;2(1):fcz046. doi:10.1093/braincomms/fcz046

106. Arboleda-Velasquez JF, Lopera F, O'Hare M, et al. Resistance to autosomal dominant Alzheimer's disease in an APOE3 Christchurch homozygote: a case report. *Nat Med*. 2019;25(11):1680-1683. doi:10.1038/s41591-019-0611-3

107. Oakley H, Cole SL, Logan S, et al. Intraneuronal beta-Amyloid Aggregates, Neurodegeneration, and Neuron Loss in Transgenic Mice with Five Familial Alzheimer's Disease Mutations: Potential Factors in Amyloid Plaque Formation. *Journal of Neuroscience*. 2006;26(40):10129-10140. doi:10.1523/JNEUROSCI.1202-06.2006

108. Forner S, Kawauchi S, Balderrama-Gutierrez G, et al. Systematic phenotyping and characterization of the 5xFAD mouse model of Alzheimer's disease. *Sci Data*. 2021;8(1):270. doi:10.1038/s41597-021-01054-y

109. Götz J, Chen F, van Dorpe J, Nitsch RM. Formation of neurofibrillary tangles in P301l tau transgenic mice induced by Abeta 42 fibrils. *Science*. 2001;293(5534):1491-1495. doi:10.1126/science.1062097

110. Mah D, Zhao J, Liu X, et al. The Sulfation Code of Tauopathies: Heparan Sulfate Proteoglycans in the Prion Like Spread of Tau Pathology. *Front Mol Biosci*. 2021;8. doi:10.3389/fmolb.2021.671458

111. Braak H, Alafuzoff I, Arzberger T, Kretzschmar H, Del Tredici K. Staging of Alzheimer disease-associated neurofibrillary pathology using paraffin sections and immunocytochemistry. *Acta Neuropathol*. 2006;112(4):389-404. doi:10.1007/s00401-006-0127-z

112. Bussière T, Giannakopoulos P, Bouras C, Perl DP, Morrison JH, Hof PR. Progressive degeneration of nonphosphorylated neurofilament protein-enriched pyramidal neurons predicts cognitive impairment in Alzheimer's disease: Stereologic analysis of prefrontal cortex area 9. *Journal of Comparative Neurology*. 2003;463(3):281-302. doi:10.1002/cne.10760

113. Paspalas CD, Carlyle BC, Leslie S, et al. The aged rhesus macaque manifests Braak stage III/IV Alzheimer's-like pathology. *Alzheimer's & Dementia*. 2018;14(5):680-691. doi:10.1016/j.jalz.2017.11.005

114. Braak H, Del Tredici K. Spreading of Tau Pathology in Sporadic Alzheimer's Disease Along Cortico-cortical Top-Down Connections. *Cerebral Cortex*. 2018;28(9):3372-3384. doi:10.1093/cercor/bhy152

115. Jicha GA, Weaver C, Lane E, et al. cAMP-Dependent Protein Kinase Phosphorylations on Tau in Alzheimer's Disease. *J Neurosci*. 1999;19(17):7486-7494. doi:10.1523/JNEUROSCI.19-17-07486.1999

116. Arnsten AFT, Datta D, Leslie S, Yang ST, Wang M, Nairn AC. Alzheimer's-like pathology in aging rhesus macaques: Unique opportunity to study the etiology and treatment of Alzheimer's disease. *Proceedings of the National Academy of Sciences*. 2019;116(52):26230-26238. doi:10.1073/pnas.1903671116

117. Kondo H, Tanaka K, Hashikawa T, Jones EG. Neurochemical gradients along monkey sensory cortical pathways: calbindin-immunoreactive pyramidal neurons in layers II and III. *European Journal of Neuroscience*. 1999;11(12):4197-4203. doi:10.1046/j.1460-9568.1999.00844.x

118. Kaufman SK, Del Tredici K, Thomas TL, Braak H, Diamond MI. Tau seeding activity begins in the transentorhinal/entorhinal regions and anticipates phospho-tau pathology in Alzheimer's disease and PART. *Acta Neuropathol*. 2018;136(1):57-67. doi:10.1007/s00401-018-1855-6

119. Lacampagne A, Liu X, Reiken S, et al. Post-translational remodeling of ryanodine receptor induces calcium leak leading to Alzheimer's disease-likepathologies and cognitive deficits. *Acta Neuropathol*. 2017;134(5):749-767. doi:10.1007/s00401-017-1733-7

120. Sepulveda-Falla D, Barrera-Ocampo A, Hagel C, et al. Familial Alzheimer's disease–associated presenilin-1 alters cerebellar activity and calcium homeostasis. *J Clin Invest*. 2014;124(4):1552-1567. doi:10.1172/JCI66407

121. Stutzmann GE, Smith I, Caccamo A, Oddo S, Laferla FM, Parker I. Enhanced ryanodine receptor recruitment contributes to Ca2+ disruptions in young, adult, and aged Alzheimer's disease mice. *J Neurosci*. 2006;26(19):5180-5189. doi:10.1523/JNEUROSCI.0739-06.2006

122. Cheung KH, Shineman D, Müller M, et al. Mechanism of Ca2+ disruption in Alzheimer's disease by presenilin regulation of InsP3 receptor channel gating. *Neuron*. 2008;58(6):871-883. doi:10.1016/j.neuron.2008.04.015

123. Park J, Wetzel I, Marriott I, et al. A 3D Human Tri-Culture System Modeling Neurodegeneration and Neuroinflammation in Alzheimer's Disease. *Nat Neurosci*. 2018;21(7):941-951. doi:10.1038/s41593-018-0175-4

124. Ghatak S, Dolatabadi N, Trudler D, et al. Mechanisms of hyperexcitability in Alzheimer's disease hiPSC-derived neurons and cerebral organoids vs isogenic controls. West AE, Zoghbi HY, Ellerby LM, eds. *eLife*. 2019;8:e50333. doi:10.7554/eLife.50333

125. Lerdkrai C, Asavapanumas N, Brawek B, et al. Intracellular Ca2+ stores control in vivo neuronal hyperactivity in a mouse model of Alzheimer's disease. *Proceedings of*

the National Academy of Sciences. 2018;115(6):E1279-E1288. doi:10.1073/pnas.1714409115

126. Martinsson I, Quintino L, Garcia MG, et al. Aβ/Amyloid Precursor Protein-Induced Hyperexcitability and Dysregulation of Homeostatic Synaptic Plasticity in Neuron Models of Alzheimer's Disease. *Front Aging Neurosci*. 2022;14:946297. doi:10.3389/fnagi.2022.946297

127. Zott B, Simon MM, Hong W, et al. A vicious cycle of β amyloid-dependent neuronal hyperactivation. *Science*. 2019;365(6453):559-565. doi:10.1126/science.aay0198

128. Cao LL, Guan PP, Liang YY, Huang XS, Wang P. Calcium Ions Stimulate the Hyperphosphorylation of Tau by Activating Microsomal Prostaglandin E Synthase 1. *Front Aging Neurosci*. 2019;11:108. doi:10.3389/fnagi.2019.00108

129. Wu JW, Hussaini SA, Bastille IM, et al. Neuronal activity enhances tau propagation and tau pathology in vivo. *Nat Neurosci*. 2016;19(8):1085-1092. doi:10.1038/nn.4328

130. Schultz MK, Gentzel R, Usenovic M, et al. Pharmacogenetic neuronal stimulation increases human tau pathology and trans-synaptic spread of tau to distal brain regions in mice. *Neurobiol Dis*. 2018;118:161-176. doi:10.1016/j.nbd.2018.07.003

131. Grbovic OM, Mathews PM, Jiang Y, et al. Rab5-stimulated up-regulation of the endocytic pathway increases intracellular beta-cleaved amyloid precursor protein carboxyl-terminal fragment levels and Abeta production. *J Biol Chem*. 2003;278(33):31261-31268. doi:10.1074/jbc.M304122200

132. Carey RM, Balcz BA, Lopez-Coviella I, Slack BE. Inhibition of dynamin-dependent endocytosis increases shedding of the amyloid precursor protein ectodomain and reduces generation of amyloid beta protein. *BMC Cell Biol*. 2005;6:30. doi:10.1186/1471-2121-6-30

133. Nuriel T, Peng KY, Ashok A, et al. The Endosomal–Lysosomal Pathway Is Dysregulated by APOE4 Expression in Vivo. *Front Neurosci*. 2017;11:702. doi:10.3389/fnins.2017.00702

134. Busche MA, Hyman BT. Synergy between amyloid-β and tau in Alzheimer's disease. *Nat Neurosci*. 2020;23(10):1183-1193. doi:10.1038/s41593-020-0687-6

135. Lasagna-Reeves CA, Castillo-Carranza DL, Guerrero-Muoz MJ, Jackson GR, Kayed R. Preparation and characterization of neurotoxic tau oligomers. *Biochemistry*. 2010;49(47):10039-10041. doi:10.1021/bi1016233

136. Gomes LA, Hipp SA, Rijal Upadhaya A, et al. Aβ-induced acceleration of Alzheimer-related τ-pathology spreading and its association with prion protein. *Acta Neuropathol*. 2019;138(6):913-941. doi:10.1007/s00401-019-02053-5

137. Griner SL, Seidler P, Bowler J, et al. Structure-based inhibitors of amyloid beta core suggest a common interface with tau. *Elife*. 2019;8:e46924. doi:10.7554/eLife.46924

138. DeVos SL, Corjuc BT, Commins C, et al. Tau reduction in the presence of amyloid-β prevents tau pathology and neuronal death in vivo. *Brain*. 2018;141(7):2194-2212. doi:10.1093/brain/awy117

139. Takahashi RH, Capetillo-Zarate E, Lin MT, Milner TA, Gouras GK. Co-occurrence of Alzheimer's disease ß-amyloid and τ pathologies at synapses. *Neurobiol Aging*. 2010;31(7):1145-1152. doi:10.1016/j.neurobiolaging.2008.07.021

140. Manczak M, Reddy PH. Abnormal interaction of oligomeric amyloid-β with phosphorylated tau: implications to synaptic dysfunction and neuronal damage. *J Alzheimers Dis*. 2013;36(2):285-295. doi:10.3233/JAD-130275

141. Ittner LM, Ke YD, Delerue F, et al. Dendritic function of tau mediates amyloid-beta toxicity in Alzheimer's disease mouse models. *Cell*. 2010;142(3):387-397. doi:10.1016/j.cell.2010.06.036

142. Pickett EK, Herrmann AG, McQueen J, et al. Amyloid Beta and Tau Cooperate to Cause Reversible Behavioral and Transcriptional Deficits in a Model of Alzheimer's Disease. *Cell Rep*. 2019;29(11):3592-3604.e5. doi:10.1016/j.celrep.2019.11.044

143. Willén K, Sroka A, Takahashi RH, Gouras GK. Heterogeneous Association of Alzheimer's Disease-Linked Amyloid-β and Amyloid-β Protein Precursor with Synapses. *J Alzheimers Dis*. 60(2):511-524. doi:10.3233/JAD-170262

144. Hermann D, Both M, Ebert U, et al. Synaptic transmission is impaired prior to plaque formation in amyloid precursor protein-overexpressing mice without altering behaviorally-correlated sharp wave-ripple complexes. *Neuroscience*. 2009;162(4):1081-1090. doi:10.1016/j.neuroscience.2009.05.044

145. Ohnishi T, Yanazawa M, Sasahara T, et al. Na, K-ATPase α3 is a death target of Alzheimer patient amyloid-β assembly. *Proceedings of the National Academy of Sciences*. 2015;112(32):E4465-E4474. doi:10.1073/pnas.1421182112

146. Arbel-Ornath M, Hudry E, Boivin JR, et al. Soluble oligomeric amyloid-β induces calcium dyshomeostasis that precedes synapse loss in the living mouse brain. *Molecular Neurodegeneration*. 2017;12(1):27. doi:10.1186/s13024-017-0169-9

147. Busche MA, Chen X, Henning HA, et al. Critical role of soluble amyloid-β for early hippocampal hyperactivity in a mouse model of Alzheimer's disease. *Proceedings of the National Academy of Sciences*. 2012;109(22):8740-8745. doi:10.1073/pnas.1206171109

148. Biasetti L, Rey S, Fowler M, et al. Elevated amyloid beta disrupts the nanoscale organization and function of synaptic vesicle pools in hippocampal neurons. *Cereb Cortex*. 2023;33(4):1263-1276. doi:10.1093/cercor/bhac134

149. Shankar GM, Bloodgood BL, Townsend M, Walsh DM, Selkoe DJ, Sabatini BL. Natural Oligomers of the Alzheimer Amyloid-β Protein Induce Reversible Synapse Loss by Modulating an NMDA-Type Glutamate Receptor-Dependent Signaling Pathway. *J Neurosci*. 2007;27(11):2866-2875. doi:10.1523/JNEUROSCI.4970-06.2007

150. Taylor HBC, Emptage NJ, Jeans AF. Long-term depression links amyloid-β to the pathological hyperphosphorylation of tau. *Cell Rep*. 2021;36(9):109638. doi:10.1016/j.celrep.2021.109638

151. Müller MK, Jacobi E, Sakimura K, Malinow R, von Engelhardt J. NMDA receptors mediate synaptic depression, but not spine loss in the dentate gyrus of adult amyloid Beta (Aβ) overexpressing mice. *Acta Neuropathol Commun*. 2018;6(1):110. doi:10.1186/s40478-018-0611-4

152. Kimura T, Whitcomb DJ, Jo J, et al. Microtubule-associated protein tau is essential for long-term depression in the hippocampus. *Philos Trans R Soc Lond B Biol Sci*. 2014;369(1633):20130144. doi:10.1098/rstb.2013.0144

153. Hu S, Begum AN, Jones MR, et al. GSK3 inhibitors show benefits in an Alzheimer's disease (AD) model of neurodegeneration but adverse effects in control animals. *Neurobiol Dis*. 2009;33(2):193-206. doi:10.1016/j.nbd.2008.10.007

154. Peineau S, Taghibiglou C, Bradley C, et al. LTP inhibits LTD in the hippocampus via regulation of GSK3beta. *Neuron*. 2007;53(5):703-717. doi:10.1016/j.neuron.2007.01.029

155. Kandimalla R, Manczak M, Yin X, Wang R, Reddy PH. Hippocampal phosphorylated tau induced cognitive decline, dendritic spine loss and mitochondrial abnormalities in a mouse model of Alzheimer's disease. *Hum Mol Genet*. 2018;27(1):30-40. doi:10.1093/hmg/ddx381

156. Ginsberg SD, Alldred MJ, Counts SE, et al. Microarray analysis of hippocampal CA1 neurons implicates early endosomal dysfunction during Alzheimer's disease progression. *Biol Psychiatry*. 2010;68(10):885-893. doi:10.1016/j.biopsych.2010.05.030

157. Jiang Y, Mullaney KA, Peterhoff CM, et al. Alzheimer's-related endosome dysfunction in Down syndrome is Aβ-independent but requires APP and is reversed by BACE-1 inhibition. *Proc Natl Acad Sci U S A*. 2010;107(4):1630-1635. doi:10.1073/pnas.0908953107

158. Hsieh H, Boehm J, Sato C, et al. AMPAR removal underlies Abeta-induced synaptic depression and dendritic spine loss. *Neuron*. 2006;52(5):831-843. doi:10.1016/j.neuron.2006.10.035

159. Du Y, Fu M, Huang Z, et al. TRPV1 activation alleviates cognitive and synaptic plasticity impairments through inhibiting AMPAR endocytosis in APP23/PS45 mouse model of Alzheimer's disease. *Aging Cell*. 2020;19(3):e13113. doi:10.1111/acel.13113

160. Zhang Y, Guo O, Huo Y, Wang G, Man HY. Amyloid-β Induces AMPA Receptor Ubiquitination and Degradation in Primary Neurons and Human Brains of Alzheimer's Disease. *J Alzheimers Dis*. 2018;62(4):1789-1801. doi:10.3233/JAD-170879

161. Ueda S, Kuzuya A, Kawata M, et al. Acute inhibition of AMPA receptors by perampanel reduces amyloid β-protein levels by suppressing β-cleavage of APP in Alzheimer's disease models. *FASEB J*. 2023;37(11):e23252. doi:10.1096/fj.202300837R

162. Colom-Cadena M, Toombs J, Simzer E, et al. Transmembrane protein 97 is a potential synaptic amyloid beta receptor in human Alzheimer's disease. *Acta Neuropathol*. 2024;147(1):32. doi:10.1007/s00401-023-02679-6

163. Palop JJ, Chin J, Roberson ED, et al. Aberrant excitatory neuronal activity and compensatory remodeling of inhibitory hippocampal circuits in mouse models of Alzheimer's disease. *Neuron*. 2007;55(5):697-711. doi:10.1016/j.neuron.2007.07.025

164. Mathys H, Peng Z, Boix CA, et al. Single-cell atlas reveals correlates of high cognitive function, dementia, and resilience to Alzheimer's disease pathology. *Cell*. 2023;186(20):4365-4385.e27. doi:10.1016/j.cell.2023.08.039

165. Deng Y, Bi M, Delerue F, et al. Loss of LAMP5 interneurons drives neuronal network dysfunction in Alzheimer's disease. *Acta Neuropathol*. 2022;144(4):637-650. doi:10.1007/s00401-022-02457-w

166. Murdock MH, Yang CY, Sun N, et al. Multisensory gamma stimulation promotes glymphatic clearance of amyloid. *Nature*. 2024;627(8002):149-156. doi:10.1038/s41586-024-07132-6

167. Arnaud L, Benech P, Greetham L, et al. APOE4 drives inflammation in human astrocytes via TAGLN3 repression and NF-κB activation. *Cell Rep*. 2022;40(7):111200. doi:10.1016/j.celrep.2022.111200

168. Liu W, Taso O, Wang R, et al. Trem2 promotes anti-inflammatory responses in microglia and is suppressed under pro-inflammatory conditions. *Hum Mol Genet*. 2020;29(19):3224-3248. doi:10.1093/hmg/ddaa209

169. Wightman DP, Jansen IE, Savage JE, et al. A genome-wide association study with 1,126,563 individuals identifies new risk loci for Alzheimer's disease. *Nat Genet*. 2021;53(9):1276-1282. doi:10.1038/s41588-021-00921-z

170. Masuda T, Amann L, Monaco G, et al. Specification of CNS macrophage subsets occurs postnatally in defined niches. *Nature*. 2022;604(7907):740-748. doi:10.1038/s41586-022-04596-2

171. Parkhurst CN, Yang G, Ninan I, et al. Microglia promote learning-dependent synapse formation through brain-derived neurotrophic factor. *Cell*. 2013;155(7):1596-1609. doi:10.1016/j.cell.2013.11.030

172. Haruwaka K, Ying Y, Liang Y, et al. Microglia enhance post-anesthesia neuronal activity by shielding inhibitory synapses. *Nat Neurosci*. 2024;27(3):449-461. doi:10.1038/s41593-023-01537-8

173. Wang C, Yue H, Hu Z, et al. Microglia mediate forgetting via complement-dependent synaptic elimination. *Science*. 2020;367(6478):688-694. doi:10.1126/science.aaz2288

174. Krasemann S, Madore C, Cialic R, et al. The TREM2-APOE Pathway Drives the Transcriptional Phenotype of Dysfunctional Microglia in Neurodegenerative Diseases. *Immunity*. 2017;47(3):566-581.e9. doi:10.1016/j.immuni.2017.08.008

175. Huang Y, Happonen KE, Burrola PG, et al. Microglia use TAM receptors to detect and engulf amyloid β plaques. *Nat Immunol*. 2021;22(5):586-594. doi:10.1038/s41590-021-00913-5

176. Boza-Serrano A, Ruiz R, Sanchez-Varo R, et al. Galectin-3, a novel endogenous TREM2 ligand, detrimentally regulates inflammatory response in Alzheimer's disease. *Acta Neuropathol*. 2019;138(2):251-273. doi:10.1007/s00401-019-02013-z

177. Reed-Geaghan EG, Savage JC, Hise AG, Landreth GE. CD14 and Toll-Like Receptors 2 and 4 Are Required for Fibrillar Aβ-Stimulated Microglial Activation. *J Neurosci*. 2009;29(38):11982-11992. doi:10.1523/JNEUROSCI.3158-09.2009

178. Ding X, Wang J, Huang M, et al. Loss of microglial SIRPα promotes synaptic pruning in preclinical models of neurodegeneration. *Nat Commun*. 2021;12(1):2030. doi:10.1038/s41467-021-22301-1

179. Yoshiyama Y, Higuchi M, Zhang B, et al. Synapse loss and microglial activation precede tangles in a P301S tauopathy mouse model. *Neuron*. 2007;53(3):337-351. doi:10.1016/j.neuron.2007.01.010

180. Gerrits E, Brouwer N, Kooistra SM, et al. Distinct amyloid-β and tau-associated microglia profiles in Alzheimer's disease. *Acta Neuropathol*. 2021;141(5):681-696. doi:10.1007/s00401-021-02263-w

181. Wang C, Xiong M, Gratuze M, et al. Selective removal of astrocytic APOE4 strongly protects against tau-mediated neurodegeneration and decreases synaptic phagocytosis by microglia. *Neuron*. 2021;109(10):1657-1674.e7. doi:10.1016/j.neuron.2021.03.024

182. Fitz NF, Nam KN, Wolfe CM, et al. Phospholipids of APOE lipoproteins activate microglia in an isoform-specific manner in preclinical models of Alzheimer's disease. *Nat Commun*. 2021;12(1):3416. doi:10.1038/s41467-021-23762-0

183. Koutsodendris N, Blumenfeld J, Agrawal A, et al. Neuronal APOE4 removal protects against tau-mediated gliosis, neurodegeneration and myelin deficits. *Nat Aging*. 2023;3(3):275-296. doi:10.1038/s43587-023-00368-3

184. Xiong M, Jiang H, Serrano JR, et al. APOE immunotherapy reduces cerebral amyloid angiopathy and amyloid plaques while improving cerebrovascular function. *Sci Transl Med*. 2021;13(581):eabd7522. doi:10.1126/scitranslmed.abd7522

185. Mahan TE, Wang C, Bao X, Choudhury A, Ulrich JD, Holtzman DM. Selective reduction of astrocyte apoE3 and apoE4 strongly reduces Aβ accumulation and plaque-related pathology in a mouse model of amyloidosis. *Mol Neurodegener*. 2022;17(1):13. doi:10.1186/s13024-022-00516-0

186. Saroja SR, Gorbachev K, Julia T, Goate AM, Pereira AC. Astrocyte-secreted glypican-4 drives APOE4-dependent tau hyperphosphorylation. *Proc Natl Acad Sci U S A*. 2022;119(34):e2108870119. doi:10.1073/pnas.2108870119

187. Eisenbaum M, Pearson A, Ortiz C, et al. ApoE4 expression disrupts tau uptake, trafficking, and clearance in astrocytes. *Glia*. 2024;72(1):184-205. doi:10.1002/glia.24469

188. Asai H, Ikezu S, Tsunoda S, et al. Depletion of microglia and inhibition of exosome synthesis halt tau propagation. *Nat Neurosci*. 2015;18(11):1584-1593. doi:10.1038/nn.4132

189. d'Errico P, Ziegler-Waldkirch S, Aires V, et al. Microglia contribute to the propagation of Aβ into unaffected brain tissue. *Nat Neurosci*. 2022;25(1):20-25. doi:10.1038/s41593-021-00951-0

190. Drago F, Lombardi M, Prada I, et al. ATP Modifies the Proteome of Extracellular Vesicles Released by Microglia and Influences Their Action on Astrocytes. *Front Pharmacol*. 2017;8:910. doi:10.3389/fphar.2017.00910

191. Kraft AW, Hu X, Yoon H, et al. Attenuating astrocyte activation accelerates plaque pathogenesis in APP/PS1 mice. *FASEB J*. 2013;27(1):187-198. doi:10.1096/fj.12-208660

192. Lian H, Litvinchuk A, Chiang ACA, Aithmitti N, Jankowsky JL, Zheng H. Astrocyte-Microglia Cross Talk through Complement Activation Modulates Amyloid Pathology in Mouse Models of Alzheimer's Disease. *J Neurosci*. 2016;36(2):577-589. doi:10.1523/JNEUROSCI.2117-15.2016

193. Fiala M, Liu QN, Sayre J, et al. Cyclooxygenase-2-positive macrophages infiltrate the Alzheimer's disease brain and damage the blood-brain barrier. *Eur J Clin Invest*. 2002;32(5):360-371. doi:10.1046/j.1365-2362.2002.00994.x

194. Haruwaka K, Ikegami A, Tachibana Y, et al. Dual microglia effects on blood brain barrier permeability induced by systemic inflammation. *Nat Commun*. 2019;10(1):5816. doi:10.1038/s41467-019-13812-z

195. Kang J, Lemaire HG, Unterbeck A, et al. The precursor of Alzheimer's disease amyloid A4 protein resembles a cell-surface receptor. *Nature*. 1987;325(6106):733-736. doi:10.1038/325733a0

196. Cousins SL, Dai W, Stephenson FA. APLP1 and APLP2, members of the APP family of proteins, behave similarly to APP in that they associate with NMDA receptors and enhance NMDA receptor surface expression. *J Neurochem*. 2015;133(6):879-885. doi:10.1111/jnc.13063

197. Hick M, Herrmann U, Weyer SW, et al. Acute function of secreted amyloid precursor protein fragment APPsα in synaptic plasticity. *Acta Neuropathol*. 2015;129(1):21-37. doi:10.1007/s00401-014-1368-x

198. Steubler V, Erdinger S, Back MK, et al. Loss of all three APP family members during development impairs synaptic function and plasticity, disrupts learning, and causes an autism-like phenotype. *EMBO J*. 2021;40(12):e107471. doi:10.15252/embj.2020107471

199. von Koch CS, Zheng H, Chen H, et al. Generation of APLP2 KO mice and early postnatal lethality in APLP2/APP double KO mice. *Neurobiol Aging*. 1997;18(6):661-669. doi:10.1016/s0197-4580(97)00151-6

200. Bergmans BA, Shariati SAM, Habets RLP, et al. Neurons generated from APP/APLP1/APLP2 triple knockout embryonic stem cells behave normally in vitro

and in vivo: lack of evidence for a cell autonomous role of the amyloid precursor protein in neuronal differentiation. *Stem Cells*. 2010;28(3):399-406. doi:10.1002/stem.296

201. Tanaka S, Shiojiri S, Takahashi Y, et al. Tissue-specific expression of three types of β-protein precursor mRNA: Enhancement of protease inhibitor-harboring types in Alzheimer's disease brain. *Biochemical and Biophysical Research Communications*. 1989;165(3):1406-1414. doi:10.1016/0006-291X(89)92760-5

202. Gralle M, Ferreira ST. Structure and functions of the human amyloid precursor protein: The whole is more than the sum of its parts. *Progress in Neurobiology*. 2007;82(1):11-32. doi:10.1016/j.pneurobio.2007.02.001

203. Müller UC, Deller T, Korte M. Not just amyloid: physiological functions of the amyloid precursor protein family. *Nat Rev Neurosci*. 2017;18(5):281-298. doi:10.1038/nrn.2017.29

204. Gralle M, Oliveira CLP, Guerreiro LH, et al. Solution Conformation and Heparin-induced Dimerization of the Full-length Extracellular Domain of the Human Amyloid Precursor Protein. *Journal of Molecular Biology*. 2006;357(2):493-508. doi:10.1016/j.jmb.2005.12.053

205. Munter LM, Voigt P, Harmeier A, et al. GxxxG motifs within the amyloid precursor protein transmembrane sequence are critical for the etiology of Aβ42. *EMBO J*. 2007;26(6):1702-1712. doi:10.1038/sj.emboj.7601616

206. Baumkötter F, Schmidt N, Vargas C, et al. Amyloid Precursor Protein Dimerization and Synaptogenic Function Depend on Copper Binding to the Growth Factor-Like Domain. *J Neurosci*. 2014;34(33):11159-11172. doi:10.1523/JNEUROSCI.0180-14.2014

207. Stahl R, Schilling S, Soba P, et al. Shedding of APP limits its synaptogenic activity and cell adhesion properties. *Front Cell Neurosci*. 2014;8:410. doi:10.3389/fncel.2014.00410

208. Morales-Corraliza J, Mazzella MJ, Berger JD, et al. In Vivo Turnover of Tau and APP Metabolites in the Brains of Wild-Type and Tg2576 Mice: Greater Stability of sAPP in the β-Amyloid Depositing Mice. *PLOS ONE*. 2009;4(9):e7134. doi:10.1371/journal.pone.0007134

209. Peters-Libeu C, Campagna J, Mitsumori M, et al. sAβPPα is a Potent Endogenous Inhibitor of BACE1. *J Alzheimers Dis*. 2015;47(3):545-555. doi:10.3233/JAD-150282

210. Milosch N, Tanriöver G, Kundu A, et al. Holo-APP and G-protein-mediated signaling are required for sAPPα-induced activation of the Akt survival pathway. *Cell Death Dis*. 2014;5(8):e1391. doi:10.1038/cddis.2014.352

211. van der Kant R, Goldstein LSB. Cellular functions of the amyloid precursor protein from development to dementia. *Dev Cell*. 2015;32(4):502-515. doi:10.1016/j.devcel.2015.01.022

212. Delport A, Hewer R. The amyloid precursor protein: a converging point in Alzheimer's disease. *Mol Neurobiol*. 2022;59(7):4501-4516. doi:10.1007/s12035-022-02863-x

213. DeBoer SR, Dolios G, Wang R, Sisodia SS. Differential Release of β-Amyloid from Dendrite- Versus Axon-Targeted APP. *J Neurosci*. 2014;34(37):12313-12327. doi:10.1523/JNEUROSCI.2255-14.2014

214. Sisodia SS. Beta-amyloid precursor protein cleavage by a membrane-bound protease. *Proc Natl Acad Sci U S A*. 1992;89(13):6075-6079.

215. Thinakaran G, Koo EH. Amyloid Precursor Protein Trafficking, Processing, and Function. *J Biol Chem*. 2008;283(44):29615-29619. doi:10.1074/jbc.R800019200

216. Toh WH, Tan JZA, Zulkefli KL, Houghton FJ, Gleeson PA. Amyloid precursor protein traffics from the Golgi directly to early endosomes in an Arl5b- and AP4-dependent pathway. *Traffic*. 2017;18(3):159-175. doi:10.1111/tra.12465

217. Das U, Scott DA, Ganguly A, Koo EH, Tang Y, Roy S. Activity-induced convergence of APP and BACE-1 in acidic microdomains via an endocytosis-dependent pathway. *Neuron*. 2013;79(3):447-460. doi:10.1016/j.neuron.2013.05.035

218. Das U, Wang L, Ganguly A, et al. Visualization of APP and BACE-1 approximation in neurons: new insights into the amyloidogenic pathway. *Nat Neurosci*. 2016;19(1):55-64. doi:10.1038/nn.4188

219. Wang J, Gleeson PA, Fourriere L. Spatial–Temporal Mapping Reveals the Golgi as the Major Processing Site for the Pathogenic Swedish APP Mutation: Familial APP Mutant Shifts the Major APP Processing Site. *Traffic*. 2024;25(3):e12932. doi:10.1111/tra.12932

220. Januário YC, Eden J, de Oliveira LS, et al. Clathrin adaptor AP-1–mediated Golgi export of amyloid precursor protein is crucial for the production of neurotoxic amyloid fragments. *Journal of Biological Chemistry*. 2022;298(8):102172. doi:10.1016/j.jbc.2022.102172

221. Thinakaran G, Teplow DB, Siman R, Greenberg B, Sisodia SS. Metabolism of the "Swedish" Amyloid Precursor Protein Variant in Neuro2a (N2a) Cells: EVIDENCE THAT CLEAVAGE AT THE "β-SECRETASE" SITE OCCURS IN THE GOLGI APPARATUS (*). *Journal of Biological Chemistry*. 1996;271(16):9390-9397. doi:10.1074/jbc.271.16.9390

222. Tan JZA, Fourriere L, Wang J, Perez F, Boncompain G, Gleeson PA. Distinct anterograde trafficking pathways of BACE1 and amyloid precursor protein from the TGN and the regulation of amyloid-β production. *Mol Biol Cell*. 2020;31(1):27-44. doi:10.1091/mbc.E19-09-0487

223. Herr UM, Strecker P, Storck SE, et al. LRP1 Modulates APP Intraneuronal Transport and Processing in Its Monomeric and Dimeric State. *Front Mol Neurosci*. 2017;10:118. doi:10.3389/fnmol.2017.00118

224. Brodeur J, Thériault C, Lessard-Beaudoin M, Marcil A, Dahan S, Lavoie C. LDLR-related protein 10 (LRP10) regulates amyloid precursor protein (APP) trafficking and processing: evidence for a role in Alzheimer's disease. *Mol Neurodegener*. 2012;7:31. doi:10.1186/1750-1326-7-31

225. Andersen OM, Reiche J, Schmidt V, et al. Neuronal sorting protein-related receptor sorLA/LR11 regulates processing of the amyloid precursor protein. *Proc Natl Acad Sci U S A*. 2005;102(38):13461-13466. doi:10.1073/pnas.0503689102

226. Hung C, Tuck E, Stubbs V, et al. SORL1 deficiency in human excitatory neurons causes APP-dependent defects in the endolysosome-autophagy network. *Cell Rep*. 2021;35(11):109259. doi:10.1016/j.celrep.2021.109259

227. Mishra S, Knupp A, Szabo MP, et al. The Alzheimer's gene SORL1 is a regulator of endosomal traffic and recycling in human neurons. *Cell Mol Life Sci*. 2022;79(3):162. doi:10.1007/s00018-022-04182-9

228. Cuccaro ML, Carney RM, Zhang Y, et al. SORL1 mutations in early- and late-onset Alzheimer disease. *Neurol Genet*. 2016;2(6):e116. doi:10.1212/NXG.0000000000000116

229. He X, Cooley K, Chung CHY, Dashti N, Tang J. Apolipoprotein Receptor 2 and X11α/β Mediate Apolipoprotein E-Induced Endocytosis of Amyloid-β Precursor Protein and β-Secretase, Leading to Amyloid-β Production. *J Neurosci*. 2007;27(15):4052-4060. doi:10.1523/JNEUROSCI.3993-06.2007

230. Ho A, Liu X, Südhof TC. Deletion of Mint proteins decreases amyloid production in transgenic mouse models of Alzheimer's disease. *J Neurosci*. 2008;28(53):14392-14400. doi:10.1523/JNEUROSCI.2481-08.2008

231. Sullivan SE, Dillon GM, Sullivan JM, Ho A. Mint Proteins Are Required for Synaptic Activity-dependent Amyloid Precursor Protein (APP) Trafficking and Amyloid β Generation *. *Journal of Biological Chemistry*. 2014;289(22):15374-15383. doi:10.1074/jbc.M113.541003

232. King GD, Perez RG, Steinhilb ML, Gaut JR, Turner RS. X11alpha modulates secretory and endocytic trafficking and metabolism of amyloid precursor protein: mutational analysis of the YENPTY sequence. *Neuroscience*. 2003;120(1):143-154. doi:10.1016/s0306-4522(03)00284-7

233. Caster AH, Kahn RA. Recruitment of the Mint3 adaptor is necessary for export of the amyloid precursor protein (APP) from the Golgi complex. *J Biol Chem*. 2013;288(40):28567-28580. doi:10.1074/jbc.M113.481101

234. Shrivastava-Ranjan P, Faundez V, Fang G, et al. Mint3/X11gamma is an ADP-ribosylation factor-dependent adaptor that regulates the traffic of the Alzheimer's Precursor protein from the trans-Golgi network. *Mol Biol Cell*. 2008;19(1):51-64. doi:10.1091/mbc.e07-05-0465

235. Henry SM, Kistler SA, Lagani GD, et al. Tight control of the APP-Mint1 interaction in regulating amyloid production. *Brain Res*. 2023;1817:148496. doi:10.1016/j.brainres.2023.148496

236. Chaufty J, Sullivan SE, Ho A. Intracellular amyloid precursor protein sorting and amyloid-β secretion are regulated by Src-mediated phosphorylation of Mint2. *J Neurosci*. 2012;32(28):9613-9625. doi:10.1523/JNEUROSCI.0602-12.2012

237. Kaden D, Voigt P, Munter LM, Bobowski KD, Schaefer M, Multhaup G. Subcellular localization and dimerization of APLP1 are strikingly different from APP and APLP2. *J Cell Sci*. 2009;122(Pt 3):368-377. doi:10.1242/jcs.034058

238. Vieira SI, Rebelo S, Domingues SC, da Cruz e Silva EF, da Cruz e Silva OAB. S655 phosphorylation enhances APP secretory traffic. *Mol Cell Biochem*. 2009;328(1-2):145-154. doi:10.1007/s11010-009-0084-7

239. Triaca V, Sposato V, Bolasco G, et al. NGF controls APP cleavage by downregulating APP phosphorylation at Thr668: relevance for Alzheimer's disease. *Aging Cell*. 2016;15(4):661-672. doi:10.1111/acel.12473

240. Vieira SI, Rebelo S, Esselmann H, et al. Retrieval of the Alzheimer's amyloid precursor protein from the endosome to the TGN is S655 phosphorylation state-dependent and retromer-mediated. *Mol Neurodegener*. 2010;5:40. doi:10.1186/1750-1326-5-40

241. Xia Y, Wang ZH, Liu P, et al. TrkB receptor cleavage by delta-secretase abolishes its phosphorylation of APP, aggravating Alzheimer's disease pathologies. *Mol Psychiatry*. 2021;26(7):2943-2963. doi:10.1038/s41380-020-00863-8

242. La Rosa LR, Perrone L, Nielsen MS, Calissano P, Andersen OM, Matrone C. Y682G Mutation of Amyloid Precursor Protein Promotes Endo-Lysosomal Dysfunction by Disrupting APP-SorLA Interaction. *Front Cell Neurosci*. 2015;9:109. doi:10.3389/fncel.2015.00109

243. Matrone C, Barbagallo APM, La Rosa LR, et al. APP is phosphorylated by TrkA and regulates NGF/TrkA signaling. *J Neurosci*. 2011;31(33):11756-11761. doi:10.1523/JNEUROSCI.1960-11.2011

244. Menon PK, Koistinen NA, Iverfeldt K, Ström AL. Phosphorylation of the amyloid precursor protein (APP) at Ser-675 promotes APP processing involving meprin β. *The Journal of Biological Chemistry*. 2019;294(47):17768. doi:10.1074/jbc.RA119.008310

245. Walter J, Schindzielorz A, Hartung B, Haass C. Phosphorylation of the beta-amyloid precursor protein at the cell surface by ectocasein kinases 1 and 2. *J Biol Chem*. 2000;275(31):23523-23529. doi:10.1074/jbc.M002850200

246. Tsatsanis A, Dickens S, Kwok JCF, Wong BX, Duce JA. Post Translational Modulation of β-Amyloid Precursor Protein Trafficking to the Cell Surface Alters Neuronal Iron Homeostasis. *Neurochem Res*. 2019;44(6):1367-1374. doi:10.1007/s11064-019-02747-y

247. Yazaki M, Tagawa K, Maruyama K, et al. Mutation of potential N-linked glycosylation sites in the Alzheimer's disease amyloid precursor protein (APP). *Neuroscience Letters*. 1996;221(1):57-60. doi:10.1016/S0304-3940(96)13285-7

248. Tienari PJ, De Strooper B, Ikonen E, et al. The beta-amyloid domain is essential for axonal sorting of amyloid precursor protein. *EMBO J*. 1996;15(19):5218-5229.

249. Schedin-Weiss S, Winblad B, Tjernberg LO. The role of protein glycosylation in Alzheimer disease. *FEBS J*. 2014;281(1):46-62. doi:10.1111/febs.12590

250. McFarlane I, Georgopoulou N, Coughlan CM, Gillian AM, Breen KC. The role of the protein glycosylation state in the control of cellular transport of the amyloid β precursor protein. *Neuroscience*. 1999;90(1):15-25. doi:10.1016/S0306-4522(98)00361-3

251. Chun YS, Kwon OH, Chung S. O-GlcNAcylation of amyloid-β precursor protein at threonine 576 residue regulates trafficking and processing. *Biochem Biophys Res Commun*. 2017;490(2):486-491. doi:10.1016/j.bbrc.2017.06.067

252. Singh Y, Regmi D, Ormaza D, et al. Mucin-Type O-Glycosylation Proximal to β-Secretase Cleavage Site Affects APP Processing and Aggregation Fate. *Front Chem*. 2022;10:859822. doi:10.3389/fchem.2022.859822

253. Tachida Y, Iijima J, Takahashi K, et al. O-GalNAc glycosylation determines intracellular trafficking of APP and Aβ production. *J Biol Chem*. 2023;299(7):104905. doi:10.1016/j.jbc.2023.104905

254. Tomita S, Kirino Y, Suzuki T. Cleavage of Alzheimer's amyloid precursor protein (APP) by secretases occurs after O-glycosylation of APP in the protein secretory pathway. Identification of intracellular compartments in which APP cleavage occurs without using toxic agents that interfere with protein metabolism. *J Biol Chem*. 1998;273(11):6277-6284. doi:10.1074/jbc.273.11.6277

255. Nakamura N, Kurosaka A. Mucin-type glycosylation as a regulatory factor of amyloid precursor protein processing. *J Biochem*. 2019;165(3):205-208. doi:10.1093/jb/mvy121

256. Watanabe T, Hikichi Y, Willuweit A, Shintani Y, Horiguchi T. FBL2 Regulates Amyloid Precursor Protein (APP) Metabolism by Promoting Ubiquitination-Dependent APP Degradation and Inhibition of APP Endocytosis. *J Neurosci*. 2012;32(10):3352-3365. doi:10.1523/JNEUROSCI.5659-11.2012

257. Gireud-Goss M, Reyes S, Tewari R, et al. The ubiquitin ligase UBE4B regulates amyloid precursor protein ubiquitination, endosomal trafficking, and amyloid β42 generation and secretion. *Mol Cell Neurosci*. 2020;108:103542. doi:10.1016/j.mcn.2020.103542

258. Maniv I, Sarji M, Bdarneh A, et al. Altered ubiquitin signaling induces Alzheimer's disease-like hallmarks in a three-dimensional human neural cell culture model. *Nat Commun*. 2023;14:5922. doi:10.1038/s41467-023-41545-7

259. Zheng Q, Song B, Li G, et al. USP25 inhibition ameliorates Alzheimer's pathology through the regulation of APP processing and Aβ generation. *J Clin Invest*. 2022;132(5):e152170. doi:10.1172/JCI152170

260. El Ayadi A, Stieren ES, Barral JM, Boehning D. Ubiquilin-1 regulates amyloid precursor protein maturation and degradation by stimulating K63-linked

polyubiquitination of lysine 688. *Proc Natl Acad Sci U S A*. 2012;109(33):13416-13421. doi:10.1073/pnas.1206786109

261. Santos SF, Tasiaux B, Sindic C, Octave JN. Inhibition of neuronal calcium oscillations by cell surface APP phosphorylated on T668. *Neurobiol Aging*. 2011;32(12):2308-2313. doi:10.1016/j.neurobiolaging.2010.01.006

262. García-González L, Pilat D, Baranger K, Rivera S. Emerging Alternative Proteinases in APP Metabolism and Alzheimer's Disease Pathogenesis: A Focus on MT1-MMP and MT5-MMP. *Front Aging Neurosci*. 2019;11:244. doi:10.3389/fnagi.2019.00244

263. Esch FS, Keim PS, Beattie EC, et al. Cleavage of amyloid beta peptide during constitutive processing of its precursor. *Science*. 1990;248(4959):1122-1124. doi:10.1126/science.2111583

264. Asai M, Hattori C, Szabó B, et al. Putative function of ADAM9, ADAM10, and ADAM17 as APP alpha-secretase. *Biochem Biophys Res Commun*. 2003;301(1):231-235. doi:10.1016/s0006-291x(02)02999-6

265. Hartmann D, de Strooper B, Serneels L, et al. The disintegrin/metalloprotease ADAM 10 is essential for Notch signalling but not for alpha-secretase activity in fibroblasts. *Hum Mol Genet*. 2002;11(21):2615-2624. doi:10.1093/hmg/11.21.2615

266. Kuhn PH, Wang H, Dislich B, et al. ADAM10 is the physiologically relevant, constitutive alpha-secretase of the amyloid precursor protein in primary neurons. *EMBO J*. 2010;29(17):3020-3032. doi:10.1038/emboj.2010.167

267. Skovronsky DM, Moore DB, Milla ME, Doms RW, Lee VM. Protein kinase C-dependent alpha-secretase competes with beta-secretase for cleavage of amyloid-beta precursor protein in the trans-golgi network. *J Biol Chem*. 2000;275(4):2568-2575. doi:10.1074/jbc.275.4.2568

268. Ibarreta D, Duchén M, Ma D, Qiao L, Kozikowski AP, Etcheberrigaray R. Benzolactam (BL) enhances sAPP secretion in fibroblasts and in PC12 cells. *Neuroreport*. 1999;10(5):1035-1040. doi:10.1097/00001756-199904060-00026

269. Nitsch RM, Kim C, Growdon JH. Vasopressin and bradykinin regulate secretory processing of the amyloid protein precursor of Alzheimer's disease. *Neurochem Res*. 1998;23(5):807-814. doi:10.1023/a:1022423813362

270. Nitsch RM, Deng M, Growdon JH, Wurtman RJ. Serotonin 5-HT2a and 5-HT2c receptors stimulate amyloid precursor protein ectodomain secretion. *J Biol Chem*. 1996;271(8):4188-4194. doi:10.1074/jbc.271.8.4188

271. Buxbaum JD, Ruefli AA, Parker CA, Cypess AM, Greengard P. Calcium regulates processing of the Alzheimer amyloid protein precursor in a protein kinase C-independent manner. *Proc Natl Acad Sci U S A*. 1994;91(10):4489-4493. doi:10.1073/pnas.91.10.4489

272. Chen M, Fernandez HL. Stimulation of beta-amyloid precursor protein alpha-processing by phorbol ester involves calcium and calpain activation. *Biochem Biophys Res Commun*. 2004;316(2):332-340. doi:10.1016/j.bbrc.2004.02.052

273. Hoey SE, Williams RJ, Perkinton MS. Synaptic NMDA Receptor Activation Stimulates α-Secretase Amyloid Precursor Protein Processing and Inhibits Amyloid-β Production. *J Neurosci*. 2009;29(14):4442-4460. doi:10.1523/JNEUROSCI.6017-08.2009

274. Rossner S, Ueberham U, Schliebs R, Perez-Polo JR, Bigl V. p75 and TrkA receptor signaling independently regulate amyloid precursor protein mRNA expression, isoform composition, and protein secretion in PC12 cells. *J Neurochem*. 1998;71(2):757-766. doi:10.1046/j.1471-4159.1998.71020757.x

275. Yogev-Falach M, Amit T, Bar-Am O, Weinstock M, Youdim MBH. Involvement of MAP kinase in the regulation of amyloid precursor protein processing by novel cholinesterase inhibitors derived from rasagiline. *FASEB J*. 2002;16(12):1674-1676. doi:10.1096/fj.02-0198fje

276. Kojro E, Postina R, Buro C, Meiringer C, Gehrig-Burger K, Fahrenholz F. The neuropeptide PACAP promotes the alpha-secretase pathway for processing the Alzheimer amyloid precursor protein. *FASEB J*. 2006;20(3):512-514. doi:10.1096/fj.05-4812fje

277. Kim C, Jang CH, Bang JH, et al. Amyloid precursor protein processing is separately regulated by protein kinase C and tyrosine kinase in human astrocytes. *Neurosci Lett*. 2002;324(3):185-188. doi:10.1016/s0304-3940(02)00217-3

278. Kleinberger G, Yamanishi Y, Suárez-Calvet M, et al. TREM2 mutations implicated in neurodegeneration impair cell surface transport and phagocytosis. *Sci Transl Med*. 2014;6(243):243ra86. doi:10.1126/scitranslmed.3009093

279. Feuerbach D, Schindler P, Barske C, et al. ADAM17 is the main sheddase for the generation of human triggering receptor expressed in myeloid cells (hTREM2) ectodomain and cleaves TREM2 after Histidine 157. *Neurosci Lett*. 2017;660:109-114. doi:10.1016/j.neulet.2017.09.034

280. Letronne F, Laumet G, Ayral AM, et al. ADAM30 Downregulates APP-Linked Defects Through Cathepsin D Activation in Alzheimer's Disease. *EBioMedicine*. 2016;9:278-292. doi:10.1016/j.ebiom.2016.06.002

281. Marcello E, Saraceno C, Musardo S, et al. Endocytosis of synaptic ADAM10 in neuronal plasticity and Alzheimer's disease. *J Clin Invest*. 2013;123(6):2523-2538. doi:10.1172/JCI65401

282. Marcello E, Epis R, Saraceno C, et al. SAP97-mediated local trafficking is altered in Alzheimer disease patients' hippocampus. *Neurobiol Aging*. 2012;33(2):422.e1-10. doi:10.1016/j.neurobiolaging.2010.09.015

283. Zimmermann M, Gardoni F, Marcello E, et al. Acetylcholinesterase inhibitors increase ADAM10 activity by promoting its trafficking in neuroblastoma cell lines. *J Neurochem*. 2004;90(6):1489-1499. doi:10.1111/j.1471-4159.2004.02680.x

284. Postina R, Schroeder A, Dewachter I, et al. A disintegrin-metalloproteinase prevents amyloid plaque formation and hippocampal defects in an Alzheimer disease mouse model. *J Clin Invest*. 2004;113(10):1456-1464. doi:10.1172/JCI200420864

285. Pastore F, Battistoni M, Sollazzo R, et al. A Bioengineering Strategy to Control ADAM10 Activity in Living Cells. *Int J Mol Sci*. 2023;24(2):917. doi:10.3390/ijms24020917

286. Cheng XS, Shi FX, Zhao KP, et al. Nmnat2 attenuates amyloidogenesis and up-regulates ADAM10 in AMPK activity-dependent manner. *Aging (Albany NY)*. 2021;13(20):23620-23636. doi:10.18632/aging.203634

287. Araki W, Kitaguchi N, Tokushima Y, et al. Trophic effect of beta-amyloid precursor protein on cerebral cortical neurons in culture. *Biochem Biophys Res Commun*. 1991;181(1):265-271. doi:10.1016/s0006-291x(05)81412-3

288. Gakhar-Koppole N, Hundeshagen P, Mandl C, et al. Activity requires soluble amyloid precursor protein alpha to promote neurite outgrowth in neural stem cell-derived neurons via activation of the MAPK pathway. *Eur J Neurosci*. 2008;28(5):871-882. doi:10.1111/j.1460-9568.2008.06398.x

289. Young-Pearse TL, Chen AC, Chang R, Marquez C, Selkoe DJ. Secreted APP regulates the function of full-length APP in neurite outgrowth through interaction with integrin beta1. *Neural Develop*. 2008;3:15. doi:10.1186/1749-8104-3-15

290. Obregon D, Hou H, Deng J, et al. Soluble amyloid precursor protein-α modulates β-secretase activity and amyloid-β generation. *Nat Commun*. 2012;3:777. doi:10.1038/ncomms1781

291. Mattson MP, Cheng B, Culwell AR, Esch FS, Lieberburg I, Rydel RE. Evidence for excitoprotective and intraneuronal calcium-regulating roles for secreted forms of the beta-amyloid precursor protein. *Neuron*. 1993;10(2):243-254. doi:10.1016/0896-6273(93)90315-i

292. Goodman Y, Mattson MP. Secreted forms of beta-amyloid precursor protein protect hippocampal neurons against amyloid beta-peptide-induced oxidative injury. *Exp Neurol*. 1994;128(1):1-12. doi:10.1006/exnr.1994.1107

293. Ohline SM, Chan C, Schoderboeck L, et al. Effect of soluble amyloid precursor protein-alpha on adult hippocampal neurogenesis in a mouse model of Alzheimer's disease. *Mol Brain*. 2022;15(1):5. doi:10.1186/s13041-021-00889-1

294. Baratchi S, Evans J, Tate WP, Abraham WC, Connor B. Secreted amyloid precursor proteins promote proliferation and glial differentiation of adult hippocampal neural progenitor cells. *Hippocampus*. 2012;22(7):1517-1527. doi:10.1002/hipo.20988

295. Caillé I, Allinquant B, Dupont E, et al. Soluble form of amyloid precursor protein regulates proliferation of progenitors in the adult subventricular zone. *Development*. 2004;131(9):2173-2181. doi:10.1242/dev.01103

296. Tian Y, Crump CJ, Li YM. Dual role of alpha-secretase cleavage in the regulation of gamma-secretase activity for amyloid production. *J Biol Chem*. 2010;285(42):32549-32556. doi:10.1074/jbc.M110.128439

297. Jäger S, Leuchtenberger S, Martin A, et al. alpha-secretase mediated conversion of the amyloid precursor protein derived membrane stub C99 to C83 limits Abeta generation. *J Neurochem*. 2009;111(6):1369-1382. doi:10.1111/j.1471-4159.2009.06420.x

298. Flammang B, Pardossi-Piquard R, Sevalle J, et al. Evidence that the amyloid-β protein precursor intracellular domain, AICD, derives from β-secretase-generated C-terminal fragment. *J Alzheimers Dis*. 2012;30(1):145-153. doi:10.3233/JAD-2012-112186

299. Dainauskas JJ, Vitale P, Moreno S, Marie H, Migliore M, Saudargiene A. Altered synaptic plasticity at hippocampal CA1–CA3 synapses in Alzheimer's disease: integration of amyloid precursor protein intracellular domain and amyloid beta effects into computational models. *Front Comput Neurosci*. 2023;17:1305169. doi:10.3389/fncom.2023.1305169

300. Pousinha PA, Mouska X, Bianchi D, et al. The Amyloid Precursor Protein C-Terminal Domain Alters CA1 Neuron Firing, Modifying Hippocampus Oscillations and Impairing Spatial Memory Encoding. *Cell Rep*. 2019;29(2):317-331.e5. doi:10.1016/j.celrep.2019.08.103

301. Long DM, Cravetchi O, Chow ES, Allen C, Kretzschmar D. The amyloid precursor protein intracellular domain induces sleep disruptions and its nuclear localization fluctuates in circadian pacemaker neurons in Drosophila and mice. *Neurobiol Dis*. 2024;192:106429. doi:10.1016/j.nbd.2024.106429

302. Higgins LS, Murphy GM, Forno LS, Catalano R, Cordell B. P3 beta-amyloid peptide has a unique and potentially pathogenic immunohistochemical profile in Alzheimer's disease brain. *Am J Pathol*. 1996;149(2):585-596.

303. Lalowski M, Golabek A, Lemere CA, et al. The "Nonamyloidogenic" p3 Fragment (Amyloid β17-42) Is a Major Constituent of Down's Syndrome Cerebellar Preamyloid *. *Journal of Biological Chemistry*. 1996;271(52):33623-33631. doi:10.1074/jbc.271.52.33623

304. Kuhn AJ, Abrams BS, Knowlton S, Raskatov JA. The Alzheimer's Disease "non-amyloidogenic" p3 peptide revisited: a case for Amyloid-α. *ACS Chem Neurosci*. 2020;11(11):1539-1544. doi:10.1021/acschemneuro.0c00160

305. Dulin F, Léveillé F, Ortega JB, et al. p3 peptide, a truncated form of Aβ devoid of synaptotoxic effect, does not assemble into soluble oligomers. *FEBS Letters*. 2008;582(13):1865-1870. doi:10.1016/j.febslet.2008.05.002

306. Deng Y, Wang Z, Wang R, et al. Amyloid-β protein (Aβ) Glu11 is the major β-secretase site of β-site amyloid-β precursor protein-cleaving enzyme 1(BACE1), and shifting the cleavage site to Aβ Asp1 contributes to Alzheimer pathogenesis. *Eur J Neurosci*. 2013;37(12):1962-1969. doi:10.1111/ejn.12235

307. Vassar R, Bennett BD, Babu-Khan S, et al. Beta-secretase cleavage of Alzheimer's amyloid precursor protein by the transmembrane aspartic protease BACE. *Science*. 1999;286(5440):735-741. doi:10.1126/science.286.5440.735

308. Haniu M, Denis P, Young Y, et al. Characterization of Alzheimer's β-Secretase Protein BACE: A PEPSIN FAMILY MEMBER WITH UNUSUAL PROPERTIES *. *Journal of Biological Chemistry*. 2000;275(28):21099-21106. doi:10.1074/jbc.M002095200

309. Farzan M, Schnitzler CE, Vasilieva N, Leung D, Choe H. BACE2, a β-secretase homolog, cleaves at the β site and within the amyloid-β region of the amyloid-β precursor protein. *Proc Natl Acad Sci U S A*. 2000;97(17):9712-9717.

310. Harada H, Tamaoka A, Ishii K, et al. Beta-site APP cleaving enzyme 1 (BACE1) is increased in remaining neurons in Alzheimer's disease brains. *Neurosci Res*. 2006;54(1):24-29. doi:10.1016/j.neures.2005.10.001

311. Hartlage-Rübsamen M, Zeitschel U, Apelt J, et al. Astrocytic expression of the Alzheimer's disease beta-secretase (BACE1) is stimulus-dependent. *Glia*. 2003;41(2):169-179. doi:10.1002/glia.10178

312. Benjannet S, Elagoz A, Wickham L, et al. Post-translational processing of beta-secretase (beta-amyloid-converting enzyme) and its ectodomain shedding. The pro- and transmembrane/cytosolic domains affect its cellular activity and amyloid-beta production. *J Biol Chem*. 2001;276(14):10879-10887. doi:10.1074/jbc.M009899200

313. Bennett BD, Denis P, Haniu M, et al. A furin-like convertase mediates propeptide cleavage of BACE, the Alzheimer's beta -secretase. *J Biol Chem*. 2000;275(48):37712-37717. doi:10.1074/jbc.M005339200

314. Shi XP, Chen E, Yin KC, et al. The pro domain of beta-secretase does not confer strict zymogen-like properties but does assist proper folding of the protease domain. *J Biol Chem*. 2001;276(13):10366-10373. doi:10.1074/jbc.m009200200

315. Charlwood J, Dingwall C, Matico R, et al. Characterization of the glycosylation profiles of Alzheimer's beta -secretase protein Asp-2 expressed in a variety of cell lines. *J Biol Chem*. 2001;276(20):16739-16748. doi:10.1074/jbc.M009361200

316. Walter J, Fluhrer R, Hartung B, et al. Phosphorylation regulates intracellular trafficking of beta-secretase. *J Biol Chem*. 2001;276(18):14634-14641. doi:10.1074/jbc.M011116200

317. Fourriere L, Cho EHJ, Gleeson PA. Segregation of the membrane cargoes, BACE1 and amyloid precursor protein (APP) throughout the Golgi apparatus. *Traffic*. 2022;23(3):158-173. doi:10.1111/tra.12831

318. Roselli S, Satir TM, Camacho R, et al. APP-BACE1 Interaction and Intracellular Localization Regulate Aβ Production in iPSC-Derived Cortical Neurons. *Cell Mol Neurobiol*. 2023;43(7):3653-3668. doi:10.1007/s10571-023-01374-0

319. Yu Y, Gao Y, Winblad B, Tjernberg LO, Schedin-Weiss S. A Super-Resolved View of the Alzheimer's Disease-Related Amyloidogenic Pathway in Hippocampal Neurons. *J Alzheimers Dis*. 2021;83(2):833-852. doi:10.3233/JAD-215008

320. Chia PZC, Toh WH, Sharples R, Gasnereau I, Hill AF, Gleeson PA. Intracellular itinerary of internalised β-secretase, BACE1, and its potential impact on β-amyloid peptide biogenesis. *Traffic*. 2013;14(9):997-1013. doi:10.1111/tra.12088

321. Choy RWY, Cheng Z, Schekman R. Amyloid precursor protein (APP) traffics from the cell surface via endosomes for amyloid β (Aβ) production in the trans-Golgi network. *Proceedings of the National Academy of Sciences*. 2012;109(30):E2077-E2082. doi:10.1073/pnas.1208635109

322. Joshi G, Chi Y, Huang Z, Wang Y. Aβ-induced Golgi fragmentation in Alzheimer's disease enhances Aβ production. *Proc Natl Acad Sci U S A*. 2014;111(13):E1230-1239. doi:10.1073/pnas.1320192111

323. Marquer C, Devauges V, Cossec JC, et al. Local cholesterol increase triggers amyloid precursor protein-Bace1 clustering in lipid rafts and rapid endocytosis. *FASEB J*. 2011;25(4):1295-1305. doi:10.1096/fj.10-168633

324. Fabelo N, Martín V, Marín R, Moreno D, Ferrer I, Díaz M. Altered lipid composition in cortical lipid rafts occurs at early stages of sporadic Alzheimer's disease and facilitates APP/BACE1 interactions. *Neurobiol Aging*. 2014;35(8):1801-1812. doi:10.1016/j.neurobiolaging.2014.02.005

325. Díaz M, Fabelo N, Martín V, Ferrer I, Gómez T, Marín R. Biophysical alterations in lipid rafts from human cerebral cortex associate with increased BACE1/AβPP interaction in early stages of Alzheimer's disease. *J Alzheimers Dis*. 2015;43(4):1185-1198. doi:10.3233/JAD-141146

326. Das B, Singh N, Yao AY, et al. BACE1 controls synaptic function through modulating release of synaptic vesicles. *Mol Psychiatry*. 2021;26(11):6394-6410. doi:10.1038/s41380-021-01166-2

327. Pratsch K, Unemura C, Ito M, Lichtenthaler SF, Horiguchi N, Herms J. New Highly Selective BACE1 Inhibitors and Their Effects on Dendritic Spine Density In Vivo. *Int J Mol Sci*. 2023;24(15):12283. doi:10.3390/ijms241512283

328. Zhu K, Xiang X, Filser S, et al. Beta-Site Amyloid Precursor Protein Cleaving Enzyme 1 Inhibition Impairs Synaptic Plasticity via Seizure Protein 6. *Biol Psychiatry*. 2018;83(5):428-437. doi:10.1016/j.biopsych.2016.12.023

329. Sachse CC, Kim YH, Agsten M, et al. BACE1 and presenilin/γ-secretase regulate proteolytic processing of KCNE1 and 2, auxiliary subunits of voltage-gated potassium channels. *FASEB J*. 2013;27(6):2458-2467. doi:10.1096/fj.12-214056

330. Kim W, Watanabe H, Lomoio S, Tesco G. Spatiotemporal processing of neural cell adhesion molecules 1 and 2 by BACE1 in vivo. *J Biol Chem*. 2021;296:100372. doi:10.1016/j.jbc.2021.100372

331. Fleck D, van Bebber F, Colombo A, et al. Dual Cleavage of Neuregulin 1 Type III by BACE1 and ADAM17 Liberates Its EGF-Like Domain and Allows Paracrine Signaling. *J Neurosci*. 2013;33(18):7856-7869. doi:10.1523/JNEUROSCI.3372-12.2013

332. Kuhn PH, Koroniak K, Hogl S, et al. Secretome protein enrichment identifies physiological BACE1 protease substrates in neurons. *EMBO J*. 2012;31(14):3157-3168. doi:10.1038/emboj.2012.173

333. Heber S, Herms J, Gajic V, et al. Mice with Combined Gene Knock-Outs Reveal Essential and Partially Redundant Functions of Amyloid Precursor Protein Family Members. *J Neurosci*. 2000;20(21):7951-7963. doi:10.1523/JNEUROSCI.20-21-07951.2000

334. Saito Y, Sano Y, Vassar R, et al. X11 proteins regulate the translocation of amyloid beta-protein precursor (APP) into detergent-resistant membrane and suppress the amyloidogenic cleavage of APP by beta-site-cleaving enzyme in brain. *J Biol Chem*. 2008;283(51):35763-35771. doi:10.1074/jbc.M801353200

335. Nigam SM, Xu S, Ackermann F, et al. Endogenous APP accumulates in synapses after BACE1 inhibition. *Neurosci Res*. 2016;109:9-15. doi:10.1016/j.neures.2016.02.002

336. Sakurai T, Kaneko K, Okuno M, et al. Membrane microdomain switching: a regulatory mechanism of amyloid precursor protein processing. *J Cell Biol*. 2008;183(2):339-352. doi:10.1083/jcb.200804075

337. Zhou B, Lu JG, Siddu A, Wernig M, Südhof TC. Synaptogenic effect of APP-Swedish mutation in familial Alzheimer's disease. *Sci Transl Med*. 2022;14(667):eabn9380. doi:10.1126/scitranslmed.abn9380

338. Furukawa K, Sopher BL, Rydel RE, et al. Increased activity-regulating and neuroprotective efficacy of alpha-secretase-derived secreted amyloid precursor protein conferred by a C-terminal heparin-binding domain. *J Neurochem*. 1996;67(5):1882-1896. doi:10.1046/j.1471-4159.1996.67051882.x

339. Copanaki E, Chang S, Vlachos A, et al. sAPPalpha antagonizes dendritic degeneration and neuron death triggered by proteasomal stress. *Mol Cell Neurosci*. 2010;44(4):386-393. doi:10.1016/j.mcn.2010.04.007

340. Taylor CJ, Ireland DR, Ballagh I, et al. Endogenous secreted amyloid precursor protein-alpha regulates hippocampal NMDA receptor function, long-term potentiation and spatial memory. *Neurobiol Dis*. 2008;31(2):250-260. doi:10.1016/j.nbd.2008.04.011

341. Rice HC, de Malmazet D, Schreurs A, et al. Secreted Amyloid-β Precursor Protein Functions as a GABABR1a Ligand to Modulate Synaptic Transmission. *Science*. 2019;363(6423):eaa04827. doi:10.1126/science.aa04827

342. Chasseigneaux S, Dinc L, Rose C, et al. Secreted amyloid precursor protein β and secreted amyloid precursor protein α induce axon outgrowth in vitro through Egr1 signaling pathway. *PLoS One*. 2011;6(1):e16301. doi:10.1371/journal.pone.0016301

343. Freude KK, Penjwini M, Davis JL, LaFerla FM, Blurton-Jones M. Soluble amyloid precursor protein induces rapid neural differentiation of human embryonic stem cells. *J Biol Chem*. 2011;286(27):24264-24274. doi:10.1074/jbc.M111.227421

344. Barger SW, Harmon AD. Microglial activation by Alzheimer amyloid precursor protein and modulation by apolipoprotein E. *Nature*. 1997;388(6645):878-881. doi:10.1038/42257

345. Meckler X, Checler F. Presenilin 1 and Presenilin 2 Target γ-Secretase Complexes to Distinct Cellular Compartments*. *Journal of Biological Chemistry*. 2016;291(24):12821-12837. doi:10.1074/jbc.M115.708297

346. Sannerud R, Esselens C, Ejsmont P, et al. Restricted Location of PSEN2/γ-Secretase Determines Substrate Specificity and Generates an Intracellular Aβ Pool. *Cell*. 2016;166(1):193-208. doi:10.1016/j.cell.2016.05.020

347. Ratovitski T, Slunt HH, Thinakaran G, Price DL, Sisodia SS, Borchelt DR. Endoproteolytic processing and stabilization of wild-type and mutant presenilin. *J Biol Chem*. 1997;272(39):24536-24541. doi:10.1074/jbc.272.39.24536

348. Podlisny MB, Citron M, Amarante P, et al. Presenilin proteins undergo heterogeneous endoproteolysis between Thr291 and Ala299 and occur as stable N- and C-terminal fragments in normal and Alzheimer brain tissue. *Neurobiol Dis*. 1997;3(4):325-337. doi:10.1006/nbdi.1997.0129

349. Kopan R, Ilagan MXG. γ-Secretase: proteasome of the membrane? *Nat Rev Mol Cell Biol*. 2004;5(6):499-504. doi:10.1038/nrm1406

350. Checler F, Afram E, Pardossi-Piquard R, Lauritzen I. Is γ-secretase a beneficial inactivating enzyme of the toxic APP C-terminal fragment C99? *J Biol Chem*. 2021;296:100489. doi:10.1016/j.jbc.2021.100489

351. Struhl G, Adachi A. Requirements for Presenilin-Dependent Cleavage of Notch and Other Transmembrane Proteins. *Molecular Cell*. 2000;6(3):625-636. doi:10.1016/S1097-2765(00)00061-7

352. Bolduc DM, Montagna DR, Gu Y, Selkoe DJ, Wolfe MS. Nicastrin functions to sterically hinder γ-secretase–substrate interactions driven by substrate transmembrane domain. *Proceedings of the National Academy of Sciences*. 2016;113(5):E509-E518. doi:10.1073/pnas.1512952113

353. Yan Y, Xu TH, Melcher K, Xu HE. Defining the minimum substrate and charge recognition model of gamma-secretase. *Acta Pharmacol Sin*. 2017;38(10):1412-1424. doi:10.1038/aps.2017.35

354. Murphy MP, Hickman LJ, Eckman CB, Uljon SN, Wang R, Golde TE. gamma-Secretase, evidence for multiple proteolytic activities and influence of membrane positioning of substrate on generation of amyloid beta peptides of varying length. *J Biol Chem*. 1999;274(17):11914-11923. doi:10.1074/jbc.274.17.11914

355. Lichtenthaler SF, Wang R, Grimm H, Uljon SN, Masters CL, Beyreuther K. Mechanism of the cleavage specificity of Alzheimer's disease gamma-secretase identified by phenylalanine-scanning mutagenesis of the transmembrane domain of the amyloid precursor protein. *Proc Natl Acad Sci U S A*. 1999;96(6):3053-3058. doi:10.1073/pnas.96.6.3053

356. Fukumori A, Steiner H. Substrate recruitment of γ-secretase and mechanism of clinical presenilin mutations revealed by photoaffinity mapping. *EMBO J*. 2016;35(15):1628-1643. doi:10.15252/embj.201694151

357. Bai X chen, Rajendra E, Yang G, Shi Y, Scheres SH. Sampling the conformational space of the catalytic subunit of human γ-secretase. Kühlbrandt W, ed. *eLife*. 2015;4:e11182. doi:10.7554/eLife.11182

358. Clemente N, Abdine A, Ubarretxena-Belandia I, Wang C. Coupled Transmembrane Substrate Docking and Helical Unwinding in Intramembrane Proteolysis of Amyloid Precursor Protein. *Sci Rep*. 2018;8(1):12411. doi:10.1038/s41598-018-30015-6

359. Bolduc DM, Montagna DR, Seghers MC, Wolfe MS, Selkoe DJ. The amyloid-beta forming tripeptide cleavage mechanism of γ-secretase. Cravatt BF, ed. *eLife*. 2016;5:e17578. doi:10.7554/eLife.17578

360. Shelar A, Bansal M. Helix perturbations in membrane proteins assist in inter-helical interactions and optimal helix positioning in the bilayer. *Biochimica et Biophysica Acta (BBA) - Biomembranes*. 2016;1858(11):2804-2817. doi:10.1016/j.bbamem.2016.08.003

361. Kamp F, Winkler E, Trambauer J, Ebke A, Fluhrer R, Steiner H. Intramembrane Proteolysis of *β*-Amyloid Precursor Protein by *γ*-Secretase Is an Unusually Slow Process. *Biophysical Journal*. 2015;108(5):1229-1237. doi:10.1016/j.bpj.2014.12.045

362. Kanatsu K, Hori Y, Ebinuma I, Chiu YW, Tomita T. Retrograde transport of γ-secretase from endosomes to the trans-Golgi network regulates Aβ42 production. *J Neurochem*. 2018;147(1):110-123. doi:10.1111/jnc.14477

363. Szaruga M, Munteanu B, Lismont S, et al. Alzheimer's-Causing Mutations Shift Aβ Length by Destabilizing γ-Secretase-Aβn Interactions. *Cell*. 2017;170(3):443-456.e14. doi:10.1016/j.cell.2017.07.004

364. Takami M, Nagashima Y, Sano Y, et al. γ-Secretase: Successive Tripeptide and Tetrapeptide Release from the Transmembrane Domain of β-Carboxyl Terminal Fragment. *J Neurosci*. 2009;29(41):13042-13052. doi:10.1523/JNEUROSCI.2362-09.2009

365. Matsumura N, Takami M, Okochi M, et al. γ-Secretase Associated with Lipid Rafts: MULTIPLE INTERACTIVE PATHWAYS IN THE STEPWISE PROCESSING OF β-CARBOXYL-TERMINAL FRAGMENT*. *Journal of Biological Chemistry*. 2014;289(8):5109-5121. doi:10.1074/jbc.M113.510131

366. Wakabayashi T, Craessaerts K, Bammens L, et al. Analysis of the γ-secretase interactome and validation of its association with tetraspanin-enriched microdomains. *Nat Cell Biol*. 2009;11(11):1340-1346. doi:10.1038/ncb1978

367. Chen AC, Kim S, Shepardson N, Patel S, Hong S, Selkoe DJ. Physical and functional interaction between the α- and γ-secretases: A new model of regulated intramembrane proteolysis. *J Cell Biol*. 2015;211(6):1157-1176. doi:10.1083/jcb.201502001

368. Liu L, Ding L, Rovere M, Wolfe MS, Selkoe DJ. A cellular complex of BACE1 and γ-secretase sequentially generates Aβ from its full-length precursor. *J Cell Biol*. 2019;218(2):644-663. doi:10.1083/jcb.201806205

369. Anderson RM, Hadjichrysanthou C, Evans S, Wong MM. Why do so many clinical trials of therapies for Alzheimer's disease fail? *The Lancet*. 2017;390(10110):2327-2329. doi:10.1016/S0140-6736(17)32399-1

370. Tse KH, Herrup K. Re-imagining Alzheimer's disease - the diminishing importance of amyloid and a glimpse of what lies ahead. *J Neurochem*. 2017;143(4):432-444. doi:10.1111/jnc.14079

371. Karran E, De Strooper B. The amyloid cascade hypothesis: are we poised for success or failure? *J Neurochem*. 2016;139 Suppl 2:237-252. doi:10.1111/jnc.13632

372. Castello MA, Soriano S. On the origin of Alzheimer's disease. Trials and tribulations of the amyloid hypothesis. *Ageing Res Rev*. 2014;13:10-12. doi:10.1016/j.arr.2013.10.001

373. Behl C, Ziegler C. Beyond Amyloid - Widening the View on Alzheimer's Disease. *J Neurochem*. 2017;143(4):394-395. doi:10.1111/jnc.14137

374. Loeffler DA. Antibody-Mediated Clearance of Brain Amyloid-β: Mechanisms of Action, Effects of Natural and Monoclonal Anti-Aβ Antibodies, and Downstream Effects. *J Alzheimers Dis Rep*. 2023;7(1):873-899. doi:10.3233/ADR-230025

375. Pantelopulos GA, Straub JE, Thirumalai D, Sugita Y. Structure of APP-C991–99 and implications for role of extra-membrane domains in function and oligomerization. *Biochimica et Biophysica Acta (BBA) - Biomembranes*. 2018;1860(9):1698-1708. doi:10.1016/j.bbamem.2018.04.002

376. Lauritzen I, Pardossi-Piquard R, Bauer C, et al. The β-Secretase-Derived C-Terminal Fragment of βAPP, C99, But Not Aβ, Is a Key Contributor to Early Intraneuronal Lesions in Triple-Transgenic Mouse Hippocampus. *J Neurosci*. 2012;32(46):16243-16255. doi:10.1523/JNEUROSCI.2775-12.2012

377. Bourgeois A, Lauritzen I, Lorivel T, Bauer C, Checler F, Pardossi-Piquard R. Intraneuronal accumulation of C99 contributes to synaptic alterations, apathy-like behavior, and spatial learning deficits in 3×TgAD and 2×TgAD mice. *Neurobiol Aging*. 2018;71:21-31. doi:10.1016/j.neurobiolaging.2018.06.038

378. Pera M, Alcolea D, Sánchez-Valle R, et al. Distinct patterns of APP processing in the CNS in autosomal-dominant and sporadic Alzheimer disease. *Acta Neuropathol*. 2013;125(2):201-213. doi:10.1007/s00401-012-1062-9

379. Tamayev R, Matsuda S, Arancio O, D'Adamio L. β- but not γ-secretase proteolysis of APP causes synaptic and memory deficits in a mouse model of dementia. *EMBO Mol Med*. 2012;4(3):171-179. doi:10.1002/emmm.201100195

380. Hamm V, Héraud C, Bott JB, et al. Differential contribution of APP metabolites to early cognitive deficits in a TgCRND8 mouse model of Alzheimer's disease. *Sci Adv*. 2017;3(2):e1601068. doi:10.1126/sciadv.1601068

381. Cavanagh C, Colby-Milley J, Bouvier D, et al. βCTF-correlated burst of hippocampal TNFα occurs at a very early, pre-plaque stage in the TgCRND8 mouse model of Alzheimer's disease. *J Alzheimers Dis*. 2013;36(2):233-238. doi:10.3233/JAD-122131

382. Tambini MD, Yao W, D'Adamio L. Facilitation of glutamate, but not GABA, release in Familial Alzheimer's APP mutant Knock-in rats with increased β-cleavage of APP. *Aging Cell*. 2019;18(6):e13033. doi:10.1111/acel.13033

383. Mondragón-Rodríguez S, Gu N, Manseau F, Williams S. Alzheimer's Transgenic Model Is Characterized by Very Early Brain Network Alterations and β-CTF Fragment Accumulation: Reversal by β-Secretase Inhibition. *Front Cell Neurosci*. 2018;12:121. doi:10.3389/fncel.2018.00121

384. Jiang Y, Rigoglioso A, Peterhoff CM, et al. Partial BACE1 Reduction in a Down Syndrome Mouse Model blocks Alzheimer-related Endosomal Anomalies and Cholinergic Neurodegeneration: Role of APP-CTF. *Neurobiol Aging*. 2016;39:90-98. doi:10.1016/j.neurobiolaging.2015.11.013

385. Kwart D, Gregg A, Scheckel C, et al. A Large Panel of Isogenic APP and PSEN1 Mutant Human iPSC Neurons Reveals Shared Endosomal Abnormalities Mediated by APP β-CTFs, Not Aβ. *Neuron*. 2019;104(2):256-270.e5. doi:10.1016/j.neuron.2019.07.010

386. Israel MA, Yuan SH, Bardy C, et al. Probing sporadic and familial Alzheimer's disease using induced pluripotent stem cells. *Nature*. 2012;482(7384):216-220. doi:10.1038/nature10821

387. Yoon SY, Choi JE, Yoon JH, Huh JW, Kim DH. BACE inhibitor reduces APP-beta-C-terminal fragment accumulation in axonal swellings of okadaic acid-induced neurodegeneration. *Neurobiol Dis*. 2006;22(2):435-444. doi:10.1016/j.nbd.2005.12.013

388. Chen HY, Wang L, Liu JF, Wang WZ, Yu CJ. Effect of the beta secretase-1 inhibitor on the amyloid C-terminal fragment of amyloid precursor protein processing in a hyperphosphorylated tau rat model. *Genet Mol Res*. 2014;13(3):6213-6227. doi:10.4238/2014.August.15.4

389. Lauritzen I, Pardossi-Piquard R, Bourgeois A, et al. Intraneuronal aggregation of the β-CTF fragment of APP (C99) induces Aβ-independent lysosomal-autophagic pathology. *Acta Neuropathol*. 2016;132(2):257-276. doi:10.1007/s00401-016-1577-6

390. Jiang Y, Sato Y, Im E, et al. Lysosomal Dysfunction in Down Syndrome Is APP-Dependent and Mediated by APP-βCTF (C99). *J Neurosci*. 2019;39(27):5255-5268. doi:10.1523/JNEUROSCI.0578-19.2019

391. Hung COY, Livesey FJ. Altered γ-Secretase Processing of APP Disrupts Lysosome and Autophagosome Function in Monogenic Alzheimer's Disease. *Cell Rep*. 2018;25(13):3647-3660.e2. doi:10.1016/j.celrep.2018.11.095

392. Kaur G, Pawlik M, Gandy SE, Ehrlich ME, Smiley JF, Levy E. Lysosomal dysfunction in the brain of a mouse model with intraneuronal accumulation of carboxyl terminal fragments of the amyloid precursor protein. *Mol Psychiatry*. 2017;22(7):981-989. doi:10.1038/mp.2016.189

393. González AE, Muñoz VC, Cavieres VA, et al. Autophagosomes cooperate in the degradation of intracellular C-terminal fragments of the amyloid precursor protein via the MVB/lysosomal pathway. *FASEB J*. 2017;31(6):2446-2459. doi:10.1096/fj.201600713R

394. Bustamante HA, Rivera-Dictter A, Cavieres VA, et al. Turnover of C99 is Controlled by a Crosstalk between ERAD and Ubiquitin-Independent Lysosomal Degradation in Human Neuroglioma Cells. *PLoS One*. 2013;8(12):e83096. doi:10.1371/journal.pone.0083096

395. Del Prete D, Suski JM, Oulès B, et al. Localization and Processing of the Amyloid-β Protein Precursor in Mitochondria-Associated Membranes. *J Alzheimers Dis*. 2017;55(4):1549-1570. doi:10.3233/JAD-160953

396. Pera M, Larrea D, Guardia-Laguarta C, et al. Increased localization of APP-C99 in mitochondria-associated ER membranes causes mitochondrial dysfunction in Alzheimer disease. *EMBO J*. 2017;36(22):3356-3371. doi:10.15252/embj.201796797

397. Vaillant-Beuchot L, Mary A, Pardossi-Piquard R, et al. Accumulation of amyloid precursor protein C-terminal fragments triggers mitochondrial structure, function, and mitophagy defects in Alzheimer's disease models and human brains. *Acta Neuropathol*. 2021;141(1):39-65. doi:10.1007/s00401-020-02234-7

398. Reddy PH, Yin X, Manczak M, et al. Mutant APP and amyloid beta-induced defective autophagy, mitophagy, mitochondrial structural and functional changes and synaptic damage in hippocampal neurons from Alzheimer's disease. *Hum Mol Genet*. 2018;27(14):2502-2516. doi:10.1093/hmg/ddy154

399. Sorrentino V, Romani M, Mouchiroud L, et al. Enhancing mitochondrial proteostasis reduces amyloid-β proteotoxicity. *Nature*. 2017;552(7684):187-193. doi:10.1038/nature25143

400. Yankner BA, Dawes LR, Fisher S, Villa-Komaroff L, Oster-Granite ML, Neve RL. Neurotoxicity of a Fragment of the Amyloid Precursor Associated with Alzheimer's Disease. *Science*. 1989;245(4916):417-420. doi:10.1126/science.2474201

401. Wolf D, Quon D, Wang Y, Cordell B. Identification and characterization of C-terminal fragments of the beta-amyloid precursor produced in cell culture. *EMBO J*. 1990;9(7):2079-2084. doi:10.1002/j.1460-2075.1990.tb07375.x

402. Pantelopulos GA, Matsuoka D, Hutchison JM, et al. Formation of extramembrane β-strands controls dimerization of transmembrane helices in amyloid precursor protein C99. *Proc Natl Acad Sci U S A*. 2022;119(52):e2212207119. doi:10.1073/pnas.2212207119

403. Winkler E, Julius A, Steiner H, Langosch D. Homodimerization Protects the Amyloid Precursor Protein C99 Fragment from Cleavage by γ-Secretase. *Biochemistry*. 2015;54(40):6149-6152. doi:10.1021/acs.biochem.5b00986

404. Perrin F, Papadopoulos N, Suelves N, et al. Dimeric Transmembrane Orientations of APP/C99 Regulate γ-Secretase Processing Line Impacting Signaling and Oligomerization. *iScience*. 2020;23(12):101887. doi:10.1016/j.isci.2020.101887

405. Higashide H, Ishihara S, Nobuhara M, Ihara Y, Funamoto S. Alanine substitutions in the GXXXG motif alter C99 cleavage by γ-secretase but not its dimerization. *J Neurochem*. 2017;140(6):955-962. doi:10.1111/jnc.13942

406. Vingtdeux V, Hamdane M, Loyens A, et al. Alkalizing Drugs Induce Accumulation of Amyloid Precursor Protein By-products in Luminal Vesicles of Multivesicular Bodies *. *Journal of Biological Chemistry*. 2007;282(25):18197-18205. doi:10.1074/jbc.M609475200

407. Lauritzen I, Bécot A, Bourgeois A, et al. Targeting γ-secretase triggers the selective enrichment of oligomeric APP-CTFs in brain extracellular vesicles from Alzheimer cell and mouse models. *Transl Neurodegener*. 2019;8:35. doi:10.1186/s40035-019-0176-6

408. Filser S, Ovsepian SV, Masana M, et al. Pharmacological inhibition of BACE1 impairs synaptic plasticity and cognitive functions. *Biol Psychiatry*. 2015;77(8):729-739. doi:10.1016/j.biopsych.2014.10.013

409. Wang H, Song L, Laird F, Wong PC, Lee HK. BACE1 Knock-Outs Display Deficits in Activity-Dependent Potentiation of Synaptic Transmission at Mossy Fiber to CA3 Synapses in the Hippocampus. *J Neurosci*. 2008;28(35):8677-8681. doi:10.1523/JNEUROSCI.2440-08.2008

410. Lombardo S, Chiacchiaretta M, Tarr A, et al. BACE1 partial deletion induces synaptic plasticity deficit in adult mice. *Sci Rep*. 2019;9:19877. doi:10.1038/s41598-019-56329-7

411. Hu X, Zhou X, He W, et al. BACE1 Deficiency Causes Altered Neuronal Activity and Neurodegeneration. *J Neurosci*. 2010;30(26):8819-8829. doi:10.1523/JNEUROSCI.1334-10.2010

412. Puzzo D, Privitera L, Fa' M, et al. Endogenous Amyloid-β is Necessary for Hippocampal Synaptic Plasticity and Memory. *Ann Neurol*. 2011;69(5):819-830. doi:10.1002/ana.22313

413. Morley JE, Farr SA, Banks WA, Johnson SN, Yamada KA, Xu L. A physiological role for amyloid-beta protein:enhancement of learning and memory. *J Alzheimers Dis*. 2010;19(2):441-449. doi:10.3233/JAD-2009-1230

414. Lewczuk P, Matzen A, Blennow K, et al. Cerebrospinal Fluid Aβ42/40 Corresponds Better than Aβ42 to Amyloid PET in Alzheimer's Disease. *J Alzheimers Dis*. 2017;55(2):813-822. doi:10.3233/JAD-160722

415. Kuperstein I, Broersen K, Benilova I, et al. Neurotoxicity of Alzheimer's disease Aβ peptides is induced by small changes in the Aβ42 to Aβ40 ratio. *EMBO J*. 2010;29(19):3408-3420. doi:10.1038/emboj.2010.211

416. Ancolio K, Dumanchin C, Barelli H, et al. Unusual phenotypic alteration of β amyloid precursor protein (βAPP) maturation by a new Val-715 → Met βAPP-770 mutation responsible for probable early-onset Alzheimer's disease. *Proc Natl Acad Sci U S A*. 1999;96(7):4119-4124.

417. Abraham JD, Promé S, Salvetat N, et al. Cerebrospinal Aβ11-x and 17-x levels as indicators of mild cognitive impairment and patients' stratification in Alzheimer's disease. *Transl Psychiatry*. 2013;3(7):e281. doi:10.1038/tp.2013.58

418. Wei W, Norton DD, Wang X, Kusiak JW. Abeta 17-42 in Alzheimer's disease activates JNK and caspase-8 leading to neuronal apoptosis. *Brain*. 2002;125(Pt 9):2036-2043. doi:10.1093/brain/awf205

419. Peters C, Bascuñán D, Opazo C, Aguayo LG. Differential Membrane Toxicity of Amyloid-β Fragments by Pore Forming Mechanisms. *J Alzheimers Dis*. 2016;51(3):689-699. doi:10.3233/JAD-150896

420. Busch L, Taleb Z al, Tsai YL, et al. Amyloid beta and its naturally occurring N-terminal variants are potent activators of human and mouse formyl peptide receptor 1. *Journal of Biological Chemistry*. 2022;298(12). doi:10.1016/j.jbc.2022.102642

421. Jang H, Arce FT, Ramachandran S, et al. Truncated β-amyloid peptide channels provide an alternative mechanism for Alzheimer's Disease and Down syndrome. *Proc Natl Acad Sci U S A*. 2010;107(14):6538-6543. doi:10.1073/pnas.0914251107

422. Huse JT, Liu K, Pijak DS, Carlin D, Lee VMY, Doms RW. Beta-secretase processing in the trans-Golgi network preferentially generates truncated amyloid species that accumulate in Alzheimer's disease brain. *J Biol Chem*. 2002;277(18):16278-16284. doi:10.1074/jbc.M111141200

423. Sohma Y, Yamasaki M, Kawashima H, et al. Comparative properties of Aβ1-42, Aβ11-42, and [Pyr^{11}]Aβ11-42 generated from O-acyl isopeptides. *Bioorg Med Chem Lett*. 2013;23(5):1326-1329. doi:10.1016/j.bmcl.2012.12.082

424. Barritt JD, Viles JH. Truncated Amyloid-β(11-40/42) from Alzheimer Disease Binds Cu2+ with a Femtomolar Affinity and Influences Fiber Assembly. *J Biol Chem*. 2015;290(46):27791-27802. doi:10.1074/jbc.M115.684084

425. Jiang D, Zhang L, Grant GPG, et al. The elevated copper binding strength of amyloid-β aggregates allows the sequestration of copper from albumin: a pathway to accumulation of copper in senile plaques. *Biochemistry*. 2013;52(3):547-556. doi:10.1021/bi301053h

426. Esmieu C, Ferrand G, Borghesani V, Hureau C. Impact of N-Truncated Aβ Peptides on Cu- and Cu(Aβ)-Generated ROS: CuI Matters! *Chemistry*. 2021;27(5):1777-1786. doi:10.1002/chem.202003949

427. Teng X, Stefaniak E, Girvan P, et al. Hierarchical binding of copperII to N-truncated Aβ4-16 peptide. *Metallomics*. 2020;12(4):470-473. doi:10.1039/c9mt00299e

428. Bouter Y, Dietrich K, Wittnam JL, et al. N-truncated amyloid β (Aβ) 4-42 forms stable aggregates and induces acute and long-lasting behavioral deficits. *Acta Neuropathol*. 2013;126(2):189-205. doi:10.1007/s00401-013-1129-2

429. Portelius E, Bogdanovic N, Gustavsson MK, et al. Mass spectrometric characterization of brain amyloid beta isoform signatures in familial and sporadic

Alzheimer's disease. *Acta Neuropathol*. 2010;120(2):185-193. doi:10.1007/s00401-010-0690-1

430. Antonios G, Saiepour N, Bouter Y, et al. N-truncated Abeta starting with position four: early intraneuronal accumulation and rescue of toxicity using NT4X-167, a novel monoclonal antibody. *Acta Neuropathol Commun*. 2013;1:56. doi:10.1186/2051-5960-1-56

431. Cabrera E, Mathews P, Mezhericher E, et al. Aβ truncated species: Implications for brain clearance mechanisms and amyloid plaque deposition. *Biochim Biophys Acta*. 2018;1864(1):208-225. doi:10.1016/j.bbadis.2017.07.005

432. Liebsch F, Kulic L, Teunissen C, et al. Aβ34 is a BACE1-derived degradation intermediate associated with amyloid clearance and Alzheimer's disease progression. *Nat Commun*. 2019;10(1):2240. doi:10.1038/s41467-019-10152-w

433. Shi XP, Tugusheva K, Bruce JE, et al. Beta-secretase cleavage at amino acid residue 34 in the amyloid beta peptide is dependent upon gamma-secretase activity. *J Biol Chem*. 2003;278(23):21286-21294. doi:10.1074/jbc.M209859200

434. Page RM, Baumann K, Tomioka M, et al. Generation of Abeta38 and Abeta42 is independently and differentially affected by familial Alzheimer disease-associated presenilin mutations and gamma-secretase modulation. *J Biol Chem*. 2008;283(2):677-683. doi:10.1074/jbc.M708754200

435. Olsson F, Schmidt S, Althoff V, et al. Characterization of Intermediate Steps in Amyloid Beta (Aβ) Production under Near-native Conditions. *J Biol Chem*. 2014;289(3):1540-1550. doi:10.1074/jbc.M113.498246

436. Wiltfang J, Esselmann H, Bibl M, et al. Highly conserved and disease-specific patterns of carboxyterminally truncated Abeta peptides 1-37/38/39 in addition to 1-40/42 in Alzheimer's disease and in patients with chronic neuroinflammation. *J Neurochem*. 2002;81(3):481-496. doi:10.1046/j.1471-4159.2002.00818.x

437. Liu L, Lauro BM, He A, et al. Identification of the Aβ37/42 peptide ratio in CSF as an improved Aβ biomarker for Alzheimer's disease. *Alzheimers Dement*. 2023;19(1):79-96. doi:10.1002/alz.12646

438. Reinert J, Richard BC, Klafki HW, et al. Deposition of C-terminally truncated Aβ species Aβ37 and Aβ39 in Alzheimer's disease and transgenic mouse models. *Acta Neuropathol Commun*. 2016;4:24. doi:10.1186/s40478-016-0294-7

439. Suárez-Calvet M, Belbin O, Pera M, et al. Autosomal-dominant Alzheimer's disease mutations at the same codon of amyloid precursor protein differentially alter Aβ production. *J Neurochem*. 2014;128(2):330-339. doi:10.1111/jnc.12466

440. Noor A, Zafar S, Shafiq M, et al. Molecular Profiles of Amyloid-β Proteoforms in Typical and Rapidly Progressive Alzheimer's Disease. *Mol Neurobiol*. 2022;59(1):17-34. doi:10.1007/s12035-021-02566-9

441. Hernandez-Guillamon M, Mawhirt S, Blais S, et al. Sequential Amyloid-β Degradation by the Matrix Metalloproteases MMP-2 and MMP-9. *J Biol Chem*. 2015;290(24):15078-15091. doi:10.1074/jbc.M114.610931

442. Liao MC, Van Nostrand WE. Degradation of soluble and fibrillar amyloid beta-protein by matrix metalloproteinase (MT1-MMP) in vitro. *Biochemistry*. 2010;49(6):1127-1136. doi:10.1021/bi901994d

443. Baranger K, Marchalant Y, Bonnet AE, et al. MT5-MMP is a new pro-amyloidogenic proteinase that promotes amyloid pathology and cognitive decline in a transgenic mouse model of Alzheimer's disease. *Cell Mol Life Sci*. 2016;73(1):217-236. doi:10.1007/s00018-015-1992-1

444. Py NA, Bonnet AE, Bernard A, et al. Differential spatio-temporal regulation of MMPs in the 5xFAD mouse model of Alzheimer's disease: evidence for a pro-amyloidogenic role of MT1-MMP. *Front Aging Neurosci*. 2014;6:247. doi:10.3389/fnagi.2014.00247

445. Langenfurth A, Rinnenthal JL, Vinnakota K, et al. Membrane-type 1 metalloproteinase is upregulated in microglia/brain macrophages in neurodegenerative and neuroinflammatory diseases. *J Neurosci Res*. 2014;92(3):275-286. doi:10.1002/jnr.23288

446. Ohuchi E, Imai K, Fujii Y, Sato H, Seiki M, Okada Y. Membrane type 1 matrix metalloproteinase digests interstitial collagens and other extracellular matrix macromolecules. *J Biol Chem*. 1997;272(4):2446-2451. doi:10.1074/jbc.272.4.2446

447. Sato H, Takino T, Kinoshita T, et al. Cell surface binding and activation of gelatinase A induced by expression of membrane-type-1-matrix metalloproteinase (MT1-MMP). *FEBS Lett*. 1996;385(3):238-240. doi:10.1016/0014-5793(96)00389-4

448. Overall CM, Tam EM, Kappelhoff R, et al. Protease degradomics: mass spectrometry discovery of protease substrates and the CLIP-CHIP, a dedicated DNA microarray of all human proteases and inhibitors. *Biol Chem*. 2004;385(6):493-504. doi:10.1515/BC.2004.058

449. Tam EM, Morrison CJ, Wu YI, Stack MS, Overall CM. Membrane protease proteomics: Isotope-coded affinity tag MS identification of undescribed MT1–matrix metalloproteinase substrates. *Proc Natl Acad Sci U S A*. 2004;101(18):6917-6922. doi:10.1073/pnas.0305862101

450. Holmbeck K, Bianco P, Caterina J, et al. MT1-MMP-deficient mice develop dwarfism, osteopenia, arthritis, and connective tissue disease due to inadequate collagen turnover. *Cell*. 1999;99(1):81-92. doi:10.1016/s0092-8674(00)80064-1

451. Ould-Yahoui A, Sbai O, Baranger K, et al. Role of matrix metalloproteinases in migration and neurotrophic properties of nasal olfactory stem and ensheathing cells. *Cell Transplant*. 2013;22(6):993-1010. doi:10.3727/096368912X657468

452. Sakamoto T, Seiki M. Cytoplasmic tail of MT1-MMP regulates macrophage motility independently from its protease activity. *Genes Cells*. 2009;14(5):617-626. doi:10.1111/j.1365-2443.2009.01293.x

453. Higashi S, Miyazaki K. Novel processing of beta-amyloid precursor protein catalyzed by membrane type 1 matrix metalloproteinase releases a fragment lacking the inhibitor domain against gelatinase A. *Biochemistry*. 2003;42(21):6514-6526. doi:10.1021/bi020643m

454. Ahmad M, Takino T, Miyamori H, Yoshizaki T, Furukawa M, Sato H. Cleavage of amyloid-beta precursor protein (APP) by membrane-type matrix metalloproteinases. *J Biochem*. 2006;139(3):517-526. doi:10.1093/jb/mvj054

455. García-González L, Paumier JM, Louis L, et al. MT5-MMP controls APP and β-CTF/C99 metabolism through proteolytic-dependent and -independent mechanisms relevant for Alzheimer's disease. *FASEB J*. 2021;35(7):e21727. doi:10.1096/fj.202100593R

456. Paumier JM, Py NA, García-González L, et al. Proamyloidogenic effects of membrane type 1 matrix metalloproteinase involve MMP-2 and BACE-1 activities, and the modulation of APP trafficking. *FASEB J*. 2019;33(2):2910-2927. doi:10.1096/fj.201801076R

457. Gomis-Rüth FX. Catalytic domain architecture of metzincin metalloproteases. *J Biol Chem*. 2009;284(23):15353-15357. doi:10.1074/jbc.R800069200

458. Rivera S, Khrestchatisky M, Kaczmarek L, Rosenberg GA, Jaworski DM. Metzincin Proteases and Their Inhibitors: Foes or Friends in Nervous System Physiology? *J Neurosci*. 2010;30(46):15337-15357. doi:10.1523/JNEUROSCI.3467-10.2010

459. Olson MW, Gervasi DC, Mobashery S, Fridman R. Kinetic Analysis of the Binding of Human Matrix Metalloproteinase-2 and -9 to Tissue Inhibitor of Metalloproteinase (TIMP)-1 and TIMP-2*. *Journal of Biological Chemistry*. 1997;272(47):29975-29983. doi:10.1074/jbc.272.47.29975

460. Morgunova E, Tuuttila A, Bergmann U, Tryggvason K. Structural insight into the complex formation of latent matrix metalloproteinase 2 with tissue inhibitor of metalloproteinase 2. *Proceedings of the National Academy of Sciences*. 2002;99(11):7414-7419. doi:10.1073/pnas.102185399

461. Sbai O, Ferhat L, Bernard A, et al. Vesicular trafficking and secretion of matrix metalloproteinases-2, -9 and tissue inhibitor of metalloproteinases-1 in neuronal cells. *Mol Cell Neurosci*. 2008;39(4):549-568. doi:10.1016/j.mcn.2008.08.004

462. Gomis-Rüth FX. Structural aspects of the metzincin clan of metalloendopeptidases. *Mol Biotechnol*. 2003;24(2):157-202. doi:10.1385/MB:24:2:157

463. Roghi C, Jones L, Gratian M, English WR, Murphy G. Golgi reassembly stacking protein 55 interacts with membrane-type (MT) 1-matrix metalloprotease (MMP) and furin and plays a role in the activation of the MT1-MMP zymogen. *FEBS J*. 2010;277(15):3158-3175. doi:10.1111/j.1742-4658.2010.07723.x

464. Limb GA, Matter K, Murphy G, et al. Matrix Metalloproteinase-1 Associates with Intracellular Organelles and Confers Resistance to Lamin A/C Degradation during Apoptosis. *The American Journal of Pathology*. 2005;166(5):1555-1563. doi:10.1016/S0002-9440(10)62371-1

465. Pei D. Identification and Characterization of the Fifth Membrane-type Matrix Metalloproteinase MT5-MMP *. *Journal of Biological Chemistry*. 1999;274(13):8925-8932. doi:10.1074/jbc.274.13.8925

466. Madzharova E, Kastl P, Sabino F, auf dem Keller U. Post-Translational Modification-Dependent Activity of Matrix Metalloproteinases. *International Journal of Molecular Sciences*. 2019;20(12):3077. doi:10.3390/ijms20123077

467. Wang P, Wang X, Pei D. Mint-3 Regulates the Retrieval of the Internalized Membrane-type Matrix Metalloproteinase, MT5-MMP, to the Plasma Membrane by Binding to Its Carboxyl End Motif EWV *. *Journal of Biological Chemistry*. 2004;279(19):20461-20470. doi:10.1074/jbc.M400264200

468. Baranger K, Khrestchatisky M, Rivera S. MT5-MMP, just a new APP processing proteinase in Alzheimer's disease? *J Neuroinflammation*. 2016;13(1):167. doi:10.1186/s12974-016-0633-4

469. Sekine-Aizawa Y, Hama E, Watanabe K, et al. Matrix metalloproteinase (MMP) system in brain: identification and characterization of brain-specific MMP highly expressed in cerebellum. *Eur J Neurosci*. 2001;13(5):935-948. doi:10.1046/j.0953-816x.2001.01462.x

470. Jaworski DM. Developmental regulation of membrane type-5 matrix metalloproteinase (MT5-MMP) expression in the rat nervous system. *Brain Res*. 2000;860(1-2):174-177. doi:10.1016/s0006-8993(00)02035-7

471. Porlan E, Martí-Prado B, Morante-Redolat JM, et al. MT5-MMP regulates adult neural stem cell functional quiescence through the cleavage of N-cadherin. *Nat Cell Biol*. 2014;16(7):629-638. doi:10.1038/ncb2993

472. Warren KM, Reeves TM, Phillips LL. MT5-MMP, ADAM-10, and N-cadherin act in concert to facilitate synapse reorganization after traumatic brain injury. *J Neurotrauma*. 2012;29(10):1922-1940. doi:10.1089/neu.2012.2383

473. Komori K, Nonaka T, Okada A, et al. Absence of mechanical allodynia and Abeta-fiber sprouting after sciatic nerve injury in mice lacking membrane-type 5 matrix metalloproteinase. *FEBS Lett*. 2004;557(1-3):125-128. doi:10.1016/s0014-5793(03)01458-3

474. Folgueras AR, Valdés-Sánchez T, Llano E, et al. Metalloproteinase MT5-MMP is an essential modulator of neuro-immune interactions in thermal pain stimulation. *Proc Natl Acad Sci U S A*. 2009;106(38):16451-16456. doi:10.1073/pnas.0908507106

475. Monea S, Jordan BA, Srivastava S, DeSouza S, Ziff EB. Membrane Localization of Membrane Type 5 Matrix Metalloproteinase by AMPA Receptor Binding Protein and Cleavage of Cadherins. *J Neurosci*. 2006;26(8):2300-2312. doi:10.1523/JNEUROSCI.3521-05.2006

476. Restituito S, Khatri L, Ninan I, et al. Synaptic Autoregulation by Metalloproteases and γ-Secretase. *J Neurosci*. 2011;31(34):12083-12093. doi:10.1523/JNEUROSCI.2513-11.2011

477. Wang X, Pei D. Shedding of membrane type matrix metalloproteinase 5 by a furin-type convertase: a potential mechanism for down-regulation. *J Biol Chem*. 2001;276(38):35953-35960. doi:10.1074/jbc.M103680200

478. Willem M, Tahirovic S, Busche MA, et al. η-Secretase processing of APP inhibits neuronal activity in the hippocampus. *Nature*. 2015;526(7573):443-447. doi:10.1038/nature14864

479. García-Ayllón MS, Lopez-Font I, Boix CP, et al. C-terminal fragments of the amyloid precursor protein in cerebrospinal fluid as potential biomarkers for Alzheimer disease. *Sci Rep*. 2017;7:2477. doi:10.1038/s41598-017-02841-7

480. Mensch M, Dunot J, Yishan SM, et al. Aη-α and Aη-β peptides impair LTP ex vivo within the low nanomolar range and impact neuronal activity in vivo. *Alzheimers Res Ther*. 2021;13(1):125. doi:10.1186/s13195-021-00860-1

481. Baranger K, Bonnet AE, Girard SD, et al. MT5-MMP Promotes Alzheimer's Pathogenesis in the Frontal Cortex of 5xFAD Mice and APP Trafficking in vitro. *Front Mol Neurosci*. 2017;9:163. doi:10.3389/fnmol.2016.00163

482. Laulagnier K, Javalet C, Hemming FJ, et al. Amyloid precursor protein products concentrate in a subset of exosomes specifically endocytosed by neurons. *Cell Mol Life Sci*. 2018;75(4):757-773. doi:10.1007/s00018-017-2664-0

483. Lee ACL, Harris JL, Khanna KK, Hong JH. A Comprehensive Review on Current Advances in Peptide Drug Development and Design. *Int J Mol Sci*. 2019;20(10):2383. doi:10.3390/ijms20102383

484. Henning-Knechtel A, Kumar S, Wallin C, et al. Designed Cell-Penetrating Peptide Inhibitors of Amyloid-beta Aggregation and Cytotoxicity. *CR-PHYS-SC*. 2020;1(2). doi:10.1016/j.xcrp.2020.100014

485. Horsley JR, Jovcevski B, Wegener KL, Yu J, Pukala TL, Abell AD. Rationally designed peptide-based inhibitor of Aβ42 fibril formation and toxicity: a potential therapeutic strategy for Alzheimer's disease. *Biochem J*. 2020;477(11):2039-2054. doi:10.1042/BCJ20200290

486. Soudy R, Kimura R, Patel A, et al. Short amylin receptor antagonist peptides improve memory deficits in Alzheimer's disease mouse model. *Sci Rep*. 2019;9(1):10942. doi:10.1038/s41598-019-47255-9

487. Walker LC, Jucker M. The Exceptional Vulnerability of Humans to Alzheimer's Disease. *Trends Mol Med*. 2017;23(6):534-545. doi:10.1016/j.molmed.2017.04.001

488. Takahashi K, Yamanaka S. Induction of pluripotent stem cells from mouse embryonic and adult fibroblast cultures by defined factors. *Cell*. 2006;126(4):663-676. doi:10.1016/j.cell.2006.07.024

489. Takahashi K, Tanabe K, Ohnuki M, et al. Induction of pluripotent stem cells from adult human fibroblasts by defined factors. *Cell*. 2007;131(5):861-872. doi:10.1016/j.cell.2007.11.019

490. Wang J, Sun S, Deng H. Chemical reprogramming for cell fate manipulation: Methods, applications, and perspectives. *Cell Stem Cell*. 2023;30(9):1130-1147. doi:10.1016/j.stem.2023.08.001

491. Straccia M, Garcia-Diaz Barriga G, Sanders P, et al. Quantitative high-throughput gene expression profiling of human striatal development to screen stem cell-derived medium spiny neurons. *Mol Ther Methods Clin Dev*. 2015;2:15030. doi:10.1038/mtm.2015.30

492. Ho SM, Hartley BJ, Julia T, et al. Rapid Ngn2-induction of excitatory neurons from hiPSC-derived neural progenitor cells. *Methods*. 2016;101:113-124. doi:10.1016/j.ymeth.2015.11.019

493. Farhy-Tselnicker I, Boisvert MM, Liu H, et al. Activity-dependent modulation of synapse-regulating genes in astrocytes. *eLife*. 10:e70514. doi:10.7554/eLife.70514

494. Zhang Y, Pak C, Han Y, et al. Rapid single-step induction of functional neurons from human pluripotent stem cells. *Neuron*. 2013;78(5):785-798. doi:10.1016/j.neuron.2013.05.029

495. Frega M, van Gestel SHC, Linda K, et al. Rapid Neuronal Differentiation of Induced Pluripotent Stem Cells for Measuring Network Activity on Micro-electrode Arrays. *J Vis Exp*. 2017;(119):54900. doi:10.3791/54900

496. Tcw J, Wang M, Pimenova AA, et al. An Efficient Platform for Astrocyte Differentiation from Human Induced Pluripotent Stem Cells. *Stem Cell Reports*. 2017;9(2):600-614. doi:10.1016/j.stemcr.2017.06.018

497. Watanabe H, Murakami R, Tsumagari K, et al. Astrocytic APOE4 genotype-mediated negative impacts on synaptic architecture in human pluripotent stem cell model. *Stem Cell Reports*. 2023;18(9):1854-1869. doi:10.1016/j.stemcr.2023.08.002

498. Das D, Sonthalia S, Stein-O.'Brien G, et al. Insights for disease modeling from single-cell transcriptomics of iPSC-derived Ngn2-induced neurons and astrocytes across differentiation time and co-culture. *BMC Biol*. 2024;22:75. doi:10.1186/s12915-024-01867-4

499. Ryan SK, Jordan-Sciutto KL, Anderson SA. Protocol for Tri-culture of hiPSC-Derived Neurons, Astrocytes, and Microglia. *STAR Protoc*. 2020;1(3):100190. doi:10.1016/j.xpro.2020.100190

500. Lancaster MA, Renner M, Martin CA, et al. Cerebral organoids model human brain development and microcephaly. *Nature*. 2013;501(7467):373-379. doi:10.1038/nature12517

501. Benito-Kwiecinski S, Lancaster MA. Brain Organoids: Human Neurodevelopment in a Dish. *Cold Spring Harb Perspect Biol*. 2020;12(8):a035709. doi:10.1101/cshperspect.a035709

502. Miura Y, Li MY, Birey F, et al. Generation of human striatal organoids and cortico-striatal assembloids from human pluripotent stem cells. *Nat Biotechnol*. 2020;38(12):1421-1430. doi:10.1038/s41587-020-00763-w

503. Pellegrini L, Albecka A, Mallery DL, et al. SARS-CoV-2 Infects the Brain Choroid Plexus and Disrupts the Blood-CSF Barrier in Human Brain Organoids. *Cell Stem Cell*. 2020;27(6):951-961.e5. doi:10.1016/j.stem.2020.10.001

504. Bardy C, van den Hurk M, Eames T, et al. Neuronal medium that supports basic synaptic functions and activity of human neurons in vitro. *Proceedings of the National Academy of Sciences*. 2015;112(20):E2725-E2734. doi:10.1073/pnas.1504393112

505. Lam M, Sanosaka T, Lundin A, et al. Single-cell study of neural stem cells derived from human iPSCs reveals distinct progenitor populations with neurogenic and gliogenic potential. *Genes Cells*. 2019;24(12):836-847. doi:10.1111/gtc.12731

506. Caiazzo M, Dell'Anno MT, Dvoretskova E, et al. Direct generation of functional dopaminergic neurons from mouse and human fibroblasts. *Nature*. 2011;476(7359):224-227. doi:10.1038/nature10284

507. Giehrl-Schwab J, Giesert F, Rauser B, et al. Parkinson's disease motor symptoms rescue by CRISPRa-reprogramming astrocytes into GABAergic neurons. *EMBO Mol Med*. 2022;14(5):e14797. doi:10.15252/emmm.202114797

508. Lin HC, He Z, Ebert S, et al. NGN2 induces diverse neuron types from human pluripotency. *Stem Cell Reports*. 2021;16(9):2118-2127. doi:10.1016/j.stemcr.2021.07.006

509. Feuer KL, Peng X, Yovo CK, Avramopoulos D. DPYSL2/CRMP2 isoform B knockout in human iPSC-derived glutamatergic neurons confirms its role in mTOR signaling and neurodevelopmental disorders. *Mol Psychiatry*. 2023;28(10):4353-4362. doi:10.1038/s41380-023-02186-w

510. Wen J, Zellner A, Braun NC, et al. Loss of function of FIP200 in human pluripotent stem cell-derived neurons leads to axonal pathology and hyperactivity. *Transl Psychiatry*. 2023;13(1):143. doi:10.1038/s41398-023-02432-3

511. Faheem M, Deneault E, Alexandrova R, et al. Disruption of DDX53 coding sequence has limited impact on iPSC-derived human NGN2 neurons. *BMC Med Genomics*. 2023;16(1):5. doi:10.1186/s12920-022-01425-3

512. Lee A, Kondapalli C, Virga DM, et al. Aβ42 oligomers trigger synaptic loss through CAMKK2-AMPK-dependent effectors coordinating mitochondrial fission and mitophagy. *Nat Commun*. 2022;13:4444. doi:10.1038/s41467-022-32130-5

513. Qu G, Merchant JP, Clatot J, et al. Targeted blockade of aberrant sodium current in a stem cell-derived neuron model of SCN3A encephalopathy. *Brain*. 2024;147(4):1247-1263. doi:10.1093/brain/awad376

514. Wang C, Ward ME, Chen R, et al. Scalable Production of iPSC-Derived Human Neurons to Identify Tau-Lowering Compounds by High-Content Screening. *Stem Cell Reports*. 2017;9(4):1221-1233. doi:10.1016/j.stemcr.2017.08.019

515. Sridharan B, Hubbs C, Llamosas N, et al. A Simple Procedure for Creating Scalable Phenotypic Screening Assays in Human Neurons. *Sci Rep*. 2019;9(1):9000. doi:10.1038/s41598-019-45265-1

516. Cheng C, Reis SA, Adams ET, et al. High-content image-based analysis and proteomic profiling identifies Tau phosphorylation inhibitors in a human iPSC-derived glutamatergic neuronal model of tauopathy. *Sci Rep*. 2021;11:17029. doi:10.1038/s41598-021-96227-5

517. van Hugte EJH, Lewerissa EI, Wu KM, et al. SCN1A-deficient excitatory neuronal networks display mutation-specific phenotypes. *Brain*. 2023;146(12):5153-5167. doi:10.1093/brain/awad245

518. Wen J, Peitz M, Brüstle O. A defined human-specific platform for modeling neuronal network stimulation in vitro and in silico. *Journal of Neuroscience Methods*. 2022;373:109562. doi:10.1016/j.jneumeth.2022.109562

519. Pré D, Wooten AT, Biesmans S, et al. Development of a platform to investigate long-term potentiation in human iPSC-derived neuronal networks. *Stem Cell Reports*. 2022;17(9):2141-2155. doi:10.1016/j.stemcr.2022.07.012

520. Meijer M, Rehbach K, Brunner JW, et al. A Single-Cell Model for Synaptic Transmission and Plasticity in Human iPSC-Derived Neurons. *Cell Reports*. 2019;27(7):2199-2211.e6. doi:10.1016/j.celrep.2019.04.058

521. Aerqin Q, Wang ZT, Wu KM, He XY, Dong Q, Yu JT. Omics-based biomarkers discovery for Alzheimer's disease. *Cell Mol Life Sci*. 2022;79(12):585. doi:10.1007/s00018-022-04614-6

522. Clark C, Rabl M, Dayon L, Popp J. The promise of multi-omics approaches to discover biological alterations with clinical relevance in Alzheimer's disease. *Front Aging Neurosci*. 2022;14:1065904. doi:10.3389/fnagi.2022.1065904

523. Berisha V, Krantsevich C, Hahn PR, et al. Digital medicine and the curse of dimensionality. *NPJ Digit Med*. 2021;4:153. doi:10.1038/s41746-021-00521-5

524. O'Connor LM, O'Connor BA, Lim SB, Zeng J, Lo CH. Integrative multi-omics and systems bioinformatics in translational neuroscience: A data mining perspective. *J Pharm Anal*. 2023;13(8):836-850. doi:10.1016/j.jpha.2023.06.011

525. Lin S, Schorpp K, Rothenaigner I, Hadian K. Image-based high-content screening in drug discovery. *Drug Discov Today*. 2020;25(8):1348-1361. doi:10.1016/j.drudis.2020.06.001

526. Zhou T, Tan L, Cederquist GY, et al. High Content Screening in hESC-Neural Progenitors Identifies Drug Candidates that Inhibit Zika Virus Infection in Fetal-like Organoids and Adult Brain. *Cell Stem Cell*. 2017;21(2):274-283.e5. doi:10.1016/j.stem.2017.06.017

527. Azorsa DO, Robeson RH, Frost D, et al. High-content siRNA screening of the kinome identifies kinases involved in Alzheimer's disease-related tau hyperphosphorylation. *BMC Genomics*. 2010;11:25. doi:10.1186/1471-2164-11-25

528. Nieland TJF, Logan DJ, Saulnier J, et al. High Content Image Analysis Identifies Novel Regulators of Synaptogenesis in a High-Throughput RNAi Screen of Primary Neurons. *PLoS One*. 2014;9(3):e91744. doi:10.1371/journal.pone.0091744

529. Mendes T, Herledan A, Leroux F, Deprez B, Lambert JC, Kilinc D. High-Content Screening for Protein-Protein Interaction Modulators Using Proximity Ligation Assay in Primary Neurons. *Current Protocols in Cell Biology*. 2020;86(1):e100. doi:10.1002/cpcb.100

530. Kolluri S, Lin J, Liu R, Zhang Y, Zhang W. Machine Learning and Artificial Intelligence in Pharmaceutical Research and Development: a Review. *AAPS J*. 2022;24(1):19. doi:10.1208/s12248-021-00644-3

531. Samuel AL. Some Studies in Machine Learning Using the Game of Checkers. *IBM Journal of Research and Development*. 1959;3(3):210-229. doi:10.1147/rd.33.0210

532. De Velasco Oriol J, Vallejo EE, Estrada K, Taméz Peña JG, Disease Neuroimaging Initiative TA. Benchmarking machine learning models for late-onset alzheimer's disease prediction from genomic data. *BMC Bioinformatics*. 2019;20:709. doi:10.1186/s12859-019-3158-x

533. Qiu S, Miller MI, Joshi PS, et al. Multimodal deep learning for Alzheimer's disease dementia assessment. *Nat Commun*. 2022;13:3404. doi:10.1038/s41467-022-31037-5

534. Liu Y, Mazumdar S, Bath PA, Alzheimer's Disease Neuroimaging Initiative. An unsupervised learning approach to diagnosing Alzheimer's disease using brain magnetic resonance imaging scans. *Int J Med Inform*. 2023;173:105027. doi:10.1016/j.ijmedinf.2023.105027

535. Joshi PS, Heydari M, Kannan S, et al. Temporal association of neuropsychological test performance using unsupervised learning reveals a distinct signature of Alzheimer's disease status. *Alzheimers Dement (N Y)*. 2019;5:964-973. doi:10.1016/j.trci.2019.11.006

536. Alexander N, Alexander DC, Barkhof F, Denaxas S. Identifying and evaluating clinical subtypes of Alzheimer's disease in care electronic health records using unsupervised machine learning. *BMC Med Inform Decis Mak*. 2021;21(1):343. doi:10.1186/s12911-021-01693-6

537. Liu X, Tosun D, Weiner MW, Schuff N, Alzheimer's Disease Neuroimaging Initiative. Locally linear embedding (LLE) for MRI based Alzheimer's disease classification. *Neuroimage*. 2013;83:148-157. doi:10.1016/j.neuroimage.2013.06.033

538. Orair GH, Teixeira CHC, Meira W, Wang Y, Parthasarathy S. Distance-based outlier detection: consolidation and renewed bearing. *Proc VLDB Endow*. 2010;3(1-2):1469-1480. doi:10.14778/1920841.1921021

539. Li W, Mo W, Zhang X, et al. Outlier detection and removal improves accuracy of machine learning approach to multispectral burn diagnostic imaging. *J Biomed Opt*. 2015;20(12):121305. doi:10.1117/1.JBO.20.12.121305

540. Ju F, Sun Y, Gao J, Hu Y, Yin B. Image Outlier Detection and Feature Extraction via L1-Norm-Based 2D Probabilistic PCA. *IEEE Trans Image Process*. 2015;24(12):4834-4846. doi:10.1109/TIP.2015.2469136

541. Polack FP, Thomas SJ, Kitchin N, et al. Safety and Efficacy of the BNT162b2 mRNA Covid-19 Vaccine. *N Engl J Med*. Published online December 10, 2020:NEJMoa2034577. doi:10.1056/NEJMoa2034577

542. Kruschke JK. Bayesian Analysis Reporting Guidelines. *Nat Hum Behav*. 2021;5(10):1282-1291. doi:10.1038/s41562-021-01177-7

543. Sasaguri H, Nilsson P, Hashimoto S, et al. APP mouse models for Alzheimer's disease preclinical studies. *EMBO J*. 2017;36(17):2473-2487. doi:10.15252/embj.201797397

544. Arnst N, Belio-Mairal P, García-González L, et al. Deficiency in MT5-MMP Supports Branching of Human iPSCs-Derived Neurons and Reduces Expression of GLAST/S100 in iPSCs-Derived Astrocytes. *Cells*. 2021;10(7):1705. doi:10.3390/cells10071705

545. Chambers SM, Fasano CA, Papapetrou EP, Tomishima M, Sadelain M, Studer L. Highly efficient neural conversion of human ES and iPS cells by dual inhibition of SMAD signaling. *Nat Biotechnol*. 2009;27(3):275-280. doi:10.1038/nbt.1529

546. Dunot J, Moreno S, Gandin C, et al. APP fragment controls both ionotropic and non-ionotropic signaling of NMDA receptors. *Neuron*. Published online June 7, 2024:S0896-6273(24)00404-5. doi:10.1016/j.neuron.2024.05.027

547. Griciuc A, Federico AN, Natasan J, et al. Gene therapy for Alzheimer's disease targeting CD33 reduces amyloid beta accumulation and neuroinflammation. *Hum Mol Genet*. 2020;29(17):2920-2935. doi:10.1093/hmg/ddaa179

548. Rafii MS, Tuszynski MH, Thomas RG, et al. Adeno-Associated Viral Vector (Serotype 2)–Nerve Growth Factor for Patients With Alzheimer Disease: A Randomized Clinical Trial. *JAMA Neurology*. 2018;75(7):834-841. doi:10.1001/jamaneurol.2018.0233

549. Castle MJ, Baltanás FC, Kovacs I, Nagahara AH, Barba D, Tuszynski MH. Postmortem Analysis in a Clinical Trial of AAV2-NGF Gene Therapy for Alzheimer's Disease Identifies a Need for Improved Vector Delivery. *Hum Gene Ther*. 2020;31(7-8):415-422. doi:10.1089/hum.2019.367

550. Eyjolfsdottir H, Eriksdotter M, Linderoth B, et al. Targeted delivery of nerve growth factor to the cholinergic basal forebrain of Alzheimer's disease patients: application of a second-generation encapsulated cell biodelivery device. *Alzheimers Res Ther*. 2016;8:30. doi:10.1186/s13195-016-0195-9

551. Tan ZJ, Peng Y, Song HL, Zheng JJ, Yu X. N-cadherin-dependent neuron-neuron interaction is required for the maintenance of activity-induced dendrite growth. *Proc Natl Acad Sci U S A*. 2010;107(21):9873-9878. doi:10.1073/pnas.1003480107

552. Cen C, Luo LD, Li WQ, et al. PKD1 Promotes Functional Synapse Formation Coordinated with N-Cadherin in Hippocampus. *J Neurosci*. 2018;38(1):183-199. doi:10.1523/JNEUROSCI.1640-17.2017

553. Asada-Utsugi M, Uemura K, Kubota M, et al. Mice with cleavage-resistant N-cadherin exhibit synapse anomaly in the hippocampus and outperformance in spatial learning tasks. *Mol Brain*. 2021;14(1):23. doi:10.1186/s13041-021-00738-1

554. Pilat D, Paumier JM, García-González L, et al. MT5-MMP promotes neuroinflammation, neuronal excitability and Aβ production in primary neuron/astrocyte cultures from the 5xFAD mouse model of Alzheimer's disease. *J Neuroinflammation*. 2022;19:65. doi:10.1186/s12974-022-02407-z

555. Segarra-Mondejar M, Casellas-Díaz S, Ramiro-Pareta M, et al. Synaptic activity-induced glycolysis facilitates membrane lipid provision and neurite outgrowth. *EMBO J*. 2018;37(9):e97368. doi:10.15252/embj.201797368

556. Heckman EL, Doe CQ. Presynaptic contact and activity opposingly regulate postsynaptic dendrite outgrowth. *Elife*. 2022;11:e82093. doi:10.7554/eLife.82093

557. Hayashita-Kinoh H, Kinoh H, Okada A, et al. Membrane-Type 5 Matrix Metalloproteinase Is Expressed in Differentiated Neurons and Regulates Axonal Growth1. *Cell Growth & Differentiation*. 2001;12(11):573-580.

558. Endo F, Kasai A, Soto JS, et al. Molecular basis of astrocyte diversity and morphology across the CNS in health and disease. *Science*. 2022;378(6619):eadc9020. doi:10.1126/science.adc9020

559. Bayraktar OA, Bartels T, Holmqvist S, et al. Astrocyte layers in the mammalian cerebral cortex revealed by a single-cell in situ transcriptomic map. *Nat Neurosci*. 2020;23(4):500-509. doi:10.1038/s41593-020-0602-1

560. O'Callaghan JP, Kelly KA, VanGilder RL, Sofroniew MV, Miller DB. Early Activation of STAT3 Regulates Reactive Astrogliosis Induced by Diverse Forms of Neurotoxicity. *PLoS One*. 2014;9(7):e102003. doi:10.1371/journal.pone.0102003

561. Sánchez-Juan P, Valeriano-Lorenzo E, Ruiz-González A, et al. Serum GFAP levels correlate with astrocyte reactivity, post-mortem brain atrophy and neurofibrillary tangles. *Brain*. 2024;147(5):1667-1679. doi:10.1093/brain/awae035

562. Du J, Yi M, Zhou F, et al. S100B is selectively expressed by gray matter protoplasmic astrocytes and myelinating oligodendrocytes in the developing CNS. *Mol Brain*. 2021;14:154. doi:10.1186/s13041-021-00865-9

563. Cirillo C, Capoccia E, Iuvone T, et al. S100B Inhibitor Pentamidine Attenuates Reactive Gliosis and Reduces Neuronal Loss in a Mouse Model of Alzheimer's Disease. *Biomed Res Int*. 2015;2015:508342. doi:10.1155/2015/508342

564. Barros C, Barateiro A, Neto A, et al. S100B inhibition protects from chronic experimental autoimmune encephalomyelitis. *Brain Commun*. 2022;4(3):fcac076. doi:10.1093/braincomms/fcac076

565. Araque A, Parpura V, Sanzgiri RP, et al. Tripartite synapses: glia, the unacknowledged partner. *Trends in Neurosciences*. 1999;22(5):208-215. doi:10.1016/S0166-2236(98)01349-6

566. de Ceglia R, Ledonne A, Litvin DG, et al. Specialized astrocytes mediate glutamatergic gliotransmission in the CNS. *Nature*. 2023;622(7981):120-129. doi:10.1038/s41586-023-06502-w

567. Armbruster M, Naskar S, Garcia JP, et al. Neuronal activity drives pathway-specific depolarization of peripheral astrocyte processes. *Nat Neurosci*. 2022;25(5):607-616. doi:10.1038/s41593-022-01049-x

568. Rothstein JD, Van Kammen M, Levey AI, Martin LJ, Kuncl RW. Selective loss of glial glutamate transporter GLT-1 in amyotrophic lateral sclerosis. *Ann Neurol*. 1995;38(1):73-84. doi:10.1002/ana.410380114

569. Peterson AR, Binder DK. Regulation of Synaptosomal GLT-1 and GLAST during Epileptogenesis. *Neuroscience*. 2019;411:185-201. doi:10.1016/j.neuroscience.2019.05.048

570. Iovino L, Giusti V, Pischedda F, et al. Trafficking of the glutamate transporter is impaired in LRRK2-related Parkinson's disease. *Acta Neuropathol*. 2022;144(1):81-106. doi:10.1007/s00401-022-02437-0

571. Chen S, Chang Y, Li L, et al. Spatially resolved transcriptomics reveals genes associated with the vulnerability of middle temporal gyrus in Alzheimer's disease. *Acta Neuropathol Commun*. 2022;10:188. doi:10.1186/s40478-022-01494-6

572. Maretzky T, Evers A, Le Gall S, et al. The Cytoplasmic Domain of A Disintegrin and Metalloproteinase 10 (ADAM10) Regulates Its Constitutive Activity but Is Dispensable for Stimulated ADAM10-dependent Shedding. *J Biol Chem*. 2015;290(12):7416-7425. doi:10.1074/jbc.M114.603753

573. Li X, Pérez L, Pan Z, Fan H. The transmembrane domain of TACE regulates protein ectodomain shedding. *Cell Res*. 2007;17(12):985-998. doi:10.1038/cr.2007.98

574. Maesako M, Houser MCQ, Turchyna Y, Wolfe MS, Berezovska O. Presenilin/γ-Secretase Activity Is Located in Acidic Compartments of Live Neurons. *J Neurosci*. 2022;42(1):145-154. doi:10.1523/JNEUROSCI.1698-21.2021

575. Baranger K, Rivera S, Liechti FD, et al. Chapter 14 - Endogenous and synthetic MMP inhibitors in CNS physiopathology. In: Dityatev A, Wehrle-Haller B, Pitkänen A, eds. *Progress in Brain Research*. Vol 214. Brain Extracellular Matrix in Health and Disease. Elsevier; 2014:313-351. doi:10.1016/B978-0-444-63486-3.00014-1

576. Zipfel P, Rochais C, Baranger K, Rivera S, Dallemagne P. Matrix Metalloproteinases as New Targets in Alzheimer's Disease: Opportunities and Challenges. *J Med Chem*. 2020;63(19):10705-10725. doi:10.1021/acs.jmedchem.0c00352

577. Afram E, Lauritzen I, Bourgeois A, et al. The η-secretase-derived APP fragment ηCTF is localized in Golgi, endosomes and extracellular vesicles and contributes to Aβ production. *Cell Mol Life Sci*. 2023;80(4):97. doi:10.1007/s00018-023-04737-4

578. Weiss GA, Watanabe CK, Zhong A, Goddard A, Sidhu SS. Rapid mapping of protein functional epitopes by combinatorial alanine scanning. *Proceedings of the National Academy of Sciences*. 2000;97(16):8950-8954. doi:10.1073/pnas.160252097

579. King GD, Cherian K, Turner RS. X11alpha impairs gamma- but not beta-cleavage of amyloid precursor protein. *J Neurochem*. 2004;88(4):971-982. doi:10.1046/j.1471-4159.2003.02234.x

580. Shrivastava-Ranjan P, Faundez V, Fang G, et al. Mint3/X11γ Is an ADP-Ribosylation Factor-dependent Adaptor that Regulates the Traffic of the Alzheimer's Precursor Protein from the Trans-Golgi Network. *Mol Biol Cell*. 2008;19(1):51-64. doi:10.1091/mbc.E07-05-0465

581. Sidransky E, Nalls MA, Aasly JO, et al. Multicenter analysis of glucocerebrosidase mutations in Parkinson's disease. *N Engl J Med*. 2009;361(17):1651-1661. doi:10.1056/NEJMoa0901281

582. Istaiti M, Revel-Vilk S, Becker-Cohen M, et al. Upgrading the evidence for the use of ambroxol in Gaucher disease and GBA related Parkinson: Investigator initiated registry based on real life data. *Am J Hematol*. 2021;96(5):545-551. doi:10.1002/ajh.26131

583. Bendikov-Bar I, Ron I, Filocamo M, Horowitz M. Characterization of the ERAD process of the L444P mutant glucocerebrosidase variant. *Blood Cells, Molecules, and Diseases*. 2011;46(1):4-10. doi:10.1016/j.bcmd.2010.10.012

584. Kopytova AE, Rychkov GN, Nikolaev MA, et al. Ambroxol increases glucocerebrosidase (GCase) activity and restores GCase translocation in primary patient-derived macrophages in Gaucher disease and Parkinsonism. *Parkinsonism & Related Disorders*. 2021;84:112-121. doi:10.1016/j.parkreldis.2021.02.003

585. Capone R, Tiwari A, Hadziselimovic A, et al. The C99 domain of the amyloid precursor protein resides in the disordered membrane phase. *Journal of Biological Chemistry*. 2021;296:100652. doi:10.1016/j.jbc.2021.100652

586. Polacco BJ, Lobingier BT, Blythe EE, et al. Profiling the proximal proteome of the activated μ-opioid receptor. *Nat Chem Biol*. Published online March 25, 2024. doi:10.1038/s41589-024-01588-3

587. Zhong X, Li Q, Polacco BJ, et al. A proximity proteomics pipeline with improved reproducibility and throughput. *Mol Syst Biol*. Published online July 1, 2024. doi:10.1038/s44320-024-00049-2

588. Sims EK, Carr ALJ, Oram RA, DiMeglio LA, Evans-Molina C. 100 years of insulin: celebrating the past, present and future of diabetes therapy. *Nat Med*. 2021;27(7):1154-1164. doi:10.1038/s41591-021-01418-2

589. COHEN R, David M, Khrestchatisky M. Transferrin receptor-binding molecules, conjugates thereof and their uses. Published online July 16, 2020. Accessed July 10, 2024. https://patents.google.com/patent/WO2020144233A1/en

590. Gammella E, Lomoriello IS, Conte A, et al. Unconventional endocytosis and trafficking of transferrin receptor induced by iron. *Mol Biol Cell*. 2021;32(2):98-108. doi:10.1091/mbc.E20-02-0129

591. Hinze C, Boucrot E. Endocytosis in proliferating, quiescent and terminally differentiated cells. *J Cell Sci*. 2018;131(23):jcs216804. doi:10.1242/jcs.216804

592. Liu K, Lei R, Li Q, et al. Transferrin Receptor Controls AMPA Receptor Trafficking Efficiency and Synaptic Plasticity. *Sci Rep*. 2016;6(1):21019. doi:10.1038/srep21019

593. Muratore CR, Rice HC, Srikanth P, et al. The familial Alzheimer's disease APPV717I mutation alters APP processing and Tau expression in iPSC-derived neurons. *Hum Mol Genet*. 2014;23(13):3523-3536. doi:10.1093/hmg/ddu064

594. Hu NW, Corbett GT, Moore S, et al. Extracellular Forms of Aβ and Tau from iPSC Models of Alzheimer's Disease Disrupt Synaptic Plasticity. *Cell Rep*. 2018;23(7):1932-1938. doi:10.1016/j.celrep.2018.04.040

595. Balez R, Steiner N, Engel M, et al. Neuroprotective effects of apigenin against inflammation, neuronal excitability and apoptosis in an induced pluripotent stem cell model of Alzheimer's disease. *Sci Rep*. 2016;6:31450. doi:10.1038/srep31450

596. Martín-Maestro P, Sproul A, Martinez H, et al. Autophagy induction by Bexarotene promotes mitophagy in Presenilin 1 familial Alzheimer's disease iPSC-derived neural stem cells. *Mol Neurobiol*. 2019;56(12):8220-8236. doi:10.1007/s12035-019-01665-y

597. Unterauer EM, Shetab Boushehri S, Jevdokimenko K, et al. Spatial proteomics in neurons at single-protein resolution. *Cell*. 2024;187(7):1785-1800.e16. doi:10.1016/j.cell.2024.02.045